Application of Ozone Nanobubbles in Wastewater Treatment

A Thesis Submitted

in Partial Fulfilment of the Requirements

for the Degree of

DOCTOR OF PHILOSOPHY

by

Priya Koundle

(2019CHZ0002)



DEPARTMENT OF CHEMICAL ENGINEERING INDIAN INSTITUTE OF TECHNOLOGY ROPAR

December, 2024

Copyright ©
Priya Koundle, Indian Institute of Technology, Ropar All Rights Reserved

 ${\it To~my~family~and~friends}$

Declaration of Originality

I hereby declare that the work which is being presented in the thesis entitled **Application** of Ozone Nanobubbles in Wastewater Treatment has been solely authored by me. It presents the result of my own independent investigation/research conducted during the time period from July, 2019 of joining the Ph.D. program to July, 2024 of Ph.D. Thesis submission under the supervision of Neelkanth Nirmalkar, Assistant Professor, and Dr. To the best of my knowledge, it is an original work, both in terms of research content and narrative, and has not been submitted or accepted elsewhere, in part or in full, for the award of any degree, diploma, fellowship, associateship, or similar title of any university or institution. Further, due credit has been attributed to the relevant state-of-the-art and collaborations (if any) with appropriate citations and acknowledgments, in line with established ethical norms and practices. I also declare that any idea/data/fact/source stated in my thesis has not been fabricated/falsified/misrepresented. All the principles of academic honesty and integrity have been followed. I fully understand that if the thesis is found to be unoriginal, fabricated, or plagiarized, the Institute reserves the right to withdraw the thesis from its archive and revoke the associated Degree conferred. Additionally, the Institute also reserves the right to appraise all concerned sections of society of the matter for their information and necessary action (if any). If accepted, I hereby consent for my thesis to be available online in the Institute's Open Access repository, inter-library loan, and the title & abstract to be made available to outside organizations.

Signature



Name: Priya Koundle

Entry Number: 2019CHZ0002

Program: PhD.

Department: Department of Chemical Engineering

Indian Institute of Technology Ropar

Rupnagar, Punjab 140001

Date: 12th December, 2024

Acknowledgement

Firstly, I want to express my deep sense of gratitude to my supervisor **Dr. Neelkanth**Nirmalkar for his extreme support and guidance during my entire journey of PhD. I

have received a great deal of technical knowledge as well as acquired good communication
skills. Under his guidance, I have got an immense opportunity to explore new problems
and learning the approach to solve them efficiently.

I am also thankful to the institute for providing me the opportunity to work as a PhD scholar. I am deeply thankful to all the faculty members of the Chemical Engineering Department, IIT Ropar for their fruitful guidance and support throughout the course. I also wish to thank all the supporting staff of the department for their immense co-operation throughout the period. I would like to thank my doctoral committee members, **Dr. Navin Gopinathan** (Department of Chemical Engineering), **Dr. Tarak Mondal** (Department of Chemical Engineering) and **Dr. Anupam Agrawal** (Department of Mechanical Engineering) for their valuable suggestions and constructive criticism during the project evaluations, which helped me to make necessary improvements in various stages of my research work.

I thank Technology Innovation Hub at the Indian Institute of Technology Ropar in the framework of National Mission on Interdisciplinary Cyber-Physical Systems (NM—ICPS) for the funding of this work. Also DST Inspire scheme DST/INSPIRE/04/2016/001163 under Department of Science and Technology.

I express my sincere thanks to my friends **Nikhil Bhatia**, **Divas Dagur** and **Ritu Parashar** at IIT Ropar for making my time here a blissful experience. Their presence and cooperation comforted me in many ways. I could never have achieved my goal without their moral support. They always helped me and encouraged me to be strong enough to surpass all my difficulties, frustrations and worries. Their assistance, suggestions made my stay cheerful at IITRPR.

Also, I would like to thank all my lab members for their extreme support, guidance, advice and encouragement. I thank **Harsh Sharma**, **Nilanjan Dutta**, **Gaurav Yadav**, **Shivi Garg**, **Saurabh Maurya** and **Alok Das** for sharing some wonderful moments with me. This thesis would not have been possible without the hearty support of my family. My deepest regards to my parents for their blessings, affection and continuous support throughout the course. Also, last but not the least, I thank **GOD**, the almighty for giving me the inner willingness, strength and wisdom to carry out this research work successfully.

Certificate

This is to certify that the thesis entitled Application of Ozone Nanobubbles in Wastewater Treatment, submitted by Priya Koundle (2019CHZ0002) for the award of the degree of Doctor of Philosophy of Indian Institute of Technology Ropar, is a record of bonafide research work carried out under my guidance and supervision. To the best of my knowledge and belief, the work presented in this thesis is original and has not been submitted, either in part or full, for the award of any other degree, diploma, fellowship, associate ship or similar title of any university or institution.

In my opinion, the thesis has reached the standard fulfilling the requirements of the regulations relating to the Degree.

Dr. Neelkanth Nirmalkar

Department of Chemical Engineering Indian Institute of Technology Ropar Rupnagar, Punjab 140001

Date: 12^{th} December, 2024

Lay Summary

Conventional water treatment systems frequently exhibit diminished efficiency at high salinity - a significant issue especially for real industrial effluents - mostly due to the creation of intricate structures between pollutants and salts. One of the primary obstacles associated with high salinity conditions is the generation of by-products that pose additional hurdles for treatment. Nanobubble (NB) technologies have received considerable attention for various applications due to their low cost, eco-friendliness, scale-up potential, process control, and unique physical characteristics. Ozonation is one of the widely used AOPs used in wastewater treatment techniques. But, there are certain limitations (i) low ozone solubilities (ii) lower mass transfer rates (iii) high energy requirements. Combining ozone with the nanobubble technology to overcome the above-mentioned limitations has been the major goal in our proposed work. The unique properties of nanobubbles such as high stability, small size, high gas transfer efficiency, oxidative potential and hydrophobicity have made nanobubbles more appealing in the field of wastewater treatment. experimental studies were performed to understand the characteristics and stability of ozone in the form of nanobubbles. From the experiments, it was found that nanobubbles enhance the process of ozonation by three major mechanisms (i) increased ozone solubility leading to increased mass transfer rates (ii) increased formation of reactive oxygen species (iii) increased number of active sites for the chemical reaction to take place. Stability of ozone nanobubbles and dissolved ozone concentrations was measured for a period of 20 days. Based on these findings, application of ozone nanobubbles in treating the organics and heavy metals present in the water were performed. The organics included antibiotics (e.g. tetracycline), dyes (e.g. green rit dye and methylene blue dye) and heavy metals (e.g. arsenic). With the application of ozone nanobubbles, 100 % removal and degradation of organic contaminants and heavy metals was achieved. The comparison efficiency of ozone nanobubbles with conventional ozone microbubbles and macrobubbles has also been presented in this work. The formation of reactive oxygen species, which is the key mechanism for the degradation of the contaminants present in the wastewater has been studied. ESR (Electron Spin Resonance) measurements and radical quenching experiments confirmed the presence of reactive oxygen species being formed during the nanobubble generation. Thus, ozone nanobubble technology can promote a chemical free, cost effective and a practical approach in the wastewater treatment industry.

Abstract

Ozone nanobubbles, in recent times, seems to have wide range of applications in wastewater treatment. Several unique characteristics of nanobubbles such as high stability, increased mass transfer rates etc. make them eminent in improving the efficiencies of the conventional advanced oxidation processes (AOPs). These properties of ozone nanobubbles have been studied in detail. Many practical applications of ozone nanobubbles have been presented. In addition, directions for future research of ozone nanobubble technology and their application in real life problems have been identified.

Ozone is known to be one of the most powerful oxidant used in wastewater treatment processes. One of the primary disadvantages associated with ozone is its restricted solubility and instability when dissolved in an aqueous solution. These characteristics impose limitations on its potential applications and need the use of specialized systems to facilitate gas-liquid interaction. In this work, the novel advanced oxidation process a so-called ozone nanobubble technology for degradation of the pollutants at high salinity conditions has been investigated. Enhancing the ozonation process through the utilization of ozone nanobubbles was studied in this work. The findings of the experiment and subsequent analysis indicate that the presence of nanobubbles enhances the process of ozonation through three key mechanisms: (i) an increased mass transfer coefficient, (ii) a higher rate of reactive oxygen species (ROS) generation attributed to the charged interface, and (iii) the nanobubble interface serving as an active surface for chemical reactions. The study showcased the degradation of methylene blue dye exhibited a much higher rate of dye degradation compared to ozone microbubbles. The confirmation of the radical degradation mechanism was achieved by the utilization of electron spin resonance (ESR) measurements. The developed process has high potential for application in industrial scale textile wastewater treatment.

In pharmaceuticals, especially antibiotics, in industrial and domestic effluents causes serious damage to the environment. Classical wastewater treatment processes, in particular conventional biological treatment methods, are not sufficient to rapidly eliminate Typically, Advanced Oxidation Processes (AOPs) based on activation of antibiotics. hydrogen peroxide, ozone or persulfate for production of particular type of radical species or singlet oxygen are used. One of the cutting edge technologies to increase effectiveness of AOPs based on ozone are nanobubbles based processes. Thus, this thesis focuses on utilization of ozone in the form of nanobubbles for degradation of tetracycline (TC). This studies revealed, that the presence of ozone nanobubbles had a substantial positive impact on the degradation of TC. This improvement may be attributed to the enhanced mass transfer and the production of reactive radicals that occur during the collapse of the nanobubbles. Identification of radical species revealed a significant contribution of hydroxyl radicals (${}^{\bullet}$ OH) and superoxide $O_2{}^{\bullet-}$ in the degradation of the antibiotic. Based on identified by LC-MS intermediates a degradation mechanism has been described. Degradation of TC and intermediates transformations include demethylation, hydroxylation, ring-opening steps as well as cleavage of C-N bonds.

Organic pollutants, especially dyes, present in substantial amounts with high molecular weight and complex structure are highly toxic and can contaminate natural waterways if improperly treated. AOPs have proven to be an effective solution for chemical wastewater treatment. Ozonation is recognized as one of the most prevalent AOPs. Nevertheless, some cases show a lowered efficiency of O₃ utilization is attributed to its inadequate distribution in the treated water causing low mass transfer coefficient as well as shorter half-life. This study demonstrates the application of ozone nanobubbles to enhance the degradation of organics under high loading conditions. We propose an integrated method that utilizes bulk nanobubbles to enhance the reactivity of ozone for the degradation of organics. The degradation of the organic pollutant by ozone nanobubbles demonstrated a threefold increase in reaction rate constants compared to microbubbles. The degradation reaction exhibited second-order kinetics by ozone nanobubbles while ozonation alone offers first-order kinetics. The efficiency of removing the organic pollutant was higher under acidic pH conditions, as well as with lower concentrations of salts and surfactants. The presence of reactive oxygen species and hydroxyl radicals was verified using scavenging tests.

Arsenic, a highly toxic element, is present in various water resources as As(III) and/or As(V). The removal of As(V) using adsorption is considered to be easier than the removal of As(III). In this work, we report the oxidation of As(III) to As(V) using ozone nanobubbles. Ozone has been widely used in the advanced oxidation process (AOP) to remove organics and inorganics in wastewater. The major advantage of ozone nanobubbles is their enhanced half-life, which leads to higher ozone solubility in water. In addition, the rate of mass transfer by using nanobubbles can be enhanced drastically. The present results revealed that ozone nanobubbles positively impacted the oxidation of As(III) to As(V). AOP process based on O₃ NBs (nanobubbles) was most efficient with 99% oxidation rates of 1 ppm of As(III) within 20 minutes at 6.5 ppm ozone concentrations. An acidic pH of 3-7 promoted quick oxidation due to the high mass transfer coefficient of ozone nanobubbles. About $\sim 70\%$ degradation of As(III) to As(V) was achieved at acidic (pH = 3) compared to \sim 39% degradation at pH =11. The presence of salt (~ 50 mM) in the solution not only hindered the ozone mass transfer coefficient but also reduced the stability of nanobubbles. The detection of reactive oxygen species, particularly hydroxyl radical was unravelled by utilizing 2-propanol as a scavenger.

Keywords: Ozone; Nanobubbles; AOPs; Reactive oxygen species; Organic contaminant; Arsenic;

List of Publications

Published Online

- Koundle P., Nirmalkar N., Momotko M., Boczkaj G., 2024 Ozone nanobubble technology as a novel AOPs for pollutants degradation under high salinity conditions. Water Research, Vol.263, 122148).
- Koundle P., Nirmalkar N.[™], Boczkaj G., 2024 Tetracycline degradation for wastewater treatment based on ozone nanobubbles advanced oxidation processes (AOPs) - focus on nanobubbles formation, degradation kinetics, mechanism and effects of water composition (In Press, Journal Pre-proof, Chemical Engineering Journal).
- Koundle P., Nirmalkar N.≅, Boczkaj G., 2024 High performance ozone nanobubbles based advanced oxidation processes (AOPs) for degradation of organic pollutants under high pollutant loading (Under Revision, Journal of Environmental Management).
- Koundle P., Goud Nandkumar G., Gopinathan N., Nirmalkar N.[™], 2024 Advanced oxidation of Arsenic (III) to Arsenic(V) using ozone nanobubbles under high salinity.
 J. Environ. Chem. Eng., Vol.12, Iss.5, 113402.

Conference/Presentations

- Koundle, P., and Nirmalkar, N., 2022. Comparison efficiency of Ozone and Oxygen Nanobubbles in Degradation of Green Rit Dye. International Conference on Nanobubbles, Nanodroplets and their Applications (Nanobubble 2022), Otto-von-Guericke- University Magdeburg, Germany, Nanobubble production 7, 98, 18-21 September.
- Kounndle, P., and Nirmalkar, N., 2022. STUDY ON DEGRADATION OF TETRACYCLINE USING OZONE NANOBUBBLES. Complex Fluid Symposium (CompFlu 22), Indian Institute of Technology, Kharagpur. 19-22 December.
- Koundle, P., Nirmalkar, N., and Boczkaj, G., 2024 Ozone nanobubble technology as a novel AOPs for pollutants degradation under high salinity conditions. International Conference on Nanobubbles, Nanodroplets and their Applications (Nanobubble 2024), Kyoto University, Uji Campus, Kyoto, Japan. 10-12 October.

^{* \}subseteq Corresponding author

Contents

ט	eclar	ation		lV
A	cknov	wledge	ment	v
\mathbf{C}	ertifi	cate		vi
L	ay Su	ımmar	y	vii
A	bstra	.ct	•	viii
Li	ist of	Publi	cations	x
Li	ist of	Figur	es	xv
Li	ist of	Table	S XX	xiii
Li	ist of	Symb	ols x	xxv
1	Intr	oduct	ion	1
	1.1	Overv	iew	1
	1.2	Introd	luction to nanobubbles	2
	1.3	Funda	amental characteristics of nanobubbles related to wastewater treatment	2
		1.3.1	Miniature size and high mass transfer efficiency	3
		1.3.2	High negative zeta potential and hydrophobocity	4
		1.3.3	Long term stability	5
		1.3.4	High oxidative potential: radical producer and scavenger	8
	1.4	Gener	ation techniques of nanobubbles	9
		1.4.1	Cavitation	9
		1.4.2	Membranes	10
		1.4.3	Ethanol-water mixing	11
		1.4.4	Electrolysis	11
	1.5	Ozone	e: a potential oxidant	12
	1.6	Applie	cations of nanobubbles	14
		1.6.1	Role of nanobubbles in floatation processes	16
		1.6.2	Role of nanobubbles in membrane cleaning/defouling	16
		1.6.3	Role of nanobubbles in advanced oxidation processes	17
		1.6.4	Role of nanobubbles in anaerobic digestion processes	18
	17	Future	e prospects and potential applications	18

xii

2	Lite	erature	e Review	21
	2.1	Litera	ature	21
		2.1.1	Ozone nanobubble technology as a novel AOPs under high salinity conditions	21
		2.1.2	Degradation of antibiotic tetracycline	23
		2.1.3	Degradation of organic contaminants from wastewater with high pollutant loading	25
		2.1.4	Oxidation of Arsenic(III) to Arsenic (V) in wastewater using ozone nanobubbles	26
	2.2	Object	etives of this work	29
	2.3	_	nization of thesis	29
3	Exp	oerime	ental Methods	31
	3.1	Exper	rimental setup	31
	3.2	Chara	acteristics and stability of ozone nanobubbles as AOPs	32
		3.2.1	Materials	32
		3.2.2	Nanobubble generation and its characterization	33
		3.2.3	ESR spin trap measurements of reactive oxygen species generated in ozone nanobubbles	35
	3.3	Degra	adation of antibiotic tetracycline using ozone nanobubbles	36
	0.0	3.3.1	Materials	36
		3.3.2	Experimental methods	36
		3.3.3	Degradation kinetics and calculating mass transfer coefficient	36
		3.3.4	Measurement of concentration of tetracycline and degradation	50
		0.0.4	pathways	39
	3.4	Degra	adation of organic pollutants under high pollutant loading	39
		3.4.1	Materials	39
		3.4.2	Experimental methods	39
		3.4.3	Color measurement, degradation analysis and radical quenching	40
	3.5	Oxida	ation of As(III) to As(V)	41
		3.5.1	Materials	41
		3.5.2	Nanobubble generation and oxidation	41
		3.5.3	Analysis of $As(V)$ and determining oxidation kinetic studies	42
4	R&	D 1: 0	Characteristics, stability and application of ozone nanobubbles	45
	4.1	Ozone	e nanobubble dynamics in salt solution	45
	4.2	Ozone	e nanobubbles in acidic and alkaline medium	48
	4.3	Mass	transfer coefficient by ozone nanobubbles	52
	4.4	Stabil	lity of ozone nanobubbles, ROS generation and dye degradation	55

Contents

5	\mathbf{R} &	D 2: 7	Tetracycline degradation for wastewater treatment based on	1
	ozo	ne nan	obubbles advanced oxidation processes (AOPs)	61
	5.1	Effect	of TC dosage on degradation kinetics	61
	5.2	Degrad	dation characteristics of TC in alkaline and acidic medium	65
	5.3	Degrad	dation kinetics in the presence of monovalent salts	67
	5.4	Degrad	dation efficiency of TC by different methods	68
	5.5	Effect	of radical scavengers and determining the degradation pathway	72
6			zone nanobubbles based advanced oxidation processes (AOPs)	
		_	ation of organic pollutants	77
	6.1		of ozone flow rate on nanobubble generation	77
	6.2		of change of initial concentration of dye	
	6.3		of change of ozone flow rates on dye degradation	80
	6.4		of pH, salts and surfactants	80
	6.5	-	arison of treatment efficiency of ozone and oxygen nanobubbles,	~ ~
			bubbles and charge possessed by nanobubbles	
	6.6	Radica	al quenching and analysis of intermediates	86
7	R &	D 4: A	${\bf Advanced\ oxidation\ of\ Arsenic(III)\ to\ Arsenic(V)\ using\ ozone}$	3
	nan	obubbl	les under high salinity	89
	7.1	Effect	of ozone flow rate on nanobubble generation	89
	7.2	Effect	of ozone flow rate on Arsenic oxidation	90
	7.3	Effect	of initial concentration of As(III)	92
	7.4	Effect	of pH	92
	7.5	Effect	of chloride ions/salts on oxidation of $As(III)$	95
	7.6	Effect	of 2-propanol as OH radical scavenger	96
8	Cor	ıclusior	1	99
	8.1	Conclu	ı <mark>sion</mark>	99
		8.1.1	Characteristics, stability and application of ozone nanobubbles	99
		8.1.2	Tetracycline degradation for wastewater treatment based on ozone	
			nanobubbles advanced oxidation processes (AOPs) $\ \ldots \ \ldots \ \ldots$	100
		8.1.3	Ozone nanobubbles based advanced oxidation processes (AOPs) for	
			degradation of organic pollutants	101
		8.1.4	Advanced oxidation of $Arsenic(III)$ to $Arsenic(V)$ using ozone nanobubbles under high salinity	101
	8.2	Scope	for future work	102
Re	efere	nces		103
A	App	pendix	A	131
В	Apı	pendix	A	133

xiv	Contents

\mathbf{C}	Appendix B	13	7
	${\rm C.1} \ \ {\rm Determination\ of\ volumetric\ mass\ transfer\ coefficient\ (Model\ development)\ .}$	13	7
D	Appendix C	14	5

List of Figures

1.1	Range of bubbles sizes and corresponding major properties [1]	2
1.2	Fundamental physio chemical properties of nanobubbles [2]	3
1.3	Nanobubble stability map from the force balance around a single nanobubble	
	[3]	5
1.4	Schematic diagram showing various nanobubble generation techniques:	
	A-hydrodynamic cavitation using venturi system, B-acoustic cavitation,	
	C–Membrane system, D–Centrifugal multiphase pump, E–electrolytic cell,	
	F-micro- and nano-sized nozzle [4]	9
1.5	(a) Size distribution of nanobubbles; (b) The time course of O_3 concentration	
	during nanobubble and macrobubble aeration scenarios; (c) Size distribution	
	of macrobubbles [5]	13
1.6	(a) Ozone concentration time profile when using nano-ozone and macro	
	ozone bubble (b) Effect of (a) pH and (b) temperature on degradation	
	kinetics of TMAH during nano-ozone/ H_2O_2 process (pH = 7, 7 10; t =	
	5, 25, 45 °C; $H_2O_2 = 100 \text{ mg/L}$; $n = 2)$ [6]	13
1.7	An overview of how NB technology can enhance water and wastewater	- 4
	treatment processes. [2]	14
1.8	(A) Illustration of microbubble, nanobubble, and micro-nanobubble	
	flotation. (B) Apatite flotation mass recovery for various tailings.	
	CB—conventional test, NB—nanobubbles, NBC—nanobubbles with a collector, NBF—nanobubbles with a frother. [7]	15
1.9	Main mechanisms behind membrane cleaning in reverse osmosis membrane	10
1.9	processes [8]	16
1 10	Photocatalyst particle stabilization by MNBs. (A) Concentration profiles	10
1.10	of TiO ₂ particles as a function of time in three different solutions: MNB	
	suspension, MaB-aerated DI water, and DI water without aeration (labeled	
	NonB). (B) Schematic illustrating the forces of a TiO ₂ particle adhered to	
	a bubble. (C) Detachment force (Fd) of a TiO ₂ particle [9]	17
1.11	A schematic overview of the role of NBs in anaerobic digestion [10]	18
3.1	Illustrative representation of the experimental set-up for the ozone	
0.1	nanobubble generation and ozone nanobubble collapse leading to ROS	
	formation, enhanced mass transfer. The dissolved ozone has been measured	
	online using the dissolved ozone analyser.	32
3.2	Working principal of (a) NTA (Nanoparticle tracking analysis) (b) DLS	
	(Dynamic light scattering)	33

xvi List of Figures

3.3	FE-SEM scan of 30 nm pore size ceramic membrane (a) overall morphology of the membrane (b) outermost/support layer (c) membrane area near channel opening (d) transition layer) (e) innermost layer (f) Image of the ceramic membrane with a zoomed view of the membrane pore channel	34
3.4	Illustrative representation of the experimental set-up for the degradation of tetracycline. The dissolved ozone has been measured online using the dissolved ozone analyser. The degradation of TC is characterized by analysis through UV Spectrophotometer and LC-MS analysis. Photography of collected samples document real change of color of treated solution, while	
	treatment.	37
3.5	Calibration plots for Tetracycline (i) 0-50 mg/L (ii) 0-450 mg/L	38
3.6	Schematic illustration of the experimental setup. The setup is run in re-circulation mode. The degraded samples are collected every 10 seconds until complete degradation. The NBs formed during the process are characterized by NTA analysis. The intermediates formed during the process are examined by LC-MS analysis	40
3.7	Illustrative representation of the experimental set-up for the oxidation of As(III) to As(V). The dissolved ozone has been measured using the dissolved ozone analyser. The NB sample was analysed using NTA and DLS. The As	
	detection was performed using spectrophotometer	42
3.8	As (V) standard calibration curve	43
4.1	Generation of ozone nanobubbles at various ozone flow rates (1-10 L/min). (a) 3D representation of the ozone nanobubbles at different flow rates of ozone (b) Comparative representation of the bubble number density against mean bubble diameter (c) Zeta potential trend at different flow rates from 1-10 L/min (d) Dissolved ozone concentration measurement at every minute for 30 minutes of the experimental run.	47
4.2	Ozone nanobubble preparation in the presence of salts at various ionic concentrations (a) The upper graph shows the trends for the bubble number density against the mean bubble diameter. The lower graph shoes the trend for the negative charge. (b) The upper graph shows the trends for the bubble number density against the mean bubble diameter. The lower graph shoes	
	the trend for the positive charge	48
4.3	Ozone nanobubble generation at acidic and alkaline medium (a) Trends for the bubble number density to that of the mean bubble diameter with respect to the change in the medium (b) The dissolved ozone concentration monitored every one minute for 30 minutes time interval (c) Zeta potential trends at various pH (d) Comparison of the scattering intensities of 100 nm mono-dispersed polystyrene latex beads with ozone nanobubbles produced	
	at 7 L/min (201.1 nm) and in the presence of trivalent salt (139.7 nm)	50

List of Figures xvii

4.4	during nanobubble generation and nanobubble dissolution (a) Comparison of mass transfer coefficient at different ozone flow rates (1-10 L/min) (b) The trends of mass transfer coefficient being the highest at acidic pH and decreasing as the pH of the medium changes to alkaline (c) At varying concentrations of monovalent salt (0.1-100 mM) (d) At varying concentrations of trivalent salt (0.1-100 mM)	53
4.5	Stability of ozone nanobubbles over a time span of 20 days followed by the application of ozone nanobubbles in dye degradation (a) The bubble number density of ozone nanobubbles (b) The dissolved ozone concentration compared to simply sparging the gas in the water (c) Pictorial and experimental degradation of methylene blue dye at different concentration (10-200 mg/L) using ozone nanobubbles.	56
4.6	Mechanism of understanding the behavior of the ozone nanobubbles during long term stability (20 days) and upon diluting the nanobubble solution into degassed water at a particular dilution ratio (1:5, 1:4, 1:6)	57
4.7	LC-MS analysis (a) m/z MS spectra at every 1 minute (b) Possible degradation pathway of methylene blue.	58
4.8	ESR spectrum of the radical adduct of DMPO. The ESR measurements were done for ozone nanobubbles in comparison to pure water taken as a control sample. The left side of the figure shows the cumulative peaks at the given magnetic field. The right side of the figure depicts the magnified versions of the peaks arranged in stacks to compare the intensity of the curves at various conditions.	59
4.9	Radical quenching experiments (a) Dye degradation trends in the presence and absence of scavengers (b) Rate constant depicting the domination presence of the reactive oxygen species	59
5.1	Effect of ozone flow rate on nanobubble generation (i) bubble size distribution (ii) scattering intensity of nanobubbles tracked at different flow rates	62
5.2	Effect of Initial concentration (100-400 mg/L) and different ozone flow rates (i) 10 L/min (ii) 5 L/min (iii) 2.5 L/min and kinetics with rate constant k at (iv) 10 L/min (v) 5 L/min (vi) 2.5 L/min ozone flow rates	63
5.3	(i) Dissolved ozone measurements in pure water and during tetracycline degradation (100-400 mg/L) (ii) highest dissolved ozone attained at different ozone flow rates at different TC concentrations (iii) Mass transfer coefficient corresponding to the ozone concentrations at different ozone flow rates and different concentrations of TC (100-400 mg/L) (iv) Comparison of molar excess of O_3 (%) to degradation efficiency (%) of TC (100-400 mg/L)	64

xviii List of Figures

5.4	Effect of acidic and alkaline mediums on degradation of TC (i) Degradation of 200 mg/L TC under different pH conditions (ii) Rate constant k under different pH conditions (iii) Online dissolved ozone measurements during degradation of TC (iv) Mass transfer coefficient of ozone at various pH	6.0
5.5	conditions	00
5.6	of ozone at various salt concentrations	67
5.7	Effect of addition of 2-propanol as an *OH scavenger (i) Degradation of TC (200 mg/L) under the influence of 1 mM 2-propanol, sodium azide and chloroform (ii) Pseudo second order rate constant at particular experimental conditions.	73
5.8	Possible degradation pathway mechanism of tetracycline through LC-MS technique.	76
6.1	Nanobubble generation at various ozone flow rates (1-10 L/min) and their characterization using NTA and DLS analysis (a) Comparative representation of BND with mean bubble diameter (b) Zeta potential trend (c) Dissolved ozone monitoring (d) Measurement of the volumetric mass transfer coefficient ($k_{\rm L}a$) at various flow rates of ozone	78
6.2	Effect of initial concentration of dye on degradation at 5 L/min ozone flow rates (a) Bubble size distribution of green rit at various concentrations (10-200 mg/L) (b) Mean bubble diameter (c) Zeta potential of the end products; (d) Varying initial concentrations of green rit (10-200 mg/L) (e) Kinetics of the reaction rate constant k (f) Varying initial concentration of methylene blue (0.5-30 mg/L) (g) The reaction rate constant of degradation of organic pollutants	79
6.3	Effect of various ozone flow rates $(2.5, 5 \text{ and } 7 \text{ L/min})$ on dye degradation (a) Green rit dye (100 mg/L) (b) Green rit dye (200 mg/L) (c) Methylene	•
6.4	blue dye (10 mg/L) (d) Methylene blue dye (20 mg/L) with rate constant k Effect of pH (4-10) on degradation of dye at a constant ozone flow rate of 5 L/min (a) 100 mg/L green rit dye (b) 200 mg/L green rit dye (c) Comparison of reaction rate constant for both green rit dye concentrations (d) 10 mg/L methylene blue dye (e) 20 mg/L methylene blue dye (f) Comparison of reaction rate constant for both methylene blue dye concentrations	81

List of Figures xix

6.5	Effect of salt concentration on dye degradation (2-100 mM) at a constant 5 L/min ozone flow rate (a) Monovalent salt (NaCl) (b) Divalent salt (CaC l_2 ·6 H_2 O) (c) Trivalent salt (AlC l_3) at 20 mg/L methylene blue dye concentration (d) Monovalent salt (NaCl) (e) Divalent salt (CaC l_2 ·6 H_2 O) (f) Trivalent salt (AlC l_3) at 200 mg/L green rit dye concentration	83
6.6	Effect of concentration of surfactant (0.3-5 cmc) (a) Anionic surfactant (SDS) at 200 mg/L GRD (b) Anionic surfactant (SDS) at 20 mg/L MB (c) Comparative trends of rate constant for SDS (d) Cationic surfactant (CTAB) at 200 mg/L GRD (e) Cationic surfactant (CTAB) at 200 mg/L MB (f) Comparative trends of rate constant for CTAB	84
6.7	Comparison efficiency in dye degradation (a) Ozone and oxygen nanobubbles (b) Oxygen nanobubbles with positive and negative charge (c) Ozone nanobubbles vs ozone microbubbles (d) Reaction rate constant k for various comparative methods depicting highest rate constant for ozone nanobubbles	86
6.8	Radical quenching experiments (a) Comparison of degradation efficiency in presence of scavengers (2-Propanol and Sodium azide) to degradation efficiency when no scavenger is present (b) Comparison of the reaction rate constant in presence and absence of scavengers	87
6.9	Analysis of intermediates being formed during ozonation by LC-MS analysis showing MS spectra and the possible degradation mechanism	88
7.1	Ozone nanobubble generation in pure water at various ozone flow rates (a) Bubble number density and mean diameter (b) Zeta potential (c) Cumulative population of ozone nanobubbles (d) Comparison of the scattering intensities of 100 nm mono-dispersed polystyrene latex beads with ozone nanobubbles produced at 3 L/min (127.2 nm) and 10 L/min (196.6 nm)	90
7.2	(a) Effect on oxidation of As(III) to As(V) at different ozone flow rates with respect to time (b) Final As(V) concentration achieved at the end of 10 minutes at different ozone flow rates (c) Reaction rate constant at various flow rates (d) Online dissolved ozone measurements during oxidation process	91
7.3	(a) Effect on oxidation of As(III) to As(V) at different initial concentrations of As(III) (b) Degradation efficiency with time achieved at the end of 20 minutes at varying As(III) initial concentration (c) Reaction rate constant following the first order kinetics (d) Mass balance of total arsenic at 1 ppm As(III) initial concentration	93
7.4	Effect on oxidation of As(III) to As(V) at varying pH (3-11) (a) As(V) final concentration vs pH after 10 minutes (b) Degradation efficiency achieved at the end of 10 minutes at different pH (c) Reaction rate constant K with at varying pH (d) Online dissolved ozone measurements during oxidation process	94

xx List of Figures

7.5	Effect of various concentration of monovalent salts (NaCl) on As(III) oxidation (a) Oxidation of As(III) to As(V) at different NaCl concentrations (1-50 mM) (b) Degradation efficiency with time achieved at different NaCl concentrations (c) Reaction rate constant K (d) Online dissolved ozone	
	measurements during oxidation process	96
7.6	Effect of addition of scavenger (2-Propanol) (a) Oxidation of As(III) to As(V) at 0.01 -0.05 M 2-Propanol concentrations (b) Degradation efficiency at different scavenger concentration (c) Reaction rate constant K (d) Online dissolved ozone measurement during oxidation process	98
B.1	Ozone nanobubble preparation in the presence of monovalent salt (NaCl) (a) 3D representation of bubble number density of NBs at different concentrations of salts (0.1-100 mM) (b) Dissolved ozone concentration at	100
B.2	every one-minute time interval for a period of 30 minutes	
D a	every one-minute time interval for a period of 30 minutes	
B.3 B.4	3D representation of Ozone nanobubble preparation at different pH (2-12). Dissolved ozone concentration during ozone dissolution (1:5) at various conditions (a) varying ozone flow rates (1-10 LPM) (b) varying pH (2-12)	134
B.5	 (c) monovalent salt (NaCl) (d) trivalent salt (AlCl₃)	134
	ratio (d) mass transfer coefficient at different conditions	135
C.1 C.2	Sample calculations for (i) k_La (ii) k_d	137
C^{2}	to degradation efficiency (%) of TC at 5 LPM	138
C.3	Comparison of dissolved ozone in pure water and during degradation of TC (100-400 mg/L) (i) 10 LPM (ii) 5 LPM (iii) 2.5 LPM	138
C.4	(i) Comparison of dissolved ozone in presence of pure water to different salt concentrations (ii) Comparison of dissolved ozone in presence of only NaCl to NaCl $+$ TC (0.1, 1, 5mM) (iii) Comparison of dissolved ozone in presence	
C.5	of only NaCl to NaCl + TC (10, 50, 100 mM)	139
	with rate constant k at 10 LPM ozone flow rates	139
C.6	LC-MS peaks with MS spectra during TC degradation at an interval of 5 minutes	140

List of Figures xxi

C.7	Stability of ozone nanobubbles at different ozone flow rates (2.5, 5 and 10	
	L/min) over a period of 30 days (i) Bubble number density (bubble.mL ⁻¹)	
	(ii) Mean bubble diameter (nm	140
C.8	Scheme 1	141
C.9	Scheme 2	142
C.10	Scheme 3	143
C.11	Scheme 4	144
D.1	Kinetic study for effect of ozone flow rates (a) 100 mg/L green rit dye (b) 200 mg/L green rit dye (c) 10 mg/L methylene blue dye (d) 20 mg/L methylene	
	blue dye	145
D.2	Kinetic study for effect of pH on (a) 100 mg/L green rit dye (b) 200 mg/L green rit dye (c) 10 mg/L methylene blue dye (d) 20 mg/L methylene blue	
	dye	146
D.3	Kinetic study on effect of salts on green rit dye (200 mg/L) (a) Monovalent	
	salt (b) Divalent salt (c) Trivalent salt (d) Rate constant k for all three salts I	146
D.4	Kinetic study on effect of salts on methylene blue dye (20 mg/L) (a) Monovalent salt (b) Divalent salt (c) Trivalent salt (d) Rate constant k	
	for all three salts	147
D.5	Kinetic study on the effect of surfactants (a) SDS on green rit dye (200 mg/L) (b) CTAB on green rit dye (200 mg/L) (c) SDS on methylene blue	
	dye (20 mg/L) (d) CTAB on methylene blue dye (20 mg/L) \dots	147
D.6	Kinetic study on (a) Comparison of ozone and oxygen MB's and NB's (b)	
	Negative and positive oxygen NB's (c) Radical scavenging experiments 1	148
D.7	Analysis of intermediates formed during ozonation of 100 mg/L methylene	
	blue by LC-MS analysis showing MS spectra and the possible degradation	
	mechanism.	148
D.8	LC chromatograms for the LC-MS analysis of the methylene blue dye 1	149

xxii List of Figures

List of Tables

1.1	Detection methods of reactive oxygen species in NB research	8
1.2	Ozone reactions [11] [12]	11
3.1	Parameters of 30 nm ceramic membrane used in nanobubble generation $$	35
4.1	Degradation products of methylene blue	58
5.1	Synergistic coefficient for different methods	71
5.2	Comparison efficiency of ozone nanobubbles with conventional AOPs	72
5.3	Comparison of operation cost of different AOPs with ozone nanobubbles	73
6.1	Comparison of operation cost of different AOPs with ozone nanohubbles	87

xxiv List of Tables

List of Symbols

ϵ_0	Permittivity of free space
ϵ_r	Relative dielectric constant
ψ	Surface potential
$ ho_e$	Local electric charge density, ${\cal C}/m^3$
$ ho_{\infty}$	Bulk ion number density
σ	Surface charge density
σ_S	Scattering cross section, nm^2
ξ	Synergistic coefficient
ζ	Surface charge on nanobubble
C^*	Saturated concentration of ozone, $\rm mg/l$
C_0	Initial concentration of ozone, $\mathrm{mg/L}$
C_t	Ozone concentration at any given time t , mg/L
k_B	Boltzmann constant
k_d	Ozone decomposition rate constant, min^{-1}
k_L	Mass transfer of liquid
k_L a	Mass transfer coefficient, min^{-1}
P_S	Scattering power, AU
P_{B0}	Gas pressure
P_{ele}	Pressure force
W_R (1	D) Electrostatic potential
В	Breadth, inches
D	Inter-spacing distance
e	Unit charge
Н	Height, inches
L	Length, inches

xxvi List of Symbols

MB Microbubbles

n Normal to the surface

NB Nanobubbles

NTA Nanoparticle tracking analysis

Q Surface chrge, Cm^{-2}

R Nanobubbles radius, nm

s Valency

T Temperature, °C

Chapter 1

Introduction

This chapter presents a summary of the properties of nanobubbles in accordance with the applications. Various methods for the generation of nanobubbles have been discussed. Combination of ozone with nanobubbles in the field of wastewater treatment as an Advanced Oxidation Process (AOP) has been thoroughly discussed. Many practical applications using ozone, air and oxygen nanobubbles have been presented. How nanobubbles are an important factor with its application in the various advanced oxidation processes (AOPs) has also been discussed. In addition, directions for future research of ozone nanobubbles technology and its potential applications has been identified.

1.1 Overview

Water pollution refers to the discharge of contaminants into subsurface groundwater or into lakes, streams, rivers and oceans to the point that the substances interfere with the beneficial use of water or with the natural functioning of ecosystems. It increases when there is any change in the chemical, physical or biological change in the quality of water. Due to the increased population and industrialization, the necessity and scarcity of drinking water has become a major concern. One of the major reasons for water pollution is the release of toxic and organic contaminants in water resulting from rapid population and industrial growth. These toxic pollutants include effluents from textile industry, antibiotics, heavy metals etc. The complete removal of the contaminants from the water is not possible due to various reasons. Therefore, in recent years there have a lot of conventional technologies which have been focusing upon the treatment of wastewater. These are referred to as Advanced oxidation processes (AOPs) which include Fenton-like, ozonation, photocatalysis, electro-catalysis, ultrasound, wet-air oxidation and many more. But these conventional technologies have shown limitations in terms of formation of sludge and by-products, operating costs and not meeting the discharge needs. With these growing challenges, there is a need for the development of a more effective and prominent technology for the wastewater treatment. In this relation, nanobubbles have gained a growing interest due to their unique properties which offer great opportunities to improve existing wastewater treatment technologies.

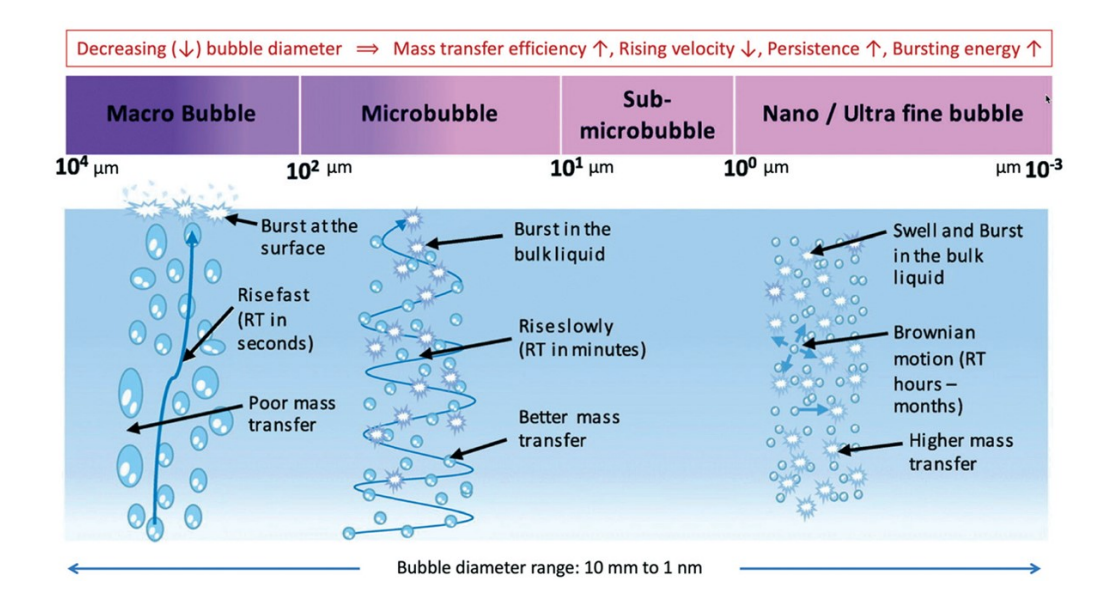


Figure 1.1: Range of bubbles sizes and corresponding major properties [1]

1.2 Introduction to nanobubbles

Nanobubbles are spherical packages of gas filled cavities with a volume equivalent diameter of less than 1 μ m [13] [3]. They are different from the conventional bubbles such as macrobubbles or microbubbles. Macro and microbubbles are larger in size than the nanobubbles and these conventional bubbles have been widely used in the wastewater treatment processes. Some of these processes include floatation, aeration, disinfection and membrane fouling. But these conventional bubbles have some limitations like they disappear quickly in water either by bursting at the surface or shrinking and collapsing within the liquid which limits their overall gas transfer efficiency. Nanobubbles, on the other hand, possess high stability and can exist in water for a longer period of time. With high stability, nanobubbles have other unique properties such as low buoyancy, high negative zeta potential, high surface area to volume ratio, and their ability to generate reactive oxygen species. A comparison of the size of the nanobubbles to the conventional bubbles along with major distinctive properties is shown in Fig. 1.1 [1]. The application of nanobubbles in wastewater treatment is regarded as a type of green technology as it helps towards chemical free processes. This technology has the potential of replacing or enhancing the potential of the conventional technologies.

1.3 Fundamental characteristics of nanobubbles related to wastewater treatment

Nanobubbles are endowed with several physio-chemical properties that distinguish them from the conventional macro and micro bubbles. The unique properties of nanobubbles have been mentioned in Fig.1.2. Further, nanobubbles are classified as surface nanobubbles

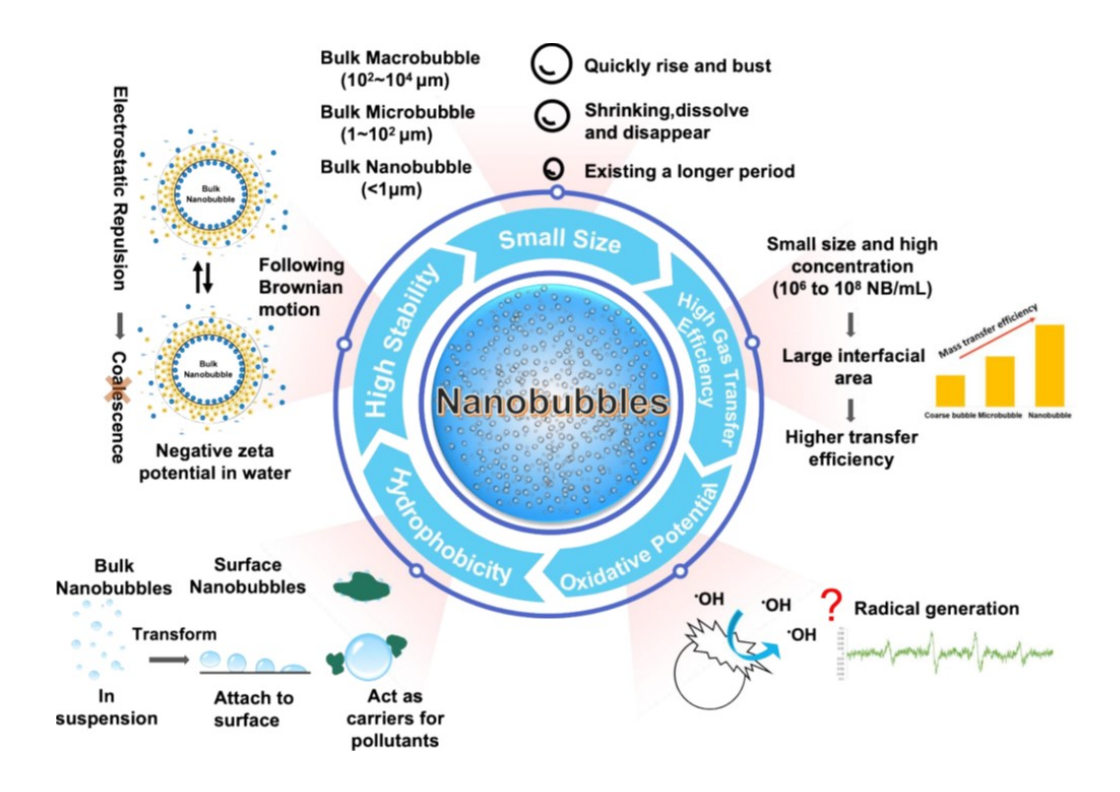


Figure 1.2: Fundamental physio chemical properties of nanobubbles [2]

(surface NBs) and bulk nanobubbles (NBs). Surface nanobubbles are define as as the nanoscopic entities that are generated directly on the surface in form of a spherical cap. When compared to NBs, they differ in terms of their mobility and have been investigated to be stable for a longer period of time. Surface NBs are majorly used in froth flotation and mineral processing applications. However, due to their immobility, surface NBs have limited applications. NBs, on the other hand, are produced in bulk of the solution as freely suspended spherical bubbles. A Brownian motion is followed by NBs in solutions. Because of this Brownian motion, it is difficult to verify or model the behaviour of these NBs. Nevertheless, many efforts have been made to investigate their fundamental properties listed below.

1.3.1 Miniature size and high mass transfer efficiency

Bubbles are classified as macrobubbles, microbubbles and nanobubbles under water according to their sizes Fig. 1.2. Macrobubbles, which are commonly used in fermentors, gas-liquid reactors and ore floatation equipment, have diameters in the range of 2-5 mm. These bubbles have a high tendency of quickly rising and bursting on the surface of the liquid. Mirobubbles, have diameters ranging from 1-100 μ m. These bubbles have a tendency to be stable in water for a few seconds and the shrink, dissolve and disappear in the bulk liquid itself. NBs on the other hand have diameters less than 1 μ m and these small spherical sizes of NBs provide a larger surface area-to-volume ratio as well as Brownian motion with negligible buoyant force. Nanobubbles are generated in huge amount (10⁶ to 10^9 NB/mL) and spread over a large area.

For gas-liquid operations, the volumetric mass transfer coefficient $(k_L a)$ is an essential measure of the aeration efficiency such as air floatation and aeration processes for treating water. The efficiency of gas-liquid mass transfer is largely dependent on the size of the bubbles. When the bubbles get smaller, there's an increased rate of gas transmission [3]. Several studies have claimed that nanobubbles can significantly increase the gas transfer efficiency in water. This further helps in enhancing the overall efficiency of the wastewater treatment processes [5]. In one instance, Han et al. [14] investigated the mass transfer coefficient $(k_{L}a)$ by varying the flow rates of the liquid and gas phases in a study where microbubbles were created using the membrane approach. When the velocity increases, the value of $(k_L a)$ exhibits a linear increase with the superficial gas velocity, reaches a maximum point, and then stabilises at a constant value. Bai et al. [15] investigated the influence of salt on the mass transfer characteristics of micro-nanobubbles produced by the compression-dissolution process. Because NaCl prevents bubble coalescence, its presence in a liquid solution causes a large increase in the interfacial area while concurrently decreasing the liquid side mass transfer coefficient (k_L) . Therefore, k_L increased when salt addition was done. Xue et al. [16] used oxygen nanobubbles to investigate the effectiveness of mass transfer $(k_L a)$ and to compare the difference between nanobubble and macrobubble aeration. The results of the aeration experiment comparing nanobubbles and macrobubbles showed that the former had k_L a values 5-8 times greater than the latter. O₂ and O₃ NBs had 1.5 and 4.7 times greater mass transfer efficiencies than coarse bubbles, according to Xiao and Xu [17] and Fan et al. [5], whereas MNBs have a 52.6% lower oxygen drop rate than coarse bubble aeration, according to Chen et al. [18].

1.3.2 High negative zeta potential and hydrophobocity

The surface characteristics of NBs determine how they behave in liquid solutions and are essential to their use. Ions disperse over the electrically charged surfaces of NBs, creating an electrical double layer that encircles the bubble. A key variable in establishing bubble stability and bubble-particle interactions, zeta potential assesses the electrical potential (i.e., the charge repulsion and attraction) at the boundary of the diffuse layer. Although it might vary depending on the situation, NBs' zeta potential usually ranges from -50 mV to -20 mV [19]. In accordance with the literature, the small radius of NBs and the strong polarity of hydroxyl ions cause dissociated hydroxyl ions to adhere to the bubble surface, whereas hydrogen ions are more readily hydrated and prefer to remain in the bulk liquid. This is the reason for the negative charge of NBs. A greater stability is indicated by a greater absolute zeta potential because the surfaces of the NBs provide a repulsive attraction that keeps them from combining [20].

Another crucial characteristic of NBs is their surface hydrophobicity, which enables them to interact with other particles through hydrophobic attraction. While connected NBs might encourage particle-particle or particle-bubble interactions by capillary bridging processes that provide an attractive attraction between two surfaces, BNBs can adsorb on hydrophobic particles and boost their mobility in the liquid [21].

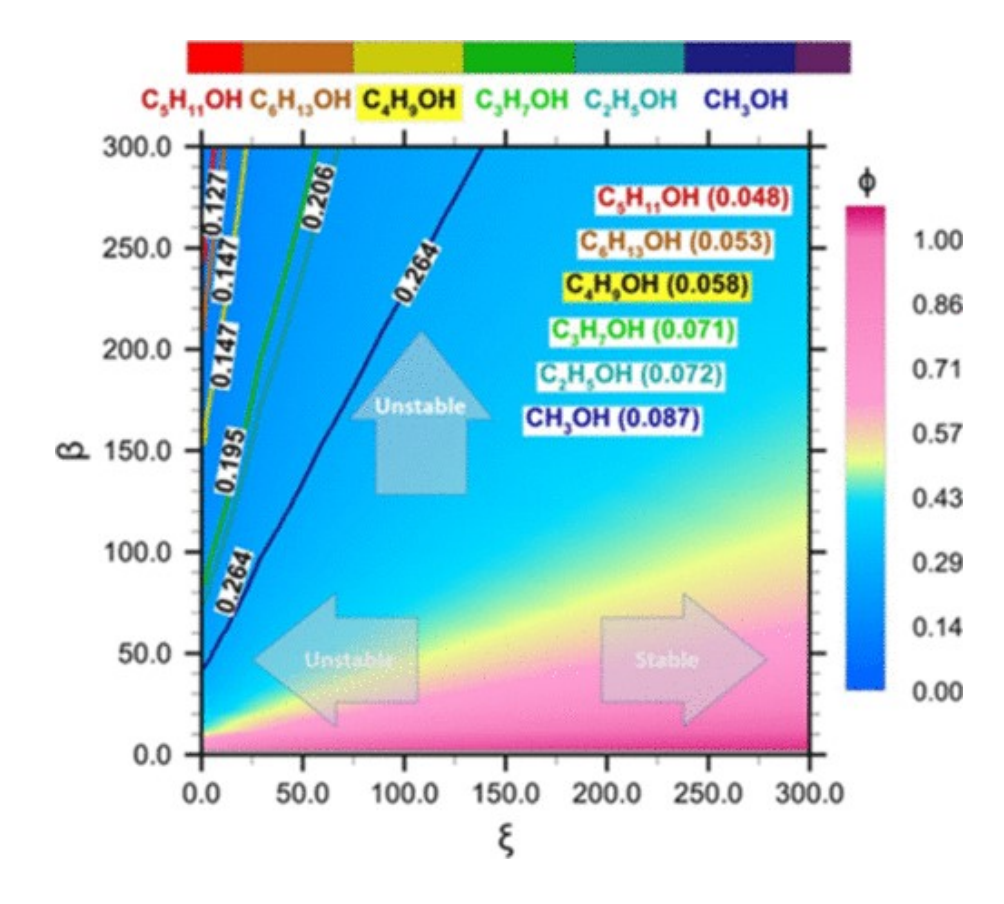


Figure 1.3: Nanobubble stability map from the force balance around a single nanobubble [3]

1.3.3 Long term stability

Amongst the various properties that NBs possesses, long term stability is the most astonishing and a peculiar property. When conventional bubbles are first generated, they usually stay that size for a while before starting to expand and finally disintegrate into the solution. On the other hand, the findings of the experiments have verified that NBs may live in water for days or months at a time. With varying starting concentrations of NBs, Nirmalkar et al. [13] tracked the temporal evolution of NBs' mean diameters and found no significant changes in their diameters for more than 170 days. Similar findings were made by Wang et al. [22], who discovered that while CO₂ NBs were less stable than 48 hours, N₂ and O₂ NBs were stable for 48 hours. This was mainly because CO₂ has a larger density and is more gas soluble.

Agarwal et al. [23] proposed a single nanobubble stability model for the nanobubbles generated in pure water and salts. Sharma et al. [3] implemented the force balance surrounding a single nanobubble to determine the NB equilibrium size in pure alcohols. The stability of a group of nanobubbles might potentially be predicted using the force balance model surrounding a single nanobubble. The electrostatic pressure operates naturally on the nanobubble surface, as previously mentioned, and it tends to enlarge the interface. The pressure that the electric double layer applies to the interface, on the other hand, is known as the ionic forces. These ionic forces that result from solving the spherical

Poisson-Boltzmann equation that were examined in a research by Tan et al. [24]. The normal force of NB is opposed by the surface tension force. The Poisson equation provides the following potential distribution around nanobubbles:

$$\frac{\partial^2 \psi}{\partial x_i^2} = -\frac{\rho_e}{\epsilon_r \epsilon_0} \tag{1.1}$$

where ρ_e , ϵ_0 and ϵ_r are the local electric charge density (C/m^3) , the permittivity of free space and the relative dielectric constant. Assuming radial distribution, the Poisson equation was further reduced to the following form:

$$\frac{1}{r^2}\frac{d}{dr}\left(r^2\frac{d\psi}{dr}\right) = -\frac{\rho_e}{\epsilon_r\epsilon_0} \tag{1.2}$$

The boundary condition at the surface of the NB was:

$$\frac{d\psi}{dn} = -\frac{\sigma_i}{\epsilon_r \epsilon_0} \tag{1.3}$$

where σ is the surface charge density and n is the normal to the surface. Further, the conservative force in terms of potential was as follows:

$$E = \frac{\partial^2 \psi}{\partial n_i} \tag{1.4}$$

where $F_{ionic} = qE$. Ionic pressure was expressed as:

$$p = \frac{F}{4\pi R_c^2} = \frac{q\sigma_i}{4\pi R_c^2 \epsilon_r \epsilon_0} \tag{1.5}$$

or

$$P_{ionic} = \frac{\sigma_i^2}{\epsilon_r \epsilon_0} \tag{1.6}$$

On the other hand, the surface of the nanobubble experiences a perpendicular force from the electrostatic pressure. The electrostatic pressure can be calculated by taking into account two hemispheres and the force that expands them. The following equation to represent electrostatic pressure was as follows:

$$P_{electrostatic} = \frac{\sigma_e^2}{2\epsilon_r \epsilon_0} \tag{1.7}$$

The surface charge density can be roughly represented as $\sigma_e \approx \sigma_i = \sigma$ when taking into account the local electro-neutrality. Thus, the forces operating on nanobubbles in equilibrium were represented as follows.

$$P_g + P_{electrostatic} = P_L + \frac{2\gamma}{R_c} + P_{ionic}$$
 (1.8)

$$P_g + \frac{\sigma_e^2}{2\epsilon_r \epsilon_0} = P_L + \frac{2\gamma}{R_c} + \frac{\sigma_i^2}{\epsilon_r \epsilon_0}$$
 (1.9)

$$or$$
 (1.10)

$$P_g = P_L + \frac{2\gamma}{R_c} + \frac{\sigma^2}{2\epsilon_r \epsilon_0} \tag{1.11}$$

The equation of state for real gas was represented as:

$$P_g = P_{B0} \left(\frac{R_0}{R_C}\right)^3 \tag{1.12}$$

where P_{B0} is the gas pressure at R_0 . When considering charge conservation, the surface charge density is expressed as follows:

$$\sigma = \frac{\epsilon_0 R_0^2}{R_c^2} \tag{1.13}$$

Upon substitution, the following equation was formed:

$$P_{B0}\left(\frac{R_0}{R_C}^3\right) = P_L + \frac{2\gamma R_0}{R_c R_0} + \frac{\sigma_0^2}{2\epsilon_r \epsilon_0} \left(\frac{R_0}{R_C}^4\right)$$

$$\tag{1.14}$$

$$or$$
 (1.15)

$$\phi^3 - \zeta \phi^2 - \beta \phi - \alpha = 0 \tag{1.16}$$

where

$$\phi = \frac{R_O}{R_C} \tag{1.17}$$

$$\alpha = \frac{P_L}{P_{B0}} \tag{1.18}$$

$$\beta = \frac{2\gamma}{R_0 P_{B0}} \tag{1.19}$$

$$\beta = \frac{2\gamma}{R_0 P_{B0}}$$

$$\zeta = \frac{\sigma_0^2}{2\epsilon_r \epsilon_0 P_{B0}}$$

$$(1.19)$$

Thus, the size of the nanobubbles could be determined by analysing the force balance which lead to a quadratic equation. This equation could be used to solve for the values of ζ , α and β as shown in Fig. 1.3. The existence of stable nanobubbles was predicted with the force balance model. The mean diameter and surface charge experimental findings were included in the mechanical stability map. The results of the experiment aligned with the stable regime of alcohol-based nanobubbles. The surface charge on the nanobubbles was represented by the parameter ζ . For given values of α and β , there was a positive association between an increase in ζ and the critical size of a single nanobubble. The surface tension that we saw in the experiments is represented by β . In conclusion, while nanobubbles may not be stable for all ζ and β values, but they were stable when their surface charge and surface tension were equal.

The development of characterisation technologies has led to a growing amount of evidence supporting the stability of NBs; nonetheless, further study is needed to construct theoretical models that characterise and explain the stability of NBs, especially BNBs, in liquid solutions. The most widely accepted explanation for the exceptional lifetime of BNBs is the electrostatic repulsion concept, which has been the subject of several ideas and models [25]. Molecular dynamics (MD) simulations have been utilised recently in BNB research to elucidate the fundamental principles driving their stability. The stabilisation mechanism of BNBs is intricate, as demonstrated by Gao et al. [26] who used molecular

docking to highlight the role of NBs' supersaturation, surface charge, interfacial molecular structure, and high inner density.

1.3.4 High oxidative potential: radical producer and scavenger

One of the most appealing aspects of NBs is thought to be their ability to produce free radicals, however the degree to which this is the case is still up for debate because it may be challenging to identify radical species. Free radicals have been found in NB solutions, according to several investigations, with hydroxyl radicals (*OH) being the most common kind. Notably, because hydrogen has a potent antioxidant effect, H₂ NBs functioned as radical scavengers whereas other forms of NBs were shown to create reactive oxygen species (ROS), as shown in Table 1.1. According to Liu et al. [32], H₂ water with NBs had higher

Table 1.1: Detection methods	s of reactive	oxygen species i	n NB research
------------------------------	---------------	------------------	---------------

NB type	Detection method and conditions	Detection results	Refs.
O_2, H_2 and O_3 NBs	Electron spin resonance (ESR) with DMPO as radical trapping agent	Superoxide radicals detected	[27]
Air NBs and O_2 NBs	ESR with DMPO as radical trapping agent	OH and methyl radical detected	[28]
O_3 NBs	OH peaks observed only when HCl was added as stimuli		[29]
Air NBs and O_2 NBs	Terephthalic acid as probe compound using a fluorescence spectrophotometer	OH was observed on applying ultrasound as stimuli	[30]
CO_2 NBs and N_2 NBs		Limited amount of OH observed when stimuli was applied	
O_3 NBs	Formaldehyde capturing method using UV-vis	OH in range of 0-32 $\mu g L^{-1}$	[5]
O_2 NBs	APF fluorescent probe using a spectrophotometer	OH detected in submicomolar level	[31]

removal efficiencies than H_2 water without NBs for four different forms of ROS (${}^{\bullet}$ OH and $O_2{}^{\bullet-}$), suggesting that NBs can alleviate oxidative stress. Hydrogen NBs have the potential to form hydrogen radicals (H^{\bullet}) [33]. However, they were unable to detect H^{\bullet} using electron paramagnetic resonance (EPR), which might be because H^{\bullet} production is sluggish and H^{\bullet} concentrations are below the detection limit. Rather, by transforming H^{\bullet} into ${}^{\bullet}$ OH by adding H_2O_2 and successfully seeing ${}^{\bullet}$ OH, they provided an indirect proof of H^{\bullet} 's existence. The exact mechanism by which NBs produce free radicals—for example, whether they self-collapse in the absence of dynamic stimuli—remains a mystery despite continuous investigation.

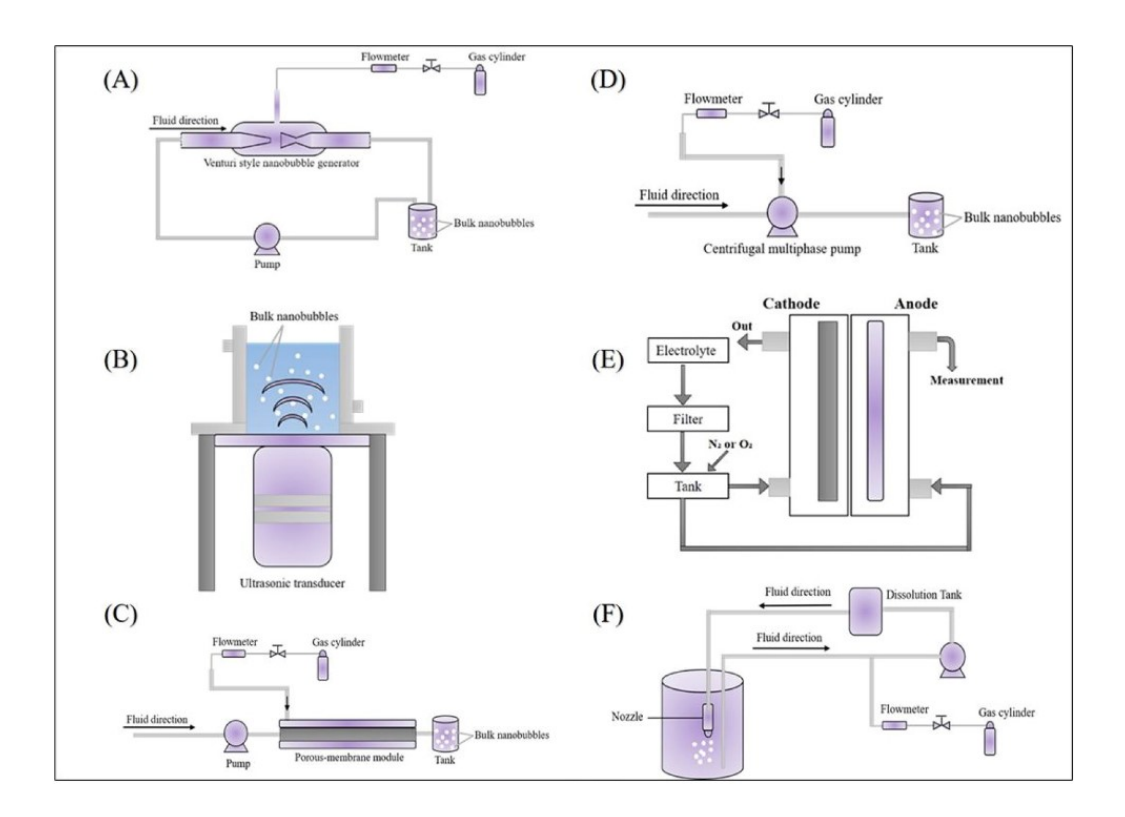


Figure 1.4: Schematic diagram showing various nanobubble generation techniques: A-hydrodynamic cavitation using venturi system, B-acoustic cavitation, C-Membrane system, D-Centrifugal multiphase pump, E-electrolytic cell, F-micro- and nano-sized nozzle [4]

1.4 Generation techniques of nanobubbles

Bulk NBs can be produced using a variety of generation techniques, such as water-solvent mixing, acoustic cavitation, hydrodynamic cavitation (HC), nano-membrane filtration, compression and decompression of gas, electrolysis, fluid oscillation, periodic pressure changes, chemical reactions, vibrations, electric fields, and so forth. The schematic diagram for a few of the commonly utilised NB generating methods is displayed in Fig. 1.4. Every approach offers benefits, and the choice depends on the particular use case. The most popular NB generating techniques are membranes and HC/acoustic cavitation, which may be employed in specially created settings for study and with a wide variety of gases. However, other techniques, like as electrolysis, are limited to using certain gases, thus the process of electrolysing water can only produce H₂ and O₂ NBs.

1.4.1 Cavitation

One of the most popular methods for creating bulk NBs is cavitation. The cavitation phenomenon is caused by bubbles that burst violently due to pressure differences. The associated cavitation is referred to as hydrodynamic cavitation (HC) when the liquid's hydrodynamic motion is the reason behind the drop in liquid pressure caused by liquid flow through a constriction such as venturi systems. Rather, the cavitation that results

is referred to as acoustic cavitation when the decrease in liquid pressure is caused by strong ultrasonic waves. Khaire and Gogate [34] have evaluated the uses of HC in food processing in a very recent study. There are four ways that cavitation can produce nanobubbles (NBs): (1) HC through a fluid flow; (2) acoustic cavitation from ultrasonic waves travelling through the bulk liquid; (3) optical cavitation from a high-intensity laser beam; and (4) particle-induced cavitation (cavitation caused by particles, such as protons, passing through the liquid). Many researchers have used techniques that use a centrifugal multi-phase pump, venturi-style cavitation, orifice plate, and throttling valve to produce bulk NBs using HC. In order to define homogeneous nucleation, Li et al. [35] investigated the production of MNBs by HC of deionised water. They discovered that while increasing fluid velocity had no effect on bubble sizes, it did change the concentration of the bubbles produced, and that the HC was capable of producing MNBs with a diameter of less than 50 μm. By utilising a needle valve and a centrifugal multi-phase pump with deionised water at room temperature, Etchepare et al. [36] showed a novel technique for producing nanobubbles by hydrodynamic cavitation. The maximum concentration of 4×10^9 bubbles per mL at 5 bar was achieved. Its size was $60-70~\mu m$ and its surface tension was 49~mN/m. Also, they said that the produced bubbles exhibited remarkable stability as, for as long as two months, the size and concentration did not significantly vary.

Acoustic cavitation bubbles are the bubbles that arise from acoustic cavitation. More than 200 nm-sized NBs are produced by acoustic cavitation when the amplitude of the acoustic pressure is quite high. Ultrasound radiation applied to water causes bubble nuclei to expand and compress producing cavitation bubbles, which eventually collapse. Nirmalkar et al. [13] investigated how bulk NB suspension was affected by sonication time at 20 kHz and 750 W of power. They observed that as the sonication period was extended, the bubble concentration went from 1.76×10^6 to 2.69×10^6 NBs/mL and thereafter grew to around 8×10^6 NBs/mL. Mo et al. [37] investigated the effects of ultrasonic exposure at 40 kHz and 300 W of power. They found that the concentration of NB steadily rose at initially.

1.4.2 Membranes

It has been established that NBs are produced by membranes having nanopores [38]. Usually, a membrane is used to force a gas phase into a water phase. Next, at the interface between the water phase and the membrane surface, size-controlled bubbles are produced. This technique of NB generation involves two steps: the bubbles' growth and their detachment. While the drag force created by the water phase pushes NBs away and separates them from the pore opening, the surface tension between the air and water keeps them close to the entrance [39]. It is thought that reducing the pore diameter is essential to getting NBs. Sharma et al. [3] studied the generation of oxygen nanobubbles in tubular multi channel ceramic membranes with pore size of 1, 5 and 10 nm. The nanobubbles with 100-150 nm of size were generated. Dhungana and Bhandari [40] described how gaseous NBs are produced using a ceramic membrane and how liquid food processing uses them. They observed foaming in their dairy protein dispersion systems when the air and CO₂

MNBs were created by HC (venturi-style), in contrast to the ceramic membrane-based technique. They also note that the continuous membrane NB production method is a straightforward approach that can be included into a continuous system, and that the working mechanism of cavitation-based approaches is complex, resulting in a lack of control over bubble size and consistency. Ahmed et al. [41] investigation looked at the effects of two distinct pore sizes—100 and 1000 nm—on the zeta potential and NB size. About 150 and 300 nm, respectively, was the diameter of the N₂ and O₂ NBs. At 60 PSI, the zeta potentials of O₂ and N₂ NBs were -38 and -45 mV, respectively.

1.4.3 Ethanol-water mixing

A straightforward method for producing NBs in large quantities is the mixing of ethanol and water, which has been extensively studied [42] and on surfaces [43]. Purified water is used to replace (pre-distilled) ethanol in the production of NBs. The dissolved gases in the combination become supersaturated when equilibrated solvents and ambient gases are combined; this might lead to the nucleation of bulk NBs. Zhang et al. [44] noted warm ethanol and water (45 °C) were shown to be more efficient in the production of NBs. They studied the morphology of NBs using TM-AFM and reported the NBs had an average height of 26 nm and a lateral dimension of 591 nm. Ethanol-water exchange was utilised by Alheshibri and Craig [42] to create 200 nm-diameter NBs; interestingly, a higher ethanol level produced fewer particles.

No. Reactions Rate constant In alkaline medium $O_3 + OH^- \rightarrow O_2 + HO_2^$ $k_1 = 40M^{-1}s^{-1}$ 1 $k_2 = 2.2 \times M^{-1} s^{-1}$ 2 $O_3 + HO_2^- \to O_3^{--} + HO_2$ $HO_2 + OH^- \rightarrow O_2^- + H_2O$ 3 pK = 4.8 $k_4 = 1.6 \times 10^9 M^{-1} s^{-1}$ $O_2^{-} + O_3 \rightarrow O_3^{-} + O_2$ 4 $O_3^{-} + H_2O \to HO^{-} + O_2 + OH^{-}$ $k_5 = 20 - 30s^{-1}$ 5 $k_6 = 6 \times 10^9 M^{-1} s^{-1}$ 6 $O_3^{-} + HO^{-} \rightarrow O_2^{-} + HO_2^{-}$ $O_3^{--} + HO^{-} \rightarrow O_3 + OH^{-}$ $O_3 + HO^{-} \rightarrow HO_3 \perp O$ $k_7 = 2.5 \times 10^9 M^{-1} s^{-1}$ 7 $k_8 = 3 \times 10^9 M^{-1} s^{-1}$ $O_3 + HO^{\cdot} \rightarrow HO_2 + O_2$ 8 In acidic medium 9 $O_3 \rightarrow O + O_2$ 10 $O + H_2O \rightarrow 2HO$ $k_{11} = 1.1 \times 10^8 M^{-1} s^{-1} \\ k_{12} \le 10^4 M^{-1} s^{-1}$ 11 $HO^{\cdot} + O_3 \to HO_2^{\cdot} + O_2$ $HO_2^{-} + O_3 \to HO^{-} + 2O_2^{-}$ 12

Table 1.2: Ozone reactions [11] [12]

1.4.4 Electrolysis

In contrast to cavitation-based generation methods, electrolytic generation produces gas nanobulks (NBs) by electrochemical reactions between various salts electrolysed on electrodes. In addition, H_2 and O_2 NBs are produced during the electrolysis of water in the presence of an acid or base. There have been several reports of bubbles forming at

the electrode surface during electrolysis [45]. Achieving a high gas concentration using electrolysis requires both the behaviour of the desired gas NBs and the concentration of gas at the electrode surface. Zhu et al. [45] reported NBs that were stable for around 24 hours, measuring about 90 nm in diameter and 5×10^8 NBs per millilitre. Similarly, Kukizaki [38] produced NBs by electrolysing water (O₂); on days two and three, the control group's bubble diameter sizes were 30, 180, and 250 nm, respectively. Yadav et al. [27] generated nanobubbles with a bubble density of 20×10^7 bubbles per mL. Their results indicated that bulk nanobubbles were electrochemically reactive even after the cessation of nanobubble production.

1.5 Ozone: a potential oxidant

Ozone is extensively employed for oxidation of pharmaceuticals in drinking water [46]. Ozone has enormous potential for treating wastewater due to its intense oxidation capabilities. One useful tool for accelerating the oxidation of pollutants by ozone is hydrogen peroxide [47]. Since it is an unstable trioxygen molecule, it needs to be produced onsite. It has an exceptional inactivation capability against aquatic pathogens such as bacteria, viruses, protozoa, and endospores because, in comparison to other widely used disinfectants (free chlorine, chlorine dioxide, and UV radiation), it is a highly powerful oxidant. When designing disinfection systems, factors like ozone concentration and contact time, which are highly dependent on operation temperature, become crucial. Furthermore, depending on the kind of organism, the pace at which ozone inactivates microorganisms can vary by up to four orders of magnitude [48].

Ozone has the ability to interact both directly and indirectly with microorganisms and pollutants. Direct reactions are very specialised and require ozone molecules. Conversely, the indirect reaction entails the production of free hydroxyl radicals (*OH) by the breakdown of ozone in water. These radicals are less selective ($E^0 = 2.07V$) and more reactive ($E^0 = 2.80 \text{ V}$) than ozone. Since hydroxyl ions have the ability to start the processes that lead to ozone breakdown, the pH of the water plays a critical role in this process. Above pH 10, the indirect route takes precedence over the direct ozonation when pH is less than 4. Both direct and indirect ozone responses can be significant in waters with a pH of 7, therefore treatment design should take them into consideration [49]. Many studies were examining the mechanism and kinetics of the fundamental events related to the degradation of ozone [50]. The following reactions in an alkaline media, as suggested by Tomiyasu et al. [11], serve as the basis for the processes interpretation. Table 1.2 provides a list of the reactions that occur in an acidic media [12]. Nevertheless, the rapid disintegration rate of dissolved ozone in water is much quicker than that in the gas phase that limits the effectiveness of ozone oxidation. Thus, there is an urgent requirement for techniques to extend the reactivity of aqueous-phase ozone, and several stabilisers have been employed to boost groundwater ozone stability [51]. Advanced oxidation processes (AOP) for eliminating organic pollutants through degradation are powerful and effective,

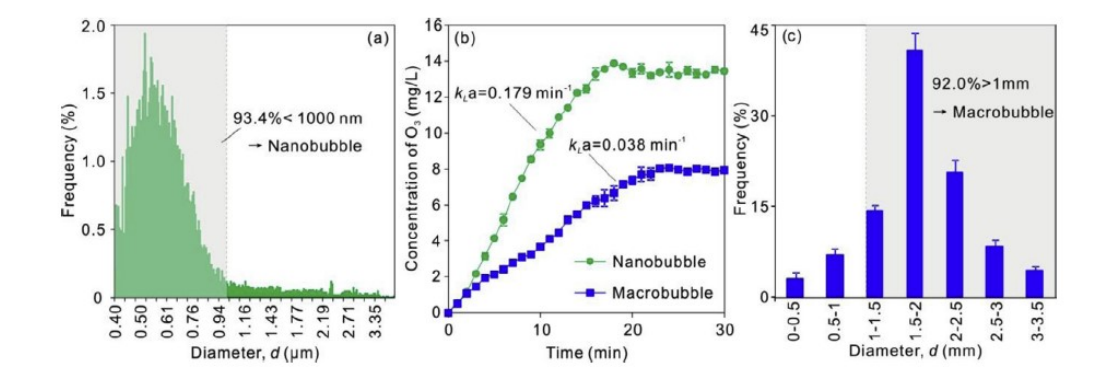


Figure 1.5: (a) Size distribution of nanobubbles; (b) The time course of O₃ concentration during nanobubble and macrobubble aeration scenarios; (c) Size distribution of macrobubbles [5]

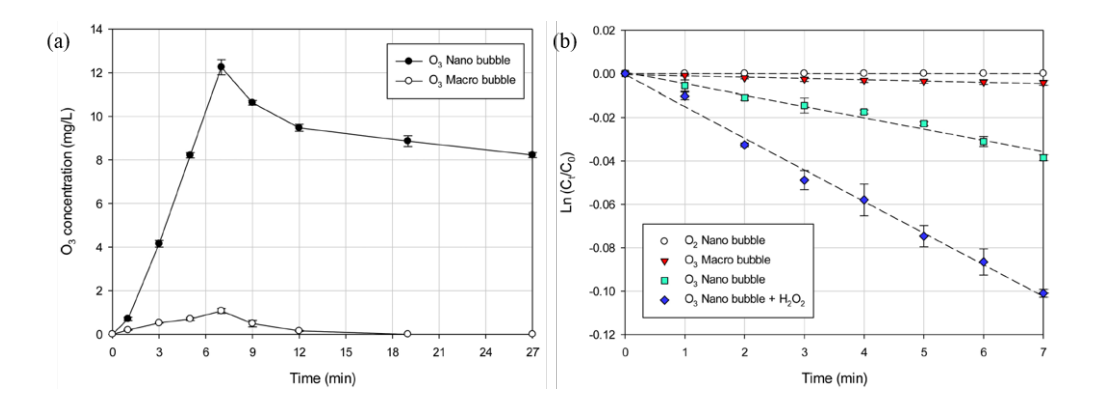


Figure 1.6: (a) Ozone concentration time profile when using nano-ozone and macro ozone bubble (b) Effect of (a) pH and (b) temperature on degradation kinetics of TMAH during nano-ozone/ H_2O_2 process (pH = 7, 7 10; t = 5, 25, 45 °C; H_2O_2 = 100 mg/L; n = 2) [6]

but they are usually restricted by their cost-effectiveness, necessitating further optimisation and improvement [6]. Ozonation combined with nanobubbles has proven to be a green technology which eliminates the above-mentioned problems by increasing the dissolution rates and half-life of O₃, ROS and hydroxyl radical formation and would permit an upgrade to more affordable, chemical-free methods. Multiple studies have demonstrated that NBs may successfully increase O₃ dissolution and lifetime, hence extending O₃'s reactivity during ozonation [1]. Fan et al. [5], for instance, discovered that NB aeration increases the dissolved O_3 concentration and mass transfer coefficient by 1.7 and 4.7 times respectively, compared to microbubble aeration shown in Fig. 1.5. According to Kim et al. [6], O₃ NBs had a half-life that was 23 times longer than O₃ microbubbles as depicted in Fig. 1.6. Additionally, Fan et al. [9] showed that NBs may increase the concentration of OH. two to three times more than MB's, which further enhanced the ozonation's removal effectiveness. According to a recent cost-benefit study, installing an ONBs generator would benefit current water treatment facilities since it would be four times less expensive overall and might result in annual savings of \$375,000 [52]. A hybrid system that uses forward osmosis (FO) and nanobubbles (NBs), two advanced technologies,

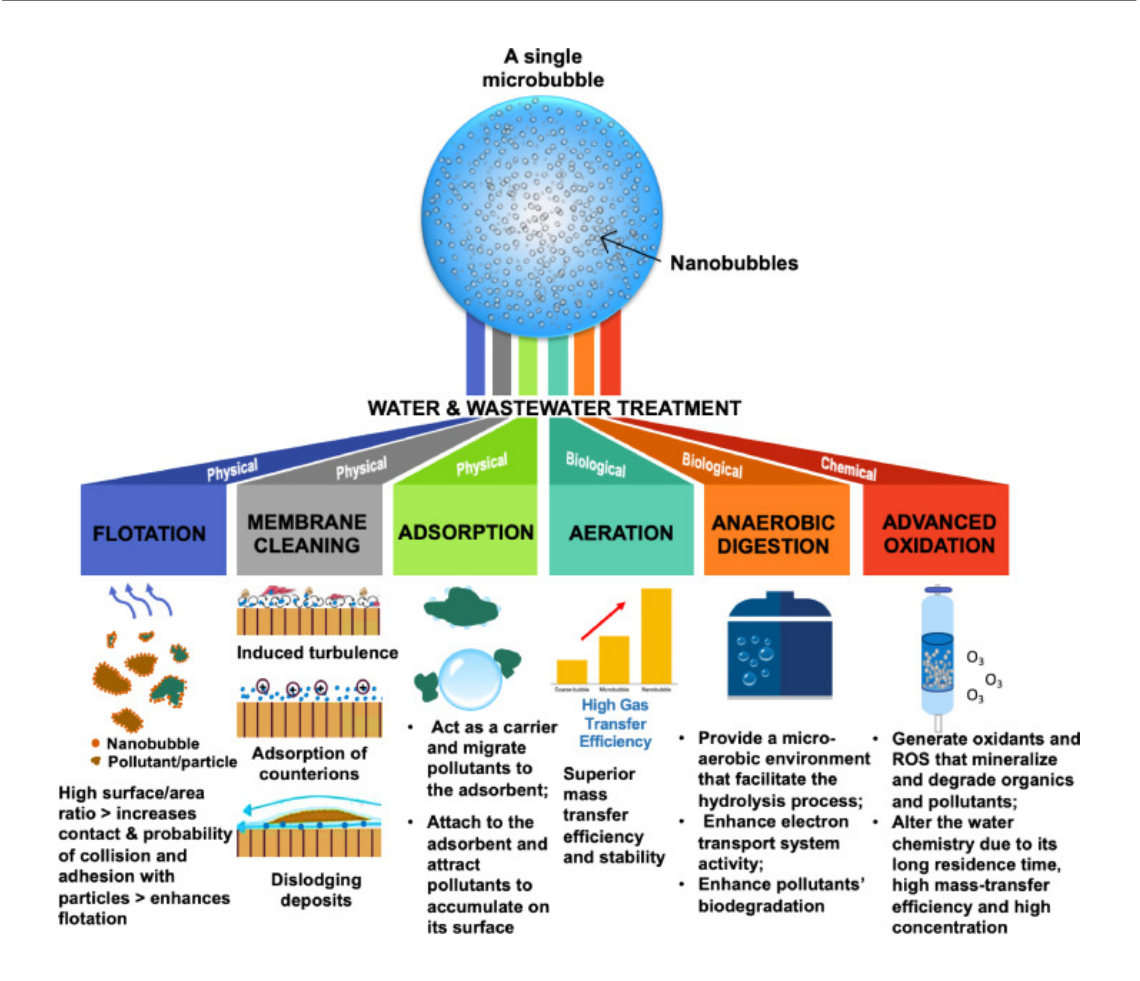


Figure 1.7: An overview of how NB technology can enhance water and wastewater treatment processes. [2]

to clean and reuse aquaculture wastewater in a way that is sustainable, energy-efficient, and effective compared to traditional methods was investigated by Farid et al. [53]. The dissolved solids and pharmaceutical chemical residues were removed from aquaculture effluents with a high efficiency (about 98%) by the FO membrane, while the NBs served as a physical membrane-cleaning agent that improved the lifetime and performance of the FO membrane. 30% of oxytetracycline was reduced using ozone NBs attributed to the formation of hydroxyl radicals that react with OTC for its oxidative decomposition. Kim et al. [6] in this work employed a nano-ozone bubble to increase the ozone/ H_2O_2 process's efficiency for the breakdown of tetramethylammonium hydroxide (TMAH), which is present in semiconductor wastewater at high concentrations. Compared to the nano-ozone solo reaction $(0.9 \times 10^{-4} \text{ min}^{-1})$, the combined process exhibited a 162-fold quicker rate constant $(1.46 \times 10^{-2} \text{ min}^{-1})$. The nano-ozone bubbles/ H_2O_2 had a half-life that was 23 times greater than the nano-ozone bubbles.

1.6 Applications of nanobubbles

Equipped with a deeper understanding of the characteristics and potential of NBs as discovered by NB research over time, the focus of NB research has begun to shift towards

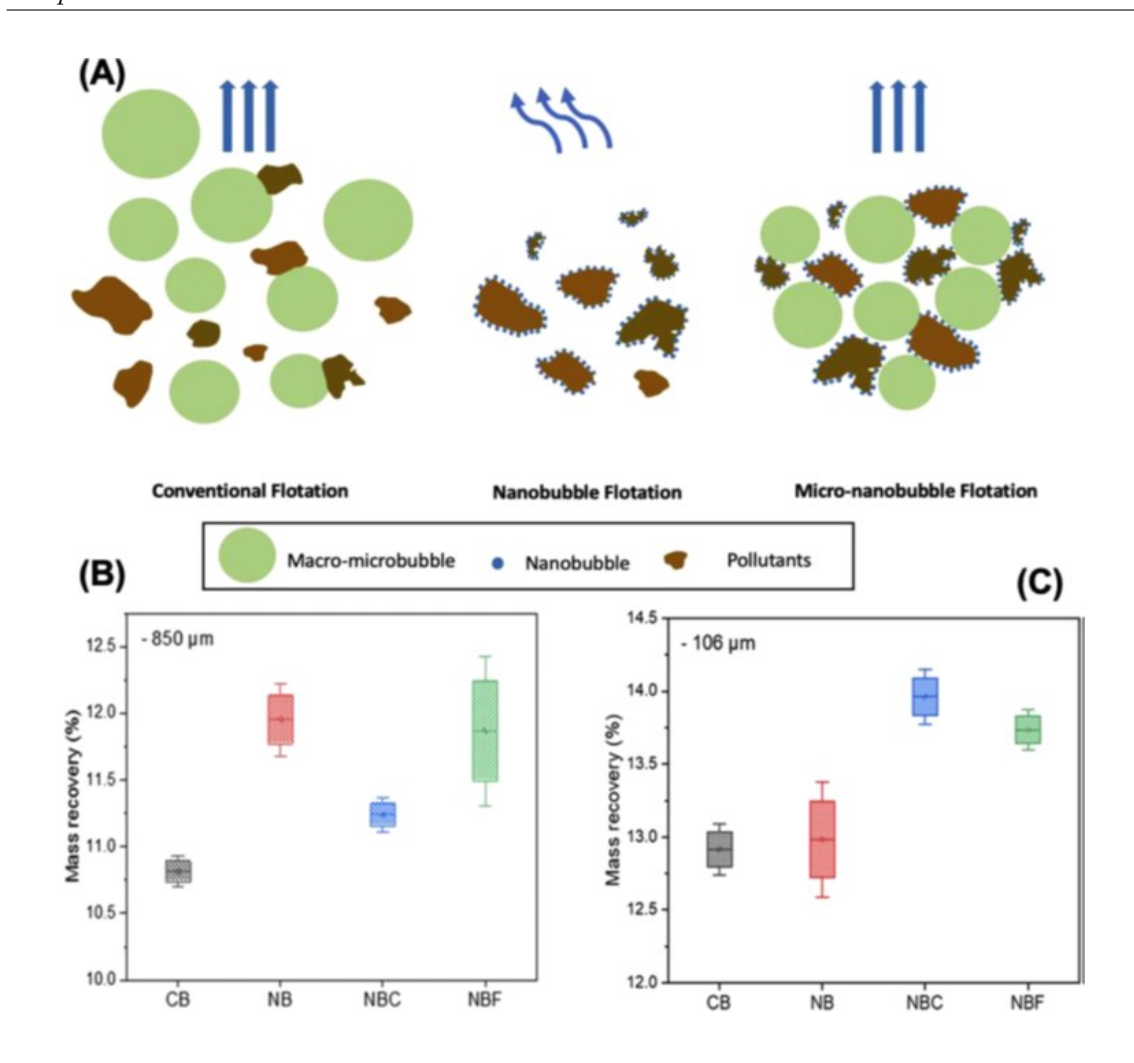


Figure 1.8: (A) Illustration of microbubble, nanobubble, and micro-nanobubble flotation. (B) Apatite flotation mass recovery for various tailings. CB—conventional test, NB—nanobubbles, NBC—nanobubbles with a collector, NBF—nanobubbles with a frother. [7]

the use of NBs in a variety of industry sectors, such as water treatment, agriculture, aquaculture, food processing, biomedical, and mineral processing. A smaller amount of study has been done on NBs' roles in membrane cleaning and adsorption. The majority of research on using NBs in water treatment processes has focused on flotation and aeration, followed by advanced oxidation processes and anaerobic digestion. These activities may be further divided into three major categories: biological processes (aeration in bioreactor and ecosystem remediation, anaerobic digestion), physical processes (flotation, membrane cleaning, and adsorption), and chemical oxidation processes. Based on previous research, Fig. 1.7 give a summary of the primary contributions made by NBs to each process. The role of NBs can be summed up as follows: (1) their small size, high density, and long-term stability allow them to be retained for longer periods of time, increasing mass transfer efficiency and water mobility; (2) their hydrophobicity allows them to act as particle carriers through hydrophobic attraction; and (3) although their contribution to ROS generation has been minimal thus far, bursting of NBs generates ROS.

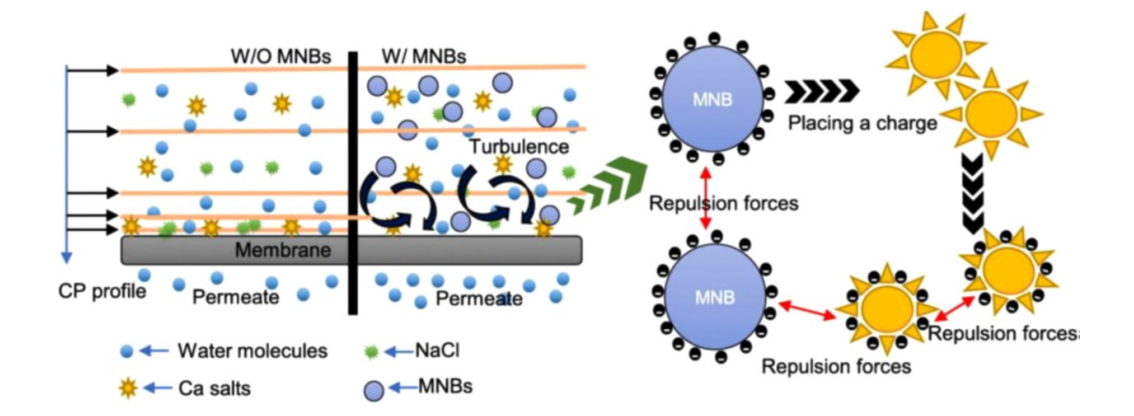


Figure 1.9: Main mechanisms behind membrane cleaning in reverse osmosis membrane processes [8]

1.6.1 Role of nanobubbles in floatation processes

For particles between 20 and 150 μ m in size, conventional flotation provides significant separation efficiency; nevertheless, recovering coarse and small particles outside of this range continues to be difficult: Particle detachment makes it harder to recover coarse particles, whereas low particle-bubble collision makes it harder to extract tiny particles [54]. In general, the likelihood of a collision and adhesion between particles/flocs increases with their size relative to bubbles. Applying NBs, which have greater surface area-to-volume ratios and are formed in bigger numbers, might thereby enhance the probability of impact and adhesion with tiny particles. Additionally, by adhering to larger bubbles, NBs can decrease the likelihood of small and coarse particles separating from larger bubbles and enhance their contact angles [55]. A schematic of the comparison of NBs to MBs has been shown in Fig. 1.8.

1.6.2 Role of nanobubbles in membrane cleaning/defouling

Modern membrane separation techniques are quite effective in removing contaminants from wastewater, however fouling during membrane operations significantly reduces the effectiveness of these procedures [56]. Numerous strategies have been put forth to address the fouling issues. Among them, gas bubbling with coarse bubbles has been a commonly employed tactic for membrane fouling mitigation; nevertheless, because huge bubbles have a limited lifespan, constant or frequent intermittent bubble generation—which consumes energy—is necessary for effective fouling management. On the other hand, because NBs are long-lasting and exhibit Brownian motion in large quantities, they can provide a steady turbidity that can aid in preventing the accumulation and deposition of particles on the membrane. Additionally, the negatively charged surface and hydrophobicity of NBs can remove positively charged ions and stop salts from binding. It's also thought that the ROS produced by NBs contributes to the direct degradation of organics as shown in Fig. 1.9 [9].

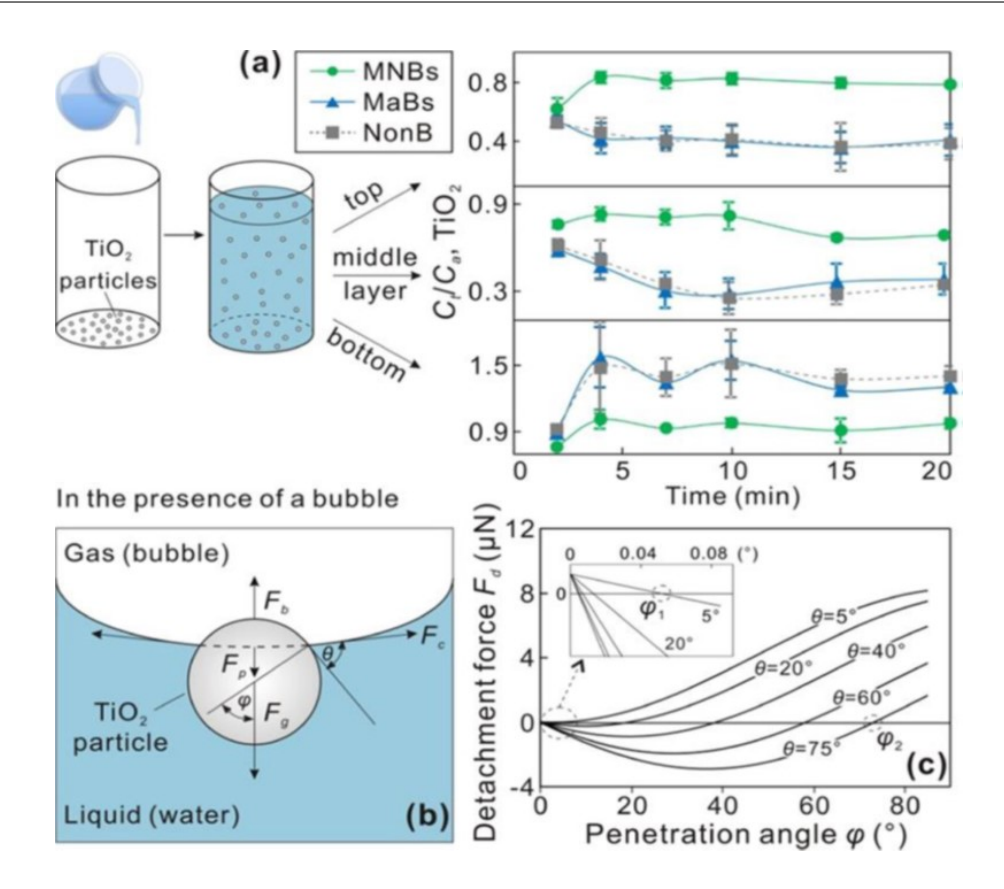


Figure 1.10: Photocatalyst particle stabilization by MNBs. (A) Concentration profiles of TiO₂ particles as a function of time in three different solutions: MNB suspension, MaB-aerated DI water, and DI water without aeration (labeled NonB). (B) Schematic illustrating the forces of a TiO₂ particle adhered to a bubble. (C) Detachment force (Fd) of a TiO₂ particle [9]

1.6.3 Role of nanobubbles in advanced oxidation processes

The use of advanced oxidation processes (AOP) to remove organic pollutants through degradation is strong and efficient, particularly when it comes to directly eradicating pathogens and stubborn contaminants in the aqueous phase. However, the cost-effectiveness of these procedures frequently places a limit on them, necessitating more improvement and optimisation. Ozonation is a frequently used AOP for water treatment (e.g., cleaning drinking water or breaking down contaminants in water bodies). It is an energy-intensive process that is made more difficult by O₃'s short half-life and poor solubility. Several investigations have demonstrated that NBs may successfully increase O₃ dissolution and lifetime, thereby extending O₃'s reactivity during ozonation [1]. In addition to ozonation, NBs have been used to support and improve other AOPs, such as photocatalysis, which is extensively studied but has a restricted use because to its low efficiency. It has been discovered that adding MNBs to the photocatalysis process improves the interfacial photoelectric effects of TiO₂/MNB suspensions, enriches oxygen in solution, increases photocatalyst light absorption, stabilises and prevents photocatalyst particle settling Fig. 1.10

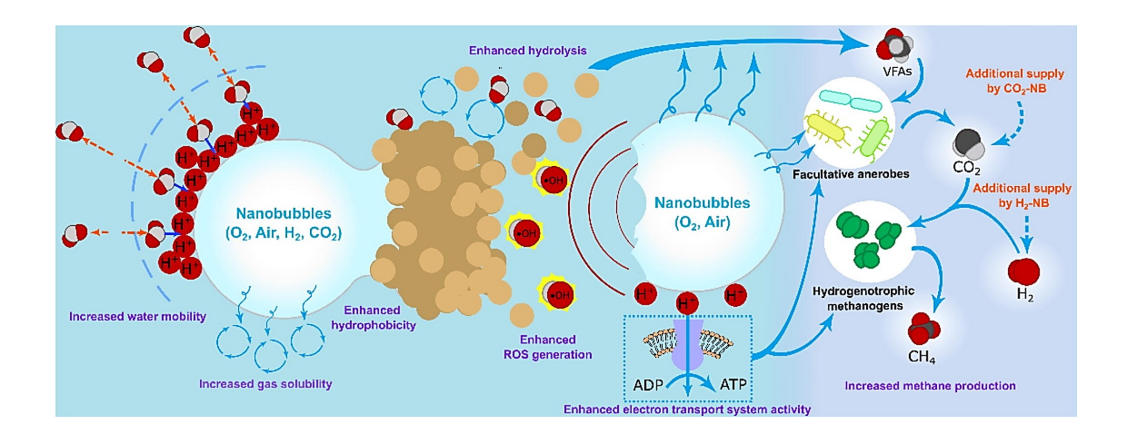


Figure 1.11: A schematic overview of the role of NBs in anaerobic digestion [10]

1.6.4 Role of nanobubbles in anaerobic digestion processes

Rich organic materials are present in wasted activated sludge (WAS), which is produced by wastewater treatment facilities and can turn into a secondary contaminant if improperly disposed of [57]. Anaerobic digestion, a commonly used green technique that uses WAS as substrates to create renewable energy, is said to have a greater production efficiency when NBs are included Fig. 1.11. The following are the roles of NBs in anaerobic digestion that have been suggested by previous research: (1) Because of their tiny size and strong zeta potential, NBs are able to transfer nutrients to the interior area of the biofilm and stimulate the activity of microorganisms and enzymes by increasing the movement of water molecules [58] (2) The NBs produced radicals can speed up the oxidative breakdown of substrates by microbes [59](3) Oxygen-containing NBs stimulate increased metabolite transport and ATP production [60] (4) Methanogens can use CO₂ and H₂ NBs as extra substrates [10].

1.7 Future prospects and potential applications

The spreading knowledge of the eye-catching characteristics of nanobubbles over the last decade have shown a great potential for this promising technology by achieving remarkable improvements in various water and wastewater treatment processes [61]. Nevertheless, the use of NB technology in the purification and treatment of water is still in its preliminary stages. Despite the increasing awareness of NBs' potential, the majority of the research on NBs that has been done so far has been restricted to lab-scale testing, which is occasionally unfeasible and calls for establishing theoretical assumptions in order to reach a result. To address the accompanying up-scaling challenges and to provide an accurate assessment of NBs' capabilities at the industrial scale, these systems must be tested at both the pilot and full-scale levels.

The potential of NBs to improve the removal or degradation efficiency of organic micro-pollutants (MPs), such as pharmaceutical active compounds (PhACs), personal care products (PCPs), and endocrine disrupting chemicals (EDCs), is another area that requires more investigation. The majority of published articles have tested NBs in distilled

or synthetic waters. As a result, it is necessary to conduct experimental studies using natural water or wastewater to learn how the various constituents, including organics, salts, suspended solids, nutrients, and other contaminants, alter the properties of NBs and manipulate their interactions. It will become harder to distinguish these components from NBs, which might have an impact on how precisely NBs can be measured for their many attributes. Therefore, to address these complications, improved characterization approaches must to be taken into consideration. Lastly, additional research must be conducted to evaluate the environmental and economic viability of NB applications in various water treatment sectors. Even though NBs have several benefits in terms of enhancing water treatment efficiency, if their cost is exorbitant, industrial implementations will not be able to immediately adopt them.

Chapter 2

Literature Review

With a brief review of literature, this chapter demonstrates the outcomes of various research works so as to identify some promising areas of research that will be addressed in the thesis. The literature has been presented for the following topics (i) Understanding the characteristics of ozone in the form of nanobubbles (ii) Degradation of antibiotic tetracycline (iii) Degradation of organic pollutants such as green rit dye and methylene blue dye (iv) oxidation of As(III) to As(V) using ozone nanobubbles. The scope and objectives of the present research work are also highlighted in this chapter.

2.1 Literature

2.1.1 Ozone nanobubble technology as a novel AOPs under high salinity conditions

Literature survey

Conventional water treatment systems frequently exhibit reduced efficiency when salinity levels rise, mostly due to the creation of complex compound between contaminants and salts. One of the primary obstacles associated with high salinity conditions is the generation of by-products that pose additional hurdles for treatment [62] [63]. The advanced oxidation techniques were often reported to be effective method of degradation of pollutants at high salinity conditions. In recent years, AOPs, for instance, hydrodynamic cavitation [64], ozonation [65], wet air oxidation [66], UV light [67], activated persulfate based processes [68], per-carbonate [69], ultrasonic [70] [71] and Fenton process [72] etc., received considerable attraction. The underlying principle of advanced oxidation is the formation of reactive oxygen species (ROS), especially hydroxyl radicals, that are able to effectively degrade organic pollutants. Ozonation is one of the AOPs which utilizes the ozone gas to degrade the contaminants in the wastewater. The major underlying challenge with ozonation is the poor gas-liquid mass transfer coefficient which leads low gas transfer efficiency [1]. The advantage of adapting ozonation for water treatment is the higher oxidation efficiency and no secondary product formation. Ozonation is an example of gas absorption with a chemical reaction where the reaction rate depends on both mass transfer and the reaction kinetics [73]. Owing to the slow dissolution of ozone gas, the mass transfer becomes a rate-limiting step [74]. The ozone transfer rate is a strong function of the concentration and size of the bubbles. By producing smaller size bubbles, the mass transfer rate can eventually be improved [75]. However, the selection of ozonation as the AOP was

reported to be expensive, indeed due to the poor gas-liquid mass transfer coefficient as well as high ozone production cost, etc. The partial oxidation may form aldehydes, organic acid, and ketones by this process [76] [77] [78]. The development of complex oxidation processes has also been given significant attention, for example, the combination of O₃ and H₂O₂, combined UV and O₃, catalytic ozonation with a metal ion, metal oxides or activated carbon. These processes indeed enhance the ozonation efficiency but also pose challenging problems such as scale-up for industrial-scale applications [79] [80] [81] [82]. In recent years, ozone microbubbles have been used for the degradation of organic compounds [82] [83] [84] [85] [86] [87]. For instance, Chu et al. [88] investigated the degradation behavior of the azo dye and C1 reactive black dye by ozone microbubbles of the size and concentration of 58 μ m and 2.9 x 10⁴ bubbles/mL. The mass transfer coefficient and reaction rate constant were reported to be 1.8 and 3.4 times higher than the conventional ozone contactor. The reactive oxygen species, especially the hydroxyl radicals contribute to the degradation of dyes. Microbubbles may enhance the degradation in two ways, namely (i) by enhancing the mass transfer rate due to higher surface area (ii) the ROS and hydroxyl radical formation is expected to enhance the degradation. The nanobubble provides a high surface area to foster the chemical reaction to form higher rate of ROS. The collapse of microbubbles formed during hydrodynamic cavitation was reported to produce hydroxyl radicals even if the gas inside the bubble is air [89]. Similarly, Khuntia et al. [90] demonstrated the quantification of hydroxyl radical generation by ozone microbubbles. The hydroxyl radical generation was reported to be less in the alkaline medium than the acidic medium [90]. Moreover, recently ozone microbubbles were used in ground water remediation [91]. In this work, we have investigated the novel advanced oxidation process where the ROS and free radicals were generated from ozone nanobubbles. Nanobubbles are long-lived colloidal bubbles that have received significant attention from the scientific community in the past decades. The nanobubbles possess unique and extraordinary properties, for instance, extra longevity [13], strong negative surface charge [92], generate reactive oxygen species [93] [31] [94] [95], the active sites for nucleation [96], ability to adsorb surfactant molecules [97], capillary bridging formation [21], increases the slip on the surface [98] etc. These properties enables the application of nanobubbles in water treatment [61], mineral processing [99], food processing [100], medical applications [101], agriculture [102] and aquaculture [103]. In this work, we have studied the ozone nanobubble behavior in the high salinity conditions. The ozone nanobubbles are further demonstrated to degrade the dyes under these adverse environmental conditions for advanced oxidation processes (AOPs) conditions.

Scope for Research

Nanobubbles are called colloidal bubbles having size 100-200 nm, expected to enhance the ozonation process further. In recent years, ozone nanobubbles are utilized to remove or degrade the residual pesticides in vegetables [104], degradation of trichloroethane in sands [105]. However, the properties and behavior of ozone nanobubbles have not

been extensively investigated despite the overwhelming applications. This work focuses on understanding the peculiar properties, ozone nanobubble dynamics and stability, estimation of mass transfer coefficient, and measurement of free radicals and ROS's during nanobubble generation. In this work, we have generated only nanobubbles rather than a mixture of micro and nanobubbles. The measured properties and mass transfer coefficient pertain to only nanobubbles. A sample of methylene blue dye was used to demonstrate the kinetics of dye degradation. The nanobubble stability model is used to explain the ozone nanobubble dynamics in the presence of salts.

2.1.2 Degradation of antibiotic tetracycline

Literature survey

Antibiotics, a class of medicines, are widely used in treatments and are recognized as a prominent category of persistent pollutants. Their presence in aqueous streams through the discharge of animal husbandry, pharmaceutical wastewater, and medical wastewater raises significant environmental concerns [106] [107] [108] [109]. Frequently used pharmaceutical medications include ibuprofen, metformin, tetracycline, and acetylsalicylic acid, among others [110]. Among the antibiotics, tetracycline is one of the broad-spectrum antibiotics, effective against infections caused by gram-positive and negative microorganisms, mycoplasma, and protozoan parasites. It is used extensively in veterinary medicine, human treatment and the agricultural industry as a feed ingredient [111] [112]. Tetracycline is often used as a growth promoter in aquaculture to amplify nutrient absorption, hence facilitating farmers in augmenting production and productivity [113]. The persistent use and inadequate handling practises contribute to the identification of tetracycline in various water matrices including surface water, ground water, sewage water, and drinking water, range from nanograms per litre (ng/L) to micrograms per litre (μ g/L) [114] [115] [116]. In the long term, tetracycline presents a substantial risk to both plant and animal life. Therefore, it is essential to create efficient remediation technology in order to guarantee the elimination of tetracycline from wastewater [117].

The COVID-19 outbreak has had a significant impact on global public health, resulting in nearly 6.5 million fatalities. The World Health Organisation has declared the COVID-19 a "public health emergency of international concern" [118] [119]. During the early stages of the pandemic, infected individuals displayed symptoms similar to bacterial pneumonia and were incorrectly treated with antibiotics that are ineffective against viral respiratory illnesses [120] [121]. High levels of antibiotics in hospital effluent have been linked to the high frequency of antibiotic treatments in medical facilities [122]. Amongst the various techniques, advanced oxidation processes such as Fenton/Fenton-like oxidation [123], photocatalysis [124] [125], electro-catalysis [126], ozone oxidation [78] [127], ultrasound [71] [128] are the best recommended technologies for the treatment of the organic pollutants present in wastewater [129]. The underlying principle of the advanced oxidation process is the generation of reactive oxygen species, including hydroxyl radicals, that help in the

degradation of the organics [130] [131]. The utilisation of AOPs, specifically ozone-based AOPs, has become prevalent in the oxidation and potential mineralization of diverse harmful and resistant organic pollutants in wastewater, intending to attain sustainable development goals (SDGs) [132]. These processes derive their efficacy from the consistent production of potent hydroxyl radicals (*OH) and ROS [133] [134]. Although there has been significant progress in the creation of very effective catalysts for catalytic ozonation processes, the stability and deactivation of these catalysts during prolonged operation have severely limited their commercial uses [135] [136]. O₃-based AOPs procedures for wastewater treatment are further hampered by the limited solubility and low mass transfer of ozone, which result in high operating costs[137] [138]. The addition of nanobubble technology to the ozonation process (O₃/NBs) holds a great potential to supplement the current conventional AOPs for efficient pollutant removal because it has a higher ROS generation rate and improved gas mass transfer efficiency than conventional ozonation technology (O₃ macrobubbles) [138] [139]. Nanobubbles are gas-filled cavities owing to some distinctive properties such as high stability [13], a high surface area to volume ratio [5], high negative zeta potential [92], low buoyancy [140], and the ability to generate radicals [29] which allow them to contribute to physical, chemical and biological water treatment processes in many ways [2]. Yang et al. [141] investigated the oxidative capacity of reactive oxygen species (ROS) produced by ozone bubbles of different sizes. The results showed the generation of ROS because of bubble shrinkage and collapse. Hydroxyl radicals were produced after the reaction between ozone and hydroxide ions. Tetracycline in its various chemical forms has been studied using the micro nanobubble technology for its removal from the wastewater. Wang et al. [94] studied the degradation of oxytetracycline using oxygen nanobubbles coupled with photodegradation. With the rise in pH (4.0-11.0), the photodegradation efficiency of OTC increased from 45 to 98 percent. Quenching tests showed that the photodegradation of OTC was mostly caused by the *OH radical as the active species [94]. Chen et al. [142] investigated the effect of activated hydrogen peroxide on the degradation of tetracycline hydrochloride using air micro and nanobubbles. Also, MNBs with ozone in wastewater treatment, improved ozone's mass transfer efficiency and boosted ozone solubility and also helped in lengthening the reaction activity. Numerous experimental research on micro-nano bubbles in combination with other processes have been conducted [91] [143].

Scope for Research

There are recent studies on the degradation of the tetracycline using oxygen [94] and air micro and nanobubbles [142], and ozone microbubbles [144]. Wang et al. [144] studied the degradation of TC using ozone microbubbles of size less than 50 µm with 500 mg/L of TC concentrations. It was evident from the rate constants that tetracycline degraded more rapidly in acidic solutions than in basic ones. Radical scavenging and mineralization experiments were also performed. However, little emphasis has been placed on investigating the associated reaction kinetics, degradation routes, and nanobubble generation. Studies

available on the degradation of the antibiotic tetracycline using ozone in the form of nanobubbles are scarce and only some preliminary attempts were published. Thus, the major objective of this work is to study the degradation of tetracycline using ozone as a potential oxidant in the form of nanobubbles. Furthermore, various parameters such as ozone flow rates (2.5-10 L/min), initial tetracycline concentration (100-400 mg/L), varying pH (4-11), addition of salts (NaCl, 0.1-100 mM) and scavenging experiments were performed. Radical quenching experiments, reaction kinetics, and liquid chromatography coupled to mass spectrometry (LC-MS) were performed owing to the explanation of the degradation mechanism of tetracycline. This study aimed to develop a catalyst-free and green technology method for the degradation of antibiotics.

2.1.3 Degradation of organic contaminants from wastewater with high pollutant loading

Literature survey

The advanced oxidation processes (AOPs) are the subject of extensive research due to their potential to degrade many harmful contaminants from wastewater [145] [146] [147]. The most widely practiced AOPs are (i) Fenton reactions (H_2O_2/Fe^{2+}) [148] [149] [150] [151] (ii) H_2O_2 and H_2O_2 -based processes [152] [146] [153] [154] (iii) ultrasound [155] (iv) ozonation [156] [157] [158] [159] [160] (v) hydrodynamic cavitation (HC) [161] [162] [163] (vi) photocatalysis and photo-electrolysis and sonophotocatalysis [157] [159] [164] [165]. These AOPs have demonstrated excellent capabilities in treating a wide range of wastewater. The AOPs provide high oxidation treatment efficiency, inconsequential secondary contamination, and the possibility for explicit and flexible disposal, either by directly mineralizing pollutants or by increasing the biodegradability of wastewater through the formation of reactive oxygen species (ROS) [166] [167] [168] [169]. From the above-mentioned processes, bubble technologies have extensively been studied in the degradation of organic contaminants from wastewater. The detailed studies based on ozone microbubbles enhanced color removal due to the strong oxidation ability [160] [156] [160]. Hydrodynamic cavitation is regarded as an excellent option since it is economical, scalable, eco-friendly, and especially useful for treating industrial wastewater [162] [163]. Hydrodynamic cavitation can be achieved by various devices such as a venturi device, pump, jet nozzle, propeller, orifice plate, and so on. When the liquid pressure falls below the vapor pressure of the liquid, the vapor cavities (bubbles) form, expand, and collapse. Intense turbulence, extremely high local pressures (10–500 MPa), and temperatures (1000–15,000 K) referred to as "hot spots," are produced as the cavity collapses [161]. The water vapor and non-condensable gases inside the cavities decompose as shown in Eq. (1) and (2), producing free radicals such as OH, H and H₂O₂. These radicals can oxidise

dissolved pollutants [170] [171].

$$H_2O \xrightarrow{HC} {}^{\bullet}OH + H^{\bullet}$$
 (2.1)

$$2^{\bullet}OH + H^{\bullet} \longrightarrow H_2O_2 \tag{2.2}$$

On the other hand, ozonation is widely known owing to its high reactivity, proven to be effective against bacteria, fungi, and viruses [172], [173]. Major attempts have been put forward in improvising the ozonation process with the inclusion of peroxides and thiosulfate [174], combining ozonation with photocatalytic/electrolytic processes [175], and using metal ions or metal oxides as catalysts [176]. In this work, we attempted to enhance the ozonation by using ozone nanobubbles. The surface potential of nanobubbles is responsible for their extraordinary stability by enhancing the repulsive electrostatic forces, high zeta potential level prevents bubbles from coalescing [20]. The ozone nanobubble/H₂O₂ process for the degradation of tetramethyl ammonium hydroxide (TMAH) showed a 162-fold faster rate constant than that of ozone nanobubbles alone followed by pseudo-first-order kinetics. The total organic carbon content removal was reported to be 65 % whereas 80 % of nitrogen was converted into nitrate (NO₃⁻) with 95 % of TMAH removal [6]. In a nutshell, ozone nanobubbles possess high reactivity in comparison to normal bubbles or microbubbles owing to their higher surface area. The rate of mass transfer is frequently the limiting factor in the gas-liquid process, and a low rate of mass transfer reduces the overall effectiveness.

Scope for Research

A major drawback of ozone is its limited solubility and stability when it is dissolved in an aqueous solution. These characteristics restrict its potential applications and require the employment of specialized equipment to promote gas-liquid interaction. In the present work, we have proposed improving the ozonation process by including ozone nanobubbles. The existence of nanobubbles may improve the ozonation process through three important mechanisms: (i) an elevated mass transfer coefficient, (ii) a greater rate of reactive oxygen species (ROS) production due to the charged interface, and (iii) the nanobubble interface acting as an active surface for chemical reactions. The main goal of this study is to find out how ozone nanobubbles break down organic pollutants in both basic and acidic environments when there are contaminated environments (salts, surfactants) and when the zeta potential changes from negative to positive. Finally, the degradation mechanism has been proposed by analyzing the reaction products using LCMS methods.

2.1.4 Oxidation of Arsenic(III) to Arsenic (V) in wastewater using ozone nanobubbles

Literature review

Arsenic (As) is a well-known carcinogenic metalloid that is classified in group 15 of the periodic table and is recognised to be extremely toxic to humans among the listed geogenic pollutants. There are two main sources of As penetration into groundwater: geogenic and anthropogenic [177] [178]. Naturally occurring microbes in groundwater oxidise organic materials to produce hydrogen carbonate and carbonic acid salt. This eventually increases the alkalinity of the solution by releasing As from the mineral surfaces. On a separate note, As and its compounds are often utilised in many applications (such as insecticides, fertilisers, medications, food additives, and wood preservatives) and can infiltrate groundwater [179] [180]. Over 94–220 million humans are exposed to contaminated groundwater containing arsenic, and 94% of them are from Asian areas [181] [182]. Any concentration of As over the recommended threshold of 10 $\mu g L^{-1}$ set by the World Health Organisation (WHO) results in dangerous conditions such as cancer, arsenicosis, hyperkeratosis, diarrhoea, diabetes mellitus, cerebrovascular disease, and hypothyroidism [183] [184]. In order to combat harmful effects of Arsenic, many researchers have summarised the numerous treatment technologies. However, most of them have been in the form of brief but critical assessments [185] [186]. The currently available technologies include membrane filtration [187], ion exchange [188], adsorption [189], electro-coagulation [190]. Amongst the advanced oxidation processes, fenton reactions [191], photocatalysis [192] etc. are included.

The selection of an As removal process for a particular location is influenced by a number of factors, including the groundwater pH, redox potential, salinity, temperature, concentration of metal sulfides and sulfate ions, presence of microorganisms and finally the oxidation state of As [193] [194]. Thus, it is challenging for scientists and engineering professionals to comprehend the extremely complex chemistry that involves the elimination of As [185]. Unfortunately, current physicochemical treatment processes are limited by their the exorbitant energy consumption and associated environmental/chemical emissions. Amongst the treatment processes, oxidation is considered to be advantageous due to its simplicity in use, low maintenance requirements, affordability and lack of additional chemical requirements. Moreover, it is suitable for domestic use in a compact module or in a municipal communal plant [195]. Conventional adsorbents and conventional arsenic removal methods struggle to remove As(III), a neutral species that is mobile. As a result, one crucial pretreatment to enhance the removal of arsenic is the oxidation of As(III) to As(V). ALSamman et al. [196] listed the most efficient anodes used in the electrochemical oxidation of As(III) to As(V). Platinum or titanium are the most significant anodes due to their $\geq 90\%$ oxidation capability. They also possess an ability to be employed for extended periods of time. Many chemical oxidation agents such as chlorine dioxide, sodium hypochlorite, manganese oxide [197], potassium ferrate [178] and hydrogen peroxide [198] have also been used in oxidation treatment [199]. Besides the above, photo chemical oxidation has also been employed by previous researchers [200]. This work examined a novel technique for oxidising As(III) using VUV lamps that produce light at both 185 and 254 nm and found that the degradation occurred due to the formation of OH radicals by photo-splitting of water. There is some evidence in the effectiveness of traditional oxygenation techniques, such as deep water aeration and artificial mixing between top and

bottom waters [201]. However, the high capital and energy expenses of these methods, inadequate capacity to fully regulate pH, and use of some hazardous oxidants that linger in water have made them unsustainable [202].

Applications of advanced oxidation methods for the removal of heavy metals from water has drawn immense attention in recent years [203] [204] [205]. Ozone, a powerful and hygienic oxidant, can convert a variety of chemical molecules into simple and more readily broken down molecular components [206]. However, there are a few limitations that prevent the industrial practice of ozonation. Firstly, the expensive manufacturing process of ozone. Secondly, the low ozone consumption owing to its poor mass transfer rates [207] [208]. In this study, we carried out the oxidation of As(III) to As(V) using ozone in the form of nanobubbles. Nanobubbles (NB) are gas-filled cavities with some distinguishing properties such as greater stability [13], high surface area to volume ratio [5], negative zeta potential [92], low buoyancy [140], and an ability to generate radicals [61]. This allows them to contribute to physical, chemical, and biological water treatment processes in many ways. According to recent reports, oxygen (O_2) , ozone (O_3) or air NB collapse to create a significant quantity of reactive oxygen species (ROS). An example is the OH radical which has a critical role in the oxidation of complex chemical molecules, nutrients, pathogenic organisms, and other contaminants [61] [30]. Earlier, Khuntia et al. [209] investigated oxidation of As(III) to As(V) using ozone microbubbles to be effective at acidic pH, the oxidation reaction rates increased with increased ozone rates and pseudo second order kinetics was followed. Recently, Han et al. [195] found that As(III) oxidation to As(V) was very effective at pH 1 by blowing O_2 nanobubbles. Tang et al. [210] studied interfacial O₂ nanobubble technology to address algal-induced hypoxia, which achieved good performance for As mitigation in eutrophic waterways by oxidising As(III) to As(V). They later sequestrated the As(V) by Iron-hydroxide under the oxic condition.

Scope for Research

Our assessment is that the research work conducted earlier is primarily directed toward the use of ozone microbubbles to oxidise arsenite. Although there are a number of recent studies available on oxidising As(III) using oxygen nanobubbles. However, little emphasis has been placed on the application of ozone in the form of nanobubbles, the reaction kinetics being followed and nanobubble generation. Hence, the major objective of this work is to study the oxidation of As(III) to As(V) in the presence of nanobubbles using ozone as a potential oxidant. It also re-examines the oxidation of As(III) to As(V) by varying conditions like the ozone flow rates, initial As(III) concentrations, pH, salt addition, etc. Finally, the presence of ${}^{\bullet}OH$ radicals was investigated using 2-propanol as a scavenging agent. This study aimed to develop a catalyst free and green technology method for the oxidation of arsenic.

2.2 Objectives of this work

The research work presented in this thesis has been divided into four major objectives which are (i) to understand the characteristics and stability of ozone nanobubbles (ii) degradation of antibiotics (iii) degradation of organic contaminants (iv) oxidation of As(III) to As(V). Our work highlights the following aspects of wastewater treatment:

- Studying the characteristics of ozone nanobubbles, their stability and mass transfer coefficient at varying ozone flow rates, pH and salt concentrations.
- Study the degradation of antibiotic tetracycline under various parameters such as initial concentration of TC, pH and varying salt concentrations. To understand the degradation mechanism by LC-MS analysis and comparison with ozone microbubbles in the degradation efficiency.
- Study the degradation of organic contaminants (green rit and methylene blue dye) at high pollutant loading conditions. The effect of presence of salts and surfactants on the degradation of organics using ozone nanobubbles. Also, calculations of degradation constants and degradation pathways using LC-MS techniques.
- Oxidation of As(III) to As(V) using ozone nanobubbles. Analyze the presence of reactive oxygen species using radical scavenging experiments. Effect of presence of salts and varying pH on the oxidation using ozone nanobubbles.

2.3 Organization of thesis

The research presented in this thesis aims to explore the application of ozone nanobubbles in the field of wastewater treatment. The introductory Chapter 1 provides an overview of the features and characteristics of nanobubbles in terms of applications. The flow of gas into the aqueous phase has been described, and correlations for predicting the volumetric mass transfer coefficient have been shown. Many practical applications including oxygen, air, and ozone microbubbles, as well as traditional techniques involving bubbles for wastewater treatment, have been demonstrated, with some now in different phases of commercialization. Other key applications of nanobubbles for wastewater treatment have been proposed, including the removal of organic and inorganic pollutants. Chapter 2 provides a quick survey of the literature and shows the findings of several research studies in order to select some prospective topics of study to be tackled in this thesis. The state-of-the-art for ozone nanobubble-based degradation of antibiotics (tetracycline), arsenic, and organic pollutants was given. This chapter also highlights the scope and purpose of the present effort. Chapter 3 describes the experimental apparatus utilised for the ozonation of all pollutants. The materials utilised in this work and their sources are listed. The experimental procedures used to conduct a thorough investigation of pollutant ozonation are also described. The procedures for preparing and characterising adsorbents are also provided. Chapter 4 starts with investigating the characteristics and

properties of ozone nanobubbles under different conditions. It deals with the generation of ozone nanobubbles under different parameters including effect of ozone flow rates, pH and different salt concentrations. Their mass transfer characteristics during the generation of ozone nanobubbles and after dissolution were also studied. The presence of reactive oxygen species formed during the generation of ozone nanobubbles was also examined using the ESR technology. One of the applications of degrading the organic methylene blue dye is also presented in this chapter. Chapter 5 presents the work on the removal of the antibiotic tetracycline from water using ozone nanobubbles. The effects of ozone feed rates, pH, different concentration of monovalent salts on ozonation have been studied. Degradation of tetracycline using oxygen nanobubbles, ozone sparging, in presence of hydrogen peroxide and a combination of ozone nanobubbles + hydrogen peroxide has also been carried out and compared with that of ozone nanobubbles. The mechanism for the degradation of tetracycline has been investigated in detail. The presence of hydroxyl radicals and reactive oxygen species has been studied by radical scavenging experiments. In Chapter 6, the work on oxidation of arsenic using ozone nanobubbles has been reported. A wide range of initial arsenic concentrations has been used in this study. The effects of ozone generation rate and pH of the aqueous medium on the efficiency of ozonation have been studied. The use of 2-propanol as the OH radical scavenger has been reported. The kinetics of oxidation of As (III) with ozone was studied and the kinetic parameters were evaluated. The effect of presence of monovalent salts on the ozonation was also studied. Chapter 7 presents the ozonation of organic contaminants green rit dye and methylene blue dye using ozone nanobubbles. This work focused on the variation of concentration of both the organic dyes with time, degradation products and kinetics of the reactions. The variation of concentration of dye with time was investigated by Spectrophotometer. The degradation mechanism was constructed from the data obtained from LC-MS. Parameters such as pH, salt concentrations (mono, di and trivalent), surfactants (SDS and CTAB) were also studied. Finally, a summary of the major findings of the works is presented in Chapter **8**. This is followed by recommendation for future works.

Chapter 3

Experimental Methods

This chapter presents the details of the experimental setup used for the generation of ozone nanobubbles, degradation of antibiotics and organic contaminants as well as oxidation of As(III) to As(V). The chemicals required, the process of how the experiments will take place, the instruments required for the characterization, methods of preparation of the solutions are provided separately in each section of this chapter.

3.1 Experimental setup

The nanobubble generation setup consisted of an oxygen concentrator (Longfian Oxygen Concentrator, MZJ10S24661, 10 L/min), an ozone generator (ISM 5-OXY, OZ-Air (India)), a nanobubble generator (Fabricated from Nanokriti Pvt. Ltd.), a dissolved ozone analyser (Q46H, Analytical Technology Inc., Collegeville, Pennsylvania, US), a circulating pump (Earth 12v Dc 150psi Diaphragm Motor Pump Diaphragm Water Pump) and an acrylic tank $(10" \times 10" \times 15" (L \times B \times H))$. Oxygen was isolated from air by the oxygen concentrator. High purity oxygen (≥98% by volume) was generated by employing pressure swing adsorption technique. This oxygen was fed to the ozone generator where oxygen was converted to ozone through corona discharge method. The ozone generator had a provision of controlling the generation rate of ozone by tuning the amount of ozone output (1-100%). The output flow rates were controlled using an inbuilt rotameter (1-10 L/min) for stable operations. The percentage of ozone in the gas mixture varied from 5-8 wt %. A pressure gauge was also installed in the ozone gas sparging line connected to the nanobubble generator. With varying ozone flow rates, the gas sparging pressure measured to be in the range of 40-50 kPa during the experiments. The experimental setup for each objective is presented in this section.

The ozone gas was passed through the nanobubble generator. The nanobubbles were generated through nanopore diffusion method in which the gas dissolved in water when passed through a ceramic membrane of 30 nm size. The mean bubble diameter of the nanobubbles varied from 120-300 nm. The generation of ozone nanobubbles was conducted in a re-circulation mode and the nanobubbles were generated continuously. The solution contained in an acrylic tank was re-circulated through the nanobubble generator. A dissolved ozone monitor (Q46H, Analytical Technology Inc., Collegeville, Pennsylvania, US) that employs a polarographic membrane sensor was used to precisely measure the amount of dissolved ozone present in water. The dissolved ozone monitor used a polarographic membrane sensor to determine the dissolved ozone concentration

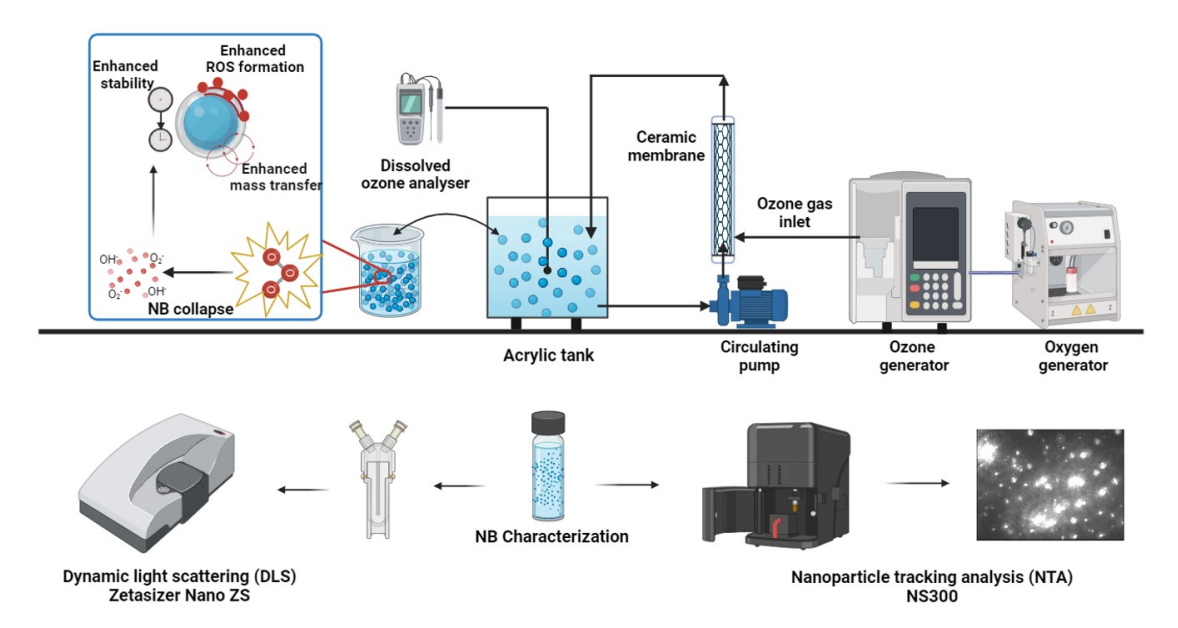


Figure 3.1: Illustrative representation of the experimental set-up for the ozone nanobubble generation and ozone nanobubble collapse leading to ROS formation, enhanced mass transfer. The dissolved ozone has been measured online using the dissolved ozone analyser.

accurately. The display range of the monitor was 0-200.0 mg/L, and the accuracy was \pm 0.1 mg/L. Calibrations for the analyser were performed beforehand using Ozone Zero Cal and Ozone Span Cal method. The excess ozone produced during the ozonation experiments were fed to the ozone destructor (OD-10, Ozone Destructor, Faraday Ozone) which was placed above the acrylic tank. The destructor works on a catalytic reaction where $\rm MnO_2$ worked as a catalyst to convert the excess ozone gas to oxygen before releasing it to the atmosphere. The experiments were performed in a room with air-conditioning. The diaphragm pump used for the re-circulation of the solution helped in maintaining the temperature at ambient conditions as the heat losses were minimized. Double distilled water (pure water) from Milli-Q Direct-16 was used in preparing all the stock solutions and in generation of ozone nanobubbles.

3.2 Characteristics and stability of ozone nanobubbles as AOPs

3.2.1 Materials

Double distilled water (pure water) (Milli-Q Direct 16, Millipore, Merck) having the electrical conductivity of $1.695~\mu Scm^{-1}$ and pH of 7.1 at a temperature of 25 °C has been used in all the experiments. Sodium chloride (NaCl, 99.5%), aluminium chloride (AlCl₃, 99.9%), sodium hydroxide (NaOH, 97%), hydrochloric acid (HCl, 37%), DMPO (5,5-Dimethyl-1-Pyrroline-N-Oxide, 98%) and ethanol were purchased from Merck chemicals.

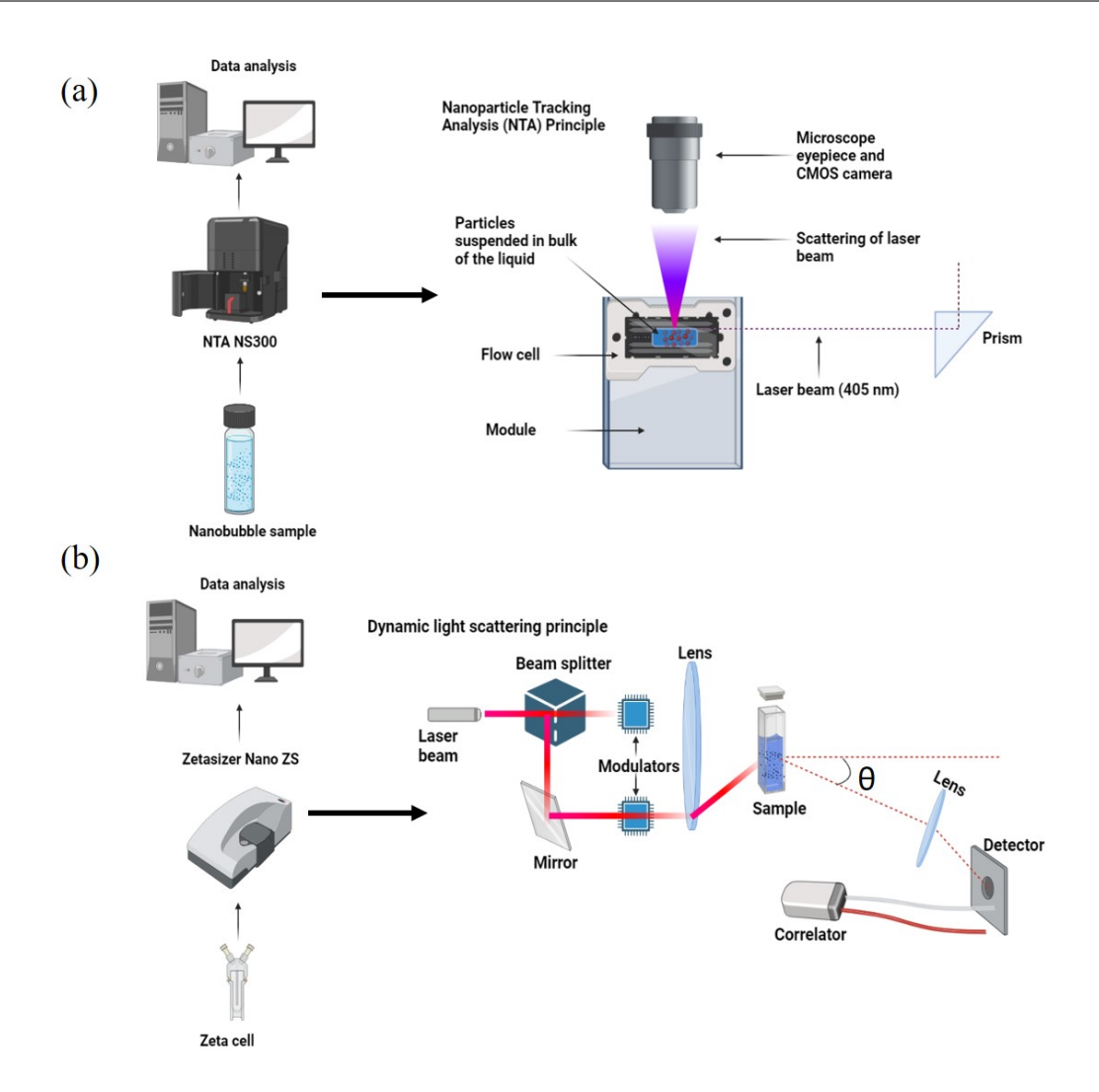


Figure 3.2: Working principal of (a) NTA (Nanoparticle tracking analysis) (b) DLS (Dynamic light scattering)

3.2.2 Nanobubble generation and its characterization

The nanobubble solutions were prepared using the ceramic membrane technique at room temperature. A 30 nm membrane was placed inside a stainless steel module for the production of nanobubbles. During the nanobubble generation stage, only nanobubbles were believed to have been formed using this approach. This was apparent by observing the lack of milky nature of the solution as it is often attributed to the presence of microbubbles [211]. Nevertheless, at increased flow rates, macrobubbles were shown to develop for milliseconds before bursting at the liquid's surface because of their powerful buoyant force. Therefore, the ozone oxidation process was primarily caused by nanobubbles.

Pure water (from the acrylic tank passed through the circulating pump) and ozone (produced from the ozone generator) were passed through the membrane module at different flow rates (1-10 L/min) at varying pH and salt concentrations (Monovalent and trivalent salts (0.01-100 mM)). The sample solutions were collected in 15 mL vials and stored for the measurement of size, number, and charge density. The pure water was placed

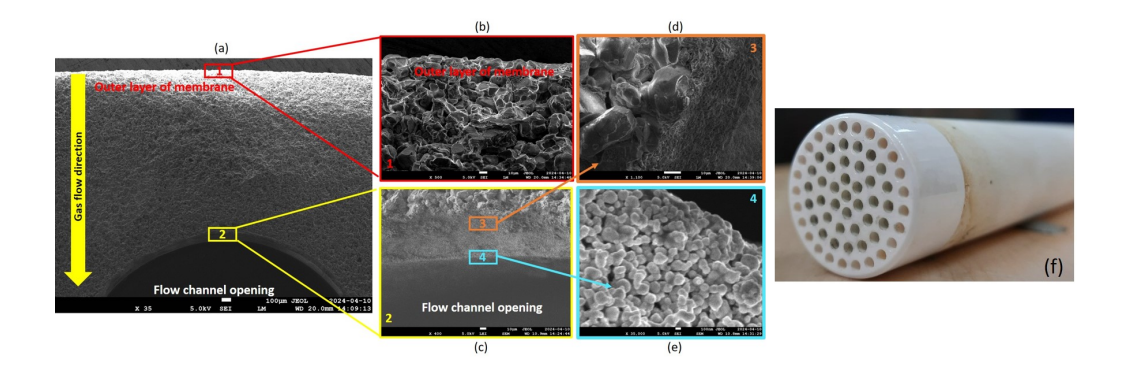


Figure 3.3: FE-SEM scan of 30 nm pore size ceramic membrane (a) overall morphology of the membrane (b) outermost/support layer (c) membrane area near channel opening (d) transition layer) (e) innermost layer (f) Image of the ceramic membrane with a zoomed view of the membrane pore channel.

in a 2 L acrylic tank, and a diaphragm pump was used for the circulation of water and gas through the membrane module as shown in Figure 3.1. The setup was run in a re-circulation mode for a period of 30 minutes. The nanobubbles were generated continuously for 30 mins and since the nanobubbles are highly stable, thus the samples are stored in 15 ml glass vials for further characterization. The bubble number density, mean bubble diameter were characterized using Nanoparticle Tacking Analysis (NTA NS300, Malvern) technique, based on the light scattering principle (details mentioned in Figure 3.2). The zeta potential of the ozone nanobubbles was measured using Zetasizer Nano ZS (Malvern) whose principle is mentioned in Figure 3.2. Online measurements for dissolved ozone concentration were carried out simultaneously. Apart from this, the ceramic membrane used for the generation of ozone nanobubbles was also characterised using FE-SEM. The cross-sectional image of the tubular channelled ceramic membrane, as well as the structural morphology of the membrane, were mapped using field emission scanning electron microscopy (FE-SEM, JSM7610F Plus, JOEL). A thin, disc-shaped membrane with a thickness of 5 mm was cut with a sharp knife and used to apply carbon coating. The results of FE-SEM have been presented in Figure 3.3 at various magnification settings. Figure 3.3 (a) depicts the overall morphology of the membrane showing the outermost layer, channel opening as well as the gas flow direction. Figures 3.3 (b) and (d) show a comparison of the cross-sectional views of the membrane's outer support layer and transition layer, respectively. The membrane's nanopore layer is shown in Figure 3.3 (e). This layer is closely packed, and next to the channel opening an extremely porous structure was seen. A magnified image of the membrane's cross-section is shown in Figure 3.3 (c), with the membrane's outer surface on the top and its first channel in the middle. As the pressurised gas sparges from the exterior to the interior of the membrane surface, the fastly moving water within the membrane channels generates shear stresses at the inner surface of the membrane, quickly breaking off the sparged gas bubbles to produce nanobubbles. Figure 3.3 (f) presents an image of the ceramic membrane with a zoomed view of the membrane pore channel. The parameters have been mentioned in Table 3.1.

Membrane size (nm)	30
Outer diameter (mm)	26.4
Channel diameter (mm)	2.0
Channels	61
Spec. membrane area (m^2/m)	0.426
Spec. crossflow velocity (m ³ /h)/(m/s)	0.85

Table 3.1: Parameters of 30 nm ceramic membrane used in nanobubble generation

3.2.3 ESR spin trap measurements of reactive oxygen species generated in ozone nanobubbles

Electron spin resonance (ESR) is the technique followed for the detection of reactive oxygen species such as centrally located oxygen species (OH radical, superoxide radical). DPMO has been preferred as the spin trapping agent since it has been used widely for detecting the free radicals [29]. The measurements of ESR were conducted in the following sequence: Firstly, ozone nanobubble sample was prepared. After the production of nanobubbles, 120 μ L of NB sample, 5 mM H₂O₂ of 30 μ L, 0.36 M DMPO of 30 μ L were mixed in the same order as mentioned simultaneously and swiftly poured in a flat quartz cell [212]. The measurements were performed using ESR instrument (Bruker BioSpin A300-9.5/12/S/W). The measurements were conducted in the X-band mode with a frequency of 9.4 GHz. The following parameters were set for the measurements to be conducted: Temperature: 250K (low temp); Power: 3.9 mW, C.field: 3300T. The calibrations were done using Ti²⁺. A minimum of 130 μ L of the sample was required to be poured in the flat quartz cell. The flat quartz cell was irradiated with UV light (280-315 nm) using a handy UV lamp with 1 × 6 W power (VL-6, MC, Vilber Lourmat, France).

In case of dye degradation, the absorbance measurements were performed using a spectrometer (DR3900, HACH). Standard solutions of methylene blue were prepared for plotting the calibration curve. For measurements, the samples were collected every 10 seconds in 15 mL glass vials. The monitored wavelength for the absorbance measurement was 668 nm for Methylene Blue [213]. The spectrophotometer was preprogramed with the calibration curve for the dye. Each sample was analyzed in duplicate. In addition, the degradation of MB was analyzed on a LC-MS (Liquid chromatography and mass spectrometry) machine (XEVO G2-XS QTOF). The mobile phase was 50:50% acetonitrile and water. ESI cation mode, C18 column with a voltage of 1.1 kV and temperature of column oven was 30 °C. The set up was run in gradient mode with 5:95 (Acetonitrile: Water) to 100% Acetonitrile 0% water [214] [215].

3.3 Degradation of antibiotic tetracycline using ozone nanobubbles

3.3.1 Materials

Tetracycline (98%) was purchased from Sigma Aldrich and was used without any further purification. Sodium chloride (NaCl, 99.5%), sodium hydroxide (NaOH, 97%), hydrochloric acid (HCl, 37%), 2-Propanol ((CH₃)₂OH, 99.5%) and ethanol were purchased from Merck chemicals. Pure water was gathered from the Milli-Q system (Milli-Q Direct-16 water purification system) having a resistivity of 18.2 M Ω .cm and pH of 7.1 at a temperature of 25 °C and that has been used in all the experiments. Before the experiment, distilled water and all stock solutions were checked using a NanoSight NS300 (Malvern Instruments, UK) for nanoscale contaminants, however, no appreciable quantities of nanoscale entities were discovered. A stock solution and the experiment water were assessed using NanoSight before the testing to rule out any prior nanoscale contamination. When handling and maintaining the experimental setup, additional safety precautions have been adopted. Disposable pipettes, vials, and syringes devoid of latex were used to avoid contamination.

3.3.2 Experimental methods

The experimental setup is presented in Figure 3.4. The stock solutions for tetracycline (TC) were prepared by adding the desired amount of tetracycline to Milli-Q water in the beaker and stirring it magnetically for 45 minutes at 600 rpm. The ozone nanobubbles were generated using the nanopore diffusion method and varying the ozone flow rates from (2.5-10 L/min, 40-50 kPa). The set up was run for a period of 30 minutes in re-circulation mode. Ozone gas was fed from the ozone generator, flow rate of which was controlled through an ozone rotameter (1-10 L/min, Flowstar Engineering Pvt. Ltd). The dissolved ozone was measured online using a dissolved ozone analyser. The excess ozone produced during the ozonation experiments were fed to the ozone destructor which was placed above the acrylic tank. The experimental protocol to study different parameters is as follows: the prepared stock solution of TC was placed in the acrylic tank and the setup was run in a re-circulation mode with ozone being fed to the nanobubble generator from the ozone generator. The experiment was run for 60 minutes and the samples were collected every five minutes. Various parameters such as ozone flow rates (2.5-10 L/min, 40-50 kPa), initial tetracycline concentration (100-400 mg/L), varying pH (4-11), addition of salts (NaCl, 0.1-100 mM) and scavenging experiments were performed.

3.3.3 Degradation kinetics and calculating mass transfer coefficient

The removal rate was calculated as in Eq. 3.1:

$$\%removal = \frac{C_{A0} - C_A}{C_{A0}} \tag{3.1}$$

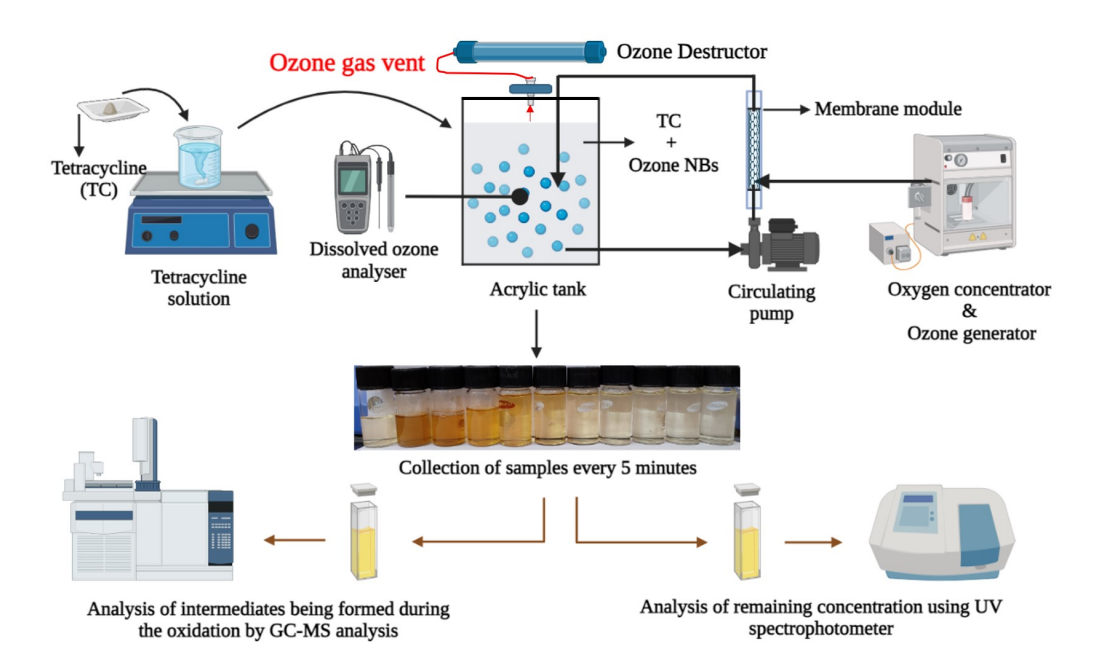


Figure 3.4: Illustrative representation of the experimental set-up for the degradation of tetracycline. The dissolved ozone has been measured online using the dissolved ozone analyser. The degradation of TC is characterized by analysis through UV Spectrophotometer and LC-MS analysis. Photography of collected samples document real change of color of treated solution, while treatment.

For the kinetic studies of TC degradation, after analysis for the correlations of zeroth, first and second order reactions [142], it was clear that the degradation of TC were observed to bear a second order kinetics as Eq. 3.2:

$$-r_A = kC_A^2 \tag{3.2}$$

Upon integrating Eq. 3.2 from t=0; $C_A=C_{A0}$ to t=t; $C_A=C_A$, we get the following expression as in Eq. 3.3.

$$\frac{1}{C_A} = \frac{1}{C_{A0}} + kt \tag{3.3}$$

where C_A is the concentration of TC at any time t, C_{A0} is the initial concentration of TC taken, t is the time and k is pseudo second order rate constant.

The volumetric mass transfer coefficient was determined by measuring the dissolved ozone concentration through a dissolved ozone analyzer. The ozone concentration was measured by passing the ozone gas through the membrane module as depicted in Figure 3.4 into the liquid tank, where the ozone analyzer was placed for the measurements. The concentration was recorded at every 1-minute interval. The mass balance equation for dissolved ozone can be given as in Eq. :

$$-\frac{dC}{dt} = k_L a(C^* - C_t) - k_d C_t \tag{3.4}$$

where C* (mg/L), C_t (mg/L), k_d, k_La and C₀ (mg/L) are the saturated concentration, concentration at any given time t (min), ozone decomposition rate constant, volumetric

mass transfer coefficient of ozone (min⁻¹) and initial concentration (mg/L), respectively. The time t is measured in minutes. At the initial condition of t=0, the concentration $C_t=C_0$. Integrating Eq. 3.4 for $k_d=0$ yields the following expression as in Eq. 3.5 [216], which is the case when pure water is being used. The reason for neglecting self-decomposition $k_d=0$ of ozone is that the entirety of the experiment was conducted while ozone nanobubble generation was taking place inside the reaction vessel. According to the recent literature it is safe to assume that the self-decomposition of the ozone would be insignificant as compared to the accumulation of ozone into the system during the ozone nanobubble generation process [141] [217].

$$ln(\frac{C^* - C_t}{C^* - C_0}) = (k_L a \ t) \tag{3.5}$$

In the present case, when TC is present in the solution, the model equation required to calculate the mass transfer coefficient can be derived from Eq. 3.4. Solving Eq. 3.4 and re-arranging the variables, the final equation is in the form Eq. 3.6. Finally, the value of k_d will be substituted in Eq. 3.6.

$$\frac{C_t}{C^*} = \frac{k_L a}{k_L a + k_d} (1 - e^{-(k_L a + k_d)t})$$
(3.6)

Consequently, the rate constant of the ozone consumed by chemical reaction over time can be measured by the following equation by determining the slope of the curve fit for the data of O_3 concentration versus time curve [141]:

$$\frac{C_t}{C^*} = e^{-k_d t} \tag{3.7}$$

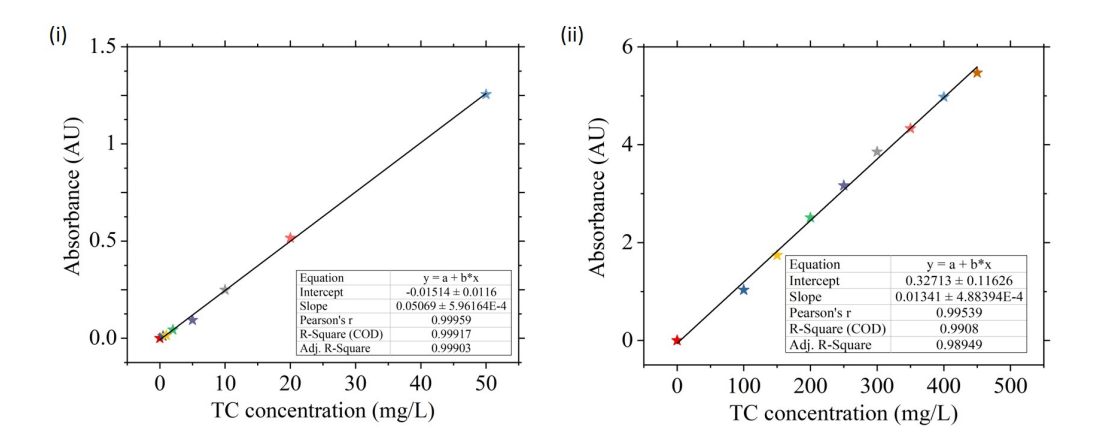


Figure 3.5: Calibration plots for Tetracycline (i) 0-50 mg/L (ii) 0-450 mg/L

3.3.4 Measurement of concentration of tetracycline and degradation pathways

A spectrophotometer (DR3900, HACH) was used for the detection of the concentration of TC remaining in the samples after the degradation. The absorbance curves were calculated and attained a maximum value at a wavelength of 357 nm [218]. The calibration curve was plotted at various concentrations of TC (0-50 mg/L, 0-400 mg/L) with R^2 =0.99 has been presented in Figure 3.5. The radicals generated during the ozonation process were qualitatively measured by radical scavenging experiments. 2-Propanol was used as a radical scavenger for $^{\bullet}$ OH radical as it inhibits the activity of the $^{\bullet}$ OH radicals. The intermediates formed during the process were analyzed by LC-MS. The degradation of TC was analyzed on a LC-MS instrument (XEVO G2-XS QTOF, Waters). An electrospray ionization (ESI) in a positive mode was used with analysis of full scan range from 0-1000 with a C18 column (Symmetry C18 Column, 4.6 mm \times 250 mm, 3.5 μ m). The set up was run with mobile phase of 50:50% acetonitrile and water [219]. Nanobubbles were characterized using Nanoparticle Tracking Analysis (NS300, Malvern).

3.4 Degradation of organic pollutants under high pollutant loading

3.4.1 Materials

The Basic Blue 9 (Methylene Blue, (MB)) with the chemical formula ($C_{16}H_{18}N_3SCl$) and green rit dye ($C_{27}H_{34}N_2O_4S$, GRD) was purchased from Sigma Aldrich. Sodium Hydoxide (NaOH, 99.5%), concentrated Hydrochloric acid (HCl, 37%), Sodium chloride (NaCl, 99.5%), Calcium Chloride Dihydrate ($CaCl_2 \cdot 2H_2O$, 99.9%) and Aluminium Chloride Anhydrous (AlCl₃, 99%) were purchased from Merck Chemicals. Sodium dodecyl sulphate (SDS, 99%), Cetyl Trimethylammonium Bromide (CTAB, 99% SRL) were purchased and used without any further purification. Ultra-pure water having an electrical conductivity of $1.695 \mu \text{ Scm}^{-1}$ and pH of 7.1 at a temperature of 25 °C has been used in all the experiments. Dye stock solutions were prepared by mixing the desired concentration of dye in pure water, followed by agitation for a period of 30 minutes at 500 rpm. Stock solutions for the surfactants were prepared by dissolving SDS and CTAB at various concentrations in pure water using a magnetic stirrer at 25 °C until completely dissolved.

3.4.2 Experimental methods

The schematic for the experimental setup shown in Figure 3.6 consists of an oxygen concentrator, ozone generator, rectangular acrylic tank of 1000 mL capacity, nanobubble generator, and a dissolved ozone analyzer. The ozone generator was used for the production of ozone from oxygen received from the concentrator with 98% purity at various flow rates (1-10 L/min). The ozone generator used here works on the principle of corona discharge. By adjusting the output percentage and the amount of oxygen, it can control the flow rate

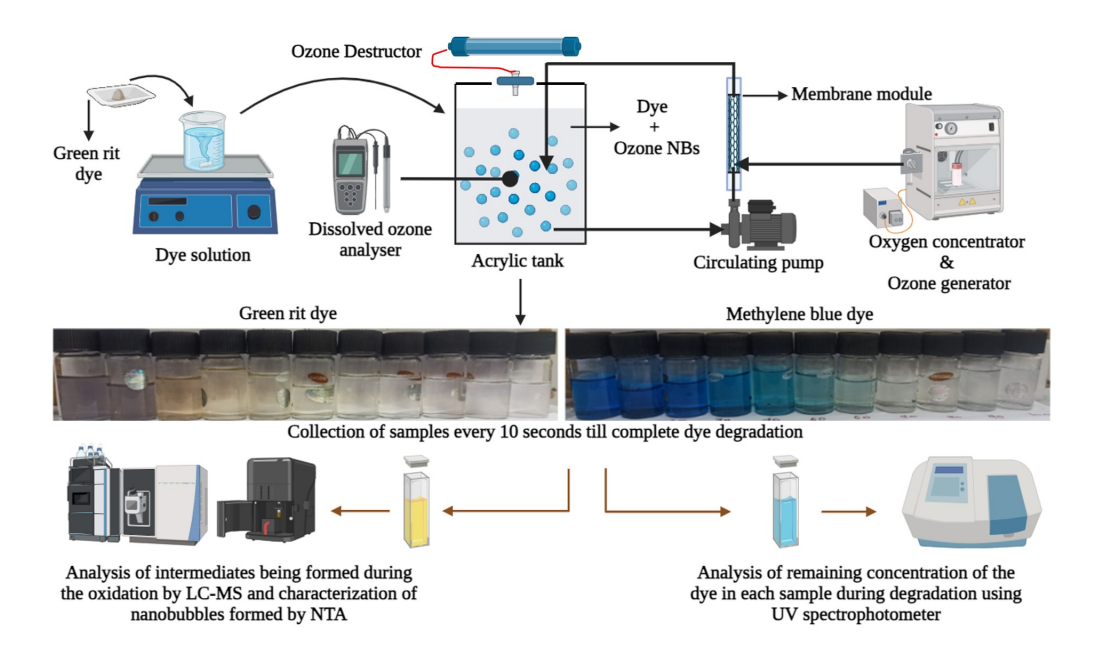


Figure 3.6: Schematic illustration of the experimental setup. The setup is run in re-circulation mode. The degraded samples are collected every 10 seconds until complete degradation. The NBs formed during the process are characterized by NTA analysis. The intermediates formed during the process are examined by LC-MS analysis.

of ozone. The online measurements of dissolved ozone were measured using the dissolved ozone analyser with a display range of the monitor at 0–200.0 mg/L with accuracy of \pm 0.1 mg/L. Nanobubbles were generated using the nanobubble module purchased from Nanokriti Technologies. A mixture of gases, comprising oxygen and ozone, was circulated through it. The organic contaminants in the tank were recirculated using the circulating pump. The system was set up to work in a re-circulation mode. The temperature of the reaction medium was kept at room temperature. Samples were thereby collected in 15-mL glass vials for further characterization of nanobubbles using NTA and DLS techniques. Batch studies were conducted to investigate the effects of initial concentration, ozone flow rates, pH, salt and surfactant additions, and ozone nanobubbles on contaminant degradation. The pH of the medium was maintained using 0.1 M NaOH and HCl solutions.

3.4.3 Color measurement, degradation analysis and radical quenching

For color measurement, standards of organic solutions were prepared in distilled water. The standards were prepared for plotting the calibration curves for the organics. For measurements, the samples were put in 15 mL glass vials and stored at room temperature. The quantity of remaining pollutant concentration in the samples was obtained at different time intervals, and it was measured using a spectrophotometer (DR-3900, HACH). The color was measured by reading the absorbance at 526 nm for green rit and 668 nm for Methylene Blue. The spectrophotometer was pre-programmed with the calibration curves of the organics, and a provided color was analyzed in every five samples in duplicate to obtain precision. Radical quenching experiments were conducted to investigate the

possible free radicals generated during the ozonation process. For the following purpose, 2-propanol (1mM) and Sodium Azide (NaN₃) (1mM) were used as trapping agents for hydroxyl radical (${}^{\bullet}$ OH) and singlet oxygen (O₂¹) respectively. The trapping agents were added to the organic solution, and the kinetics were studied to see the effect of the trapping agents on the degradation efficiency of the organics.

Also, the analysis of the intermediates formed during ozonation was detected by using an LC-MS (Liquid Chromatography-Mass Spectroscopy) instrument (XEVO G2-XS QTOF, Waters). C18 column (Symmetry C18 Column, 4.6 mm \times 250 mm, 3.5 μ m) was used for separation of dye particles. The mass spectrometer was outfitted with an electrospray ionisation source and ran in positive polarity with a voltage of 1.1 kV, and temperature of the column oven was 30°C. The mobile phase was consisted of acetonitrile and water [214][215]. The setup was run in gradient mode from 5% to 95% in 16 minutes. The mass range was run from 50-1400 m/z.

3.5 Oxidation of As(III) to As(V)

3.5.1 Materials

Chemicals: Arsenic trioxide (As₂O₃, 99% assay, Merck, India), 3 M of NaOH and hydrochloric acid (35% assay, Merck, India). Reagents: Arsenic standard solution (H₃AsO₄ in HNO₃, Merck, India), Ammonium Molybdate Tetrahydrate((NH₄)₆Mo₇O₂₄.4H₂O), Antimony Potassium Tartrate Hemihydrate (C₄H₄O₇ksb.1/2 H₂O, 99.5% extrapure AR) and L-Ascorbic acid (C₄H₈O₆, 99.7% extrapure AR). Anion exchanger: Dowex resin 1 X 8 (Chloride form, Alfa Aesar, India). All experiments utilised pure water (pH = 7.1 and an electrical conductivity of 1.695 μ Scm⁻¹) collected from a Milli-Q Direct-16 water purification system at a temperature of 25 °C.

3.5.2 Nanobubble generation and oxidation

The details of the experimental setup including preparation of stock solutions, ozone nanobubbles, dissolved ozone monitoring, nanobubble characterization and arsenic content measurements are presented in Figure 3.7. In this study, ozone nanobubbles were produced using the nanopore diffusion technique at room temperature. Arsenic(III) oxide stock solutions were prepared by mixing the desired amount of As(III) oxide to one litre of pure water and stirring the solution for a period of 45 minutes at 500 rpm. Henceforth, the prepared sample stock solution was transferred to an acrylic tank where ozonation takes place. Ozone from an ozone generator and stock solution was fed to the nanobubble generator (NanoKriti Pvt. Ltd.) for oxidation process to take place for the degradation. Ozone gas was produced by providing oxygen from an oxygen concentrator with a purity of 98% at desired flow rates (1-10 L/min) to the ozone generator where ozone was produced by the corona discharge principle. The ozone flow rate was controlled with the aid of

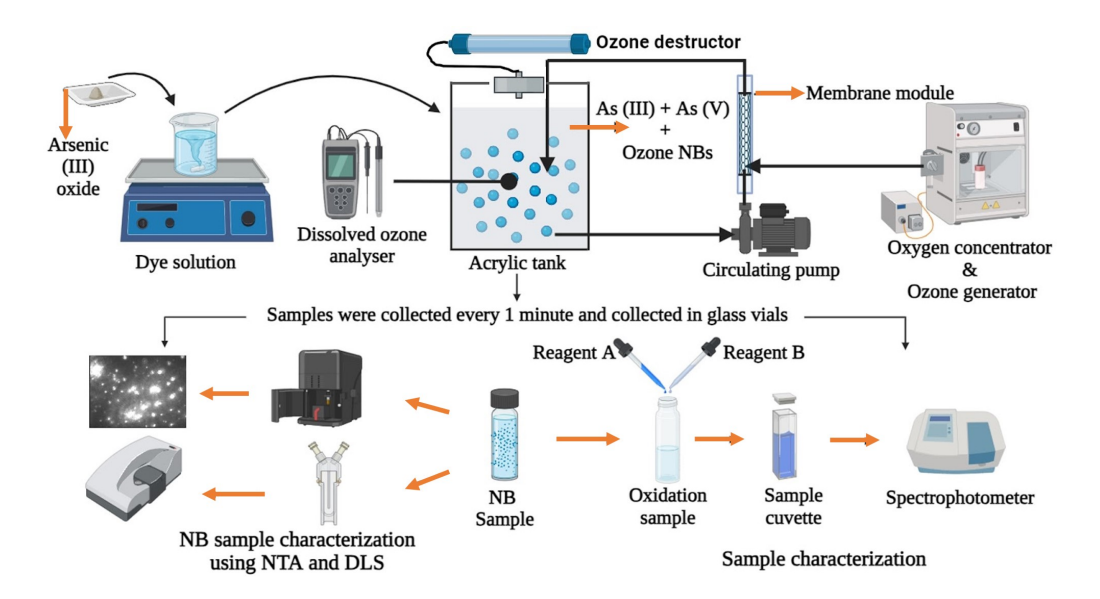


Figure 3.7: Illustrative representation of the experimental set-up for the oxidation of As(III) to As(V). The dissolved ozone has been measured using the dissolved ozone analyser. The NB sample was analysed using NTA and DLS. The As detection was performed using spectrophotometer.

a rotameter. A dissolved ozone monitor. Ozonation experiments were carried out for a period of 10-20 minutes. The experiments were performed in triplicate and repeated three times. The standard deviation was calculated and presented as error bars. These error bars depict the precision of the measurements. Smaller error bars indicate a more precise measurement, while a larger error bar suggests greater uncertainty.

For various parameters to be studied, the experimental protocol was as follows: For nanobubble generation at different flow rates: A 1 ppm (1000 mL volume) arsenic stock solution was run at ozone flow rates for 30 minutes. Further the nanobubbles were characterised using NTA and Zetasizer. For effect of ozone flow rates on As(III) oxidation: The setup was run for a period of 10 minutes in which samples were gathered every 1 minute. The As(III) concentrations were kept constant at 1 ppm. For effect of initial concentration of As(III), various concentrations of As(III)oxide (1, 2, 3, and 4 ppm) were prepared. Samples were collected every 2 minutes in an experimental run of 20 minutes. To understand the effect of addition of chloride ions, a set of experiments were run for a period of 30 minutes and samples were collected every 3 minutes at 3 L/min ozone flow rates at various concentrations (1-50 mM) of NaCl.

3.5.3 Analysis of As(V) and determining oxidation kinetic studies

As(V) concentration was determined using UV-spectroscopy. The method used for the measurements is called the molybdenum blue technique [220][221]. The procedure involved the preliminary synthesis of two reagents A and B. Reagent A was prepared by combining two separate solutions: 100 ml of 0.35 g of antimony potassium tartrate hemihydrate $(C_4H_4O_7KSb.0.5H_2O)$ and 100 ml of 10 g of ammonium molybdate tetrahydrate

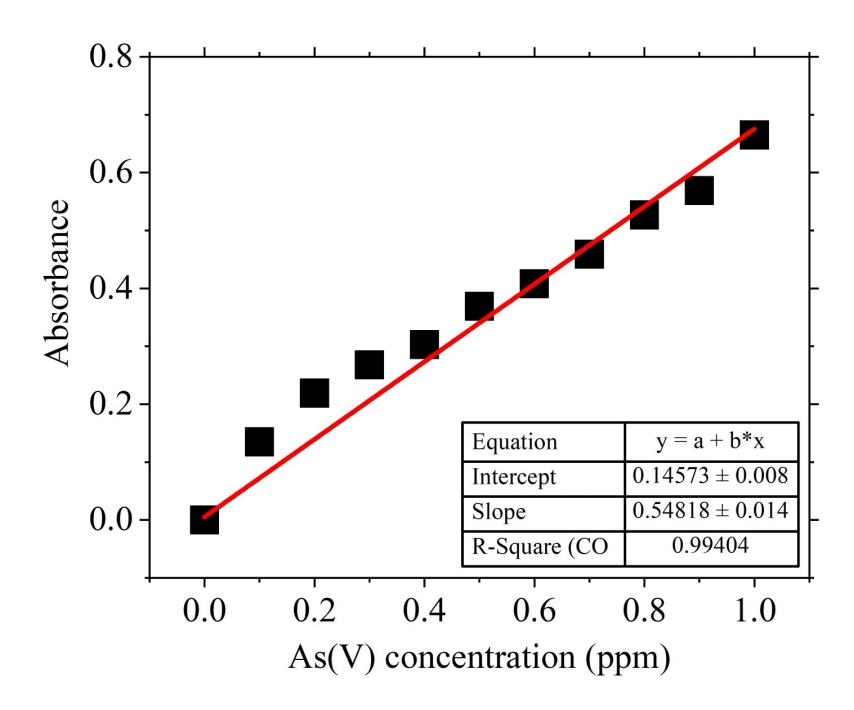


Figure 3.8: As (V) standard calibration curve

((NH₄)₆Mo₇O₂₄.4H₂O). Reagent B was prepared by dissolving 1g of L-ascorbic acid in 50 ml of milliQ water [222] [223]. Upon oxidation, the samples were collected for measuring the Arsenic(V) concentration. In 10 mL of the oxidation sample, 2 mL of Reagent A and 1 mL of Reagent B were added. A blue color was imparted to the sample to measure the amount of Arsenic(V) present in the sample. The wavelength of 874 nm was fixed based on color intensity specification. The standard calibration procedure for the same has been presented in Figure 3.8. The molybdenum blue method was utilised for calibration. The molybdenum blue method is based on the production of arsenomolybdate from the reaction of ammonium molybdate and arsenate has been suggested for the determination of As(V) concentrations ranging from 0 to 1 ppm, and then add 2 ml of reagent A and 1 ml of reagent B were added to each standard solution [221] [224] [225] [226]. Based on the requirements for colour intensity, these standard solutions were used to establish the wavelength of 874 nm. After identifying the wavelength, a curve was created using standard arsenate solutions ranging from 0 to 1 ppm. Using the molybdenum blue method and a reference calibration graph, we further assessed an unknown concentration of As(V). The concentration vs time data were evaluated for each set of experiments. After analysing the correlations for zeroth, first and second order, it was clear that the degradation of As(III) followed first order kinetics. The kinetics of the reactions were determined using the following equations:

$$-\frac{dC_{A}}{dt} = kC_{A} \tag{3.8}$$

where C_{AO} is the initial concentration (ppm) of As(III), C_A is the concentration at any time t (ppm) of As(III), k is the rate constant (min⁻¹) and t is the time (minutes). Integrating the Eq. 3.8 from t=0 to t=t, and taking an initial condition, for t=0, C_A to C_{AO} , we get

$$-ln \frac{C_{\rm A}}{C_{\rm AO}} = kt \tag{3.9}$$

From the experimental concentration trends, the dataset fitted the first order kinetics with ${\bf R}^2=0.99.$

Chapter 4

R&D 1: Characteristics, stability and application of ozone nanobubbles

This chapter presents the work on understanding the characteristics of ozone nanobubbles under various parameters such as varying ozone generation flow rates, pH, varying salt concentrations. The effect of using ozone in the form of ozone nanobubbles to enhance the volumetric mass transfer coefficient has also been studied. The effect of various parameters mentioned above has been extensively studied and compared for nanobubble generation and nanobubble dissolution. The long term stability of ozone nanobubbles has also been investigated. A brief study on the rapid degradation of methylene blue dye using ozone nanobubble as an application in wastewater treatment is also investigated.

4.1 Ozone nanobubble dynamics in salt solution

The nanopore gas diffusion method is utilized to generate the ozone nanobubbles in pure water, where nanobubble forms by shear provided on the wall of the nanopore. The size of the nanobubbles are formed strongly depends on the shear rate in the channel of the membrane. It is intuitive that higher the shear rates the smaller the size of the nanobubbles. From both fundamental and practical viewpoints, it is customary to understand the ozone nanobubble dynamics and stability in the presence of salts due to the reactive nature of the ozone gas. The gas flow rate for ozone nanobubble is varied from 1 to 10 L/min, and it is characterized by the bubble number density, mean diameter, and bubble size distribution as shown in Fig. 4.1. Evidently, the bubble size distribution was observed to be wider at a low ozone flow rate, whilst it gradually turned to a narrow distribution by increasing the ozone gas flow rate. This is attributed to the fact that nanobubble pinch-off time from the nanopore is expected to be relatively higher than that of the high flow rate. Such delay may result in the larger size of nanobubbles. Furthermore, the area under the bubble size distribution curve also increases with the ozone gas flow rate. This, in turn, indicates the higher nanobubble count with the increasing ozone gas flow rate. Fig. 4.1 (b) shows the bubble number density of the nanobubbles and mean diameter. The bubble number density (BND) monotonically increases with the ozone flow rate up to 6 L/min, and it levels off to a constant value further after supersaturation of the gas, whereas the mean size of the nanobubble decreases with the ozone flow rate and levels off to a constant value. The higher area under the distribution curve denotes the higher bubble density is evident from Fig. 4.1 (a). The zeta potential of the ozone nanobubbles also increases with the ozone flow rate (see Fig. 4.1(c)). The dissolved ozone concentration was measured with time, and the maximum dissolved ozone concentration was observed to be decreased with the ozone flow rate as shown in Fig. 4.1 (d). In a nutshell, the salient features of ozone nanobubble generation are as follows: (i) the higher the ozone flow rate higher the bubble number density, (ii) the mean diameter decreases with the flow rate, (iii) the higher negative zeta potential with a higher flow rate. From the preceding discussion, it is clear that the ozone nanobubble sample possesses a negative zeta potential and yields a higher bubble number density. On the other hand, the mean diameter of the nanobubble decreases with the flow rate. All else being equal, the size of the nanobubble were observed to have dependence on zeta potential. The surface charge on the bubbles becomes significant in the micro and nano-scale phenomena. The charge interface is expected to exert the electrostatic force along the outward normal to the bubble. Let us consider a spherical charged nanobubble of radius R_0 and the surface charge Q. From electrodynamics, the force exerts by a similar charge oriented in a spherical inner interface to be given by Eq. 4.1:

$$P_{ele} = \frac{Q^2}{8\pi\epsilon\sigma R^2} = \frac{\sigma^2}{2\epsilon\epsilon_0} \tag{4.1}$$

On the other hand, the surface tension force exerts towards the centre of the nanobubble and it acts in opposite direction to that of electrostatic force. Evidently, the electrostatic force $(\sim 1/R_0^4)$ will dominate over the surface tension $(\sim 1/R_0)$ when bubble size decreases. When the bubble shrinks the charged interface gives rise to the formation of electric double layer. The net coulombic force exerted by the counter ion to the interface acts along the radial direction whilst the net coulombic interaction force at the interface acts tangentially to the interface. All in all, the surface charge is expected to be important in determining the stable size of the nanobubbles. Therefore, perturbation in the ions in the nanobubbles sample may provide the more information about the bubble dynamics. Therefore, generating ozone nanobubbles in salt solution may serve the purpose of understanding the bubble dynamics at high salinity condition (see Fig. 4.2). All else being equal, the bubble number density increases with the salt concentration whilst the mean diameter decreases. This can also be witnessed through the 3D distribution curves in Appendix A (see Fig. B.1 (a) and B.2 (a)). The negative zeta potential increase with the NaCl concentration (see 4.2 (a)). Similar trends were observed for AlCl₃ as shown in Fig. 4.2 (b). This is in stark contrast with air/oxygen nanobubbles in the salt solution, where the negative zeta potential decreases with the salt concentration [227]. The plausible mechanism of such contrasting behavior is owing to the fact that ozone is a reactive gas and decomposes by the following reactions in the presence of NaCl [228]:

$$O_3 + OH^- \longrightarrow O^{3-} + OH^- \tag{4.2}$$

$$O_3 + 2Cl^- \longrightarrow O^{3-} + Cl_2 \tag{4.3}$$

The decomposition of ozone with and without the presence of salt into O₃- may be

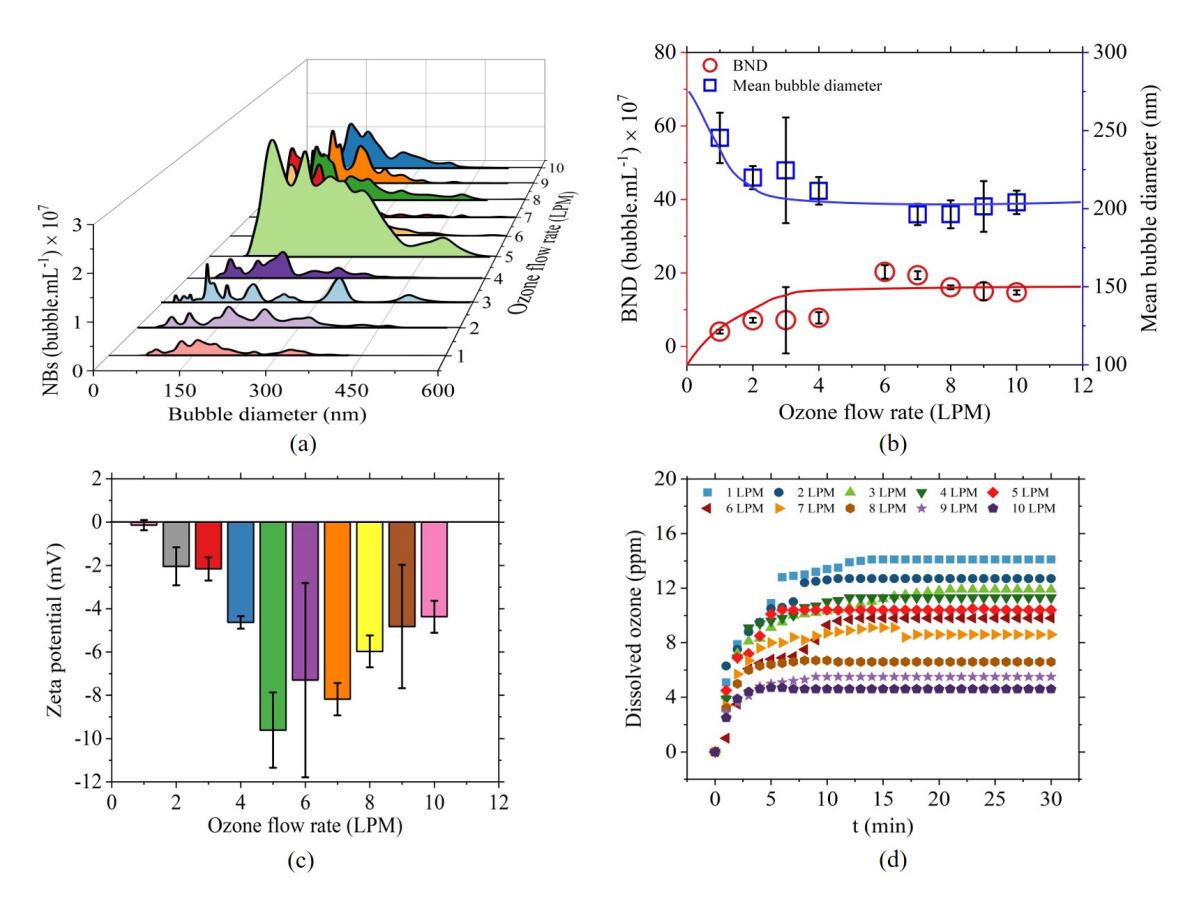


Figure 4.1: Generation of ozone nanobubbles at various ozone flow rates (1-10 L/min). (a) 3D representation of the ozone nanobubbles at different flow rates of ozone (b) Comparative representation of the bubble number density against mean bubble diameter (c) Zeta potential trend at different flow rates from 1-10 L/min (d) Dissolved ozone concentration measurement at every minute for 30 minutes of the experimental run.

responsible for the higher negative zeta potential of the nanobubbles. The extent of the formation of O_3^- may be enhanced by the higher volumetric flow rate of the ozone gas in the absence of NaCl. The variation of the amount of dissolved ozone with the salt concentrations can be referred to figures present in Appendix A (Fig. B.1 (b) and B.2 (b)). From the results, it can be seen, that with the increase in salt content, the concentration of dissolved ozone decreases. On the other hand, the presence of chloride ions also facilitates the formation of O_3 , as shown in eq (2). In conclusion, the ozone nanobubble dynamics are observed to be in contrast with the air/oxygen nanobubbles both in the presence and absence of the salts. The mean diameter of the nanobubbles was observed to decrease with the flow rate and salt concentration. On the other hand, negative zeta potential increases with both the flow rate and salt concentration. However, the bubble number density increases with the flow rate and salt concentration. These trends may be examined by the force balance around the nanobubble interface. The forces acting on the stable nanobubble are mainly electrostatic forces due to similar ions adsorbed at the interface; surface tension force acts towards the center of the nanobubbles; the intra-nanobubble electrostatic forces are expected to act to compress the nanobubble further. The electrostatic force at the charged interface tends to expand the nanobubbles;

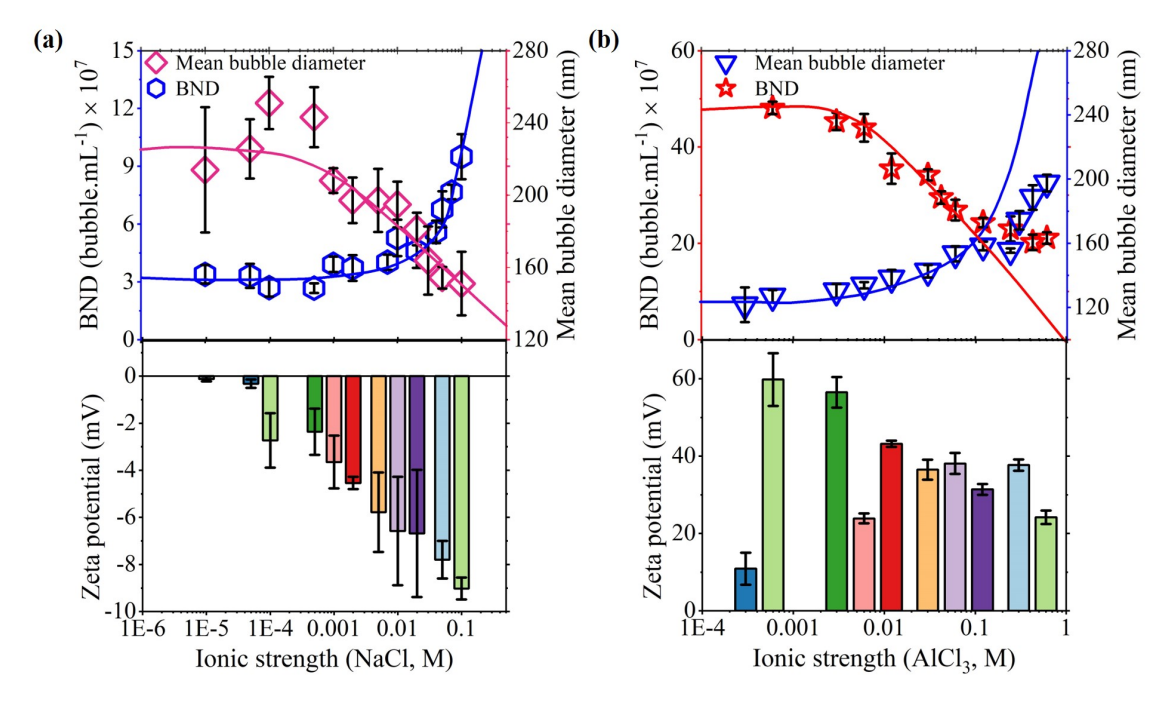


Figure 4.2: Ozone nanobubble preparation in the presence of salts at various ionic concentrations (a) The upper graph shows the trends for the bubble number density against the mean bubble diameter. The lower graph shoes the trend for the negative charge. (b) The upper graph shows the trends for the bubble number density against the mean bubble diameter. The lower graph shoes the trend for the positive charge.

therefore, a higher value of the zeta potential may result in a higher equilibrium size of the nanobubbles. However, the experimental results reported here exhibit just the opposite of this speculation. On the other hand, the intra-nanobubble force directly depends on the concentration of the neighboring nanobubbles. In the present case, it seems that the intra-nanobubble force is more dominating than the electrostatic force on the interface of individual nanobubbles. The intra-nanobubble force increases with nanobubble concentration, and therefore the equilibrium size of the nanobubble should decrease with nanobubble concentration. These are the exact trends observed in both effect of ozone flow rate and the effect of salt, where the mean diameter of the nanobubble decreases with the nanobubble concentration.

4.2 Ozone nanobubbles in acidic and alkaline medium

As noted earlier, the ozone nanobubble dynamics are completely opposite to the air/oxygen nanobubble due to the reactive nature of the ozone gas. This hypothesis can be further tested by creating nanobubbles in the acidic and alkaline medium. The effect of pre-adjustment of pH has been investigated on the bubble number density, mean diameter, and zeta potential of ozone nanobubbles. The adjustment of the pH was made prior to the nanobubble generation. The pH was adjusted using NaOH (0.1 M) and HCl (0.1 M). The setup was run for a time period of 30 minutes. The ozone concentration was measured by online probe method. The corresponding results are shown in Fig. 4.3 regarding zeta

potential, bubble number density, and dissolved ozone for varying pH values. The bubble number density exhibits an overall increase in the trend, whereas the mean bubble diameter decreases monotonically with pH. This is due to the fact that the zeta potential increases with pH and therefore, the size should decrease by the following scaling analysis. By comparing the surface tension and electrostatic force by the same order of the magnitude, the following expression can be written as Eq. 4.4:

$$\theta\left(\frac{2\gamma}{R_0}\right) \sim \theta\left(\frac{\sigma^2}{2\epsilon_0}\right)$$
 (4.4)

The surface charge density is $\sigma = Q/4 \pi R_0^2$ and thus, the scaling for the stable nanobubble can be written as follows:

$$R_0 \sim \left(\frac{Q}{8\pi\gamma}\right)^{1/3} \tag{4.5}$$

From Eq. 4.5 suggest the stable size of the nanobubbles varies $R_0 \sim Q^{1/3}$ and thus, for a single stable nanobubbles the zeta potential should increase the equilibrium nanobubble size. On the other hand, the swarm of the nanobubble also exert an electrostatic repulsion and the order of the magnitude can be much higher than that of a single nanobubble. Clearly, the stable size of the nanobubble must decrease with increase in the surface charge due to the inter-nanobubble repulsion force.

The bubble number density ranges from 1×10^7 to 7×10^8 (see Fig. B.3). The negative value of the zeta potential of the nanobubble increased quasi-linear with the pH and reached to substantially high magnitudes (around -50 mV at 12 pH) at high pH values. From a colloidal stability viewpoint, the higher zeta potential gives rise to higher total interaction energy. Given that nanobubbles may form at any pH level in water as long as there is enough dissolved gas to produce the requisite nuclei [13]. However, many nanobubbles cannot endure at low zeta potential values due to a shortage of ${}^{\bullet}$ OH ions necessary to create a charged nanobubble interface. Alkaline solutions provide a better medium for the creation and stability of ozone nanobubbles than acidic solutions due to the high zeta potential in alkaline solutions, which is evidence of robust electrostatic interaction providing stability to the system. Since the nanobubbles are charged and therefore, the nanobubble coalescence is expected to be negligible. This behavior is similar to that of air/oxygen nanobubbles [13]. However, the composition of the nanobubble interface depends on how ozone decomposition occurs in acidic and alkaline mediums. The ozone decomposition in the presence of OH, may react by the following reaction mechanism [229]:

$$O_3 + OH^- \longrightarrow O_2 + HO^{2-} \tag{4.6}$$

$$O_3 + HO^{2-} \longrightarrow O_2^{\bullet-} + HO^{\bullet} + O_2 \tag{4.7}$$

$$O_3 + O_2^{\bullet -} \longrightarrow O_3^{\bullet -} + O_2^{\bullet}$$
 (4.8)

$$O_3 + H_2O \longrightarrow HO^{\bullet} + OH^- + O_2$$
 (4.9)

Evidently, the reaction between O₃⁻ and [•]OH yields two additional ozone molecules, and

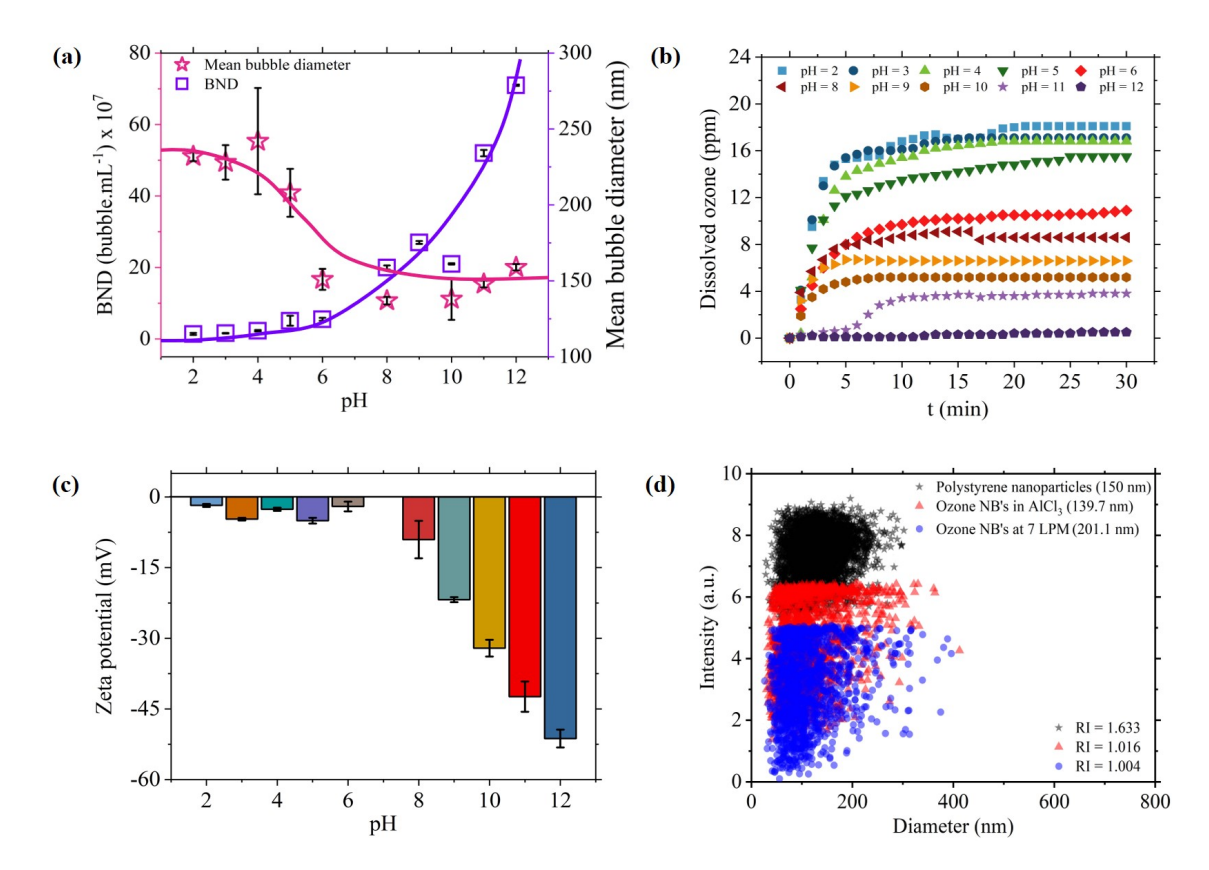


Figure 4.3: Ozone nanobubble generation at acidic and alkaline medium (a) Trends for the bubble number density to that of the mean bubble diameter with respect to the change in the medium (b) The dissolved ozone concentration monitored every one minute for 30 minutes time interval (c) Zeta potential trends at various pH (d) Comparison of the scattering intensities of 100 nm mono-dispersed polystyrene latex beads with ozone nanobubbles produced at 7 L/min (201.1 nm) and in the presence of trivalent salt (139.7 nm).

a new *OH regenerates when the pH of the solution increases. The ozone decomposition in the acidic and alkaline mediums has been discussed extensively elsewhere [230]. The ozone decomposition rate in an alkaline medium is much higher than that of an acidic medium. This fact can be verified by measuring the dissolved ozone by varying the pH of the water (see Fig. 4.3 (b)). The dissolved ozone in an acidic medium is observed to be much higher than that in an alkaline medium due to the fact that ozone decomposes much faster in the alkaline medium. Now, it is reasonably clear that the ozone reacts with water to produce *OH, which may be the plausible reason for a quasi-linear relationship between the negative zeta potential and pH. (see Fig. 4.3 (c)). Since the sliding plane is expected to have a negative charge at pH = 7, lowering the pH value with H⁺ ions (from HCl) neutralizes the negative charge. This brings the absolute value of the negative zeta potential closer to zero, weakening the electrostatic potential between two spherical nanobubbles. The following expression of electrostatic potential is expected to also be valid for nanobubbles [231]:

$$W_R(D) = \frac{64k_B T R \rho_{\infty}}{\kappa^2} \tanh^2(\frac{ze\psi_0}{4k_B T}) exp(-\kappa D)$$
(4.10)

Where $W_R(D)$, R, k_B , T, s, ψ_O , e, ρ_∞ and D are respectively, electrostatic potential, bubble radius, Boltzmann constant, temperature, valency, surface potential, unit charge, bulk ion number density, and inter-spacing distance. In alkaline solutions, however, the negative zeta potential rises, reaching a value of roughly -32 mV at pH = 10. This clearly indicates the higher electrostatic interaction potential in the alkaline medium from Eq. 4.8. In a nutshell, we observed when the water pH was altered prior to the production of the nanobubbles, namely, that alkaline media are more favorable to nanobubble stability than acidic media. This trend is consistent with air/oxygen nanobubbles despite the fact that O_3^- is reactive in water. The products of the ozone with water reaction are ROS and •OH. It may be speculated that excess formation of •OH adsorbed at the nanobubble interface leads to the enhanced negative zeta potential of the nanobubble sample. In other words, the colloidal stability of the nanobubbles in an alkaline medium is higher than the acidic [13] [92], and therefore, the bubble number density of the nanobubbles is increased significantly in the alkaline medium (see Fig. 4.3 (a)). Finally, we reached the conclusion that ozone nanobubbles in alkaline and acidic medium behave similarly to that of air/oxygen nanobubbles. Despite the reactive nature of the ozone, the alkaline medium favors the generation of ozone nanobubbles. However, the dissolved ozone in water was observed to be much smaller in the alkaline medium due to the higher ozone reactivity. On the other hand, in the case of air/oxygen nanobubbles, the dissolved oxygen was not affected by altering the pH of the water.

In addition to the ozone nanobubble dynamics in the presence under salinity conditions and the influence of the pH of the water, we have investigated the refractive index of the ozone nanobubbles. This is particularly important to support the scientific proof of the existence of the nanobubble. The NanoSight NS300 measures the light scattering from the nanobubbles in addition to particle tracking. The time and number averaged value of the highest scattering power P_S(AU) is selected to calculate the refractive index. The instrument calibration is carried out using the reference polystyrene nanoparticles. However, it should be emphasized that in consistent illumination influences NTA instruments frequently and the light scattering also depends on the distance to the optical focus [232]. Measurements are performed using the scattering intensity of polystyrene nanoparticles of four distinct sizes (50, 100, 150, and 200 nm) and a refractive index of 1.630. The measured scattering intensity has been utilized to calculate the scattering cross-section σ_S (nm²) by comparing it with the Mie theory. The particle size, the refractive index of the chosen medium and material, and the wavelength of the light source are also necessary for the theoretical scattering cross-section, which is performed by the open-source MieConScat software. The Mie scattering is an analytical solution to the Maxwell equations for scattering from a spherical dielectric object. The scattering cross-section σ_{Mie} estimated using Mie theory matches the measured P_S value. The linear regression yields the instrument constant, $\sigma_{Mie}/P_S = 0.0673$. Additionally, it should be highlighted that the selected method of utilizing the maximum intensities of the time average and number averages of the particles and the maximum scattering intensity/power

of a single particle was found to have a negligible difference in the calculation of the refractive index for nanobubbles. The refractive index of the ozone nanobubbles in pure water and in the presence of AlCl₃ were estimated to be 1.004 and 1.016, respectively, which is close to the refractive index of gas-filled bubbles. The representative light scattering intensity of the polystyrene nanosphere and ozone nanobubbles are shown in Fig. 4.3 (d). The scattering intensity of the nanobubbles is measured to be smaller than that of the particles. One can explain this by using approximated relations when the particle is smaller than the wavelength of light. The scattering cross-section varies $Q_{scat} \propto 1/\lambda^4$ and refractive index n $\propto 1/\lambda$. This implies that the scattering cross section should vary as $Q_{scat} \propto n^4$ (see Bohren and Huffman [233]). Perhaps this could be the plausible reason for predicting a smaller scattering cross-section. It is also noted that scattering intensity and cross-section follow a proportional relationship. To summarize this part, it can be concluded that the ozone nanobubbles generated in the water and salt solution are indeed nanobubbles as the refractive index of the nano-entities is close to 1.00.

4.3 Mass transfer coefficient by ozone nanobubbles

From the practical standpoint, the volumetric mass transfer coefficient of ozone nanobubbles is required for detailed process design calculations. There are several methods employed for volumetric mass transfer coefficient in the literature, namely, gas absorption, sodium sulfite oxidation method, and physical methods. Since ozone is a reactive gas and it leads to the formation of intermediate chemicals. Therefore, the chemical methods are not suitable for the volumetric mass transfer coefficient measurement. On the contrary, the dynamic desorption and absorption method is a physical method, and it requires only the concentration of the gas in the liquid over time. This work determines the volumetric mass transfer coefficient by measuring the dissolved ozone concentration through a dissolved ozone analyzer. The ozone concentration was measured by passing the ozone gas through the membrane into the liquid tank, where the ozone analyzer was placed for the measurements. The concentration was recorded at every 1-minute interval. The mass balance equation for dissolved ozone can be given as Eq. 4.11:

$$\frac{dC}{dt} = k_L a(C^* - C_t) - k_d C_t \tag{4.11}$$

where C^* (mg/L), C_t (mg/L), k_d , C_0 (mg/L), k_L a are the saturated concentration, concentration at any given time t (min), ozone decomposition rate constant, initial concentration and volumetric mass transfer coefficient respectively. The time t is measured in minutes. At initial condition of t=0, the concentration $C_t=C_O$. The reason for neglecting self-decomposition of ozone is that the entirety of the experiment was conducted while ozone nanobubble generation was taking place inside the reaction vessel. According to the recent literature it is safe to assume that the self decomposition of the ozone would be insignificant as compared to the accumulation of ozone into the system during the ozone nanobubble generation process [141] [216]. Also, Fan et al. [216] and [217] measured the

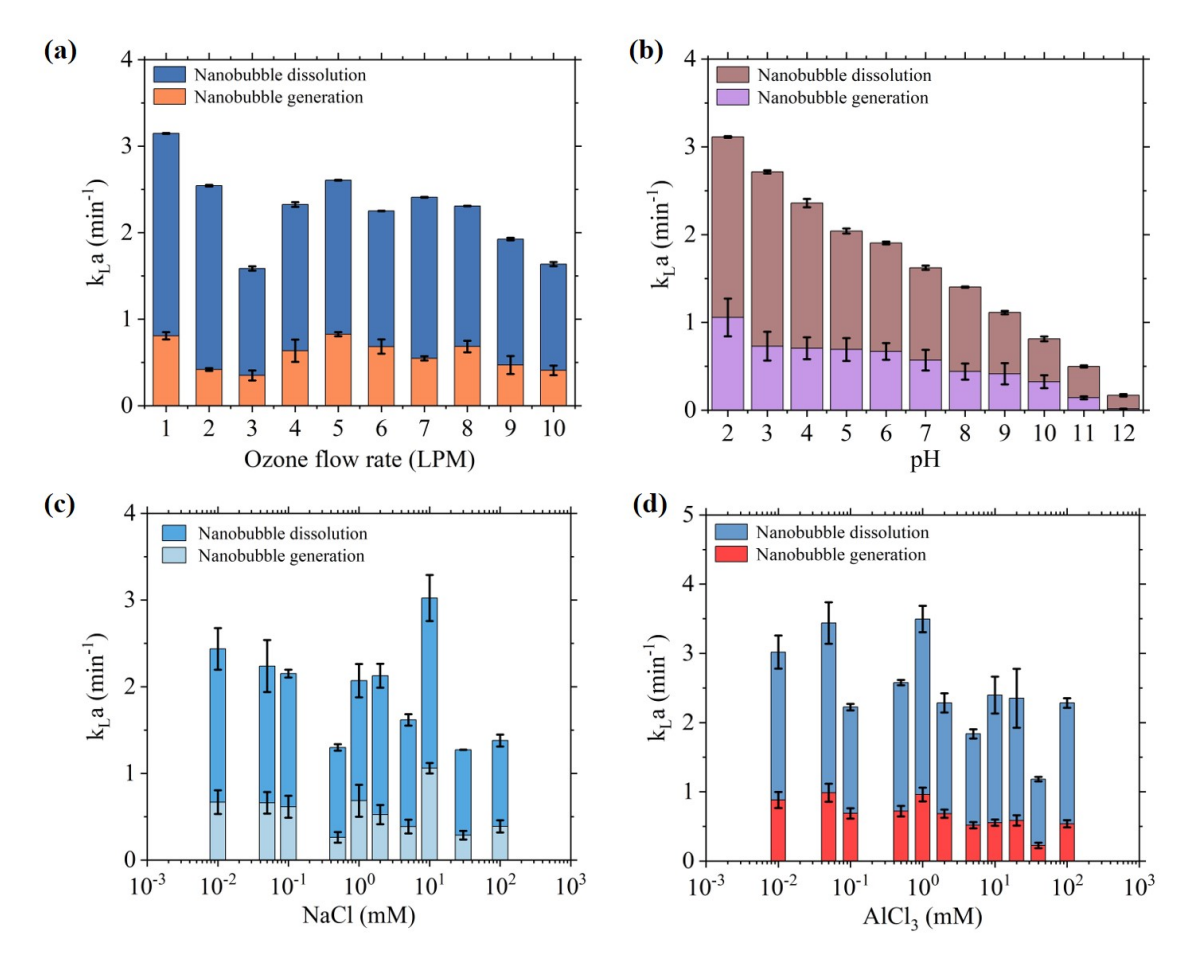


Figure 4.4: Comparative study of the mass transfer coefficients of ozone nanobubbles during nanobubble generation and nanobubble dissolution (a) Comparison of mass transfer coefficient at different ozone flow rates (1-10 L/min) (b) The trends of mass transfer coefficient being the highest at acidic pH and decreasing as the pH of the medium changes to alkaline (c) At varying concentrations of monovalent salt (0.1-100 mM) (d) At varying concentrations of trivalent salt (0.1-100 mM)

mass transfer coefficient where the ozone decomposition rate was neglected as it was very slow. Therefore, integrating Eq. 4.11 for $k_d = 0$ yields the following expression as Eq. 4.12:

$$ln\left(\frac{C^* - C_t}{C^* - C_0}\right) = (k_L a)t \tag{4.12}$$

The ozone concentration is measured over a period of time and eq. (10) is used to estimate the volumetric mass transfer coefficient. The volumetric mass transfer coefficient decreases with the ozone flow rate, pH, and presence of the salt. In other words, the ozone transfer hinders by the high ozone flow rate and the presence of salts. At neutral pH, the maximum and minimum values of $k_L a$ are 0.8 and 0.4 min⁻¹ at 1 and 3 L/min (see Fig. 4.4). On the other hand, the $k_L a$ in the acidic medium approaches 1.0 min⁻¹. Similarly, the $k_L a$ in the presence of salt varies from 0.5 to 1.0 min⁻¹. It should be noted that these $k_L a$ calculated values are during nanobubble generation. This may also contain the contribution of the bigger size of the bubbles. We have carried out a series of dilution experiments similar to the experiments employed in a previous study in order to quantify the volumetric transfer

coefficient that is solely attributed to the ozone nanobubbles [234]. The ozone nanobubbles suspensions were first prepared by our experimental setup and then nanobubbles were characterized by NTA. A 200 mL of degassed water (with no dissolved ozone level) is taken into a beaker, and 50 mL of the ozone nanobubble suspension is mixed in it. After the dilution, we used the following equation Eq. 4.13 to determine the ozone concentration in the diluted sample based on the ozone increment level:

Moreover, we have recorded the rate of increment of dissolved ozone in the diluted solution

$$Ozone\ content(mg/L) = \frac{K(200+50)}{50} = K \times 5 \tag{4.13}$$

with time. These dissolved ozone versus time data have been used for the calculation of ozone mass transfer coefficient. Since it is a polarographic sensor, the water must be flowing to provide the currents needed for the online readings. A tiny amount of the ozone sample solution was extracted, and it was agitated in a beaker using magnetic beads to produce strong currents. The polarographic sensor was positioned close to the beaker wall, where the measurements were taken, and the stirring created the flowing conditions. The experiments were repeated three times to verify repeatability and determine whether the measurements were accurate. To investigate the effect of changing the dilution ratio, further experiments were performed at 1:4 and 1:6 dilution ratios for the reproducibility of the results. The plots obtained have been shown in Fig. B.5 in Appendix A. Similar to the nanobubble generation case, the volumetric mass transfer coefficient decreases with pH, the presence of salt, and the ozone flow rate. The ozone transfer hinders by the low ozone flow rate and the presence of salts during both nanobubble generation and dissolution. At pH = 7, the maximum and minimum values of $k_L a$ are 3.2 and 0.42 min⁻¹ at 1 and 3 L/min. On the other hand, the $k_L a$ in the acidic medium approaches 3.1 min⁻¹. Similarly, the $k_L a$ in the presence of salt varies from 1.5 to 3.5 min⁻¹. From the preceding discussion, it is fairly clear that the mass transfer coefficient by nanobubble dissolution is significantly higher than that of nanobubble generation. The size of the nanobubble during generation can be speculated to be higher than the stable nanobubbles. Therefore, the volumetric mass transfer coefficient is higher during nanobubble dissolution than the nanobubble generation. Smaller bubble provides a large interfacial area for mass transfer, and higher Laplace pressure accelerates the gas diffusion from the nanobubble to the bulk water. The mass transfer enhancement was also attempted by using various membrane contactors in the recent past. For instance, Sabelfeld and Geißen [235] have investigated the ozone mass transfer using linear and helical hollow fiber membrane contactors. The ozone mass transfer rate was reported to bear a positive correlation with increasing gas pressure, ozone gas concentration, and gas and liquid velocities. The helical structure may undergo the secondary flow; therefore, the mass transfer rate was reported to be a 6-fold increase with respect to the linear hollow fiber membrane. Similarly, Wang et al. [236] utilized the polytetrafluoroethylene (PTFE) hollow fiber membrane contactor along with an ultrasound field. Both the membrane contactor and ultrasound enhanced the mass transfer coefficient. Evidently, it may be attributed to the higher interfacial area. The maximum value of the $k_L a$ was reported to be 0.73 min⁻¹ using a PTFE hollow fiber membrane contactor in the presence of the ultrasound, and 0.5154 min⁻¹ at an ozone flow rate of 5 L/min. It is to be noted that these membrane contactor only generates microbubbles. For instance, Wang et al. [236] reported the mean size of the microbubbles to be 52.78 μm . The nanobubble volumetric mass transfer coefficient at an ozone flow rate of 5 L/min was found to be 0.8 min⁻¹, which is $\sim 30\%$ enhancement in the $k_L a$. However, it is to be noted that such comparisons are not highly recommended because the volumetric mass transfer coefficient also depends on the volume of the liquid used for ozonation. In a nutshell, the mass transfer coefficient by nanobubble dissolution is estimated to be 3-fold higher than that of the nanobubble generation. The present analysis also suggests that the nanobubble mass transfer coefficient is significantly higher than the microbubbles.

4.4 Stability of ozone nanobubbles, ROS generation and dye degradation

Nanobubbles possess exceptional longevity, which is the most unique feature that they can survive for days or even weeks [237] [238]. However, ozone is a reactive gas in water, and it decomposes in the water very fast. The half-life of the ozone in water is often estimated to be the order of 20-30 minutes [239]. Under these conditions, it is interesting to examine the ozone nanobubble behavior over a period of time. We have studied the long-term stability of ozone nanobubbles by measuring the bubble number density, mean bubble diameter, zeta potential, and dissolved ozone concentration over three weeks. The NB suspensions were taken at different ozone flow rates ranging from 1-10 L/min. The experimental setup was run for 30 minutes, and the sample solutions were collected in impenetrable glass vials and preserved. The samples were withdrawn and analyzed at particular time intervals. No significant drop in nanobubble density was observed. Similarly, the mean diameter has no noticeable changes (see Fig. 4.5). However, the dissolved ozone concentration drops significantly over a period of time (see Fig. 4.5 (b)). This is attributed to ozone decomposition in water as the half-life of the ozone in water is 20-30 minutes. It is also to be noted that only dissolved ozone is expected to decompose. However, the ozone inside the nanobubble may not decompose due to being isolated from the bulk water. If this hypothesis is true, then ozone can be preserved in the liquid phase in the form of nanobubbles. Evidently, the dissolved ozone concentration gradually decreases and completely disappears in a day or so when we sparge the ozone. On the other hand, the dissolved ozone concentration was reported to be 1-2 ppm even after 21 days. This clearly indicates that ozone nanobubbles preserve the ozone in the water. Hence the lifespan of ozone increases when it is delivered in the form of nanobubbles as compared to the conventional ozone bubbles [1]. The fact that their mean bubble diameters remain constant over time shows that bubble coalescence, bubble rupture, or Ostwald ripening have no major influence. As a result, we believe that the continuous surface charge possessed

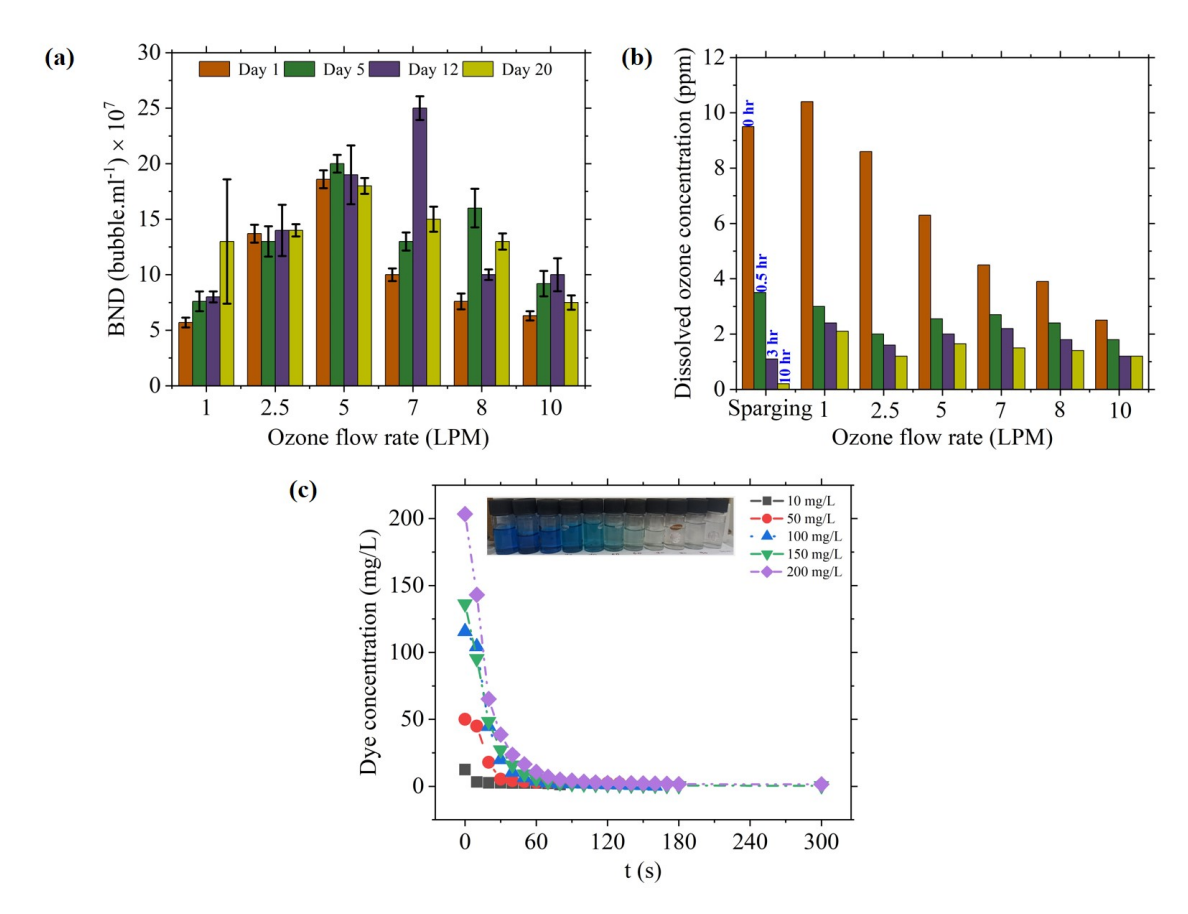


Figure 4.5: Stability of ozone nanobubbles over a time span of 20 days followed by the application of ozone nanobubbles in dye degradation (a) The bubble number density of ozone nanobubbles (b) The dissolved ozone concentration compared to simply sparging the gas in the water (c) Pictorial and experimental degradation of methylene blue dye at different concentration (10-200 mg/L) using ozone nanobubbles.

by the nanobubbles is responsible for their stability [13].

Fig. 4.6 illustrates the mechanism of understanding the behavior of ozone nanobubbles during long term stability over 20 days and variation in the dissolved ozone upon dilution of nanobubble solution in degassed water. The ozone nanobubbles are used to degrade the standard methylene blue dye. Fig. 4.5 (c) shows the degradation kinetics for varying initial concentrations. The concentration of the dye is determined by UV-spectrophotometry, and clearly, the complete degradation of the dye was observed for all the initial concentrations. The complete degradation of dye was verified using the LC-MS analysis. The samples were analysed over a time period of four minutes having measurements done at 0, 1, 2, 3 and 4 minutes. Fig. 4.7 shows a full mass spectrum scan obtained from a 100 mg/L 1 solution of methylene blue The peak at m/z = 284 corresponds to the M^+ molecular ion of methylene blue The peak at m/z = 285 is a result of C^{13} isotopes in the methylene blue molecule [240]. Because the strong oxidizing free radicals act on different MB atoms, the degradation pathway can be divided to route I and route II [241]. The peak at m/z 279 corresponds to loss of methyl groups from MB. The peaks at m/z 319 and 279 are due to consecutive additions of hydroxyl ions in the MB molecule The breaking of the MB molecule was suggested by the presence of peaks at m/z = 167, 122 and 143.

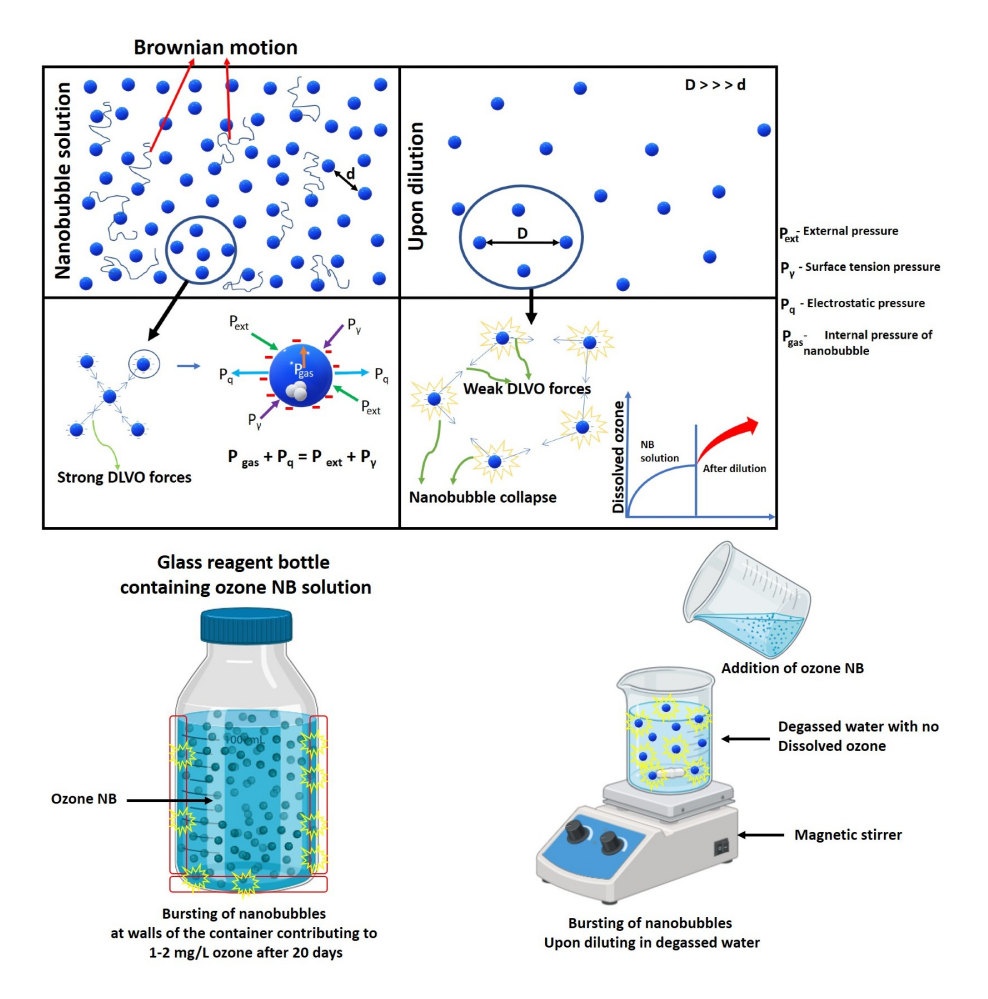


Figure 4.6: Mechanism of understanding the behavior of the ozone nanobubbles during long term stability (20 days) and upon diluting the nanobubble solution into degassed water at a particular dilution ratio (1:5, 1:4, 1:6).

From the mass analysis the degradation pathway is shown in Fig 4.7 [242]. The cation inside the MB molecule underwent partial isomerization, resulting in the formation of product P3. In P3 the methyl group was bonded to N, making it susceptible to attack by OH. In an alternative scenario, the cation underwent demethylation resulting in the production of product P5, as a consequence of being subjected to a strong shock wave during the processes of thermal cracking and bubble rupture [243]. Moreover, an additional mechanism of degradation included the hydroxylation of MB molecules by hydroxyl radicals (•OH), leading to the production of polyhydroxy compounds. aforementioned compounds underwent further nitration and demethylation processes by OH oxidation and cavitation phenomena, resulting in the formation of products P2 and P4. Furthermore, the carbon-sulfur bond experienced cleavage, leading to the disruption of the ring structure and the subsequent generation of products P6, P7, and P8. Finally they are mineralized into some inorganic substances such as CO₂, H₂O, NO₃⁻ and SO₄²-[244] [245] [215]. All the products formed are mentioned in Table 4.1. The total time required to degrade the 30 mg/L dye was 110 seconds by ozone nanobubbles whilst the same sample required 20-25 minutes by simple ozonation by spargers. As noted earlier,

Product	m/z	Chemical formula
P1	319	$C_{16}H_{21}N_3O_2S$
P2	304	$\mathrm{C}_{16}\mathrm{H}_{20}\mathrm{N}_{2}\mathrm{O}_{2}\mathrm{S}$
P3	285	$C_{16}H_{19}N_3S$
P4	279	$\mathrm{C}_{13}\mathrm{H}_{15}\mathrm{N}_{2}\mathrm{O}_{3}\mathrm{S}$
P5	256	$C_{14}H_{14}N_3S$
P6	167	$C_8H_{11}NO_2$
P7	143	$C_5H_6NO_2S$
P8	122	$C_7H_{10}N_2$

Table 4.1: Degradation products of methylene blue

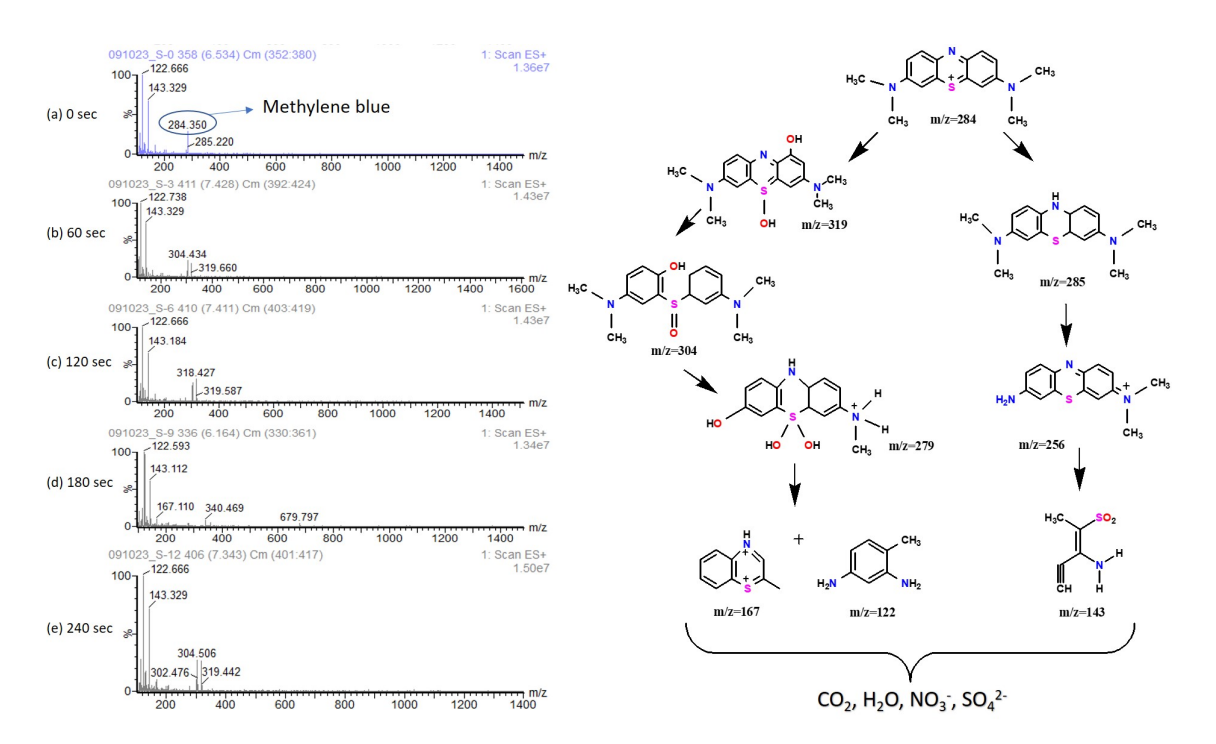


Figure 4.7: LC-MS analysis (a) m/z MS spectra at every 1 minute (b) Possible degradation pathway of methylene blue.

the ozone reacts with water and forms reactive oxygen species (ROS). The reactive oxygen species are responsible for the dye degradation. The ozonation process is the gas absorption with a chemical reaction where the overall degradation rate depends on both mass transfer and the reaction kinetics[73]. The rate-determining steps are often the slowest step, and therefore, the mass transfer becomes a rate-limiting step[74]. The dye degradation is facilitated by ozone nanobubbles due to the extraordinary properties of the nanobubbles: (i) the high volumetric mass transfer coefficient fosters the overall dye degradation rate (ii) high inner Laplace pressure enhances the formation of the ROS and hydroxyl radical (iii) The nanobubble provides an active surface area for the chemical reaction which also contributes to overall dye degradation rate. The ozone decomposition reactions speculated the formation of reactive oxygen species (ROS) like O_2^{\bullet} . We have investigated the radical formation by electron spin resonance spectroscopy measurements. Two types of solutions were used, namely pure water and ozone nanobubbles. Fig. 4.8 shows the corresponding

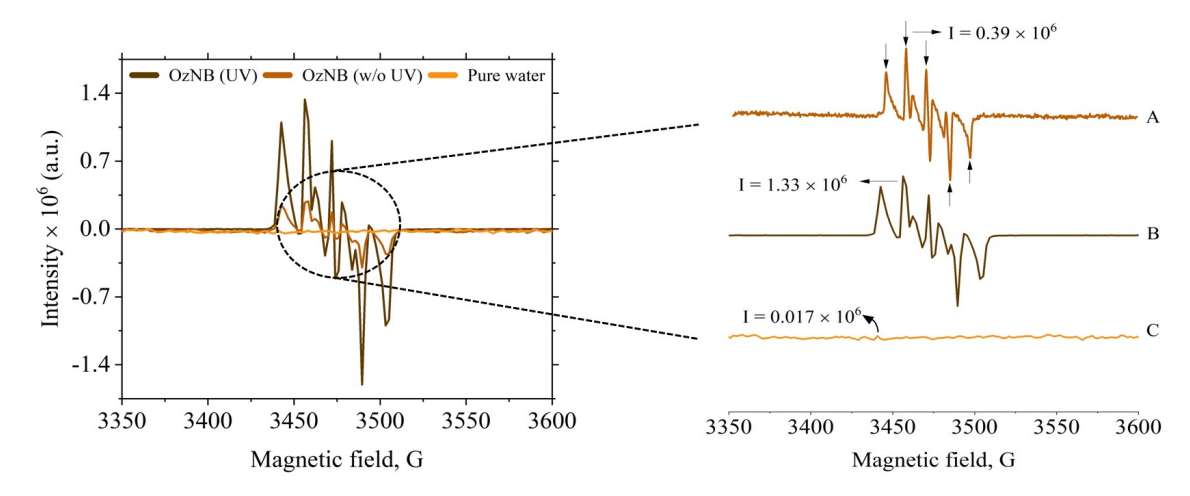


Figure 4.8: ESR spectrum of the radical adduct of DMPO. The ESR measurements were done for ozone nanobubbles in comparison to pure water taken as a control sample. The left side of the figure shows the cumulative peaks at the given magnetic field. The right side of the figure depicts the magnified versions of the peaks arranged in stacks to compare the intensity of the curves at various conditions.

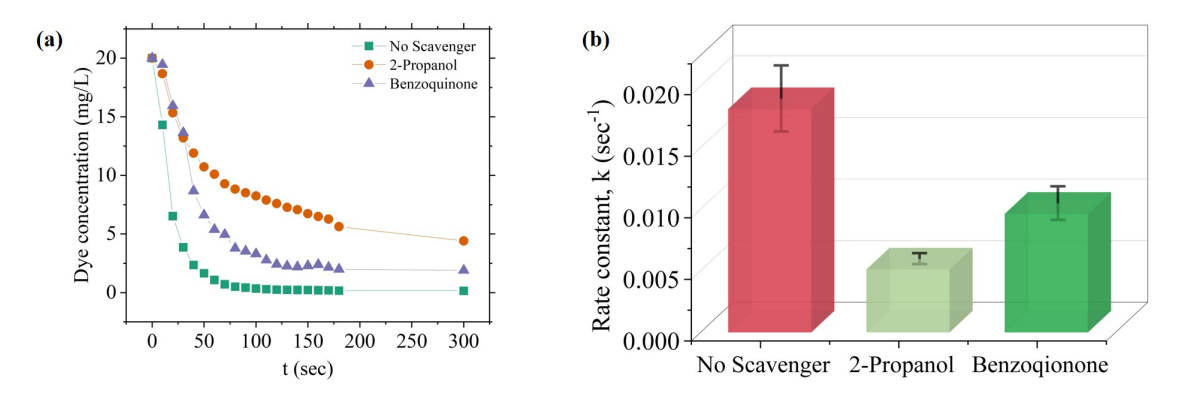


Figure 4.9: Radical quenching experiments (a) Dye degradation trends in the presence and absence of scavengers (b) Rate constant depicting the domination presence of the reactive oxygen species.

ESR spectra. It can be seen that no peaks are being formed in the case of water. This implies that there is no formation of reactive oxygen species. On the other hand, the peaks are formed in the case of ozone nanobubbles. Also, when measurements were performed without UV light, the spectra formed were of very low intensity. But when irradiated with a UV light source, the intensity increased to a greater extent. The ESR spectra reported here resemble the spectra of the O_2^{\bullet} . In summary, ozone nanobubbles offer enhanced volumetric mass transfer coefficient together with high inner Laplace pressure, which fosters the formation of ROS. In addition, the nanobubble interface provides an active surface area for dye degradation. All these factors contribute to and accelerate the overall rate of dye degradation.

In this study, radical quenching experiments were performed in order to identify the reactive oxygen species that were formed during the process of ozonation. 1 mM of 2-Propanol and 1 mM of Benzoquinone (BQ) were used as scavengers for trapping the reactive oxygen species such as hydroxyl radical (${}^{\bullet}$ OH) and superoxide (${}^{\circ}$ O₂) respectively.

All experiments were conducted at pH 7. As depicted in Fig 4.9 (a), the concentration profile for the degradation of methylene blue dye (20 mg/L) fitted very well with the pseudo first order kinetics correlation. Fig 4.9 (b) shows the values of the rate constant for the pseudo first order reaction. From the graph, it was observed that the value of the rate constant decreased to 0.00511 sec⁻¹ on the addition of 2-Propanol thereby indicating the presence of (•OH) radicals and their dominant role in the degradation of dye. With the addition of BQ, the k value dropped to 0.00676 sec⁻¹ suggesting that O₂•- also contributed majorly in the degradation of dye. Whereas, when no scavenger was added, the k value came out to be 0.01812 sec⁻¹ which confirms the formation of the reactive species during the process. The results were in well agreement with the previous reports in which these ROS coexisted in the nanobubble solution [94].

Chapter 5

R&D 2: Tetracycline degradation for wastewater treatment based on ozone nanobubbles advanced oxidation processes (AOPs)

This chapter deals with the degradation of antibiotic tetracycline, ozone nanobubble generation, degradation kinetics, pathways and different water compositions. The various parameters such as ozone flow rates, tetracycline concentrations, effect of pH and salts have been investigated. Comparison efficiency of ozone nanobubbles to conventional bubbles and ozone microbubbles has been studied. Cost estimation of the process of this study has been compared to some conventional process involved in degradation of tetracycline. The presence of reactive oxygen species has been studied on the basis chemical method for the detection of ROS by radical scavenging experiments.

5.1 Effect of TC dosage on degradation kinetics

The generation of ozone nanobubbles was performed using nanopore diffusion methods. Ozone nanobubbles were characterized by nanoparticle tracking analysis (NTA), as shown in Fig. 5.1. The bubble number density shows a positive correlation with the ozone flow rate. Furthermore, to ascertain the contamination, the nanobubble refractive index (RI) was estimated, and the refractive index was close to unity, confirming that the measurement relates to nanobubbles [3]. The stability of ozone nanobubbles was studied over a period of 30 days (results presented in Appendix B Fig. C.7). Nanobubbles seem to disappear at a slower rate at high concentration of ozone nanobubbles as in the case of 10 L/min. Even after 30 days, a considerable amount of nanobubbles are still present in the solution. Meanwhile, the mean bubble diameter experiences a relatively small but significant increase from 230 to 260 nm in case of 2.5 L/min of ozone flow rates.

To study the effect of the initial concentration of TC and ozone intake, the experiments were performed at different reaction conditions. The initial concentrations of TC were varied from 100-400 mg/L. The flow rates of ozone were taken from the start of 2.5 standard litre per minute (L/min), 5 L/min to the highest of 10 L/min values. The setup was run in a re-circulation mode and ozone was fed to the reactor to produce ozone nanobubbles. The

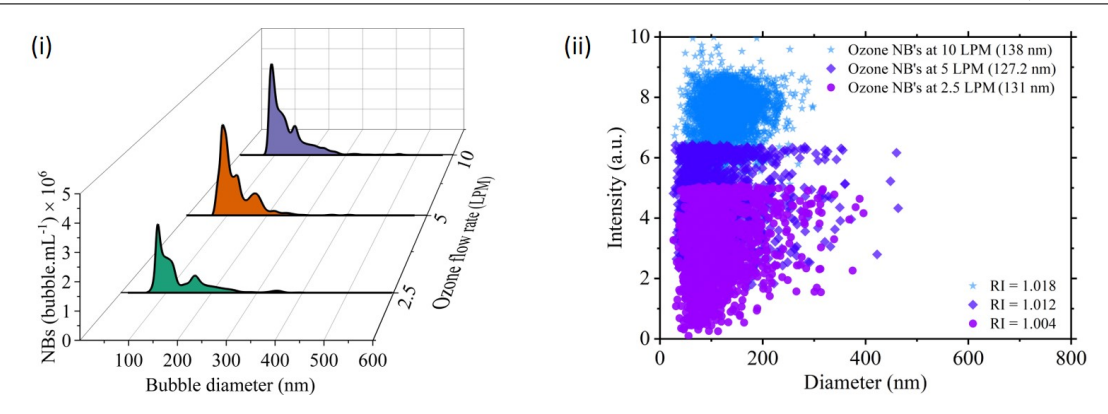


Figure 5.1: Effect of ozone flow rate on nanobubble generation (i) bubble size distribution (ii) scattering intensity of nanobubbles tracked at different flow rates.

amount of ozone being fed to the reactor plays a major role in the degradation process as it is an important aspect on which the degradation is dependent. The nanobubble characterization at different ozone flow rates was done using NTA (Nanoparticle Tracking Analysis, Malvern). The results of the characterization are depicted in Fig. 5.2. Based on the obtained results, it can be clearly depicted that at 10 L/min, the highest amount of nanobubbles are being formed with the highest intensity. The results for varying initial concentration of TC and ozone intake are depicted in Fig. 5.2 where the trends for the decrease in the concentration of TC are shown. From Fig. 5.2 (i), (ii), and (iii), it can be evaluated that the lower the concentration of the antibiotic, the lesser is the time needed for the quantitative degradation. The initial concentration of 100 mg/L achieves 100% degradation within 15 minutes in the case of 10 L/min ozone flow rate. Subsequently at 5 and 2.5 L/min, the time taken is 30 and 35 minutes respectively. Following this, as the concentration of TC is increased from 100 to 400, the time needed to obtain 100% degradation also increases. This phenomenon is observed in respect to all studied conditions (ozone flow rate values). The rate constant was calculated for each set of experiments and their values were compared. Fig. 5.2 (iv), (v) and (vi) show that the reaction kinetics follows the second order reaction with coefficient of determination, R^2 0.98. It can be clearly noticed, that at 10 L/min the reaction rates were the highest with a value of 0.01285 L mg⁻¹min⁻¹ at 100 mg/L of TC.

Overall, based on this part of experiments, it can be concluded that the best degradation results were achieved at 10 L/min as the highest rate constants were achieved here. The probable reason for this would be the amount of dissolved ozone present at that particular flow rate. Since ozone is acting as the prime free radical source responsible for the degradation of tetracycline, the amount of ozone being generated during these experiments plays a vital role. The online measurements were done for the dissolved ozone during the degradation process at each initial concentration of TC as well as when no antibiotic was present. Also, the molar ratio (Ozone/TC), degradation efficiency of TC and molar excess of ozone were compared to find out the plausible reason for the degradation. The results obtained are depicted in Fig. 5.3. The results depicted in Fig. 5.3 were presented for a particular flow rate at 10 L/min. Fig. 5.3 (i) presented the amount

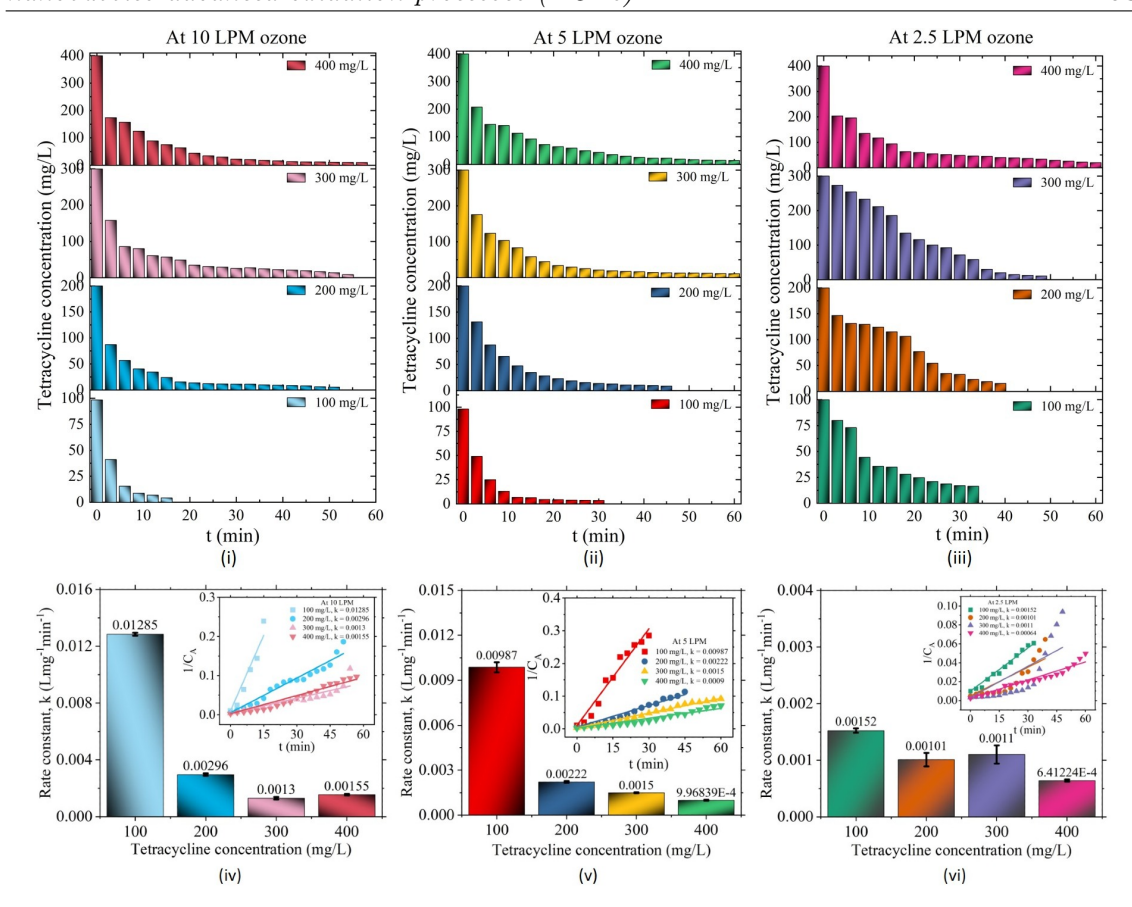


Figure 5.2: Effect of Initial concentration (100-400 mg/L) and different ozone flow rates (i) 10 L/min (ii) 5 L/min (iii) 2.5 L/min and kinetics with rate constant k at (iv) 10 L/min (v) 5 L/min (vi) 2.5 L/min ozone flow rates.

of dissolved ozone present when no antibiotic was there compared to dissolved ozone at various concentrations of TC when degradation processes were taking place. The amount of excess ozone (mmol/L) at every point of time during the degradation process is illustrated. From Fig. 5.3, it can be concluded that the amount of excess ozone was being produced at each point of time. At 100 mg/L of TC concentration, since lower concentrations of contaminants were present here, a lower amount of dissolved ozone was utilised to degrade the contaminant. This can further be explained through online dissolved ozone measurements. The dissolved ozone concentration when no TC was present to various TC concentrations (100-400 mg/L) are presented in Fig. 5.3 (ii). From the graph, it was evident that with increase in TC concentrations, the dissolved ozone decreased as compared to the case of without TC. The difference between these concentrations would provide the amount of excess ozone present at each point as shown in Fig. 5.3 (i). Upon addition of TC from 100-400 mg/L, the consumption of ozone to degrade the contaminant has been depicted here where we found out that higher amount of ozone is required at higher concentrations of TC. So, out of 12 ppm of ozone concentration, 7 ppm has been consumed for the degradation of TC while the rest 5 ppm is still present as in Fig. 5.3 (ii). Therefore, at a low concentration of TC, the amount of excess ozone was measured to be more as compared to those at higher concentrations e.g. 400 mg/L. Also, the dissolved

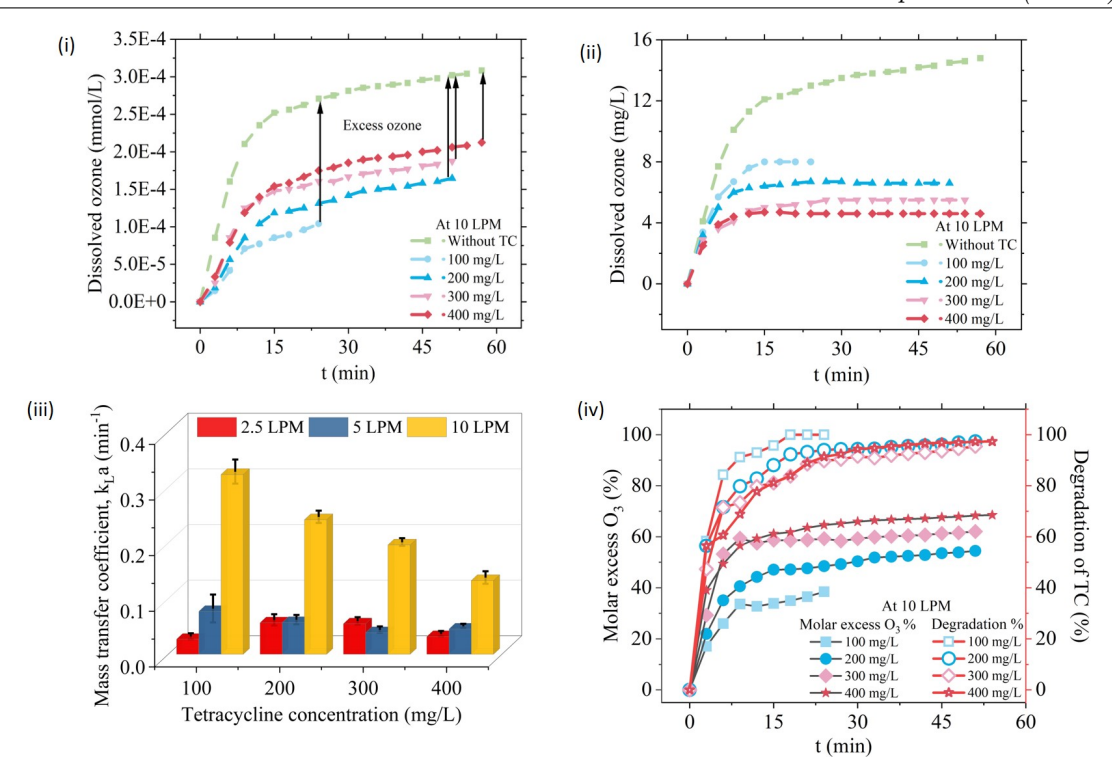


Figure 5.3: (i) Dissolved ozone measurements in pure water and during tetracycline degradation (100-400 mg/L) (ii) highest dissolved ozone attained at different ozone flow rates at different TC concentrations (iii) Mass transfer coefficient corresponding to the ozone concentrations at different ozone flow rates and different concentrations of TC (100-400 mg/L) (iv) Comparison of molar excess of O_3 (%) to degradation efficiency (%) of TC (100-400 mg/L).

ozone measurements at each point of time during the degradation has been presented in Appendix B (Fig. C.3) with comparison to when no TC was present at every ozone flow rate and TC concentration. The mass transfer coefficient for each concentration of TC at different flow rates is shown in Fig. 5.3 (iii). The mass transfer coefficients were measured and it can be inferred that higher amount of dissolved ozone concentrations lead to increased MTC rates. At 10 L/min, 8 ppm concentration of ozone is achieved with a mass transfer coefficient of 0.32309 min⁻¹. On the other hand, lower dissolved ozone concentrations at 2.5 and 5 L/min resulted in lower MTC values. Therefore, it can be concluded that higher the ozone flow rates, more is the dissolved ozone concentration leading to greater mass transfer rates and better degradation kinetics at the corresponding flow rates of ozone. This can be explained by the fact that higher concentrations of nanobubbles were being formed at higher flow rates. Also, increased flow rate leads to higher turbulence which creates better mixing conditions. This further helps in increasing the ozone mass transfer coefficients. The molar ratio (Ozone/TC) at each point of time was calculated and is depicted in Fig. 5.3 (iv). Increasing trends of molar ratio prove that excess ozone is present at each time during the degradation process. When the degradation efficiency of TC was compared to excess molar ozone as shown in Fig. 5.3 (iv), it could be seen that each point of degradation % corresponds to molar excess ozone %. Based on these observations, it can be concluded that molar excess of ozone serves as the limiting factor responsible for the degradation of the antibiotic. Similar trends were achieved for 2.5 and 5 L/min ozone flow rates (presented Appendix B Fig. C.2).

5.2 Degradation characteristics of TC in alkaline and acidic medium

The initial pH of the solution plays a vital role in the degradation mechanism of TC as it affects the formation of reactive radicals during the degradation and the chemical activity of the ozone bubbles being formed during the process[142] [94]. Fig 5.4 represents the experiments performed under various pH values. The effect of pH was carried out at a constant concentration of TC (200 mg/L) and constant ozone flow rates of 10 L/min. The pH values were varied from 4-11. Ozone molecules under acidic conditions may undergo the following reactions [12]:

$$O_3 \longrightarrow O + O_2$$
 (5.1)

The dissociation process produces the O atom, which is thought to be the precursor for •OH in acidic ozone solutions [246].

$$O + H_2O \longrightarrow 2OH^{\bullet}$$
 (5.2)

On the other hand, ozone in the presence of OH⁻ (basic conditions) may be activated by the following mechanism [229]:

$$O_3 + OH^- \rightarrow O_2 + HO_2^-$$
 (5.3)

$$O_3 + HO_2^- \rightarrow O_2^{\bullet -} + {}^{\bullet}OH + O_2 \tag{5.4}$$

$$O_3 + O_2^{\bullet -} \longrightarrow O_3^{\bullet -} + O_2^{\bullet} \tag{5.5}$$

$$O_3 + H_2O \longrightarrow {}^{\bullet}OH + OH^- + O_2 \tag{5.6}$$

From Fig. 5.4 (i), TC degradation reached a value of 96.05% at pH = 4 while the degradation efficiency decreased as pH was raised to 11 with 94.39%. Acidic medium favors the degradation of TC which is consistent with literature [247] [248]. The plausible reason for the efficient degradation could be the high mass transfer coefficient of ozone at low pH. Furthermore, the reaction followed pseudo-second-order kinetics as depicted in Fig. 5.4 (ii) with rate constant k values being highest at pH 4 (0.00266 L mg⁻¹min⁻¹) and lowest at pH 11 (0.00179 L mg⁻¹min⁻¹). The concentration of dissolved ozone increases as the pH drops. Similar trends were reported [249]. When the pH dropped from 6.8 to 2.7 at 35°C, the solubility of ozone in water increased from 6.8 ppm to 39.6 ppm. Also, Henry's law constant of ozone tends to decrease at lower pH thereby leading to a higher solubility of ozone at acidic pH [250] [251]. While at basic pH, the presence of OH catalyses the decomposition of ozone leading to decreased dissolved ozone concentrations [252].

The pH of the solution plays a significant role as it affects the ionization of tetracycline

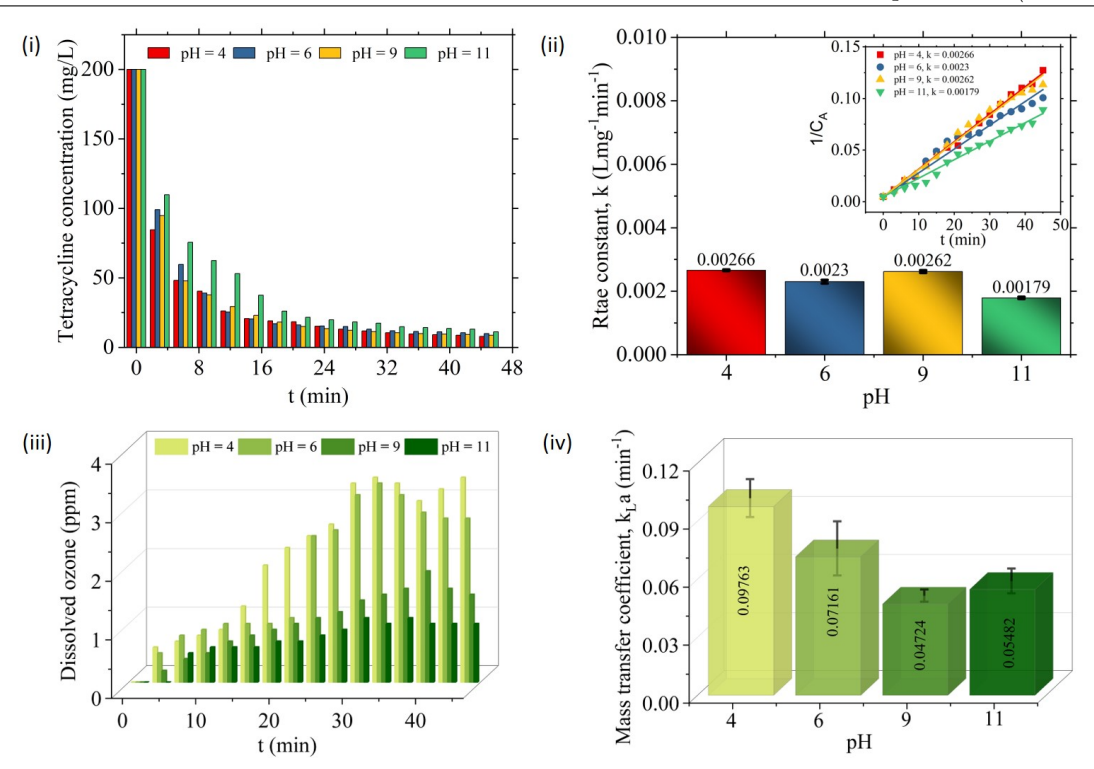


Figure 5.4: Effect of acidic and alkaline mediums on degradation of TC (i) Degradation of 200 mg/L TC under different pH conditions (ii) Rate constant k under different pH conditions (iii) Online dissolved ozone measurements during degradation of TC (iv) Mass transfer coefficient of ozone at various pH conditions.

due to its pKa values. The pKa values for TC are pKa1 (3.3), pKa2 (7.7) and pKa3 (9.5) [253]. When pH < pKa1 i.e. pH < 3.3, TC tends to exist in its protonated form (TC⁺) and most TC molecules have not lost their first proton yet. When pKa1 < pH < pKa2, TC is partially ionized as it is present in both forms ((TC⁺ and TC⁻). At pKa2, when pH > 7.7, TC tends to exist in deprotonated form (TC⁻) where most TC molecules have lost both protons. The degradation efficiencies were found to be almost similar at pH 4 and 9 with a value of 96.05% and 95.59% respectively within 35 minutes. This can be explained by the fact that dissolved ozone concentration was found to be the highest in respect to these two pH values. Further, their mass transfer coefficients were also the highest among other pH values as depicted in Fig. 5.4 (iv). The pH plays an important role in the activity of ozone as the mechanism of free radical generation changes with the pH. There are two mechanisms possible in which the ozone reacts at different pHs. In acidic pH, direct ozone attack is prominent while in basic mediums, ozone decomposes to form OH radicals and ROS which further react with the organic compounds [218]. However, the degradation efficiencies at pH 4 and 9 were insignificant as after 15 minutes of ozonation, degradation of tetracycline reached more than 90 %, and all slightly increased to approximately 96%. Only at pH = 11, the degradation curve is different from those of other pH values. It follows from the amount of dissolved ozone (Fig. 5.4 (iii)). It can be elucidated that no dissolved ozone was detected during the first five minutes of the experiments, beyond which it gradually increased from 0.5 to 1.2 ppm at the end of the reactions. While, for

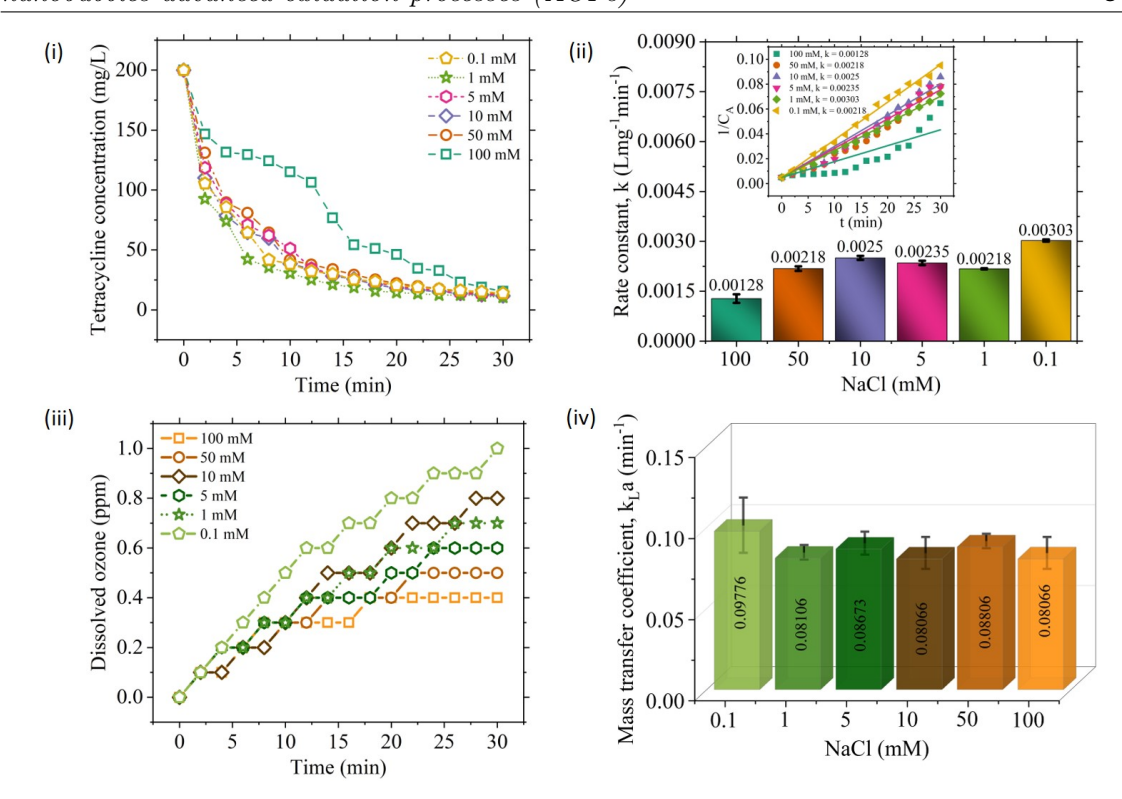


Figure 5.5: Influence of monovalent salt addition on degradation of TC (i) Degradation of 200 mg/L TC under different NaCl concentrations (0.1-100 mM) (ii) Rate constant k at under different NaCl concentrations (iii) Online dissolved ozone measurements during degradation of TC (iv) Mass transfer coefficient of ozone at various salt concentrations.

other pH values the dissolved ozone ranged from 3-4 ppm. The rate constants suggest that there was a negligible difference in the kinetics of the degradation reactions. Thus, TC was readily degraded by direct ozonation ($^{\circ}$ OH generated by ozone and H₂O) throughout the procedure, making the difference in TC degradation at different pH levels insignificant.

5.3 Degradation kinetics in the presence of monovalent salts

To investigate the effect of the presence of salts, monovalent salts were selected for this particular study. A sodium chloride (NaCl) was used in the concentration range of 0.1-100 mM. The experimental setup was run for 30 minutes and the concentrations were measured within intervals of 3 minutes intervals. The dissolved ozone concentrations were also measured online during the experiments. A presentation of how the dissolved ozone plays a major role is depicted in Fig. C.4 (in Appendix B). From the trends, it can be stated that the ozone concentrations decrease in presence of salts as compared to that in DI water (Fig. C.4 (i), Appendix B). Also, dissolved ozone curves were compared when only salt was present to ozone concentration during degradation of TC. The graphs showed (Fig. C.4' (ii) and (iii), Appendix B) the difference in the dissolved ozone thereby claiming the amount of ozone being consumed for TC degradation. The results for the effects of salt on the degradation of TC are represented in Fig. 6. Following the observations from Fig. 5.5

(i), it can be exclaimed that the presence of salts or an increase in the concentration of salts declines the overall degradation of TC. The degradation of tetracycline majorly depends upon the amount of ozone being dissolved by ozone nanobubbles which has been displayed in Fig. 5.5 (ii). Dissolved ozone is the highest at 0.1 mM salt concentration with 1 ppm ozone concentration followed by 0.75 ppm at 10 mM salt concentration. Similarly, the mass transfer coefficients decrease with an increase in salt concentration (see Fig. 5.5 (iii)). The highest mass transfer coefficient values were obtained at 0.1- and 1-mM concentrations of salt and the degradation rate is highest at these two concentrations. The plausible mechanism for this can be explained by phenomenon termed as salting out effect.

The presence of salts affects the efficiency of ozone dissolution and its ability to react with the organic contaminant (TC). Higher salt concentrations reduce the contact time between ozone and TC because of the low solubility, leading to lower degradation rates and overall treatment efficiency. The dissolved ozone measured decreased with increase in salt concentrations, owing to the higher ozone decomposition rates in the presence of chloride ions. Based on the reaction kinetics, it was observed that the degradation of the TC by O₃ nanobubble follows the pseudo 2nd order reaction kinetics as shown in Fig. 5.5 (ii). The reaction rate constant was measured for various salt concentrations and it was almost the same with a negligible difference as depicted by the concentration profiles overlapping each other except for 100 mM salt concentration. Now, comparing the degradation efficiencies when no salts were present in the system, it can be observed that in the absence of salts the degradation was higher with 98.44% while when the salt is added, the degradation efficiency lowers down to 94%, thereby inhibiting the role of ozone in the presence of salts [254]. Furthermore, in the presence of salt, ozone also reacts with chloride ions, and therefore, it hinders the degradation of TC. The ozone reacts with chloride ions by following a reaction mechanism [255] [256]:

$$O_3 + Cl^- \longrightarrow O_2^{\bullet} + OCl^- \tag{5.7}$$

$$O_3 + OCl^- \rightarrow 2O_2^{\bullet} + Cl^- \tag{5.8}$$

These two equations (14 and 15) might be used to simulate ozone disintegration in the presence of chloride ions, which would explain the decrease in ozone lifespan and further its dissociation to superoxide radical ions. Compared to the hydroxyl radicals and ozone itself, the oxidation potential of superoxide radicals is lower. Therefore, presence of salts in the reaction systems dissociates ozone into less oxidation potential radicals thereby decreasing the overall degradation efficiency of TC.

5.4 Degradation efficiency of TC by different methods

To study the effect of ozone in different forms, experiments were carried out under 4 different reaction systems namely (i) O_3 NBs (ii) O_3 MBs (iii) O_2 MBs (iv) O_3 Sparging. The effect of adding H_2O_2 to each of the above reaction systems was also evaluated. H_2O_2 is considered to increase the overall oxidation potential when combined with ozone

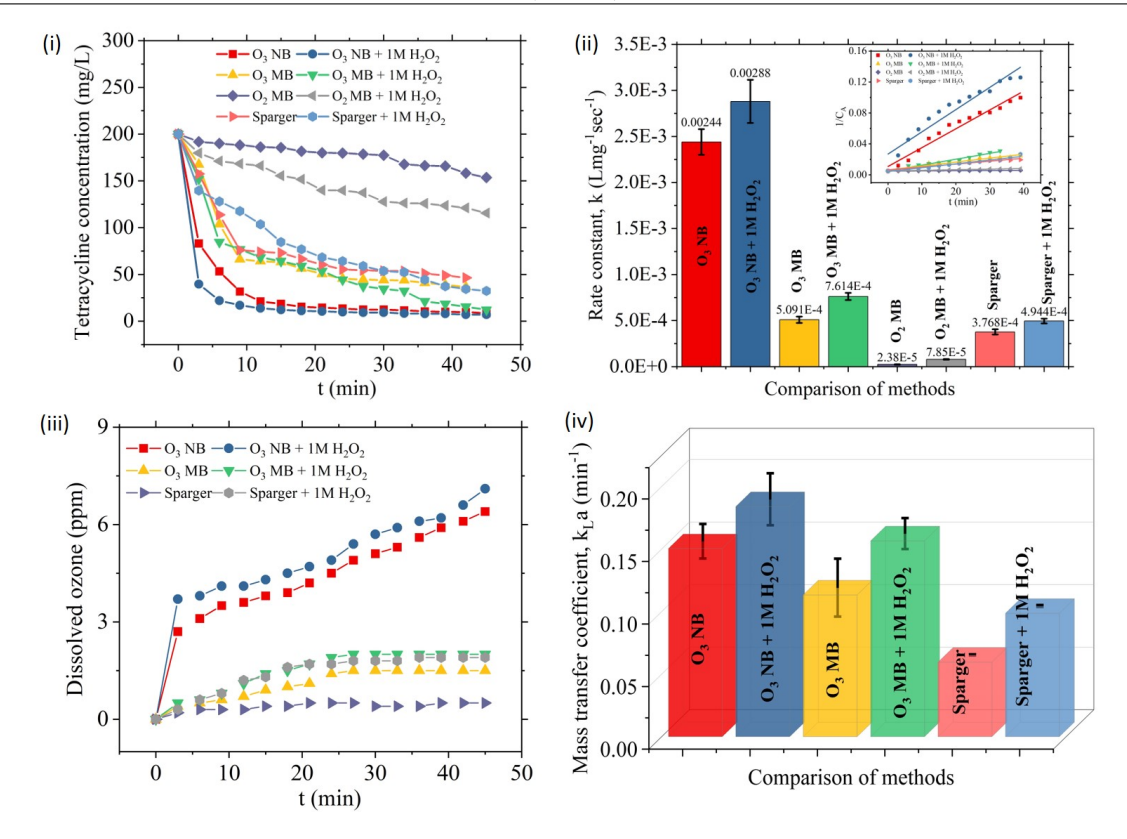


Figure 5.6: (i) Comparison efficiency of different methods (ii) Pseudo second-order rate constants (iii) Dissolved ozone in ppm during each experimental condition (iv) Mass transfer coefficient for ozone at a constant concentration of Tetracycline (200 mg/L) at 10 L/min ozone and oxygen flow rates.

in AOPs. The first system studied the effect of O₃ NBs alone and in combination with 1 M H₂O₂. The second system consisted of O₃ MBs (prepared by MNB400 + SBT50, Riverforest Corp) alone and in the presence of 1 M H₂O₂. In the third system, the effect of oxygen MBs was measured in absence and presence of 1M H₂O₂. The fourth system comprised of ozone being sparged directly to the stock solution through a sparger (G4 fritz quartz disc, 10 μ m) in absence and presence of 1M H_2O_2 . As described in the experimental setup, the stock solutions were prepared in Milli-Q water with an initial value of tetracycline to be kept constant at 200 mg/L. The flow rates of oxygen and ozone were also conserved at 10 L/min. The experiments were run for 45 minutes and the change in concentration of TC, rate constants, and mass transfer coefficients were measured. All the results of the above-mentioned experiments are depicted in Fig. 5.6. The degradation curve represented in Fig. 5.6 (i) clearly illustrates that no significant amount of degradation of TC was observed in the case of oxygen microbubbles as compared to the ozone microbubbles through sparging. Within 45 minutes, 23.17% degradation was achieved while the degradation increased to 42.17% in case when O₂ MBs were combined with 1M H₂O₂. Whilst in the case when ozone was being sparged to the reactor, degradation efficiency of 76.75% was attained while adding 1M H₂O₂ increased the degradation efficiency to 81.75%. The effect of adding hydrogen peroxide served as a classic description of the peroxone process [257] [258]. By means of electron transfer,

the H_2O_2 will facilitate the O_3 's breakdown; conversely, the O_3 will activate (a so-called peroxone process) the H_2O_2 , producing ${}^{\bullet}OH$ and $HO_2{}^{\bullet}$ which can be shown in Eq. 15 [257]:

$$H_2O_2 + O_3 \longrightarrow HO^{\bullet} + HO_2^{\bullet} + O_2$$
 (5.9)

Further, when O_3 reacts with a ${}^{\bullet}OH$, it can produce less reactive radicals like $HO_2{}^{\bullet}$, which O_3 can then transform into ${}^{\bullet}OH$ and O_2 as shown in Eq. 17 and 18 [259] [260]:

$$HO^{\bullet} + O_3 \longrightarrow O_2 + HO_2^{\bullet}$$
 (5.10)

$$O_3 + HO_2^{\bullet} \longrightarrow 2O_2 + HO^{\bullet}$$
 (5.11)

Thus, adding H₂O₂ enhances the degradation efficiency. To study the advantage of using ozone nanobubbles, comparison of ozone nanobubbles with microbubbles was also studied. For O₃ MBs, the degradation efficiency was 83.85% while in case of 1M H₂O₂, it increased to 93.85% as shown in Fig. 5.6 (i). Out of the four systems compared, the best degradation results were achieved for O₃ NBs as the degradation efficiency reached a maximum value of 95.73% and 96.51% for O_3 NBs + 1M H_2O_2 . These results can further be concluded by calculating the rate constants as shown in Fig. 5.6 (ii). From Fig. 5.6 (iii) it can be concluded that the highest concentration of dissolved ozone was produced in the presence of ozone nanobubbles + 1M H₂O₂ with the concentration of 7.1 ppm which further decomposes and forms radicals as mentioned above due to the peroxone reactions. In case of microbubbles, the dissolved ozone 1.5 and 2 ppm in absence and presence of 1M H₂O₂. Subsequently, when ozone was sparged in the presence or absence of 1M H₂O₂, the concentrations reached 1.9 and 0.5 ppm, respectively. Depending upon the concentration measurements, the mass transfer coefficient was calculated for each system as depicted in Fig. 5.6 (iv). Clearly, the mass transfer coefficient was the highest for ozone nanobubbles $+ 1 \text{M H}_2\text{O}_2 \text{ (0.16401 min}^{-1}), \text{ O}_3 \text{ NBs alone (0.15045 min}^{-1}), \text{ O}_3 \text{ MBs} + 1 \text{M H}_2\text{O}_2 \text{ (0.14658)}$ min-1), O_3 MBs alone (0.11335 min⁻¹) followed sparger + 1M H_2O_2 (0.07199 min⁻¹) and lastly sparging ozone (0.00853 min⁻¹).

Furthermore, Fig. 5.6 (ii) shows the kinetics of the degradation of tetracycline under different conditions. The kinetic study showed that the degradation of TC exhibited a strong match with the pseudo-2nd-order reaction kinetics. The k value of TC degradation for NB + 1M H₂O₂ (0.00288 L mg⁻¹min⁻¹) was 4 times higher than that of O₂ MBs + 1M H₂O₂ (0.0000785 L mg⁻¹min⁻¹) and 3 times higher than that of O₃ MBs + 1M H₂O₂ (0.000761 L mg⁻¹min⁻¹). The findings of this study show that the incorporation of ozone nanobubbles improved the effectiveness of degradation of tetracycline (TC). This can also be validated by calculating the synergistic index (ξ) which can be determined by contrasting the rate constants of the sole processes to that of the combined processes [64]:

$$\xi = \frac{k_{(combined\ process)}}{k_{(sole\ process)}} \tag{5.12}$$

Process	$k (Lmg^{-1}min^{-1})$	ξ	$rac{Efficiency}{Conacttime}$ (%/min)
O ₃ NBs	0.00244	-	95.73/45 min
$O_3 \text{ NBs} + 1 \text{ M H}_2O_2$	0.00288	1.177	96.71/45 min
O_3 Sparger	0.000376	-	$76.75/45 \min$
O_3 Sparger $+ 1$ M H_2O_2	0.000494	1.294	$81.75/45 \; \mathrm{min}$
$1 \text{ M H}_2\text{O}_2$	0.000006	_	$17.23/45 \min$
$O_3 \text{ MBs}$	0.000509	_	$83.85/45 \min$
O_3 MBs 1 M H_2O_2	0.000761	1.478	$93.85/45 \min$
$O_2 \text{ MBs}$	0.0000238	_	23.17/45 min
O_2 MBs 1 M H_2O_2	0.0000785	2.634	$42.17/45 \min$

Table 5.1: Synergistic coefficient for different methods

where $k_{sole\ process}$ will be the rate constant of individual process and $k_{combined\ process}$ will be the sum of all the rate constants of the processes mentioned in the table. Higher values of ξ demonstrates lower influence in the degradation using O_3 in various processes. Following the above formula, the synergistic coefficient values are depicted in the Table 5.1.

The observed enhancement may be attributed to three variables, namely: (a) the influence of ozone in the degradation mechanism, which facilitated the generation of reactive radicals responsible for the degradation of TC (b) the stability of nanobubbles is much greater compared to regular ozone sparging. Moreover, nanobubbles exhibit a prolonged release of ozone into water, resulting in an extended duration of ozone supply. Consequently, nanobubbles provide enhanced efficiency in delivering a greater amount of ozone throughout the oxidation process (c) the increased surface area of nanobubbles has the potential to enhance mass transfer efficiency throughout the degradation process. Reactive oxygen species and radicals, such as superoxide and hydroxyl radicals [141] [261], are also produced during the collapse of the nanobubble, and this might help with the TC breakdown.

In addition, to provide valuable insights on the efficiency and sustainability of using ozone nanobubbles, a quantitative comparison with the conventional AOP degradation techniques such as Fenton/Fenton like, photodegradation, photocatalysis etc. has been presented in Table 5.2. Parameters like degradation rates, formation of by-products, energy consumption and other operational parameters have been taken from the previous literature. These findings from the literature have been compared to the present work as in Table 5.2. Amongst all the AOPs listed, 100% degradation of the antibiotic was achieved in O₃/H₂O₂/UV as well as in O₃ NBs. But in case of conventional O₃, complete mineralization of antibiotic TC was not achieved. Presence of organic intermediates with high m/z values were still present even after 100% degradation. While in case of O₃ NBs, complete degradation was achieved at varying ozone flow rates (2.5-10 L/min). Since 100% degradation efficiencies were achieved at all the varying concentrations, it is an important aspect to optimize the ozone flow rates in order to provide a cost and energy efficient process. While at 10 L/min the time taken was 15 minutes, but for same reaction conditions 40 minutes were required in case of 2.5 L/min. The amount of electricity being

Table 5.2: Comparison efficiency of ozone nanobubbles with conventional AOPs.

AOPs	Conditions	By-products	Degradation $\%$	Energy	Ref.
Fenton	$H_2O_2 = 0.3 \text{ mM}$	Sludge	76%	Low	[262]
	$({ m Fe}^{2+}=0.3~{ m mM})$	formation			
Fenton-like	$H_2O_2 = 100 \text{ mM}$	Sludge	94%	Low	[263]
	$Fe0@CeO_2$ catalyst	formation			
Photo-	MIL-53 (Fe)/UV	No by-	99.7% (80 mins)	High	[264]
catalysis		products			
Photo-	Indirect photolysis	Biochar,	89.95%	High	[114]
degradation		syngas			
$O_3/H_2O_2/UV$	$O_3 = 0.012 \text{ mM}$	High molecular	99%	High	[265]
	$(H_2O_2 = 0-5.9 \text{ mM})$	mass organics			
	$(\lambda=254\;\mathrm{nm})$	(Not			
		mineralised)			
O ₃ NBs	$6\text{-}12 \text{ mg/L O}_3$	No by-	100% (15 mins)	High	Present
		products	$(10 \mathrm{\ L/min})$		work.
			100% (25 mins)		
			$(5 \mathrm{\ L/min})$		
			100% (40 mins)		
			$(2.5~\mathrm{L/min})$		

consumed would be less when the degradation process is run for a smaller period of time. Considering the above parameters, the best operational conditions would be to run the set-up at 10 L/min in order to achieve rapid degradation and saving energy costs since very less time is required to achieve 100% degradation.

Further, cost estimation of several oxidation processes for tetracycline degradation and their combinations have been presented in Table 5.3 [144]. The operational costs have been calculated for millibubble O_3 , Milli bubble O_3 + Fenton, Milli bubble O_3 + Ultrasound, Millibubble O_3 + Ultrasound + Fenton with the degradation of tetracycline using ozone nanobubbles in the present work. The removal %, TC concentration and running time for each method with operation cost per run has been mentioned in Table 5.3. From the table, it can be clearly depicted that the cost was the lowest for ozone nanobubbles even at higher range of TC (400 mg/L) of 0.072 USD/run compared to other conventional methods. Here the costs were calculated based on electricity prices in Ropar, India (Rs 8 KWh⁻¹) and further converted to US \$ equivalents (1 Rs. = 0.012 US \$ as in July 2024). Thus, application of ozone nanobubbles is cheaper than other conventional methods.

5.5 Effect of radical scavengers and determining the degradation pathway

It has been discovered that the generation of nanobubbles leads to the release of reactive oxygen species [266] which can be explained by a hypothesis termed as Rayleigh collapse [267]. It states the generation of ROS occurs through hydrodynamic cavitation such as sonication etc. where extreme pressure and temperature conditions (10 MPa and

Methods	TC Removal	TC Conc.	Running	Operation
	(%)	$(\mathrm{mg/L})$	${f time}$	\mathbf{Cost}
				$(\mathrm{USD/run})$
Milli bubble	98	50	10 min	0.539
O_3 + Fenton				
Milli bubble	98	50	20 min	0.655
O_3 + Ultrasound				
Milli bubble O ₃	98	50	20 min	0.313
Millibubble O ₃ +	98	50	$10 \min$	0.371
Ultrasound +				
Fenton				
O ₃ NBs				$(\mathrm{USD/run})$
(Present study)				
1 mg/L	100	1	0.83 min	0.0013
10 mg/L	100	10	1.67 min	0.0026

50

100

400

2 min

 $15 \min$

 $45 \min$

0.0032

0.024

0.072

50 mg/L

100 mg/L

400 mg/L

100

100

100

Table 5.3: Comparison of operation cost of different AOPs with ozone nanobubbles

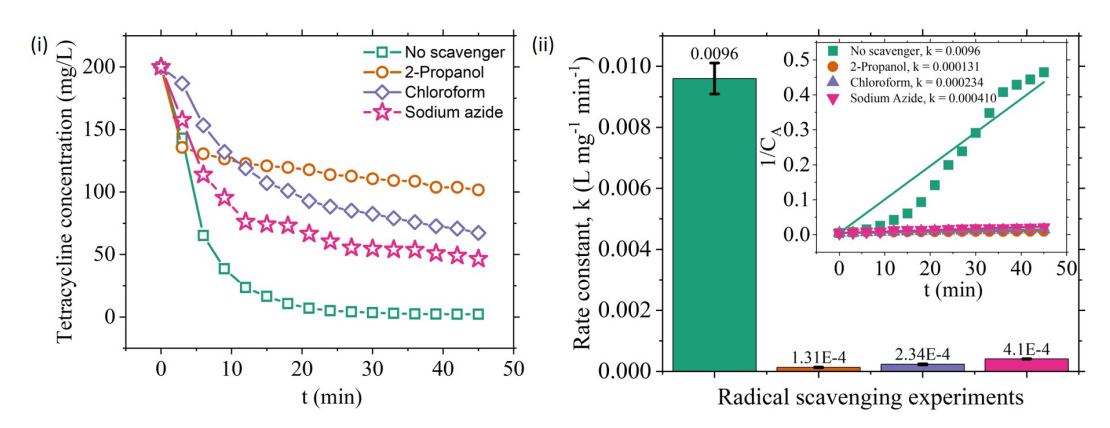


Figure 5.7: Effect of addition of 2-propanol as an *OH scavenger (i) Degradation of TC (200 mg/L) under the influence of 1 mM 2-propanol, sodium azide and chloroform (ii) Pseudo second order rate constant at particular experimental conditions.

5000 K) result in NB collapse. In these circumstances, it would be advantageous for water to molecularly dissociate into hydrogen atoms (*H) and hydroxyl radicals (*OH) [268]. Nevertheless, some studies showing no ROS during nanobubble generation. For instance, Chae et al. [267] found that benzoic acid degradation was not seen in the presence of oxygen nanobubbles, even when sonication was utilized to accelerate the collapse process. There was no electron paramagnetic resonance (EPR) signal. Further, it was suggested that the pressure and temperature generated by the collapse of nanobubbles would be lower than that of hydrodynamic cavitation, which might limit their capacity to facilitate the dissociation of water. However, Yadav et al. [27] measured the formation of ROS in nanobubbles (mixture of oxygen, hydrogen and ozone) produced through electrochemical generation methods where ESR (electron spin resonance) technique was used for the analysis. It was found that the spectrum exhibits discernible peaks that

bear resemblance to the presence of superoxides in the nanobubble sample. The radical quenching experiments were performed to examine the role that indirect radical oxidation (${}^{\bullet}$ OH, O_2^{\bullet} , ${}^{1}O_2$) and direct ozone molecule oxidation play in the tetracycline's degradation. Many researchers have utilised 2-Propanol, Sodium azide, chloroform (CLF) as a scavenger of the OH, O₂ and O₂ radicals respectively in oxidation experiments to comprehend the impacts of direct and indirect oxidation pathways because of the strong response it has with the radicals mentioned above [269] [270] [94] [70]. In order to assess the total scavenging of •OH, O_2 •-, 1O_2 radical production by ozone nanobubbles, each scavenger with a concentration of 1 mM were introduced at the start of the process. Fig. 5.7 (i) represents the degradation of TC in the presence and absence of radical scavengers and Fig. 5.7 (ii) depicts the pseudo second-order rate kinetics for the experimental runs. It can be elucidated that in the presence of radical scavengers, the degradation efficiency decreases. The TC removal achieved a level of roughly 99% when it was oxidised without the addition of any scavenger. Upon the addition of 1 mM 2-Propanol, the removal of TC shows a drop reaching a level of around 49.19%, 1 mM Chloroform shows a drop to 66.37% and 1 mM sodium azide decreases the TC efficiency to 76.75%. This observation suggests that the degradation process of tetracycline was impeded due to the scavenging action of 2-Propanol on OH radicals, chloroform on O₂ and sodium azide on O₂. The kinetics have been displayed in Fig. 5.7 (ii) where the reaction rate constants have been measured and as mentioned earlier, it follows pseudo second-order kinetics. The rate constant when no scavengers were used was 0.0096 L mg-1min-1, then it decreased to 0.000410, 0.000234 and further decreased to a value of 0.000131 L mg-1min-1 at 1 mM sodium azide, CLF and 2-propanol respectively, thereby indicating the presence of radicals. Lower values of rate constant imply higher presence of that specific radical in the degradation process.

Given the notable improvement in the degradation efficiency of tetracycline using ozone nanobubbles, it becomes imperative to ascertain the degradation route associated with this novel synergistic activity. Consequently, a comprehensive investigation was conducted, specifically employing liquid chromatography–mass spectrometry (LC-MS). To investigate the degradation routes further, LC-MS analysis was used to identify the intermediates formed during the degradation process. The mass spectra at a time interval of 15 minutes are shown in Fig. S6. The mass spectra of the intermediates have been provided in Table S1 presented in supporting information. The intensity of the mass spectrum and the proposed structure of the main intermediates has been presented. In Figure S6 at 0 minutes, in the first spectra, a peak of tetracycline (m/z = 445.263) was observed [271] [272] [273]. The spectra majorly displayed the intermediate products with m/z values of 445, 410, 363, 340 and 227. Notably, the degradation pathways of TC include demethylation, decarbonylation, hydrolysis, ozonolysis, decarboxylation and alcohol oxidation [274] [275]. Under the constant light, active species (h+, ${}^{\bullet}OH$, and $O_2{}^{\bullet-}$) attacked the TC molecules and their intermediates, breaking them down into secondary products with a reduced

Therefore, it can be concluded that ${}^{\bullet}$ OH radicals played predominant role followed by O_2^{\bullet}

and ${}^{1}O_{2}$.

molecular weight.

TC molecule (m/z = 445) when attacked by ozone $(O_3 \text{ addition})$ during the initial stages of ozonation forms an intermediate P1 (molozonide) which is a transient and relatively an unstable compound. Further P1 rapidly decomposes to P2 (ozonide) which eventually breakdown to carbonyl compound (P3) after the oxidative step. P3 fragmented into P4 (m/z = 410) and P25 (m/z = 340). The fragmentation of P3 through oxidative demethylation, oxidation of amine, imine hydrolysis, subsequent ozonolysis and decarboxylation lead to the formation of P25 (m/z = 340). Whereas P4 may further disintegrate by 1,2,3-tricarbonyl oxidation followed by ozonation of C=C double bond at P11 to decarboxylation leading to the formation of an intermediate P15 (m/z =362) (Fig. 5.8). P15 further breaks down into intermediate P18 (m/z = 226) upon decarboxylation and alcohol oxidation forming a polar intermediate (Fig. 5.8). equivalent degradation products were formed when TC molecules were progressively dislodged, it was anticipated that these products would eventually disintegrate into CO₂, H₂O, NH₄⁺ molecules, and other intermediates [229]. Depending upon the above degradation analysis, the chemical equation and process for the breakdown of TC by ozone nanobubbles can be presented as [229] [142] [253]:

$$TC + O_3 \rightarrow Products \ k = 0.01285 Lmg^{-1}min^{-1}$$
 (5.13)

$$O_3 + OH^- \to O_2 + HO_2^-$$
 (5.14)

$$O_3 + HO_2^- \to O_2^{\bullet} + {}^{\bullet}OH + O_2 \tag{5.15}$$

$$O_3 + O_2^{\bullet -} \to O_3^{\bullet -} + O_2^{\bullet} \tag{5.16}$$

$$O_3 + H_2O \to {}^{\bullet}OH + OH^- + O_2$$
 (5.17)

$${}^{\bullet}OH + TC \rightarrow intermediates \rightarrow CO_2 + H_2O$$
 (5.18)

$$O_2^{\bullet -} + TC \rightarrow intermediates \rightarrow CO_2 + H_2O$$
 (5.19)

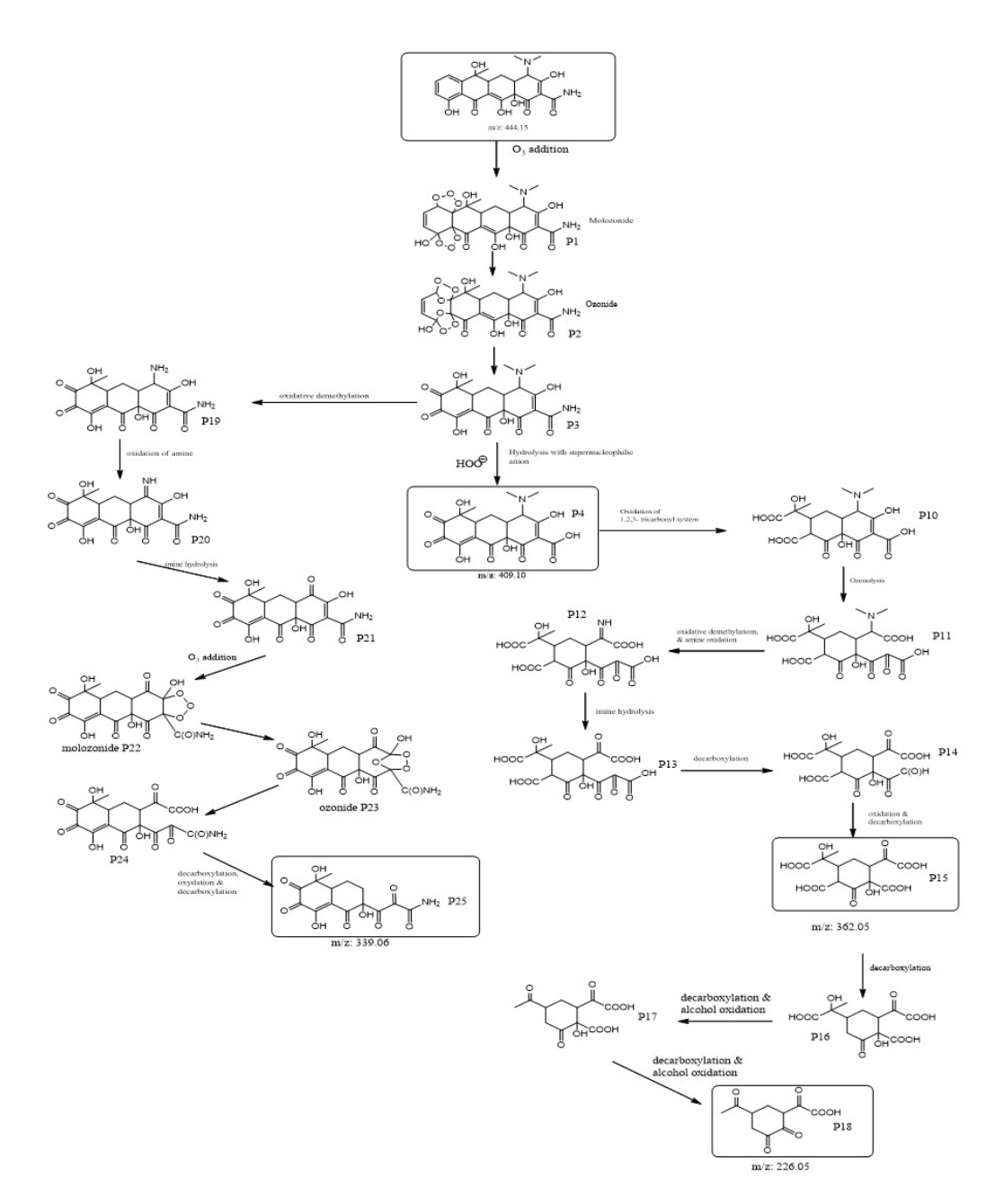


Figure 5.8: Possible degradation pathway mechanism of tetracycline through LC-MS technique.

Chapter 6

R&D 3: Ozone nanobubbles based advanced oxidation processes (AOPs) for degradation of organic pollutants

This chapter presents the degradation of two organic contaminants namely green rit dye and methylene blue dye using ozone nanobubbles. The work focused on the parameters such as variations in initial concentrations of organic contaminants, varying pH, presence if salts and surfactants, comparison efficiency with oxygen nanobubbles and microbubbles and effect of charge possessed by nanobubbles. The degradation products from methylene blue dye were investigated using LC-MS techniques. The presence of reactive oxygen species in the degradation process was studied using the radical scavenging experiments. The variation of concentration of both the dyes was investigated using UV-Visible spectrophotometer.

6.1 Effect of ozone flow rate on nanobubble generation

Ozone NBs were generated using the nanopore diffusion method. The experiments were run at various flow rates of ozone (1-10 L/min) being fed to the reactor. The characteristics such as bubble number density, mean bubble diameter, and zeta potential were measured as shown in Fig. 6.1. The mean size was in the range of 120 - 250 nm with a bubble number density ranging from 5×10^7 -18 $\times 10^7$ bubbles/mL. Whereas the ozone NBs possessed a negative zeta potential of magnitude ranging from -7 to -14.7 mV. The effect of various flow rates of ozone on the bubble number density as well as the mean bubble diameter is shown in Fig. 6.1 (a). It can be elucidated from the figure that up to 5 L/min ozone flow rates, the bubble number density increases and then gradually decreases up to 10 L/min. Whereas the mean bubble diameter increases when the ozone flow rate increases. On the other hand, the zeta potential magnitude increases as the ozone flow rate increases (Fig. 6.1 (b)). From Fig. 6.1 (c) it can be seen that ozone flow rates play a major role in the generation of NBs as well as the amount of dissolved ozone present in the NB solution. It can be observed that the dissolved ozone remains higher at smaller flow rates of ozone. This is attributed to the fact that the retention time for ozone conversion in the Corona discharge tube is higher at a low flow rate. Therefore, ozone concentrations are higher at low flow rates. Also, the volumetric mass transfer coefficient was estimated at each flow rate, as shown in Fig. 6.1 (d). The highest value was achieved at 5 L/min with a value of 0.8195 min⁻¹. In a nutshell, we can conclude from the following experiments that (i) the

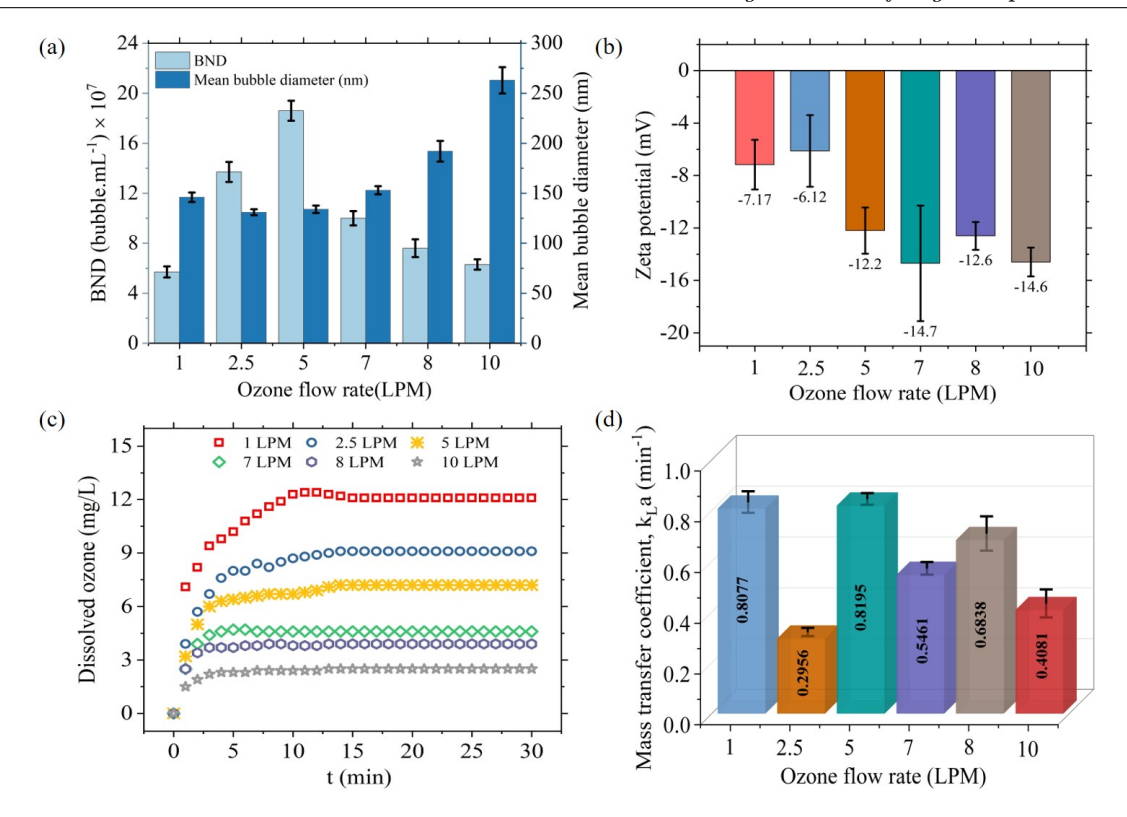


Figure 6.1: Nanobubble generation at various ozone flow rates (1-10 L/min) and their characterization using NTA and DLS analysis (a) Comparative representation of BND with mean bubble diameter (b) Zeta potential trend (c) Dissolved ozone monitoring (d) Measurement of the volumetric mass transfer coefficient (k_La) at various flow rates of ozone

bubble number density attains a maximum at 5 L/min giving the highest negative zeta potential and the lowest nanobubble diameter; (ii) the ozone concentration reaches 7 ppm at 5 L/min ozone flow rate, and the highest mass transfer coefficient was achieved at 5 L/min. Therefore, a 5 L/min flow rate was chosen for further degradation experiments.

6.2 Effect of change of initial concentration of dye

Initially, the concentrations of organic pollutants (GRD and MB) were chosen as 10-200 mg/L and 0.5-30 mg/L, respectively. For each concentration, the solutions were prepared and introduced individually to the reactor. The measurements of the following parameters (a) residual concentration of the organic pollutants (b) dissolved ozone concentration (c) characteristics of NBs formed at the end of the experiments (end product) were measured. The ozone flow rates as noted from the previous sections were kept constant at 5 L/min and all the solutions were at a constant pH of 6.5. When the ozone bubbles are generated in the contaminated solution, the concentration of the organics is gradually reduced to a colorless solution for both organic pollutants. Fig. 6.2 indicates the degradation of organic contaminants in the presence of ozone nanobubbles. Fig. 6.2 (a-c) represents the results for the NTA and DLS analysis of the nanobubbles formed during the degradation process in 5 minutes. The ozone nanobubbles generated in the contaminated solution exhibit a



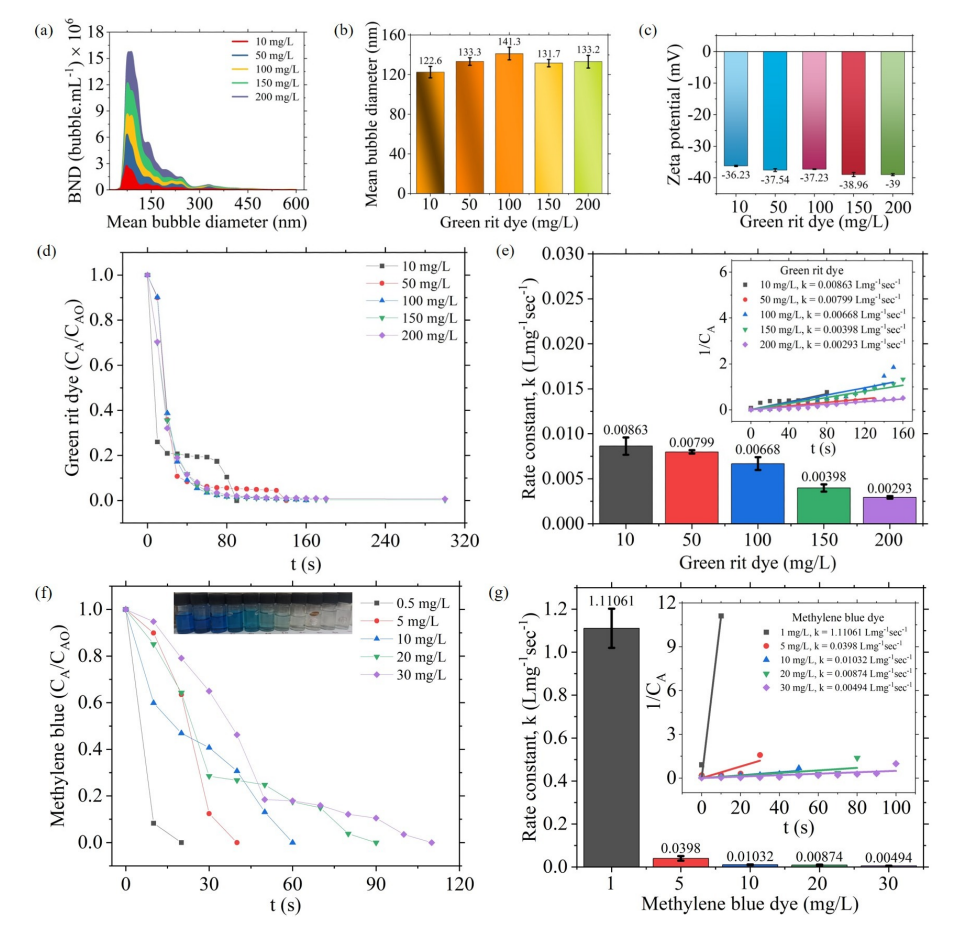


Figure 6.2: Effect of initial concentration of dye on degradation at 5 L/min ozone flow rates (a) Bubble size distribution of green rit at various concentrations (10-200 mg/L) (b) Mean bubble diameter (c) Zeta potential of the end products; (d) Varying initial concentrations of green rit (10-200 mg/L) (e) Kinetics of the reaction rate constant k (f) Varying initial concentration of methylene blue (0.5-30 mg/L) (g) The reaction rate constant of degradation of organic pollutants

positive correlation with the contaminant concentration as shown in Fig. 6.2 (a). The plausible reason for the higher bubble number density is the stabilization of nanobubbles by the organic molecules. On the other hand, the mean bubble diameter (Fig. 6.2 (b)) and zeta potential (Fig. 6.2 (c)) are also observed to increase slightly. The diameter ranges from 120-130 nm while the charge possessed by the nanobubbles was in the range -36 to -39 mV. The change in color and concentration of organics are depicted in the form of pictorial representation as shown in Fig. 6.2 (d) and (e). The results show that the lower the initial dye concentration, the lesser the time required for the degradation to occur as expected. It was observed that 90 % of the contaminant had vanished within the first three minutes. After five minutes, 100 % of the contaminant had been degraded and the concentration had dropped below the detection limit.

Assuming that the degradation process is expressed by second-order reaction, the time versus $1/C_A$ was fitted well by a single exponential, $1/C_0 + k t$, where k is the rate constant, C is the concentration at time t and C₀ is the initial concentration. The value of the pseudo-second-order rate constant k increased linearly with the concentration of both

contaminants. The rate constant k was calculated using the above and is shown in Fig. 6.2 (e) and (g). It can be concluded that the magnitude of the rate constant k was higher in the case of MB as compared to the GRD. At 0.5mg/L MBD, the rate constant k value was highest at 1.11061 L mg⁻¹ sec⁻¹ while 0.00863 L mg⁻¹ sec⁻¹ was the value at 100 mg/L for GRD.

6.3 Effect of change of ozone flow rates on dye degradation

Ozone is a powerful oxidant that possesses a redox potential of 2.07 mV and therefore, it is used in wastewater treatment and advanced oxidation processes [65]. The amount of ozone dissolved in water plays a major role in disintegration of the organic contaminants present in the wastewater. From the previous section, it was observed that the concentration of nanobubbles was the highest at 5 L/min followed by 2.5 and 7 L/min with dissolved ozone concentrations of 6.5, 9, and 4.5 ppm respectively. Therefore, this study examined the effect of changing the ozone flow rates on the degradation of both organic pollutants. Fig. 6.3 presents the degradation kinetics of both organic pollutants at various concentrations along with the reaction rate constants to determine the quickest degradation feasible at a given flow rate. Similarly, Fig. 6.3 (a) and (b) depict the effect of ozone flow rates on varying concentrations of the contaminants. It is to be noted that the best results were achieved for the ozone flow rate of 5 L/min. Whereas, no significant amount of difference was noted for 2.5 and 7 L/min of ozone flow rates for the degradation of GRD. A similar observation was made for various concentrations of MB as shown in Fig 6.3 (c) and (d). The kinetic fits for all the flow rates at different concentrations are mentioned in Appendix C (Fig. D.1 (a), (b), (c) and (d)). The rate of degradation was faster for the higher dissolved ozone concentration and higher number of nanobubbles formed. The reaction rate constant was estimated to be the highest at 5 L/min of ozone flow rates where we had achieved the maximum amount of ozone nanobubbles. The concentration curves observed are more steeper in the case of 5 L/min thereby implying that the rate constant should be higher at this value. Thus, the degradation of organic contaminants is affected both by the dissolved ozone concentration as well as the amount of NBs present in the solution. Clearly, at 2.5 L/min, although the dissolved ozone concentration is higher, but the density of NBs is lower. Similarly, in the case of 7 L/min, both ozone concentration and the nanobubble density are lower. Therefore, at 5 L/min, where the NB concentration is the highest with an ozone concentration of 6.5 ppm, the degradation is the fastest. In a nutshell, the degradation rate depends on the ozone flow rate, the concentration of ozone, and nanobubble density during the degradation process.

6.4 Effect of pH, salts and surfactants

During the ozonation process, there are two major mechanisms involved in the degradation. Direct attack by ozone molecule and indirect attack by •OH radical. Interestingly, the pH

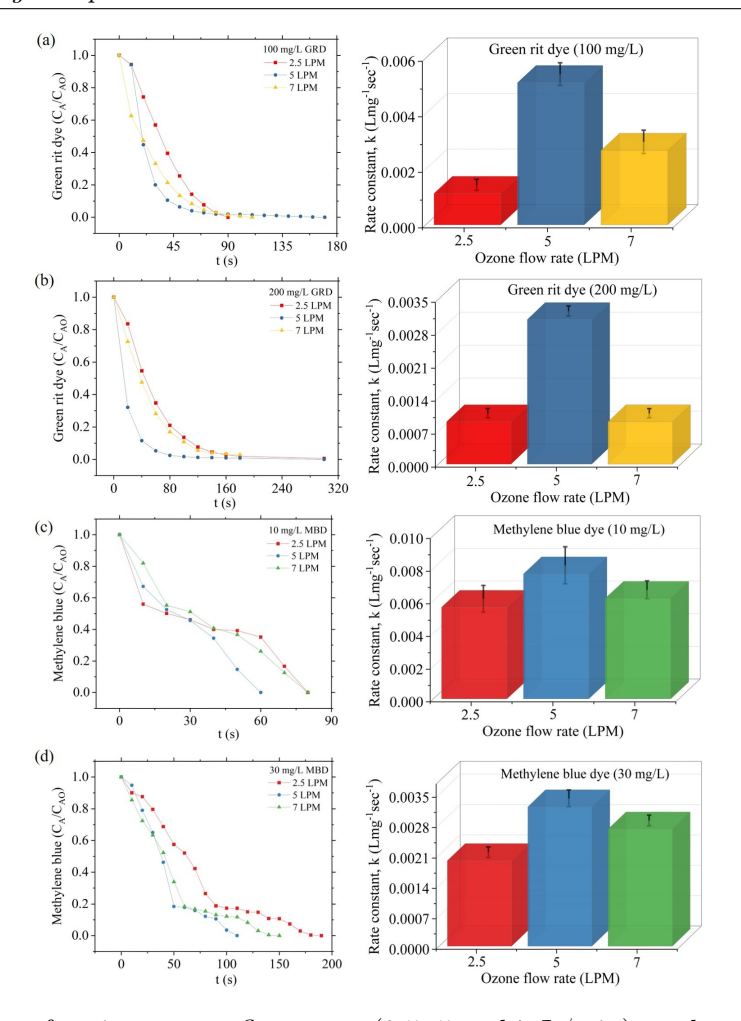


Figure 6.3: Effect of various ozone flow rates (2.5, 5 and 7 L/min) on dye degradation (a) Green rit dye (100 mg/L) (b) Green rit dye (200 mg/L) (c) Methylene blue dye (10 mg/L) (d) Methylene blue dye (20 mg/L) with rate constant k

level of the solution has a major impact on the formation of the OH radicals. In an acidic medium or at lower pH levels, direct attack by ozone molecule is dominant, whereas at higher pH or basic medium, OH radical attack plays a major role [218]. In this study, the pH of the contaminant solution was varied from 4-10 at two extreme concentrations of organic pollutants. Fig. 6.4 (a) and (b) depict the trends of the effect of pH on MB degradation. Two concentrations of 10 and 20 mg/L were considered for this study. The degradation efficiency is higher at a higher pH (basic medium) than at a lower pH (acidic medium). At higher pH, there are more chances of generation of hydroxyl radical by the collapse of NB leading to a second mechanism of hydroxyl radicals to be dominant in this case. The rate constant for degradation is represented in Fig. 6.4 (c) where it is observed that higher pH results in higher values of k. A decrease in the overall pH of the solution has been noted during the ozonation process. This might imply that the organics degrade into more acidic intermediates during the process leading to a lowering of the overall pH of the solution. Also, a significant amount of organic contaminant degradation was observed for both acidic as well as basic media. The reaction kinetics follows the pseudo-second-order and it has been shown in Appendix C (Fig. D.2).

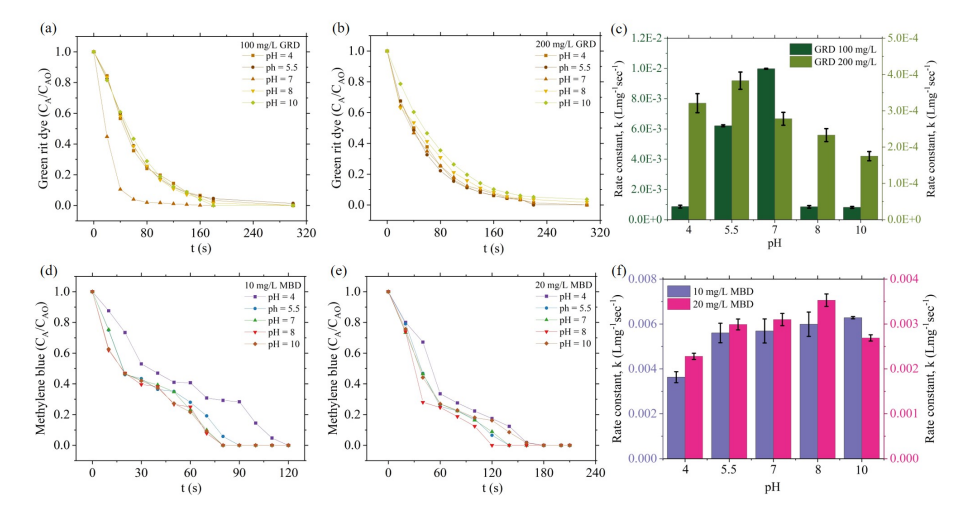


Figure 6.4: Effect of pH (4-10) on degradation of dye at a constant ozone flow rate of 5 L/min (a) 100 mg/L green rit dye (b) 200 mg/L green rit dye (c) Comparison of reaction rate constant for both green rit dye concentrations (d) 10 mg/L methylene blue dye (e) 20 mg/L methylene blue dye (f) Comparison of reaction rate constant for both methylene blue dye concentrations

The phenomenon known as the "salting-out effects" occurs when the concentration of salt in an aqueous salt solution causes a reduction in the solubility of gases. Since presence of salts lowers the gas solubility, thus it would also slow down the degradation. To study these effects, mono- and multivalent chloride salts was explored on the degradation of organic contaminants by the use of ozone nanobubbles. Fig. 6.5 (a) and (d) show the degradation at various concentrations of the monovalent salt (Sodium Chloride). As shown in the figure, the salt had a similar effect on the degradation efficiency of both organic contaminants. With the increase in the salt concentration, the overall degradation efficacy increased. The presence of salt in the organic solution prohibited the extent of degradation up to a certain extent. This result can be concluded from the fact that when only ozone nanobubbles are used, the degradation% reaches a value of 99.28% and 100% for GRD and MB, respectively. On the contrary, when salt is added to the solution, the percentage degradation goes down to 96.52% and 86.25% for GRD and MB, respectively. Similar trends were observed for the divalent (Fig. 6.5 (b) and (e)) and trivalent (Fig. 6.5 (c) and (f)) salts.

Comparing the degradation efficiency of the three types of salts, the highest degradation efficiencies were obtained for the monovalent salts followed by divalent and trivalent salts. The rate constants have been estimated for all three salts shown in Appendix C (Fig. D.3 and D.4). The residual organic concentration in the end product was found to increase as the valency of the salts increased. Moreover, the time required for 100% degradation increased upon increasing the salt concentration. It is widely known that adding salts results in the screening of EDL (electric double layer) of nanobubbles, which in turn reduces bubble number density and zeta potential and increases mean size [227]. Zeta potential on the other hand reduces for NaCl but remains negative, drops down to zero for calcium chloride, and changes to positive charge for the trivalent salt [92]. Therefore, it may be concluded that the reason for reduced degradation efficiency at higher salt concentrations

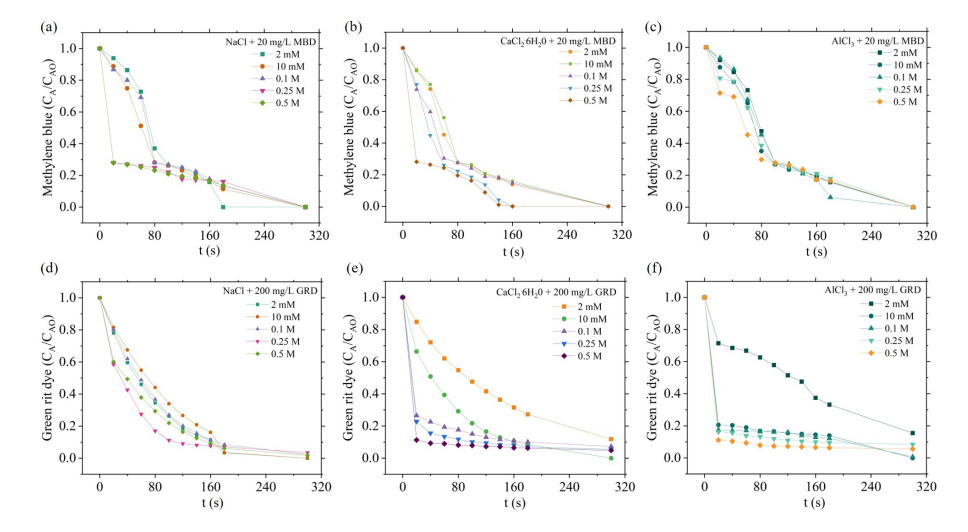


Figure 6.5: Effect of salt concentration on dye degradation (2-100 mM) at a constant 5 L/min ozone flow rate (a) Monovalent salt (NaCl) (b) Divalent salt (CaCl₂· $6H_2O$) (c) Trivalent salt (AlCl₃) at 20 mg/L methylene blue dye concentration (d) Monovalent salt (NaCl) (e) Divalent salt (CaCl₂· $6H_2O$) (f) Trivalent salt (AlCl₃) at 200 mg/L green rit dye concentration

is due to reduced nanobubble stability accompanied by smaller nanobubble number density and higher nanobubble mean size.

Fig. 6.6 (a) and (b) demonstrate the degradation of GRD and MB at a range of SDS concentration (0.3-5 cmc) (critical micelle concentration) (0.1 cmc, equivalent to 0.82 mM, [92]. When no SDS was added (SDS = 0 mM), the highest absorbance for GRD is 526 nm, and consequently for MB is 668 nm which is consistent with the literature reports [276]. Upon addition of SDS, the maximum absorbance saw a change within a range of ± 2 . At a GRD concentration of 200 mg/L, the degradation of dye increased with increasing SDS concentration as depicted by the reduced absorbance. As the surfactant concentration is increased from 0.3 to 1 CMC, the degradation efficiency of GRD has also increased. This degradation may be caused by any two of the following mechanisms. The first is due to the creation of pre-micelles that take up the dye molecules, while the second is due to additional surfactant monomers suppressing electrostatic contact between dye molecules [276]. At 8 mM of SDS (CMC value of SDS) that corresponds to 1 CMC, the highest amount of degradation was achieved. At concentrations above CMC, the degradation efficiency decreased. Thereby, it can be concluded from the results that up to the CMC concentration of SDS, the degradation of GRD increased.

For 20 mg/L of MB as shown in Fig. 6.6 (b), depicted that as the concentration of SDS increases, the degradation efficacy for MB dye decreases. For MB, the dimer may formed at a lower concentration of SDS. Since the MB solution is more turbid and concentrated, the dye requires less amount of surfactant to form the dimer. The lower the amount of SDS present in the MB solution, the greater will be the degradation efficiency. The interaction between dye-surfactants in aqueous solutions has been studied extensively. From the earlier studies, it has been established that both electrostatic and hydrophobic

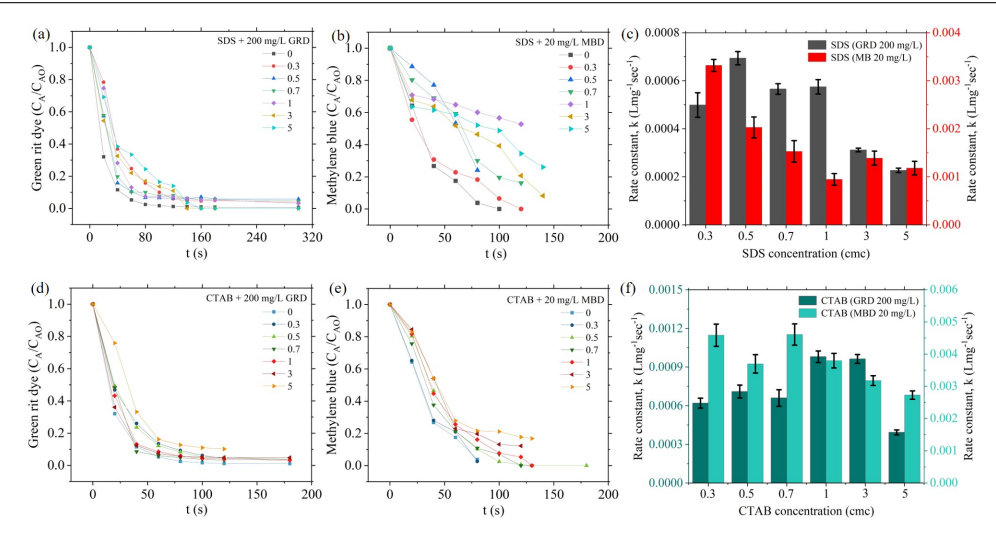


Figure 6.6: Effect of concentration of surfactant (0.3-5 cmc) (a) Anionic surfactant (SDS) at 200 mg/L GRD (b) Anionic surfactant (SDS) at 20 mg/L MB (c) Comparative trends of rate constant for SDS (d) Cationic surfactant (CTAB) at 200 mg/L GRD (e) Cationic surfactant (CTAB) at 20 mg/L MB (f) Comparative trends of rate constant for CTAB

forces are important for the interaction between the ionic dyes and surfactants. The dye interactions with opposite-charged surfactants are mostly coulombic in nature. Whereas when the same charge is possessed by the surfactant and dye, the interactions can occur only if the hydrophobic forces can overcome the electrostatic ones. The degradation in the presence of cationic (CTAB) surfactant concentration (0.3-5 CMC) has also been studied as shown in Fig. 6.6 (d) and (e). Although for MB, the charge possessed by the surfactant and dye were the same [276], the hydrophobic forces were stronger than the electrostatic forces that led to the degradation of the dye molecules to a colorless solution. Noting the trend for the different concentrations of surfactant (CTAB) used, the best results were achieved for 0.3 CMC equivalent to 2.46 mM of CTAB. Unlike with CTAB, where peak degradation efficiency was observed at an intermediate concentration, we observed the highest degradation efficiency at the lowest SDS concentration (0.3 cmc). The rate constant calculated at each concentration of the SDS and CTAB are represented in Fig. 6.6 (c) and (f) respectively (kinetic fits presented in Appendix C (Fig. D.5)). In both figures, it can be observed that the rate constant k decreases with an increase in the surfactant concentration for MB. Whereas for GRD, the k increased initially with CTAB concentration but started decreasing after the CTAB concentration was increased beyond 1 cmc. Thus from the results it can therefore be concluded that (a) Despite the nature of the surfactant, GRD degrades at a higher rate with lower surfactant concentrations (b) the concentration of surfactant plays an important role in the degradation process. The lower the amount of surfactant used, the quicker will be the degradation.

6.5 Comparison of treatment efficiency of ozone and oxygen nanobubbles, microbubbles and charge possessed by nanobubbles

Throughout the literature, many articles have reported the degradation of organic pollutants extensively in review articles [155] [160] [150] [165]. Chu et al. [88] studied the ozonation of CI Reactive Black 5 using microbubbles and compared the efficiency with bubble column reactor. The pseudo-first-order rate constant was 3.2–3.6 times greater at the same starting dye concentration compared to the bubble contactor, and the overall mass transfer coefficient was 1.8 times higher. Bui and Han [277] studied the degradation of GRD using positively charged oxygen nanobubbles. Ma et al. [278] coupled Fenton and micro-nanobubbles for degradation of Congo red dye and achieved 94% degradation results. Following the literature, a set of experiments was performed to compare the treatment efficiency of ozone, oxygen microbubbles, and nanobubbles. At pH 6.5, 200 mg/L of GRD was treated with both types of nanobubbles (ozone and oxygen). From Fig 6.7 (a), it can be inferred that there was a significant amount of difference in the treatment efficiency of ozone and oxygen NBs. However, the collapse of oxygen nanobubbles may lead to the formation of hydroxyl radicals. From the experiments, a very small amount of degradation of organic (36.8 %) was observed in the case of oxygen nanobubbles. Whereas for ozone nanobubbles, complete degradation was achieved. In the case of oxygen nanobubbles, at acidic pH, the formation of hydroxyl radicals is not that significant. The only possible mechanism here would be the formation of hydroxyl radicals by the collapse of NBs leading to the degradation of the organic product. In addition to hydroxyl radicals from the ozone nanobubbles, ozone molecules also directly play a role in the degradation mechanism. As a consequence, the findings clearly show that dye breakdown utilizing oxygen nanobubbles would be extremely slow and practically insignificant.

The positively charged oxygen NBs having a zeta potential of +10 mV were attained by adding 2 mM Al³⁺ (Aluminium Hydroxide) to the solution. Adding Aluminium hydroxide lead to the formation of Al³⁺, Al (OH)⁺⁺ and Al(OH)⁺₂ [277]. Fig. 6.7 (b) indicates the degradation rates of the GRD in the presence of negatively and positively charged oxygen NBs. Considering the GRD concentration of 200 mg/L, the degradation efficacy was more prominent in the case of negatively charged NBs as compared to positively charged ones. Explicitly, in the absence of Al⁺, the degradation rate reached a maximum of 57.2%. In contrast, the positively charged oxygen NBs could remove upto 47.31% after 60 minutes of the reaction time.

There has been a lot of debate on the working of microbubbles with nanobubbles in the advanced oxidation processes. When compared for the formation of reactive oxygen species and mass transfer, the burst of nanobubbles would provide a more effective means of increasing the number of ROS formation as well as an enhancement of the mass transfer coefficient [266]. A comparative study was conducted to observe the degradation efficiency of ozone microbubbles to nanobubbles. The results are depicted in Fig. 6.7 (c). It

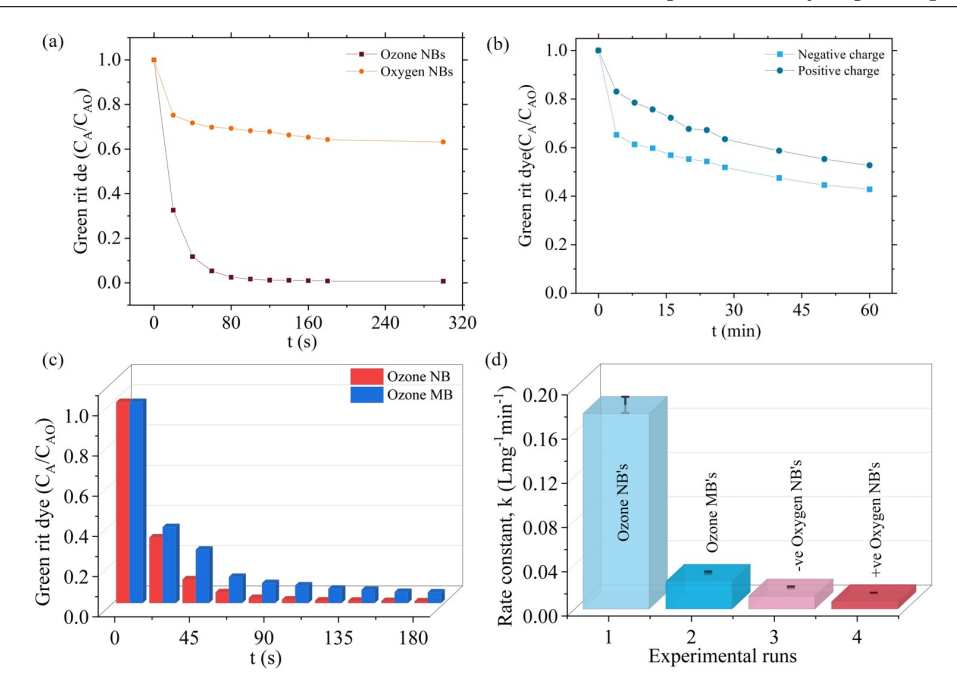


Figure 6.7: Comparison efficiency in dye degradation (a) Ozone and oxygen nanobubbles (b) Oxygen nanobubbles with positive and negative charge (c) Ozone nanobubbles vs ozone microbubbles (d) Reaction rate constant k for various comparative methods depicting highest rate constant for ozone nanobubbles

can be depicted that the ozone nanobubbles degrade the dye faster as compared to the microbubbles. The time required for the complete degradation of dye is 100 seconds in the case of nanobubbles. This can also be presented in the form of a kinetic study where the rate constant k when compared for all the systems gives the highest value for ozone NB's followed by ozone MB's, -ve Oxygen NB's, and +ve Oxygen NB's as depicted in Fig. 6.7 (d).

Additionally, the cost estimation of various conventional dye degradation methods and hybrid advanced oxidation processes have been compared to the ozone nanobubble technology on the basis of removal percentage, time taken and unit operation cost. The cost comparison was done for methylene blue dye as the main contaminant. Cost estimation of several processes for MB degradation have been presented in Table 6.1 [279]. From the table, it can be clearly depicted that the cost was the lowest for ozone nanobubbles even at a higher range of TC (400 mg/L) of 0.072 USD/run compared to other conventional methods. Here the costs were calculated based on electricity prices in Ropar, India (Rs 8 KWh⁻¹) and further converted to US \$ equivalents (1 Rs. = 0.012 US \$ as in July 2024). Thus, application of ozone nanobubbles is cheaper than other conventional methods.

6.6 Radical quenching and analysis of intermediates

It has been reported in many studies that the NB collapse leads to the formation of reactive oxygen species (ROS) that majorly include short-lived radicals - hydroxyl (${}^{\bullet}$ OH), superoxide (${\rm O_2}^{\bullet-}$) and singlet oxygen (${\rm O_2^1}$) [61]. These ROS cannot be quantified

87

Table 6.1: Comparison of operation cost of different AOPs with ozone nanobubbles

Type of process	Removal	Time taken (min.)	Unit operation cost
(Conventional/Hybrid AOPs)	efficiency (%)		$(\mathrm{USD/m^3})$
Chemical coagulation	93	28.41	1.99
Electro-Fenton	90.3	60	3.13
Fenton's Oxidation	24	120	2.50
Ozonation	95	25	29.69
Photo-Fenton process	100	120	0.91
Present Study	Removal	Time taken (min.)	Unit operation cost
(Ozone nanobubbles)	efficiency (%)		(USD/run)
Green rit dye (200 mg/L)	100	2	0.0032
Methylene blue (1 mg/L)	100	0.33	0.0009
Methylene blue (30 mg/L)	100	1.67	0.0026

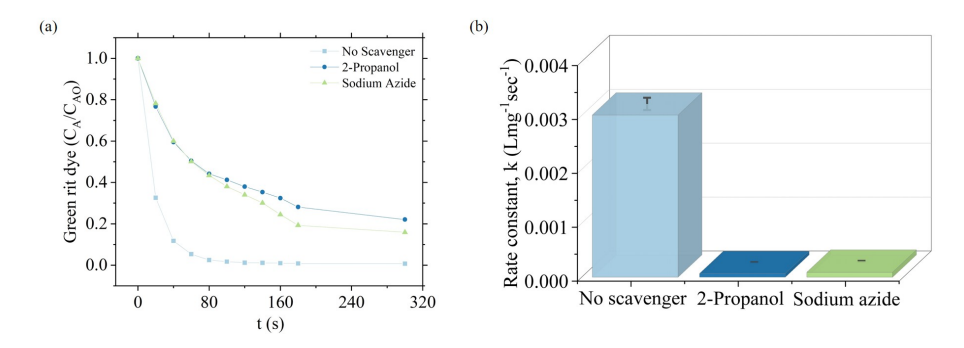


Figure 6.8: Radical quenching experiments (a) Comparison of degradation efficiency in presence of scavengers (2-Propanol and Sodium azide) to degradation efficiency when no scavenger is present (b) Comparison of the reaction rate constant in presence and absence of scavengers

directly. So there concentration is measured with respect to their reactivity towards certain chemicals used as probes or quenchers. In this study, radical quenching experiments were performed in order to identify the reactive oxygen species that were formed during the process of ozonation. 1 mM of 2-Propanol and 1 mM of NanN₃ were used as scavengers for trapping the reactive oxygen species such as hydroxyl radical (*OH) and singlet oxygen (O_2^1) respectively. All experiments were conducted at pH 7. As depicted in Fig. 6.8 (a), the concentration profile for the degradation of GRD (200 mg/L) fitted very well with the pseudo second-order kinetics. Fig. 6.8 (b) shows the values of the rate constant for the pseudo-second-order reaction. From the graph, it was observed that the value of the rate constant decreased to 0.0000689 L mg⁻¹ min⁻¹ with the addition of 2-propanol which indicates the presence of OH radicals and their dominant role in the degradation of dye. With the addition of NaN₃, the k value climbed up to 0.0000921 L mg⁻¹ min⁻¹ suggesting that singlet oxygen (O_2^1) also contributed to the degradation of contaminant. Whereas, when no scavenger was added, the k value increased to 0.00301 L mg⁻¹ min⁻¹ which confirms the formation of the reactive species during the process. The results were in good agreement with the previous reports in which these ROS coexisted in the nanobubble solution [94]. Whilst the *OH radicals were the most important oxidant in the system as

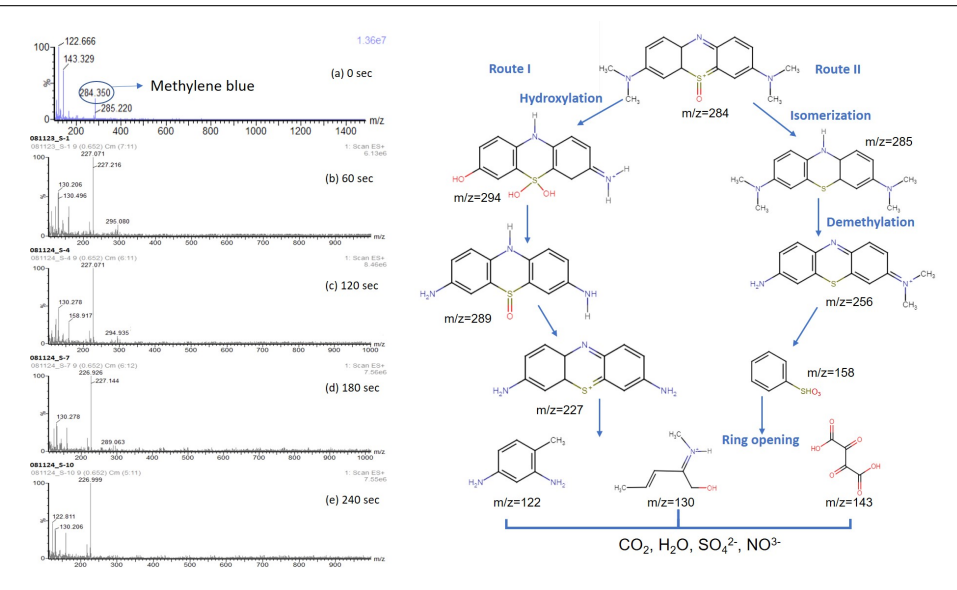


Figure 6.9: Analysis of intermediates being formed during ozonation by LC-MS analysis showing MS spectra and the possible degradation mechanism

compared to (O_2^1) . Hence, it can be inferred that ${}^{\bullet}OH$ radicals are predominant active species in the degradation process.

Further, the intermediates during the ozonation process in the presence of surfactant (SDS) were performed using LCMS analysis. The results are depicted in Fig. 6.9. From the MS spectra, it can be depicted that no peaks appear at m/z = 284.35 after 120 seconds of the treatment, indicating that the whole MB has been destroyed [215]. Nonetheless, in the mass spectrum, some peaks appear at m/z values of 294, 289, 285, 256, 227, 158, 143, 130 and 122. Upon dissolving MB in water, Cl ionizes to form Cl⁻, corresponding to the peak at m/z = 284. Two routes may be distinguished in the degradation pathway: route I and route II. This is because of the powerful oxidizing free radicals [241] and ozone itself. In route II, the cation in the MB molecule underwent either partial isomerization to form product at peak m/z = 285 in which the methyl group was linked with N, which was readily attacked by $^{\bullet}$ OH or demethylation to generate product at peak m/z = 256 due to the action of ROS during bubble rupture [245] [243]. m/z = 256 kept demethylating in response to the same action, forming products m/z = 158 and m/z = 143. m/z = 158 and m/z = 143 underwent a sequence of events, including hydroxylation, nitration, bond, and ring breaking, and ultimately mineralized. On the other degradation route I, MB molecules were first attacked by ozone, which hydroxylates them to create polyhydroxy compounds (m/z = 294). After that it was nitrated and demethylated by O and cavitation effects, resulting in products m/z = 289 and m/z = 227. Additionally, the ring was opened to create products m/z = 130 and m/z = 122, the C-S bond was broken, and the mixture eventually mineralized entirely [280] [245]. Similar analysis were performed for degradation of 100 mg/L methylene blue organic pollutant the results of which are presented in Appendix C (Fig. D.7).

Chapter 7

R&D 4: Advanced oxidation of Arsenic(III) to Arsenic(V) using ozone nanobubbles under high salinity

In this chapter, The work on oxidation of As(III) using ozone nanobubbles has been reported. The effects of ozone flow rates, initial arsenic(iii) concentrations, effect of varying pH and presence of salts has been investigated. The use of 2-propanol as the ${}^{\bullet}OH$ radical scavenger has also been reported. The degradation kinetics has also been studied in this work. The generation of ozone nanobubbles through nanopore diffusion method is also been reported in this work.

7.1 Effect of ozone flow rate on nanobubble generation

The nanopore diffusion method was utilized to generate ozone nanobubbles in pure water [3]. The effect of ozone flow rate on mean bubble diameter and bubble density are presented in Fig. 7.1 (a). The bubble density ranged from 3×10^7 to 6×10^7 bubbles.mL-1 with a mean bubble diameter ranging from 125-190 nm (Fig. 7.1 (a)). Ozone nanobubbles typically possessed a negative zeta potential, with a maximum magnitude of -11 mV (Fig. 7.1 (b)). The bubble density monotonically increases with an ozone flow rate up to 3 L/min, and it levels off to a decreasing value until 10 L/min, whereas the mean bubble diameter increases with the ozone flow rates and levels off to a constant value of 200 nm. On the other hand, zeta potential measurements in Fig. 7.1 (b) progressed to a maximum as the ozone flow rate increased from 1 to 3 L/min, followed by a gradual decrease with increasing flow rates. This is attributed to the fact that at higher flow rates, the bubble density decreases, decreasing the zeta potential magnitude. The cumulative population of nanobubbles at distinct flow rates were depicted in Fig. 7.1 (c). The sharpness of the curve reflected a smaller size of the mean bubble diameter, as illustrated for 3 L/min results. Fig. 7.1 (d) showed the representative light scattering intensity of ozone nanobubbles generated using 3 and 10 L/min ozone flow rates. They were compared against commercial 150 nm polystyrene nanoparticles. The scattering intensity of the nanobubbles was measured to be smaller than that of the polystyrene particles. Relative to the refractive index of gas-filled polystyrene bubbles (1.633), the ozone nanobubbles refractive indices in pure water were calculated to be 1.018 and 1.002 at 3 and 10 L/min, respectively. Thus, it can

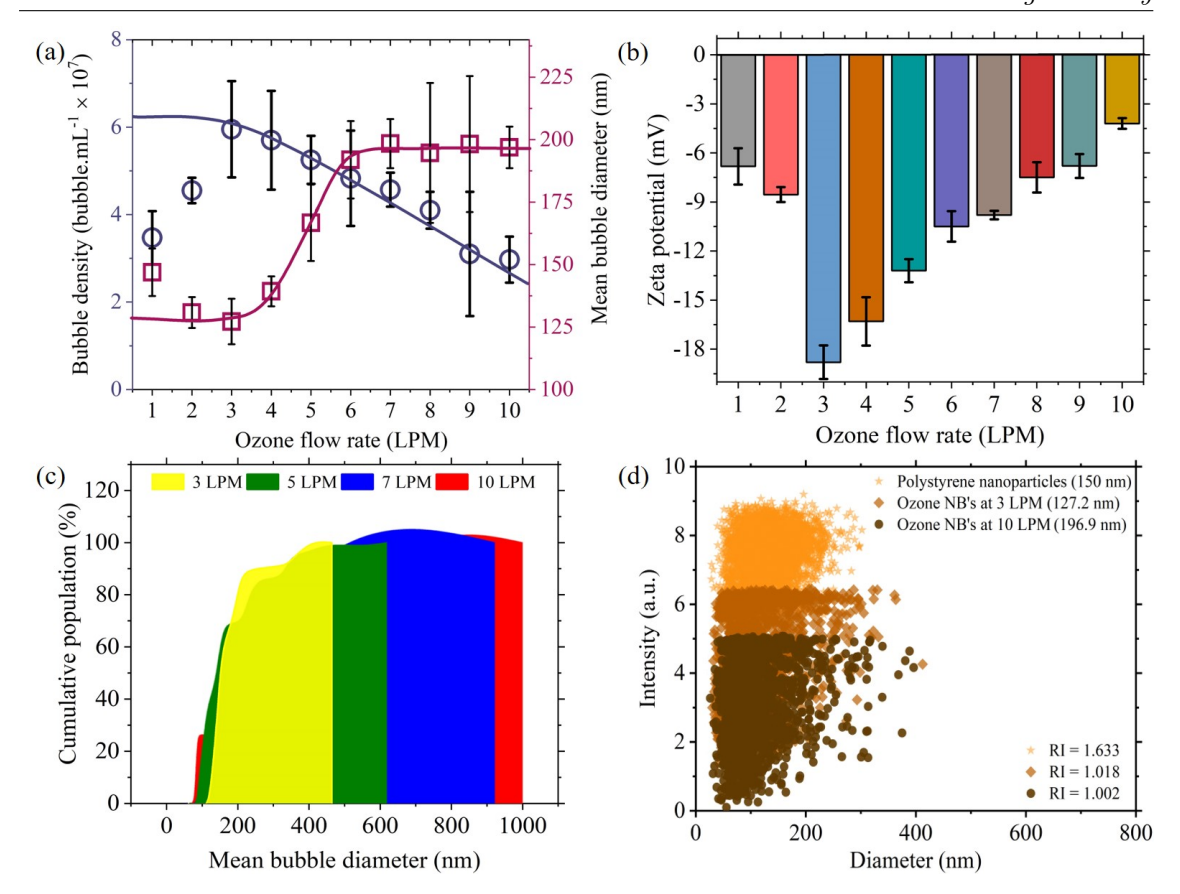


Figure 7.1: Ozone nanobubble generation in pure water at various ozone flow rates (a) Bubble number density and mean diameter (b) Zeta potential (c) Cumulative population of ozone nanobubbles (d) Comparison of the scattering intensities of 100 nm mono-dispersed polystyrene latex beads with ozone nanobubbles produced at 3 L/min (127.2 nm) and 10 L/min (196.6 nm)

be said that only nanobubbles were being produced during the generation and degradation processes. To summarize, during the generation and degradation processes. To summarize, it can be concluded that the ozone nanobubbles generated in pure water were undoubtedly nanobubbles as their refractive index was close to 1.00, as in the case of nano-entities [23].

7.2 Effect of ozone flow rate on Arsenic oxidation

To study the effect of ozone flow rates and ozone intake, the experiments were performed at different conditions. The amount of As(III) oxidized to As(V) was measured with reaction rate kinetics. Online measurements of dissolved ozone concentrations were also performed. Although the change in ozone flow rate was over one order of magnitude, but it was found that the degradation was more at 3 L/min with 60% conversion rates. In addition to that, the oxidation was rapid and effective even at other flow rates (1-10 L/min).

Fig. 7.2 (a) and (b) depicted the concentration profiles and final concentration of As(V), respectively, at each individual flow rate. Fig. 7.2 (b) showed that oxidation of As(III) to As(V) was higher at 3 L/min than at other flow rates. This can be attributed to the

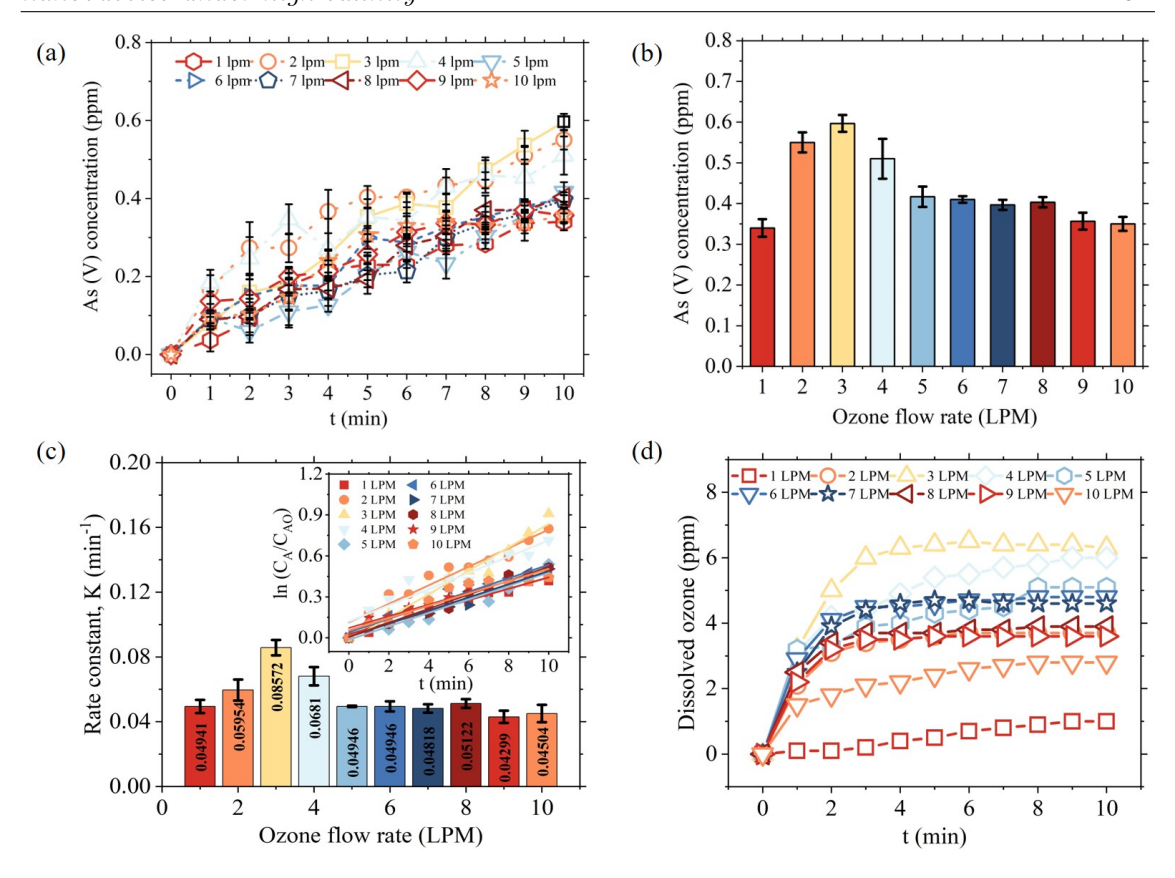


Figure 7.2: (a) Effect on oxidation of As(III) to As(V) at different ozone flow rates with respect to time (b) Final As(V) concentration achieved at the end of 10 minutes at different ozone flow rates (c) Reaction rate constant at various flow rates (d) Online dissolved ozone measurements during oxidation process

fact that the highest amount of dissolved ozone (6.5 ppm) was achieved at 3 L/min of ozone flow rates, as depicted in Fig. 7.2 (d). This also corresponds to the higher As(V) observed in Fig. 7.2 (b). Thus, higher conversion rates, i.e. As(III) to As(V), were achieved when higher concentrations of dissolved ozone were present [281] [209]. This can also be confirmed by the rate kinetics performed at each flow rate, as depicted in Fig. 7.2 (c). The kinetics followed the first-order reaction with the highest rate constant K at 3 L/min (0.08572 min⁻¹). Thus, it can be said that the higher the concentration of ozone, the higher the degradation efficiency, and the higher will be their rate constant. Also form Fig. 7.1 (a), it was observed that the nanobubbles formed were highest in concentration at 3 L/min thereby increasing the mass transfer coefficient of ozone. The rate kinetics were also examined, and the rate constant, K, is represented in Fig. 7.2 (c). It showed that the degradation process of As(III) matched well with first-order kinetics (\mathbb{R}^2 = 0.96). The highest rate constant of 0.08572 min⁻¹ was observed at 3 L/min. This implied that the amount of dissolved ozone concentration played a major role in the degradation of As(III). Henceforth, for further experiments 3 L/min was chosen for oxidation reactions of As(III).

7.3 Effect of initial concentration of As(III)

The effect of initial concentrations of arsenic has been presented in this section. The ozone intake rates were fixed at 3 L/min for these experimental runs, and other parameters were also held constant. Fig. 7.3 (a) illustrates the oxidation of As(III) to As(V) at different initial concentrations. The amount of dissolved ozone was essentially the same since the ozone flow rates were kept constant at 3 L/min, translating to a dissolved ozone concentration of 6.8 ppm. The degrading efficiency as a function of time has been depicted in Fig. 7.3 (b). The initial concentration of As(III) increased the oxidation time. As oxidation with ozone proceeded, the As(III) gradually converted to As(V). The degradation efficiency reached 98% and 96% within 18 and 20 minutes (for 1 ppm and 2-4 ppm of As(III) concentrations) respectively. It is observed that the degradation enhances over time and that the initial concentration of As(III) had no effect on the dissolved ozone concentration. This can be explained by determining the reaction rate constant, as shown in Fig. 7.3 (c). The reaction followed first-order kinetics. The reaction rate constant values were reported to be 0.07346 min⁻¹, 0.0633 min⁻¹, 0.05967 min⁻¹ and 0.06434 min⁻¹, respectively, for 1, 2, 3, and 4 ppm. The minor difference in the obtained rate constants concluded that the initial concentration of As(III) did not affect the degradation efficiency until the ozone concentrations were kept constant at a particular value (6.8 ppm in this case). The mass balance of arsenic concentration was also calculated and presented in Fig. 7.3 (d). As increasingly more As(III) was oxidized, the concentration of As(V) within the reactor increased. The total arsenic concentration remained constant throughout the experiments, indicating mass conservation [209].

7.4 Effect of pH

pH is considered to be a critical factor for oxidation processes. Prior literature work reports findings related to As(III) oxidation in the pH range of 3–9. Driehaus et al. [178] used manganese oxide to oxidise As(III) at pH levels ranging from 5 to 10. However, the impact of pH on the rate of oxidation was not studied by them. Conversely, Sorlini and Gialdini [282] have showed variations in the oxidation rates with hypochlorite, monochloramine, potassium permanganate, and chlorine dioxide at the pH range of 5-8 while employing. Hug and Leupin [283] found that As(III) oxidation by H_2O_2 was sluggish at neutral and acidic pH values. Khuntia et al. [209] investigated the effect of ozone microbubbles on the oxidation of As(III) to As(V) at pH ranging from 5-9 and found that acidic pH = 6 gave better oxidation results as compared to basic pH = 9. Han et al. [195] concluded As(III) oxidation to As(V) was 97% effective at pH 1 by blowing O_2 nanobubbles by studying the oxidation in the pH range from 1-10.

In the current study, the pH effect (3 to 11) on the oxidation of As(III) with ozone nanobubbles was investigated. The studies were conducted at a constant ozone flow rate of 3 L/min (6 -7 ppm ozone concentration) and 1 ppm of initial As(III). The pH of the

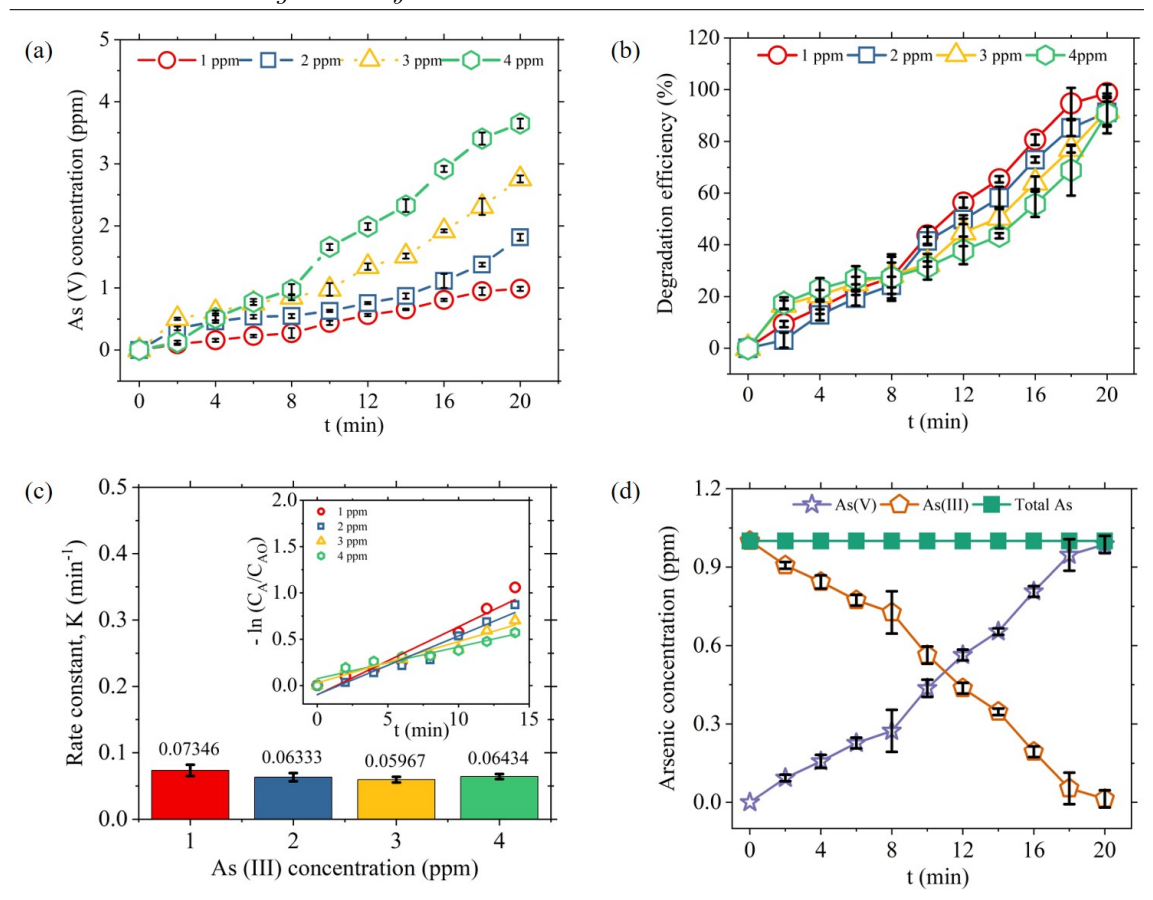


Figure 7.3: (a) Effect on oxidation of As(III) to As(V) at different initial concentrations of As(III) (b) Degradation efficiency with time achieved at the end of 20 minutes at varying As(III) initial concentration (c) Reaction rate constant following the first order kinetics (d) Mass balance of total arsenic at 1 ppm As(III) initial concentration

solution was varied with 1M NaOH and 1M HCl solutions. The studies were carried out to determine the highest conversion rates at pH levels (3, 5, 7, 9, and 11) over the course of 10 minutes. The following reactions elucidated how the products of As(III) and ozone reaction vary with pH [284] [285]: At pH 6.5:

$$H_3 As O_3 + O_3 \longrightarrow H_2 As O_4^- + O_2 + H^+$$
 (7.1)

At pH 8.5:

$$H_3 As O_3 + O_3 \longrightarrow H As O_4^{2-} + O_2 + 2H^+$$
 (7.2)

Fig. 7.4 represents the oxidation results of As(III) to As(V), degradation efficiency, rate kinetics, and dissolved ozone concentration. Fig. 7.4 (a) concluded that As(III) oxidation to As(V) decreased as we shifted the pH from acidic to alkaline. Within a time span of 10 minutes, the degradation efficiency reached a maximum of 70% at pH 3 and a minimum of 39% at pH 11 as depicted in Fig. 7.4 (b). This can further be justified by calculating the reaction rate kinetics, as shown in Fig. 7.4 (c). It was found that the reaction followed first-order kinetics. The rate constant K at pH 3, with a value of 0.10854 min⁻¹, was the maximum, while the lowest K was associated with conditions set at pH 11 (0.04605 min⁻¹).

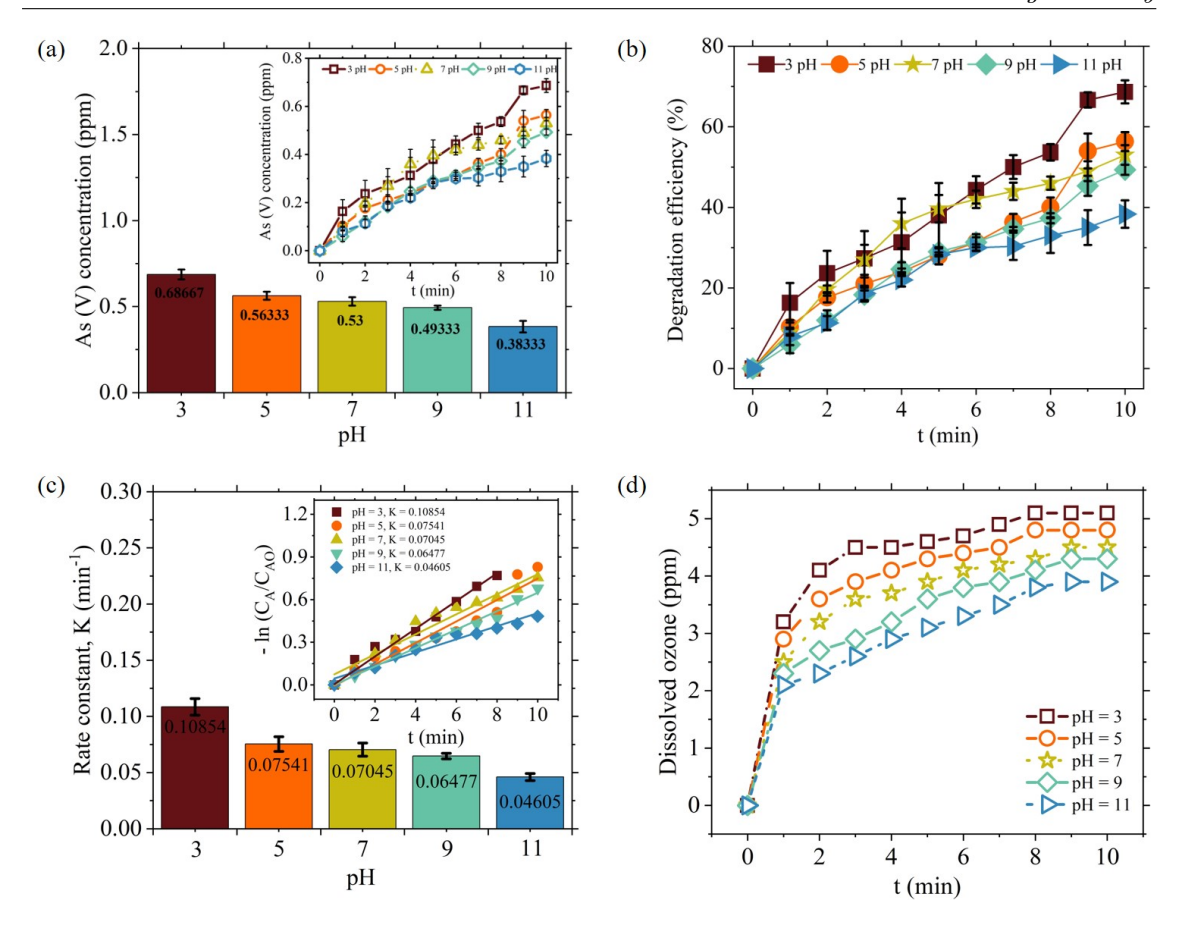


Figure 7.4: Effect on oxidation of As(III) to As(V) at varying pH (3-11) (a) As(V) final concentration vs pH after 10 minutes (b) Degradation efficiency achieved at the end of 10 minutes at different pH (c) Reaction rate constant K with at varying pH (d) Online dissolved ozone measurements during oxidation process

It was also found that the amount of dissolved ozone was higher in acidic pH conditions relative to basic pH. The dissolved ozone concentration profiles have been displayed in Fig. 7.4 (d). They illustrated ozone concentrations to be 5 ppm and 4 ppm at 3 and 11 pH, respectively. We, therefore, inferred that the higher the amount of dissolved ozone present, the better the oxidation and the greater the degradation efficiency.

pH has had a major effect on ozone activity because the mechanism that produces free radicals differs depending on pH. At varying pH, ozone can react through two distinct methods. In basic media, ozone breaks down to produce ROS and *OH radicals, whereas direct ozone attack has proven to be more prevalent in acidic pH environments [229]. The decomposition of ozone in acidic media can be explained through the following reaction, where the proton H+ reacts with ozone to form O2 and water [286] [287] [258]:

$$O_3 + 2H^+ + 2e^- \longrightarrow O_2 + H_2O$$
 (7.3)

When O_3 interacts with OH^- , it breaks down two additional ozone molecules and regenerates the OH^- ion. The absence or lack of an acceptor drastically alters the situation. Ozone chain disintegration happens through reactions involving ${}^{\bullet}OH$ and $HO_2{}^{\bullet}$ radicals.

Chain termination happens when these radicals recombine. The decomposition of ozone with OH⁻ is as follows[288] [287] [229]:

$$O_3 + OH^- \rightarrow O_2 + HO_2^-$$
 (7.4)

$$O_3 + HO_2^- \rightarrow O_2^{-} + OH^{-} + O_2$$
 (7.5)

$$O_3 + O_2^{--} \rightarrow O_3^{--} + O_2^{--}$$
 (7.6)

$$O_3 + H_2O \rightarrow OH^- + OH^- + O_2$$
 (7.7)

In addition to the ozone's aforementioned reaction processes at basic and acidic pH values, variations in the pH of the solution also affect As(III) speciation [289]. The dominant species H₃AsO₃ dissociated into H₂AsO₃-, H₂AsO₃²⁻ and AsO₃²⁻. The increased oxidation of As(III) at pH 3 was probably due to the dependence of each of these kinds of As(III)'s interaction rates with ozone. During the initial 5 minutes of the response, minor but significant changes were similar to the results reported in Moore et al. [289] where oxidation of As(III) was done with birnessite.

7.5 Effect of chloride ions/salts on oxidation of As(III)

Salts are known to have a physical and chemical influence on the oxidation of ozone. Ozone undergoes physical alterations to its solubility and mass transfer. Generally, the presence of salts lowers the gas solubility. In solutions containing salt, a shift in the solubility of ozone has been reported earlier by Rischbieter et al. [290] and Sotelo et al. [291]. This phenomenon was termed as the "salting out effect". Sotelo et al. [291] studied that at lower pH of 2.5, phosphate and chloride ions were found to increase the decomposition rates of ozone [291]. Ozone's half-life period was halved in the presence of 0.1 M NaCl due to the direct interaction between ozone and the chloride anion as shown in the following reactions [256]:

$$O_3 + Cl^- \longrightarrow O_2^{\bullet} + OCl^- \tag{7.8}$$

$$O_3 + OCl^- \rightarrow 2O_2^{\bullet} + Cl^- \tag{7.9}$$

Thus, this section focused on the effect of the addition of monovalent salt (NaCl) (1, 2, 3, 10, 25 and 50 mM NaCl) on the oxidation of As(III) (at 1 ppm). The results are depicted in Fig. 6. The evolution of As(V) concentrations was shown for different concentrations of NaCl in Fig. 7.5 (a). It was found that as the salt concentration increased, the oxidation of As(III) to As(V) gradually decreased. The degradation efficiency reached 100% within 30 minutes for low salt concentrations (1mM and 2mM). However, once the salt concentration exceeded 2 mM, the degradation efficiency dropped to 78%, 30%, 25% and 18% at 3, 10, 25 and 50 mM NaCl concentrations, respectively (refer 7.5 (b)). These results were further validated by the values of the rate constant obtained from the fit of a first-order kinetics

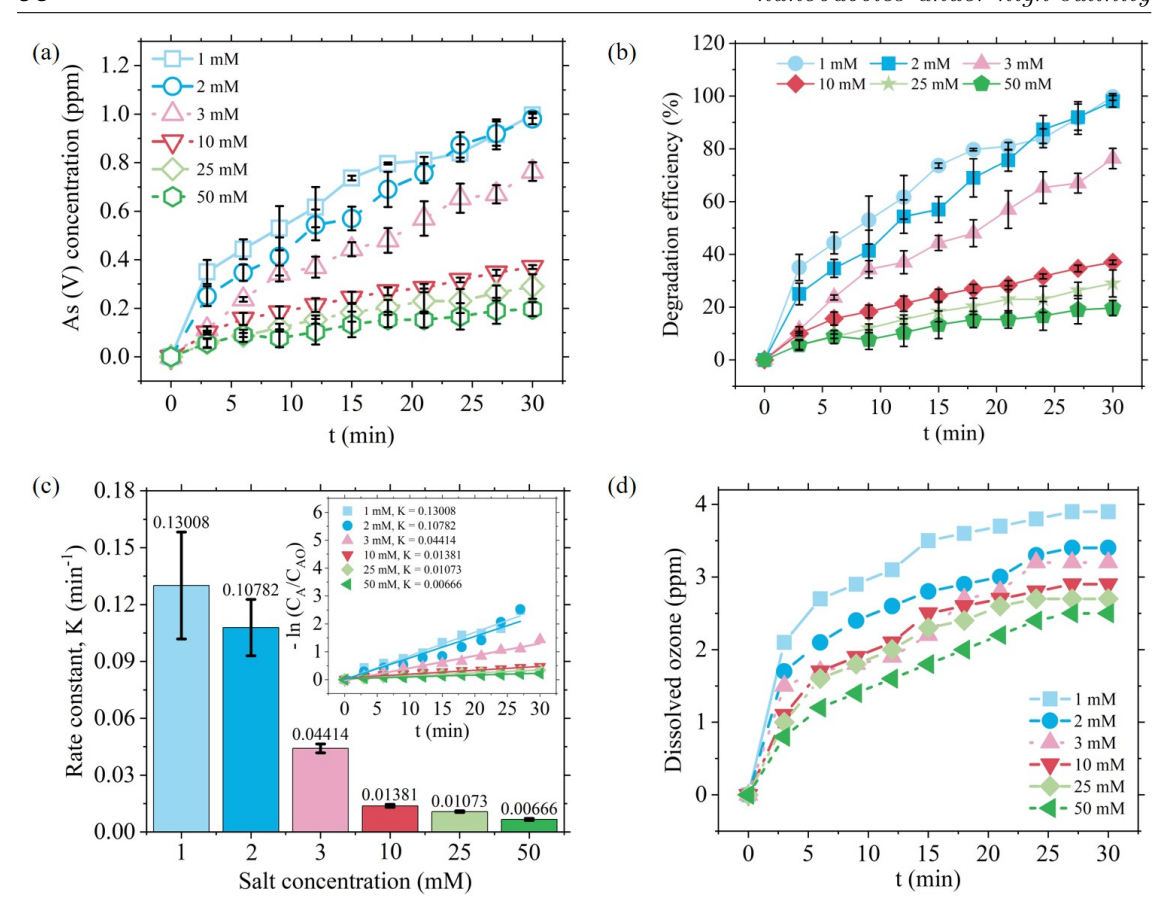


Figure 7.5: Effect of various concentration of monovalent salts (NaCl) on As(III) oxidation (a) Oxidation of As(III) to As(V) at different NaCl concentrations (1-50 mM) (b) Degradation efficiency with time achieved at different NaCl concentrations (c) Reaction rate constant K (d) Online dissolved ozone measurements during oxidation process

model (R^2 = 0.98) as given in Fig. 7.5 (c) values at 50 mM NaCl (0.00666 min⁻¹). Thus, these results correlated with those obtained for the degradation efficiency. The reaction of ozone with chloride ions leads to the formation of superoxide radicals ($O_2^{\bullet-}$) as described in reactions 10 and 11. Although ($O_2^{\bullet-}$) is a reactive oxygen species with a redox potential of 0.55 V, it is very low relative to ozone (E^0 = 2.07 V) [257]. The lower degradation efficiency at higher salt concentrations could be attributed to the lower redox potential of the superoxide radical. The dissolved ozone concentrations, depicted in Fig. 7.5 (d), showed that dissolved ozone decreased for higher salt concentrations. This explains the salting-out effect, where higher concentrations of salts hinder the mass transfer efficiency of ozone gas, thereby decreasing the dissolved ozone concentrations. The results further indicate that the lower the dissolved ozone concentrations, the lower the mass transfer efficiency, leading to lower oxidation rates.

7.6 Effect of 2-propanol as OH radical scavenger

Ozone can create hydroxyl radicals in aqueous media under specific circumstances (i.e. basic pH) [292]. One of the key processes in the oxidation of any organic or inorganic

material is the production of hydroxyl radicals from ozone. The *OH radical may react with a wide range of substances that are usually resistant to ozone oxidization due to its high standard redox potential (2.8 V) compared to the standard redox potential of ozone (2.07 V). Takahashi et al. [29] studied the formation of hydroxyl radicals in bulk nanobubbles through electron spin resonance (ESR) technology. It was anticipated that the source of the hydroxyl radical spin-adducts would be bulk nanobubbles. Michailidi et al. [28] confirmed the formation of hydroxyl radicals due to the collapse of the oxygen and air nanobubbles using electron paramagnetic resonance (EPR) under ambient conditions. As(III) can typically be oxidized by hydroxyl radicals, molecular ozone, or a combination of the two during ozonation. Therefore, radical scavenging experiments were performed to confirm whether the hydroxyl radicals are being generated during ozonation and whether they are responsible for As(III) oxidation. The existence of OH radicals and all the relative contributions of molecular ozone to the oxidation of As(III) was investigated by employing 2-propanol as an *OH radical scavenger. Fig. 7.6 (a) elucidated the effect of 2-Propanol as a radical scavenger at three different concentrations of 0.01, 0.02 and 0.05 M [209]. Adding 0.01 M of 2-propanol hardly affected the conversion of As(III) to As(V). Nevertheless, increasing the concentration from 0.01 to 0.05 M, the degradation efficiency decreased from 95% to 80% over the duration of 30 minutes as shown in Fig. 7.6 (b). The rate kinetics calculations illustrated in Fig. 7.6 (c) depicted that the presence of 2-Propanol affected the degradation efficiency by inhibiting the activity of OH radicals. The highest rate constant K following the first order kinetics was when no scavenger was used (0.13815 min⁻¹) was achieved compared to K at 0.05 M 2-Propanol (0.05907 min⁻¹). The noticeable impact of 2-propanol on the ozone nanobubble-mediated oxidation of As(III) validated the involvement of hydroxyl radicals. It is evident that the OH radicals serve as an efficient oxidant for As(III) since 2-propanol scavenged these radicals. This decrease in the degradation efficiency in the presence of 2-Propanol can also be attributed to the fact that the amount of dissolved ozone produced at each condition varied as shown in Fig. 7.6 (d). As(III) is expected to react with both *OH radicals and molecular ozone at pH values of 5 and 6. Various studies [209], [283] and [293] reported the formation of As(IV) intermediates upon the reaction of arsenic oxide with hydroxyl radicals which further oxidised to As(V). The reactions between As(III) and hydroxyl radicals are as follows:

$$As(OH)_3 + OH^{\bullet} \longrightarrow As(OH)_4$$
 (7.10)

$$As(OH)_2O^- + OH^{\bullet} \longrightarrow As(OH)_3O^-$$
 (7.11)

$$As(OH)_4 \longrightarrow H_2 AsO_3 + H_2 O$$
 (7.12)

$$As(OH)_4 \longrightarrow HAsO_3^- + H^+ + H_2O \tag{7.13}$$

$$H_2ASO_3 \longrightarrow HAsO_3^- + H^+$$
 (7.14)

$$As(OH)_2O^- + O^- \longrightarrow AsO_3^{2-} + H_2O$$
 (7.15)

The pH determines the formation of the As(IV) species. While As(OH)₃O⁻ was discovered in the pH range of 8.5–10, the species As(OH)₄ was seen at pH < 6. At pH > 3, the

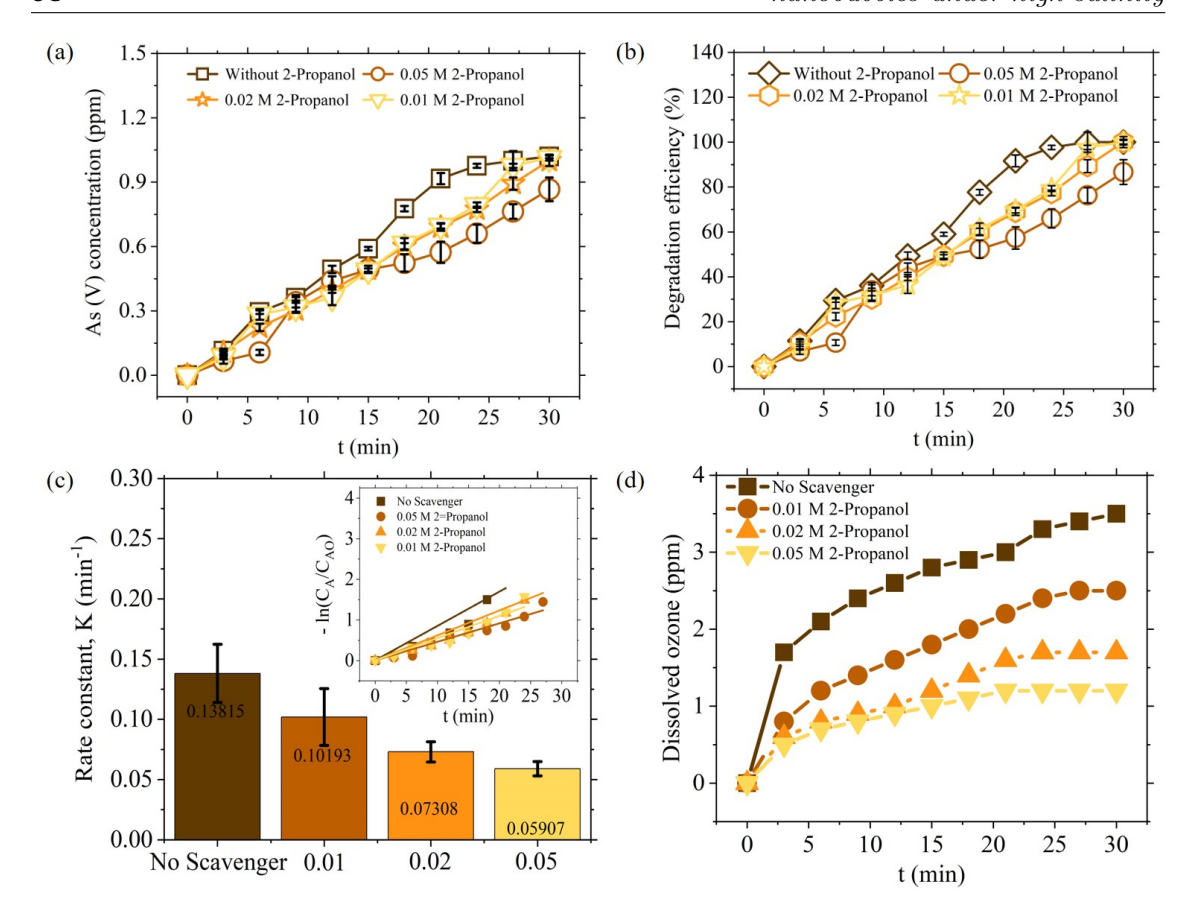


Figure 7.6: Effect of addition of scavenger (2-Propanol) (a) Oxidation of As(III) to As(V) at 0.01-0.05 M 2-Propanol concentrations (b) Degradation efficiency at different scavenger concentration (c) Reaction rate constant K (d) Online dissolved ozone measurement during oxidation process

species $HAsO_3^-$ and AsO_3^{2-} develop. Therefore, As(IV) would exist as $As(OH)_4$, $HAsO_3^-$, and AsO_3^{2-} in the event that ozone microbubbles produced ${}^{\bullet}OH$ radicals in an acidic environment. It was not anticipated that the species $As(OH)_3O^-$ would arise under these circumstances. Every As(IV) species oxidises further to become As(V) [293] [209].

Chapter 8

Conclusion

This chapter summarizes the conclusions drawn from each objective and provides recommendation for future work.

8.1 Conclusion

In this work, the characteristics and stability of ozone nanobubbles in advanced oxidation processes (AOPs) under different parameters have been studied. How nanobubbles help in enhancing the solubility and mass transfer coefficient of ozone in wastewater treatment has been investigated. Along with that, application of ozone nanobubbles in treating the various contaminants present in wastewater such as antibiotics, organic contaminants like dyes and heavy metals. The effects of several important parameters such as pH, ozone generation rates, presence of salts and surfactants have been presented. Degradation kinetics, measurement of mass transfer coefficient and degradation pathways have been studied in detail for each contaminant. The salient accomplishments and the major conclusions are briefly present as per different sections.

8.1.1 Characteristics, stability and application of ozone nanobubbles

- The peculiar properties of the (O_3^-) nanobubbles and their application in dye degradation were investigated in this work. The ozone decomposes into superoxide anions (O_3^-) with and without the presence of salt and the higher negative zeta potential of the nanobubbles was perhaps due to the O_3^- . The rate of formation of O_3^- may be further enhanced by the high ozone flow rate of the ozone gas. The presence of chloride ions also facilitates the formation of O_3^- which reflects on the zeta potential of nanobubbles.
- The (O_3^-) nanobubble dynamics were observed to be in stark contrast with the air/oxygen nanobubbles both in the presence and absence of the salts. The surface charge of Air/oxygen nanobubbles decreases with salt concentration whilst ozone nanobubbles increase. (O_3^-) nanobubbles in alkaline and acidic medium behave similarly to that air/oxygen nanobubbles.
- Despite the reactive nature of the ozone, the alkaline medium favors the generation of ozone nanobubbles. However, the dissolved ozone in water was observed to be much smaller in the alkaline medium due to the faster ozone degradation. On the

other hand, in the case of air/oxygen nanobubbles, the dissolved oxygen does not affect by altering the pH of the water.

- The refractive index of the ozone nanobubbles in pure water and in the presence of $AlCl_3$ were estimated to be 1.004 and 1.016, respectively, which is close to the refractive index of gas-filled bubbles.
- he mass transfer coefficient by nanobubble dissolution is estimated to be 3-fold higher than that of the nanobubble generation. The present analysis also suggests that the nanobubble mass transfer coefficient is significantly higher than the microbubbles.
- The radical generation property of ozone nanobubbles was analyzed using the DMPO spin-trap ESR method. The results conclude the formation of reactive oxygen species, as can be observed by the peaks obtained in the ESR spectra.
- The long-term stability of the nanobubble suspensions was reported to be several weeks and the bubble size distribution preserves its structure, although the peak gradually decreases with time.
- The dye degradation is facilitated by ozone nanobubbles due to the extraordinary properties of the nanobubbles like high volumetric mass transfer coefficient, high inner Laplace pressure and nanobubble provides an active surface area for the chemical reaction which also contributes to overall dye degradation rate.

8.1.2 Tetracycline degradation for wastewater treatment based on ozone nanobubbles advanced oxidation processes (AOPs)

- The results indicated that employing ozone nanobubbles at a lower pH level (pH = 4) and lower salt concentrations (0.1mM NaCl) resulted in enhanced ozone concentration, as well as more effective degradation of tetracycline compared to other combinations.
- The degradation kinetics follow pseudo-second-order kinetics using ozone nanobubbles which is better compared to first-order kinetics reported for sole ozonation. It is to be noted here that comparisons were made based on the same reactor volume.
- After comparing the effectiveness of other methods, it was found that using ozone in the form of nanobubbles produced the best degradation efficiency.
- Preserving the high potential of ozonation requires avoiding the presence of *OH radical scavengers, such as 2-Propanol, as the oxidation process of *OH radicals are one of the essential processes in the mineralization of organic molecules.
- The presence of intermediates was verified through LC-MS analysis. O₃ and •OH has the ability to target the ortho or para position of the phenol ring on TC.

Additional oxidation causes the unstable intermediates to ultimately breaking down into inorganic compounds like CO_2 , H_2O , and NH_4^+ .

• the best results with parameters for 100% degradation were at 100 mg/L of TC at 8 mg/L (10 L/min) concentrations of dissolved ozone within 20 minutes of time span.

8.1.3 Ozone nanobubbles based advanced oxidation processes (AOPs) for degradation of organic pollutants

- Ozone nanobubbles increased the degradation efficiency by 2.8 times when compared
 to oxygen nanobubbles. Quenching experiments were also performed to demonstrate
 the formation of reactive oxygen species.
- It was found that the negative charge possessed by nanobubbles and the production of reactive oxygen species (*OH, O₂) along with ozone molecule were the fundamental reasons for degradation.
- A higher amount of nanobubble concentration yields better degradation rates. At 5 LPM, high density of nanobubbles 19×10^7 with 145 nm mean bubble diameter gave 100% degradation with highest rate constants at each concentration of the organic pollutant followed by 7 and 2.5 LPM ozone flow rates.
- High-density nanobubbles enhance the production of ROS which leads to higher removal rates. Ozone nanobubble treatments decreases the pH of the water and it was observed that this can be due to the formation of intermediates (aldehydes, acids, etc).
- Alkaline medium favors the contaminant degradation. On comparing the effectiveness with oxygen nanobubbles, ozone nanobubbles were more efficient with 99% removal rates. The reaction kinetics follows the second-order kinetics while oxygen nanobubbles [277] and air nanobubbles [213] offer first-order kinetics.
- Addition of salts and surfactants hinders the degradation rate.

8.1.4 Advanced oxidation of Arsenic(III) to Arsenic(V) using ozone nanobubbles under high salinity

- Highest nanobubble density was achieved when ozone flow rate was set at 3 LPM and introduced by the nanopore diffusion method to the reactor system. A bubble density of 6.2×10^7 bubbles.mL⁻¹, zeta potential of -11 mV and mean bubble diameter of 125 nm was achieved.
- The oxidation of As(III) to As(V) was affected by parameters such as ozone flow rates and initial concentration of arsenite. The rate of oxidation increased with increasing ozone concentrations. The dissolved ozone concentration reached a maximum at 3 LPM. Hence, it was considered as an optimum operating condition for oxidation to take place providing 99% conversion of As(III) to As(V).

- One of the factors regulating the oxidation of As(III) was the medium pH. The conversion of As(III) was faster in acidic conditions (pH 3 and 4) with 70 and 60% degradation efficiency as compared to basic conditions (pH 9 and 11). The latter was associated with a degradation efficiency of 45 and 39% respectively. This behaviour is most likely caused by the fluctuation in As(III) speciation with pH.
- Salt addition had a negative impact. It decreased the degradation efficiency from 100 to 19% as the concentration of salt increased from 1 to 50 mM. The plausible reason for this can be explained by the salting out effect which hinders the solubility of ozone.
- ROS, •OH radical and molecular ozone were found to be the key species responsible for the oxidation process. 2-propanol confirmed the presence of •OH radical during the conversion of As(III) to As(V). The As(III) oxidation kinetics could be described by a first order model.

8.2 Scope for future work

In this work, understanding ozone nanobubbles under different water conditions, their characteristics and stability along with its application in the degradation of various contaminants such as antibiotics, organic pollutants and heavy metals has been performed. However, this work can further be put into practical applications, thus providing some future aspects.

- Ozone nanobubbles can be a substitute for the chemical sterilization method such as chlorine, UV, etc. due to the extraordinary stability of the nanobubbles. Ozone nanobubbles can also eliminate the problem of short-term sterilization like UV.
- Ozonation in the effluent treatment plant is considered to be expensive and suffers from the scale-up problem. Ozone nanobubble offers cost reduction by process intensification and facilitates the scale-up for industrial-scale applications.
- The enhanced mass transfer coefficient due to ozone nanobubbles increases the overall rate of dye degradation. This aspect can be utilized in the process design calculation in disinfection and wastewater treatment applications to reduce the cost of the treatment.
- Optimization of parameters such as ozone consumption, cost effectiveness, energy
 consumption can be studied. On the other hand, it is worth exploring the degradation
 mechanism of other types of antibiotics having different structural characteristics by
 ozone in the form of nanobubbles.
- Comparison of the conventional AOPs with the ozone nanobubbles in terms of degradation rates, efficiency, by-product formation and energy consumption can be carried out to get better insights on the advantages of ozone nanobubbles.

- [1] Petroula Seridou and Nicolas Kalogerakis. Disinfection applications of ozone micro-and nanobubbles. *Environmental Science: Nano*, 8(12):3493–3510, 2021. doi: https://doi.org/10.1039/D1EN00700A.
- [2] Mingyi Jia, Muhammad Usman Farid, Jehad A Kharraz, Nallapaneni Manoj Kumar, Shauhrat S Chopra, Am Jang, John Chew, Samir Kumar Khanal, Guanghao Chen, and Alicia Kyoungjin An. Nanobubbles in water and wastewater treatment systems: small bubbles making a big difference. *Water Research*, page 120613, 2023.
- [3] Harsh Sharma, Mohit Trivedi, and Neelkanth Nirmalkar. Do nanobubbles exist in pure alcohol? *Langmuir*, 2024.
- [4] Karthik S Babu and Jayendra K Amamcharla. Generation methods, stability, detection techniques, and applications of bulk nanobubbles in agro-food industries: A review and future perspective. *Critical Reviews in Food Science and Nutrition*, 63 (28):9262–9281, 2023.
- [5] Wei Fan, Wengang An, Mingxin Huo, Dan Xiao, Tao Lyu, and Jingyu Cui. An integrated approach using ozone nanobubble and cyclodextrin inclusion complexation to enhance the removal of micropollutants. Water Research, 196:117039, 2021. doi: https://doi.org/10.1016/j.watres.2021.117039.
- [6] Tae-Kyoung Kim, Taeyeon Kim, Inae Lee, Kyungho Choi, and Kyung-Duk Zoh. Removal of tetramethylammonium hydroxide (tmah) in semiconductor wastewater using the nano-ozone h2o2 process. *Journal of Hazardous Materials*, 409:123759, 2021. doi: https://doi.org/10.1016/j.jhazmat.2020.123759.
- [7] Vitalis Chipakwe, Rickard Jolstera, and Saeed Chehreh Chelgani. Nanobubble-assisted flotation of apatite tailings: Insights on beneficiation options. *ACS omega*, 6(21):13888–13894, 2021.
- [8] HNP Dayarathne, Sanghyun Jeong, and Am Jang. Chemical-free scale inhibition method for seawater reverse osmosis membrane process: Air micro-nano bubbles. *Desalination*, 461:1–9, 2019.
- [9] Wei Fan, Yuhang Li, Chunliang Wang, Yutong Duan, Yang Huo, Brielle Januszewski, Meng Sun, Mingxin Huo, and Menachem Elimelech. Enhanced photocatalytic water decontamination by micro—nano bubbles: measurements and mechanisms. Environmental Science & Technology, 55(10):7025–7033, 2021.

[10] Wachiranon Chuenchart, Renisha Karki, Ty Shitanaka, Kyle Rafael Marcelino, Hui Lu, and Samir Kumar Khanal. Nanobubble technology in anaerobic digestion: A review. *Bioresource technology*, 329:124916, 2021.

- [11] Hiroshi Tomiyasu, Hiroshi Fukutomi, and Gilbert Gordon. Kinetics and mechanism of ozone decomposition in basic aqueous solution. *Inorganic Chemistry*, 24(19): 2962–2966, 1985.
- [12] Knud Sehested, Hanne Corfitzen, Jerzy Holcman, Christian H Fischer, and Edwin J Hart. The primary reaction in the decomposition of ozone in acidic aqueous solutions. Environmental science & technology, 25(9):1589–1596, 1991.
- [13] Neelkanth Nirmalkar, AW Pacek, and Mostafa Barigou. On the existence and stability of bulk nanobubbles. *Langmuir*, 34(37):10964–10973, 2018. doi: https://doi.org/10.1021/acs.langmuir.8b01163.
- [14] Yang Han, Yefei Liu, Hong Jiang, Weihong Xing, and Rizhi Chen. Large scale preparation of microbubbles by multi-channel ceramic membranes: hydrodynamics and mass transfer characteristics. The Canadian Journal of Chemical Engineering, 95(11):2176–2185, 2017.
- [15] Mei Bai, Zhibin Liu, Jinpeng Zhang, and Liangliang Lu. Prediction and experimental study of mass transfer properties of micronanobubbles. *Industrial & Engineering Chemistry Research*, 60(22):8291–8300, 2021.
- [16] Shan Xue, Yihan Zhang, Taha Marhaba, and Wen Zhang. Aeration and dissolution behavior of oxygen nanobubbles in water. *Journal of colloid and interface science*, 609:584–591, 2022.
- [17] Wanting Xiao and Guoren Xu. Mass transfer of nanobubble aeration and its effect on biofilm growth: Microbial activity and structural properties. Science of the Total Environment, 703:134976, 2020.
- [18] Ben Chen, Sining Zhou, Ning Zhang, Huiyu Liang, Lianpeng Sun, Xin Zhao, Jingyi Guo, and Hui Lu. Micro and nano bubbles promoted biofilm formation with strengthen of cod and tn removal synchronously in a blackened and odorous water. Science of the Total Environment, 837:155578, 2022.
- [19] Weiguang Zhou, Liming Liu, Baonan Zhou, Li Weng, Junguo Li, Cheng Liu, Siyuan Yang, Changning Wu, and Ke Liu. Electrokinetic potential reduction of fine particles induced by gas nucleation. *Ultrasonics Sonochemistry*, 67:105167, 2020.
- [20] Fernanda Yumi Ushikubo, Takuro Furukawa, Ryou Nakagawa, Masatoshi Enari, Yoshio Makino, Yoshinori Kawagoe, Takeo Shiina, and Seiichi Oshita. Evidence of the existence and the stability of nano-bubbles in water. *Colloids and Surfaces A: Physicochemical and Engineering Aspects*, 361(1-3):31–37, 2010.

[21] Marc A Hampton and Anh V Nguyen. Nanobubbles and the nanobubble bridging capillary force. *Advances in colloid and interface science*, 154(1-2):30–55, 2010. doi: https://doi.org/10.1016/j.cis.2010.01.006.

- [22] Qiaozhi Wang, Hui Zhao, Na Qi, Yan Qin, Xuejie Zhang, and Ying Li. Generation and stability of size-adjustable bulk nanobubbles based on periodic pressure change. *Scientific reports*, 9(1):1118, 2019.
- [23] Kalyani Agarwal, Mohit Trivedi, Claus-Dieter Ohl, and Neelkanth Nirmalkar. On nanobubble dynamics under an oscillating pressure field during salting-out effects and its dlvo potential. *Langmuir*, 2023. doi: https://doi.org/10.1021/acs.langmuir. 2c03085.
- [24] Beng Hau Tan, Hongjie An, and Claus-Dieter Ohl. How bulk nanobubbles might survive. *Physical review letters*, 124(13):134503, 2020.
- [25] Pratik A Satpute and James C Earthman. Hydroxyl ion stabilization of bulk nanobubbles resulting from microbubble shrinkage. *Journal of Colloid and Interface* Science, 584:449–455, 2021.
- [26] Zhan Gao, Wangxia Wu, Weitao Sun, and Bing Wang. Understanding the stabilization of a bulk nanobubble: A molecular dynamics analysis. *Langmuir*, 37 (38):11281–11291, 2021.
- [27] Gaurav Yadav, Neelkanth Nirmalkar, and Claus-Dieter Ohl. Electrochemically reactive colloidal nanobubbles by water splitting. *Journal of Colloid and Interface Science*, 663:518–531, 2024.
- [28] Elisavet D Michailidi, George Bomis, Athanasios Varoutoglou, George Z Kyzas, George Mitrikas, Athanasios Ch Mitropoulos, Eleni K Efthimiadou, and Evangelos P Favvas. Bulk nanobubbles: Production and investigation of their formation/stability mechanism. Journal of colloid and interface science, 564:371–380, 2020.
- [29] Masayoshi Takahashi, Yasuyuki Shirai, and Shigetoshi Sugawa. Free-radical generation from bulk nanobubbles in aqueous electrolyte solutions: Esr spin-trap observation of microbubble-treated water. *Langmuir*, 37(16):5005–5011, 2021.
- [30] Ahmed Khaled Abdella Ahmed, Xiaonan Shi, Likun Hua, Leidy Manzueta, Weihua Qing, Taha Marhaba, and Wen Zhang. Influences of air, oxygen, nitrogen, and carbon dioxide nanobubbles on seed germination and plant growth. *Journal of Agricultural and Food Chemistry*, 66(20):5117–5124, 2018.
- [31] Shu Liu, Seiichi Oshita, Saneyuki Kawabata, Yoshio Makino, and Takahiko Yoshimoto. Identification of ros produced by nanobubbles and their positive and negative effects on vegetable seed germination. *Langmuir*, 32(43):11295–11302, 2016. doi: https://doi.org/10.1021/acs.langmuir.6b01621.

[32] Shu Liu, Seiichi Oshita, Dang Quoc Thuyet, Masanao Saito, and Takahiko Yoshimoto. Antioxidant activity of hydrogen nanobubbles in water with different reactive oxygen species both in vivo and in vitro. *Langmuir*, 34(39):11878–11885, 2018.

- [33] Shu Liu, Jiayao Li, Seiichi Oshita, Mohammed Kamruzzaman, Minming Cui, and Wenhong Fan. Formation of a hydrogen radical in hydrogen nanobubble water and its effect on copper toxicity in chlorella. ACS Sustainable Chemistry & Engineering, 9(33):11100–11109, 2021.
- [34] Rajeshree A Khaire and Parag R Gogate. Application of hydrodynamic cavitation in food processing. In *Design and optimization of innovative food processing techniques assisted by ultrasound*, pages 317–342. Elsevier, 2021.
- [35] Haipeng Li, Artin Afacan, Qingxia Liu, and Zhenghe Xu. Study interactions between fine particles and micron size bubbles generated by hydrodynamic cavitation.

 Minerals engineering, 84:106–115, 2015.
- [36] R Etchepare, A Azevedo, S Calgaroto, and J Rubio. Removal of ferric hydroxide by flotation with micro and nanobubbles. Separation and Purification Technology, 184: 347–353, 2017.
- [37] Chen-Ran Mo, Jing Wang, Zhou Fang, Li-Min Zhou, Li-Juan Zhang, and Jun Hu. Formation and stability of ultrasonic generated bulk nanobubbles. *Chinese Physics B*, 27(11):118104, 2018.
- [38] Masato Kukizaki. Microbubble formation using asymmetric shirasu porous glass (spg) membranes and porous ceramic membranes—a comparative study. *Colloids and Surfaces A: Physicochemical and Engineering Aspects*, 340(1-3):20–32, 2009.
- [39] Masato Kukizaki and Masahiro Goto. Size control of nanobubbles generated from shirasu-porous-glass (spg) membranes. Journal of membrane science, 281(1-2): 386–396, 2006.
- [40] Pramesh Dhungana and Bhesh Bhandari. Development of a continuous membrane nanobubble generation method applicable in liquid food processing. *International Journal of Food Science & Technology*, 56(9):4268–4277, 2021.
- [41] Ahmed Khaled Abdella Ahmed, Cuizhen Sun, Likun Hua, Zhibin Zhang, Yanhao Zhang, Wen Zhang, and Taha Marhaba. Generation of nanobubbles by ceramic membrane filters: The dependence of bubble size and zeta potential on surface coating, pore size and injected gas pressure. *Chemosphere*, 203:327–335, 2018.
- [42] Muidh Alheshibri and Vincent SJ Craig. Generation of nanoparticles upon mixing ethanol and water; nanobubbles or not? *Journal of colloid and interface science*, 542:136–143, 2019.

[43] Shi-Tao Lou, Zhen-Qian Ouyang, Yi Zhang, Xiao-Jun Li, Jun Hu, Min-Qian Li, and Fu-Jia Yang. Nanobubbles on solid surface imaged by atomic force microscopy. Journal of Vacuum Science & Technology B: Microelectronics and Nanometer Structures Processing, Measurement, and Phenomena, 18(5):2573–2575, 2000.

- [44] Xue H Zhang, Nobuo Maeda, and Vincent SJ Craig. Physical properties of nanobubbles on hydrophobic surfaces in water and aqueous solutions. *Langmuir*, 22(11):5025–5035, 2006.
- [45] Jie Zhu, Hongjie An, Muidh Alheshibri, Lvdan Liu, Paul MJ Terpstra, Guangming Liu, and Vincent SJ Craig. Cleaning with bulk nanobubbles. *Langmuir*, 32(43): 11203–11211, 2016.
- [46] Thomas A Ternes, Martin Meisenheimer, Derek McDowell, Frank Sacher, Heinz-Jürgen Brauch, Brigitte Haist-Gulde, Gudrun Preuss, Uwe Wilme, and Ninette Zulei-Seibert. Removal of pharmaceuticals during drinking water treatment. Environmental science & technology, 36(17):3855–3863, 2002.
- [47] Chedly Tizaoui, Latifa Bouselmi, Loubna Mansouri, and Ahmed Ghrabi. Landfill leachate treatment with ozone and ozone/hydrogen peroxide systems. *Journal of hazardous materials*, 140(1-2):316–324, 2007.
- [48] Clemens Von Sonntag and Urs Von Gunten. Chemistry of ozone in water and wastewater treatment. IWA publishing, 2012.
- [49] Christiane Gottschalk, Judy Ann Libra, and Adrian Saupe. Ozonation of water and waste water: A practical guide to understanding ozone and its applications. John Wiley & Sons, 2010.
- [50] Davide Gardoni, A Vailati, and Roberto Canziani. Decay of ozone in water: a review. Ozone: Science & Engineering, 34(4):233–242, 2012.
- [51] Adam Dettmer, Raymond Ball, Thomas B Boving, Naima A Khan, Tanner Schaub, Nilusha Sudasinghe, Carlos A Fernandez, and Kenneth C Carroll. Stabilization and prolonged reactivity of aqueous-phase ozone with cyclodextrin. *Journal of contaminant hydrology*, 196:1–9, 2017.
- [52] Janitha Hewa Batagoda, Shaini Dailsha Aluthgun Hewage, and Jay N Meegoda. Nano-ozone bubbles for drinking water treatment. *Journal of Environmental Engineering and Science*, 14(2):57–66, 2018.
- [53] Muhammad Usman Farid, Paula Jungwon Choi, Jehad A Kharraz, Jia-Yong Lao, Sophie St-Hilaire, Yuefei Ruan, Paul Kwan Sing Lam, and Alicia Kyoungjin An. Hybrid nanobubble-forward osmosis system for aquaculture wastewater treatment and reuse. Chemical Engineering Journal, 435:135164, 2022.

[54] Saeed Farrokhpay, Lev Filippov, and Daniel Fornasiero. Flotation of fine particles: A review. *Mineral Processing and Extractive Metallurgy Review*, 42(7):473–483, 2021.

- [55] Hainan Wang, Wenqing Yang, Xiaokang Yan, Lijun Wang, Yongtian Wang, and Haijun Zhang. Regulation of bubble size in flotation: A review. Journal of Environmental Chemical Engineering, 8(5):104070, 2020.
- [56] Jehad A Kharraz, Muhammad Usman Farid, David Jassby, and Alicia Kyoungjin An. A systematic study on the impact of feed composition and substrate wettability on wetting and fouling of omniphobic and janus membranes in membrane distillation. *Journal of Membrane Science*, 641:119873, 2022.
- [57] Hongxiao Guo, Margreet J Oosterkamp, Fabio Tonin, Alexander Hendriks, Revathy Nair, Jules B van Lier, and Merle de Kreuk. Reconsidering hydrolysis kinetics for anaerobic digestion of waste activated sludge applying cascade reactors with ultra-short residence times. Water Research, 202:117398, 2021.
- [58] Xuezhi Wang, Tian Yuan, Zitao Guo, Hanlin Han, Zhongfang Lei, Kazuya Shimizu, Zhenya Zhang, and Duu-Jong Lee. Enhanced hydrolysis and acidification of cellulose at high loading for methane production via anaerobic digestion supplemented with high mobility nanobubble water. *Bioresource technology*, 297:122499, 2020.
- [59] Xiaojing Yang, Jingmin Nie, Yu Wei, Ziwen Zhao, Kazuya Shimizu, Zhongfang Lei, and Zhenya Zhang. Simultaneous enhancement on lignin degradation and methane production from anaerobic co-digestion of waste activated sludge and alkaline lignin supplemented with n2-nanobubble water. Bioresource Technology Reports, 11:100470, 2020.
- [60] Xuezhi Wang, Tian Yuan, Zhongfang Lei, Motoyoshi Kobayashi, Yasuhisa Adachi, Kazuya Shimizu, Duu-Jong Lee, and Zhenya Zhang. Supplementation of o2-containing gas nanobubble water to enhance methane production from anaerobic digestion of cellulose. Chemical Engineering Journal, 398:125652, 2020.
- [61] Ariel J Atkinson, Onur G Apul, Orren Schneider, Sergi Garcia-Segura, and Paul Westerhoff. Nanobubble technologies offer opportunities to improve water treatment. *Accounts of chemical research*, 52(5):1196–1205, 2019. doi: https://doi.org/10.1021/acs.accounts.8b00606.
- [62] Fei Yang, Bo Sheng, Zhaohui Wang, Ying Xue, Jianshe Liu, Tianyi Ma, Richard Bush, Hrvoje Kušić, and Yanbo Zhou. Performance of uv/acetylacetone process for saline dye wastewater treatment: Kinetics and mechanism. *Journal of Hazardous Materials*, 406:124774, 2021. doi: https://doi.org/10.1016/j.jhazmat.2020.124774.
- [63] Jucai Wei, Lin Shi, and Xu Wu. Electrochemical advanced oxidation process with simultaneous persulfate and hydrogen peroxide on-site generations for high salinity

wastewater. Separation and Purification Technology, 310:123147, 2023. doi: https://doi.org/10.1016/j.seppur.2023.123147.

- [64] Kirill Fedorov, Kumaravel Dinesh, Xun Sun, Reza Darvishi Cheshmeh Soltani, Zhaohui Wang, Shirish Sonawane, and Grzegorz Boczkaj. Synergistic effects of hybrid advanced oxidation processes (aops) based on hydrodynamic cavitation phenomenon—a review. *Chemical Engineering Journal*, 432:134191, 2022. doi: https://doi.org/10.1016/j.cej.2021.134191.
- [65] Chhaya V Rekhate and JK Srivastava. Recent advances in ozone-based advanced oxidation processes for treatment of wastewater-a review. Chemical Engineering Journal Advances, 3:100031, 2020. doi: https://doi.org/10.1016/j.ceja.2020.100031.
- [66] Jianlong Wang and Shizong Wang. Reactive species in advanced oxidation processes: Formation, identification and reaction mechanism. *Chemical Engineering Journal*, 401:126158, 2020. doi: https://doi.org/10.1016/j.cej.2020.126158.
- [67] Qi Yang, Yinghao Ma, Fei Chen, Fubing Yao, Jian Sun, Shana Wang, Kaixin Yi, Lihua Hou, Xiaoming Li, and Dongbo Wang. Recent advances in photo-activated sulfate radical-advanced oxidation process (sr-aop) for refractory organic pollutants removal in water. Chemical Engineering Journal, 378:122149, 2019. doi: https://doi.org/10.1016/j.cej.2019.122149.
- [68] Zhila Honarmandrad, Xun Sun, Zhaohui Wang, Muhd Naushad, and Grzegorz Boczkaj. Activated persulfate and peroxymonosulfate based advanced oxidation processes (aops) for antibiotics degradation—a review. Water Resources and Industry, page 100194, 2022. doi: https://doi.org/10.1016/j.wri.2022.100194.
- [69] Dagang Lin, Yu Fu, Xiaodie Li, Lingli Wang, Meiru Hou, Dongdong Hu, Qingchao Li, Zhen Zhang, Chunxiao Xu, Sifan Qiu, et al. Application of persulfate-based oxidation processes to address diverse sustainability challenges: A critical review. Journal of Hazardous Materials, 440:129722, 2022. doi: https://doi.org/10.1016/j.jhazmat.2022.129722.
- [70] Kirill Fedorov, Manoj P Rayaroth, Noor S Shah, and Grzegorz Boczkaj. Activated sodium percarbonate-ozone (spc/o3) hybrid hydrodynamic cavitation system for advanced oxidation processes (aops) of 1, 4-dioxane in water. *Chemical Engineering Journal*, 456:141027, 2023. doi: https://doi.org/10.1016/j.cej.2022.141027.
- [71] Luyao Wang, Dan Luo, Oualid Hamdaoui, Yasser Vasseghian, Malwina Momotko, Grzegorz Boczkaj, George Z Kyzas, and Chongqing Wang. Bibliometric analysis and literature review of ultrasound-assisted degradation of organic pollutants. Science of The Total Environment, 876:162551, 2023. doi: https://doi.org/10.1016/j.scitotenv. 2023.162551.

[72] Danhui Liang, Nan Li, Jingkun An, Jian Ma, Yu Wu, and Hongbo Liu. Fenton-based technologies as efficient advanced oxidation processes for microcystin-lr degradation. *Science of the Total Environment*, 753:141809, 2021. doi: https://doi.org/10.1016/j. scitotenv.2020.141809.

- [73] Sameena N Malik, Prakash C Ghosh, Atul N Vaidya, and Sandeep N Mudliar. Hybrid ozonation process for industrial wastewater treatment: Principles and applications: A review. *Journal of Water Process Engineering*, 35:101193, 2020. doi: https://doi.org/10.1016/j.jwpe.2020.101193.
- [74] Marie M Mitani, Arturo A Keller, Orville C Sandall, and Robert G Rinker. Mass transfer of ozone using a microporous diffuser reactor system. *Ozone: science & engineering*, 27(1):45–51, 2005. doi: https://doi.org/10.1080/01919510590908995.
- [75] Ines Nitoi, Tatiana Oncescu, and Petruta Oancea. Mechanism and kinetic study for the degradation of lindane by photo-fenton process. *Journal of Industrial and Engineering Chemistry*, 19(1):305–309, 2013. doi: https://doi.org/10.1016/j.jiec. 2012.08.016.
- [76] Hazal Öztürk, Sibel Barışçı, and Ozge Turkay. Paracetamol degradation and kinetics by advanced oxidation processes (aops): Electro-peroxone, ozonation, goethite catalyzed electro-fenton and electro-oxidation. *Environmental Engineering Research*, 26(2), 2021. doi: https://doi.org/10.4491/eer.2018.332.
- [77] Andre Fernandes, Michał Gągol, Patrycja Makoś, Javed Ali Khan, and Grzegorz Boczkaj. Integrated photocatalytic advanced oxidation system (tio2/uv/o3/h2o2) for degradation of volatile organic compounds. Separation and Purification Technology, 224:1–14, 2019. doi: https://doi.org/10.1016/j.seppur.2019.05.012.
- [78] André Fernandes, Patrycja Makoś, Javed Ali Khan, and Grzegorz Boczkaj. Pilot scale degradation study of 16 selected volatile organic compounds by hydroxyl and sulfate radical based advanced oxidation processes. *Journal of cleaner production*, 208:54–64, 2019. doi: https://doi.org/10.1016/j.jclepro.2018.10.081.
- [79] Gang Pan, Guangzhi He, Meiyi Zhang, Qin Zhou, Tolek Tyliszczak, Renzhong Tai, Jinghua Guo, Lei Bi, Lei Wang, and Honggang Zhang. Nanobubbles at hydrophilic particle-water interfaces. *Langmuir*, 32(43):11133-11137, 2016. doi: https://doi.org/ 10.1021/acs.langmuir.6b01483.
- [80] Dubasi Govardhana Rao, R Senthilkumar, J Anthony Byrne, and S Feroz. Wastewater treatment: advanced processes and technologies. CRC Press, 2012.
- [81] R Rosal, A Rodriguez, and M Zerhouni. Enhancement of gas-liquid mass transfer during the unsteady-state catalytic decomposition of ozone in water. Applied Catalysis A: General, 305(2):169–175, 2006. doi: https://doi.org/10.1016/j.apcata. 2006.02.059.

[82] Gerald Ruppert, Rupert Bauer, and Günter Heisler. Uv-o3, uv-h2o2, uv-tio2 and the photo-fenton reaction-comparison of advanced oxidation processes for wastewater treatment. *Chemosphere*, 28(8):1447–1454, 1994. doi: https://doi.org/10.1016/0045-6535(94)90239-9.

- [83] U Sathya, M Nithya, N Balasubramanian, et al. Evaluation of advanced oxidation processes (aops) integrated membrane bioreactor (mbr) for the real textile wastewater treatment. *Journal of environmental management*, 246:768–775, 2019. doi: https://doi.org/10.1016/j.jenvman.2019.06.039.
- [84] Y Satyawali and M Balakrishnan. Wastewater treatment in molasses-based alcohol distilleries for cod and color removal: a review. *Journal of environmental management*, 86(3):481–497, 2008. doi: https://doi.org/10.1016/j.jenvman.2006.12.024.
- [85] Won-Tae Shin, Arshia Mirmiran, Sotira Yiacoumi, and Costas Tsouris. Ozonation using microbubbles formed by electric fields. Separation and purification technology, 15(3):271–282, 1999. doi: https://doi.org/10.1016/S1383-5866(98)00107-5.
- [86] Liang Sun, Can Wang, Min Ji, XiaoFang Liu, et al. Cod removal and biodegradability enhancement of pharmaceutical wastewater using a multilayer internal electrolysis reactor. *Asian Journal of Chemistry*, 24(1):112–116, 2012. doi: https://doi.org/10.1080/09593330903229164.
- [87] Liya Fu, Changyong Wu, Yuexi Zhou, Jiane Zuo, Guangqing Song, and Yu Tan. Ozonation reactivity characteristics of dissolved organic matter in secondary petrochemical wastewater by single ozone, ozone/h2o2, and ozone/catalyst. *Chemosphere*, 233:34–43, 2019. doi: https://doi.org/10.1016/j.chemosphere.2019.05.207.
- [88] Li-Bing Chu, Xin-Hui Xing, An-Feng Yu, Yu-Nan Zhou, Xu-Lin Sun, and Benjamin Jurcik. Enhanced ozonation of simulated dyestuff wastewater by microbubbles. *Chemosphere*, 68(10):1854–1860, 2007. doi: https://doi.org/10.1016/j.chemosphere. 2007.03.014.
- [89] Masayoshi Takahashi, Kaneo Chiba, and Pan Li. Formation of hydroxyl radicals by collapsing ozone microbubbles under strongly acidic conditions. *The Journal of Physical Chemistry B*, 111(39):11443–11446, 2007. doi: https://doi.org/10.1021/jp074727m.
- [90] Snigdha Khuntia, Subrata Kumar Majumder, and Pallab Ghosh. Quantitative prediction of generation of hydroxyl radicals from ozone microbubbles. *Chemical Engineering Research and Design*, 98:231–239, 2015. doi: https://doi.org/10.1016/j. cherd.2015.04.003.

[91] Liming Hu and Zhiran Xia. Application of ozone micro-nano-bubbles to groundwater remediation. *Journal of Hazardous Materials*, 342:446–453, 2018. doi: https://doi.org/10.1016/j.jhazmat.2017.08.030.

- [92] Neelkanth Nirmalkar, AW Pacek, and Mostafa Barigou. Interpreting the interfacial and colloidal stability of bulk nanobubbles. *Soft matter*, 14(47):9643–9656, 2018. doi: https://doi.org/10.1039/C8SM01949E.
- [93] Xiaohong Sun, Jingrao Chen, Wenhong Fan, Shu Liu, and Mohammed Kamruzzaman. Production of reactive oxygen species via nanobubble water improves radish seed water absorption and the expression of aquaporin genes. *Langmuir*, 38 (38):11724–11731, 2022. doi: https://doi.org/10.1021/acs.langmuir.2c01860.
- [94] Lei Wang, Jafar Ali, Zhibin Wang, NA Oladoja, Rong Cheng, Changbo Zhang, Gilles Mailhot, and Gang Pan. Oxygen nanobubbles enhanced photodegradation of oxytetracycline under visible light: Synergistic effect and mechanism. *Chemical Engineering Journal*, 388:124227, 2020. doi: https://doi.org/10.1016/j.cej.2020. 124227.
- [95] Masato Yamaguchi, Teng Ma, Daisuke Tadaki, Ayumi Hirano-Iwata, Yoshihiko Watanabe, Hiroyasu Kanetaka, Hiroshi Fujimori, Emiko Takemoto, and Michio Niwano. Bactericidal activity of bulk nanobubbles through active oxygen species generation. *Langmuir*, 37(32):9883–9891, 2021. doi: https://doi.org/10.1021/acs.langmuir.1c01578.
- [96] Isaac D Tegladza, Guihong Lin, Chang Liu, and Xuehong Gu. Control of crystal nucleation, size and morphology using micro-/nanobubbles as green additives—a review. Separation and Purification Technology, page 123232, 2023. doi: https://doi.org/10.1016/j.seppur.2023.123232.
- [97] Jeong Il Lee and Jong-Min Kim. Role of anionic surfactant in the generation of bulk nanobubbles by ultrasonication. *Colloid and Interface Science Communications*, 46: 100578, 2022. doi: https://doi.org/10.1016/j.colcom.2021.100578.
- [98] Christopher Vega-Sánchez, Sam Peppou-Chapman, Liwen Zhu, and Chiara Neto. Nanobubbles explain the large slip observed on lubricant-infused surfaces. *Nature Communications*, 13(1):351, 2022. doi: https://doi.org/10.1038/s41467-022-28016-1.
- [99] A Azevedo, H Oliveira, and J Rubio. Bulk nanobubbles in the mineral and environmental areas: Updating research and applications. *Advances in Colloid and Interface Science*, 271:101992, 2019. doi: https://doi.org/10.1016/j.cis.2019.101992.
- [100] Khanh Kim Thi Phan, Tuyen Truong, Yong Wang, and Bhesh Bhandari. Formation and stability of carbon dioxide nanobubbles for potential applications in food processing. *Food Engineering Reviews*, 13:3–14, 2021. doi: https://doi.org/10.1007/s12393-020-09233-0.

[101] Anastasios Foundas, Ramonna I Kosheleva, Evangelos P Favvas, Margaritis Kostoglou, Athanasios C Mitropoulos, and George Z Kyzas. Fundamentals and applications of nanobubbles: A review. Chemical Engineering Research and Design, 2022. doi: https://doi.org/10.1016/j.cherd.2022.11.013.

- [102] Kyle Rafael Marcelino, Li Ling, Sumeth Wongkiew, Hua Thai Nhan, KC Surendra, Ty Shitanaka, Hui Lu, and Samir Kumar Khanal. Nanobubble technology applications in environmental and agricultural systems: Opportunities and challenges. Critical Reviews in Environmental Science and Technology, pages 1–26, 2022. doi: https://doi.org/10.1080/10643389.2022.2136931.
- [103] Nguyen Vu Linh, Thao Thu Mai, Saengchan Senapin, Sophie St-Hilaire, Channarong Rodkhum, Ha Thanh Dong, et al. Impacts of oxygen and ozone nanobubbles on bacteriophage in aquaculture system. *Aquaculture*, 551:737894, 2022. doi: https://doi.org/10.1016/j.aquaculture.2022.737894.
- [104] R Pandiselvam, R Kaavya, Yasendra Jayanath, Kornautchaya Veenuttranon, Piraya Lueprasitsakul, V Divya, Anjineyulu Kothakota, and SV Ramesh. Ozone as a novel emerging technology for the dissipation of pesticide residues in foods—a review. Trends in Food Science & Technology, 97:38–54, 2020. doi: https://doi.org/10.1016/j.tifs. 2019.12.017.
- [105] Bingzhi Li and Jiang Zhu. Simultaneous degradation of 1, 1, 1-trichloroethane and solvent stabilizer 1, 4-dioxane by a sono-activated persulfate process. *Chemical Engineering Journal*, 284:750–763, 2016. doi: https://doi.org/10.1016/j.cej.2015.08. 153.
- [106] Yu-Xiang Lu, Heyang Yuan, Hameer Chand, You Wu, Yu-Li Yang, Heng Liang, and Hai-Liang Song. Impacts of draw solutes on the fate of tetracycline in an osmotic membrane bioreactor: Role of the combination between membrane fouling and microorganisms. *Journal of Hazardous Materials*, 459:132246, 2023.
- [107] Akash Balakrishnan, Mahendra Chinthala, Rajesh Kumar Polagani, and Dai-Viet N Vo. Removal of tetracycline from wastewater using g-c3n4 based photocatalysts: A review. *Environmental Research*, page 114660, 2022. doi: https://doi.org/10.1016/j.envres.2022.114660.
- [108] Yujie Ben, Caixia Fu, Min Hu, Lei Liu, Ming Hung Wong, and Chunmiao Zheng. Human health risk assessment of antibiotic resistance associated with antibiotic residues in the environment: A review. *Environmental research*, 169:483–493, 2019. doi: https://doi.org/10.1016/j.envres.2018.11.040.
- [109] Edmond Sanganyado and Willis Gwenzi. Antibiotic resistance in drinking water systems: Occurrence, removal, and human health risks. Science of the Total Environment, 669:785–797, 2019. doi: https://doi.org/10.1016/j.scitotenv.2019.03. 162.

[110] Akash Balakrishnan and Mahendra Chinthala. Comprehensive review on advanced reusability of g-c3n4 based photocatalysts for the removal of organic pollutants. *Chemosphere*, 297:134190, 2022. doi: https://doi.org/10.1016/j.chemosphere.2022. 134190.

- [111] Armağan Önal. Overview on liquid chromatographic analysis of tetracycline residues in food matrices. *Food Chemistry*, 127(1):197–203, 2011. doi: https://doi.org/10.1016/j.foodchem.2011.01.002.
- [112] Ian Chopra. Glycylcyclines: third-generation tetracycline antibiotics. *Current opinion in Pharmacology*, 1(5):464–469, 2001. doi: https://doi.org/10.1016/S1471-4892(01)00081-9.
- [113] Geetha Gopal, Hema Sankar, Chandrasekaran Natarajan, and Amitava Mukherjee. Tetracycline removal using green synthesized bimetallic nzvi-cu and bentonite supported green nzvi-cu nanocomposite: A comparative study. *Journal of environmental management*, 254:109812, 2020. doi: https://doi.org/10.1016/j.jenyman.2019.109812.
- [114] Jesús J López-Peñalver, Manuel Sánchez-Polo, Carla V Gómez-Pacheco, and José Rivera-Utrilla. Photodegradation of tetracyclines in aqueous solution by using uv and uv/h2o2 oxidation processes. *Journal of Chemical Technology & Biotechnology*, 85(10):1325–1333, 2010.
- [115] Ilho Kim and Hiroaki Tanaka. Photodegradation characteristics of ppcps in water with uv treatment. *Environment international*, 35(5):793–802, 2009. doi: https://doi.org/10.1016/j.envint.2009.01.003.
- [116] Jaimy Scaria, KV Anupama, and PV Nidheesh. Tetracyclines in the environment: An overview on the occurrence, fate, toxicity, detection, removal methods, and sludge management. Science of The Total Environment, 771:145291, 2021. doi: https://doi.org/10.1016/j.scitotenv.2021.145291.
- [117] Reza Darvishi Cheshmeh Soltani, Masumeh Mashayekhi, Masumeh Naderi, Grzegorz Boczkaj, Sahand Jorfi, and Mahdi Safari. Sonocatalytic degradation of tetracycline antibiotic using zinc oxide nanostructures loaded on nano-cellulose from waste straw as nanosonocatalyst. *Ultrasonics Sonochemistry*, 55:117–124, 2019.
- [118] Sanjeeb Mohapatra, Sumedha Bhatia, Kavindra Yohan Kuhatheva Senaratna, Mui-Choo Jong, Chun Min Benjamin Lim, G Reuben Gangesh, Jia Xiong Lee, Goh Shin Giek, Callie Cheung, Lin Yutao, et al. Wastewater surveillance of sars-cov-2 and chemical markers in campus dormitories in an evolving covid- 19 pandemic. Journal of Hazardous Materials, 446:130690, 2023.
- [119] (2020 World Health Organization et al. Clinical management of covid-19: interim guidance, 27 may 2020. Technical report, World Health Organization, 2020.

[120] Anthony Harrington, Van Vo, Katerina Papp, Richard L Tillett, Ching-Lan Chang, Hayley Baker, Shirley Shen, Amei Amei, Cassius Lockett, Daniel Gerrity, et al. Urban monitoring of antimicrobial resistance during a covid-19 surge through wastewater surveillance. Science of The Total Environment, 853:158577, 2022.

- [121] Priya Nori, Kelsie Cowman, Victor Chen, Rachel Bartash, Wendy Szymczak, Theresa Madaline, Chitra Punjabi Katiyar, Ruchika Jain, Margaret Aldrich, Gregory Weston, et al. Bacterial and fungal coinfections in covid-19 patients hospitalized during the new york city pandemic surge. *Infection Control & Hospital Epidemiology*, 42(1): 84–88, 2021.
- [122] Leshan Cai, Jiayu Sun, Fen Yao, Yumeng Yuan, Mi Zeng, Qiaoxin Zhang, Qingdong Xie, Shiwei Wang, Zhen Wang, and Xiaoyang Jiao. Antimicrobial resistance bacteria and genes detected in hospital sewage provide valuable information in predicting clinical antimicrobial resistance. Science of The Total Environment, 795:148815, 2021.
- [123] Lifa Ge, Yamei Yue, Wei Wang, Fatang Tan, Shenghua Zhang, Xinyun Wang, Xueliang Qiao, and Po Keung Wong. Efficient degradation of tetracycline in wide phrange using mgncn/mgo nanocomposites as novel h2o2 activator. Water Research, 198:117149, 2021.
- [124] Arif Nawaz, Muhammad Atif, Adnan Khan, Mohsin Siddique, Nisar Ali, Falak Naz, Muhammad Bilal, Tak H Kim, Malwina Momotko, Hameed Ul Haq, et al. Solar light driven degradation of textile dye contaminants for wastewater treatment—studies of novel polycationic selenide photocatalyst and process optimization by response surface methodology desirability factor. Chemosphere, 328:138476, 2023.
- [125] Houfeng Xiong, Shuangshi Dong, Jun Zhang, Dandan Zhou, and Bruce E Rittmann. Roles of an easily biodegradable co-substrate in enhancing tetracycline treatment in an intimately coupled photocatalytic-biological reactor. *Water research*, 136:75–83, 2018.
- [126] Wanlin Yang, Zejun Deng, Libin Liu, Kechao Zhou, Lingcong Meng, Li Ma, Qiuping Wei, et al. Co-generation of hydroxyl and sulfate radicals via homogeneous and heterogeneous bi-catalysis with the eo-ps-ef tri-coupling system for efficient removal of refractory organic pollutants. *Water Research*, 243:120312, 2023.
- [127] Wei-Ran Han, Wen-Long Wang, Tie-Jun Qiao, Wei Wang, Hang Su, Chen-Xin Xu, and Qian-Yuan Wu. Ozone micro-bubble aeration using the ceramic ultrafiltration membrane with superior oxidation performance for 2, 4-d elimination. Water Research, 237:119952, 2023.
- [128] Yangrui Huang, Lei Li, Xinmiao Luan, Xinmin Wei, Huaizheng Li, Naiyun Gao, and Juanjuan Yao. Ultrasound-enhanced coagulation for cyanobacterial removal: Effects

of ultrasound frequency and energy density on coagulation performance, leakage of intracellular organic matters and toxicity. Water Research, 201:117348, 2021.

- [129] Gonggong Lu, Xiang Li, Wei Li, Yang Liu, Ningruo Wang, Zhicheng Pan, Guisheng Zhang, Yongli Zhang, and Bo Lai. Thermo-activated periodate oxidation process for tetracycline degradation: Kinetics and byproducts transformation pathways. *Journal of Hazardous Materials*, 461:132696, 2024.
- [130] Yanan Shang, Xing Xu, Baoyu Gao, Shaobin Wang, and Xiaoguang Duan. Single-atom catalysis in advanced oxidation processes for environmental remediation. *Chemical Society Reviews*, 50(8):5281–5322, 2021.
- [131] Chencheng Dong, Wenzhang Fang, Qiuying Yi, and Jinlong Zhang. A comprehensive review on reactive oxygen species (ros) in advanced oxidation processes (aops). *Chemosphere*, page 136205, 2022.
- [132] André Fernandes, Patrycja Makoś, Zhaohui Wang, and Grzegorz Boczkaj. Synergistic effect of tio2 photocatalytic advanced oxidation processes in the treatment of refinery effluents. *Chemical Engineering Journal*, 391:123488, 2020.
- [133] Jun Ma, Ming-Hao Sui, Zhong-Lin Chen, and Li-Ning Wang. Degradation of refractory organic pollutants by catalytic ozonation—activated carbon and mn-loaded activated carbon as catalysts. *Ozone: Science and Engineering*, 26(1): 3–10, 2004.
- [134] Rebekah Oulton, Jason P Haase, Sara Kaalberg, Connor T Redmond, Michael J Nalbandian, and David M Cwiertny. Hydroxyl radical formation during ozonation of multiwalled carbon nanotubes: performance optimization and demonstration of a reactive cnt filter. *Environmental science & technology*, 49(6):3687–3697, 2015.
- [135] Can He, Jianbing Wang, Chunrong Wang, Chunhui Zhang, Pin Hou, and Xieyang Xu. Catalytic ozonation of bio-treated coking wastewater in continuous pilot-and full-scale system: Efficiency, catalyst deactivation and in-situ regeneration. *Water Research*, 183:116090, 2020.
- [136] Chao Shan, You Xu, Ming Hua, Min Gu, Zhichao Yang, Peng Wang, Zhenda Lu, Weiming Zhang, and Bingcai Pan. Mesoporous ce-ti-zr ternary oxide millispheres for efficient catalytic ozonation in bubble column. Chemical Engineering Journal, 338: 261–270, 2018.
- [137] Changjian Li, Shaofeng Yuan, Feng Jiang, Yunfei Xie, Yahui Guo, Hang Yu, Yuliang Cheng, He Qian, and Weirong Yao. Degradation of fluopyram in water under ozone enhanced microbubbles: Kinetics, degradation products, reaction mechanism, and toxicity evaluation. *Chemosphere*, 258:127216, 2020.

[138] Gwiwoong Nam, Mohamed M Mohamed, and Jinho Jung. Enhanced degradation of benzo [a] pyrene and toxicity reduction by microbubble ozonation. *Environmental Technology*, 42(12):1853–1860, 2021.

- [139] Chao Wu, Pan Li, Shengji Xia, Shuo Wang, Yue Wang, Jun Hu, Zhengqian Liu, and Shuili Yu. The role of interface in microbubble ozonation of aromatic compounds. *Chemosphere*, 220:1067–1074, 2019.
- [140] Tao Lyu, Shubiao Wu, Robert JG Mortimer, and Gang Pan. Nanobubble technology in environmental engineering: revolutionization potential and challenges, 2019.
- [141] Xiaolong Yang, Li Chen, Seiichi Oshita, Wenhong Fan, and Shu Liu. Mechanism for enhancing the ozonation process of micro-and nanobubbles: Bubble behavior and interface reaction. *ACS ES&T Water*, 3(12):3835–3847, 2023.
- [142] Zhengbo Chen, Min Fu, Chenxi Yuan, Xueli Hu, Jinwu Bai, Rui Pan, Peng Lu, and Min Tang. Study on the degradation of tetracycline in wastewater by micro-nano bubbles activated hydrogen peroxide. *Environmental Technology*, 43(23):3580–3590, 2022.
- [143] Pan Li, Masayoshi Takahashi, and Kaneo Chiba. Degradation of phenol by the collapse of microbubbles. *Chemosphere*, 75(10):1371–1375, 2009.
- [144] Chikang Wang, Chien-Yu Lin, and Guan-Yun Liao. Feasibility study of tetracycline removal by ozonation equipped with an ultrafine-bubble compressor. Water, 13(8): 1058, 2021.
- [145] M Suresh Kumar, SH Sonawane, and Aniruddha B Pandit. Degradation of methylene blue dye in aqueous solution using hydrodynamic cavitation based hybrid advanced oxidation processes. Chemical Engineering and Processing: Process Intensification, 122:288–295, 2017.
- [146] Flavia Leticia Moissa, Mateus Mittersteiner, Rafael Saugo, Tamely Cristine Floriani, and Paulo Cesar de Jesus. Kinetic behavior of ci reactive blue 182 towards oxidation with h2o2/uv and h2o2/naoh systems. *Journal of Molecular Liquids*, 264:675–682, 2018.
- [147] Yu-Gyeong Kang, Hakwon Yoon, Chung-Seop Lee, Eun-Ju Kim, and Yoon-Seok Chang. Advanced oxidation and adsorptive bubble separation of dyes using mno2-coated fe3o4 nanocomposite. Water research, 151:413-422, 2019.
- [148] Mark Daniel G de Luna, James I Colades, Chia-Chi Su, and Ming-Chun Lu. Comparison of dimethyl sulfoxide degradation by different fenton processes. *Chemical engineering journal*, 232:418–424, 2013.
- [149] Muhammad Muslim, Md Ahsan Habib, Tajmeri Selima Islam, Iqbal Mohmmad Ismail, and Abu Jafar Mahmood. Decolorization of diazo dye ponceau s by fenton process. *Pak. J. Anal. Environ. Chem.*, 14(2), 2013.

[150] Meiqiang Cai, Jie Su, Yizu Zhu, Xiaoqing Wei, Micong Jin, Haojie Zhang, Chunying Dong, and Zongsu Wei. Decolorization of azo dyes orange g using hydrodynamic cavitation coupled with heterogeneous fenton process. *Ultrasonics sonochemistry*, 28:302–310, 2016.

- [151] Chuanwei Wu, Weiming Chen, Zhepei Gu, and Qibin Li. A review of the characteristics of fenton and ozonation systems in landfill leachate treatment. *Science of The Total Environment*, 762:143131, 2021.
- [152] Emine Basturk and Mustafa Karatas. Decolorization of antraquinone dye reactive blue 181 solution by uv/h2o2 process. *Journal of photochemistry and Photobiology A: Chemistry*, 299:67–72, 2015.
- [153] Edson C Paz, Luci R Aveiro, Victor S Pinheiro, Felipe M Souza, Verônica B Lima, Fernando L Silva, Peter Hammer, Marcos RV Lanza, and Mauro C Santos. Evaluation of h2o2 electrogeneration and decolorization of orange ii azo dye using tungsten oxide nanoparticle-modified carbon. Applied Catalysis B: Environmental, 232:436–445, 2018.
- [154] Jiabin Pang, Fenglian Fu, Weibin Li, Lijun Zhu, and Bing Tang. Fe-mn binary oxide decorated diatomite for rapid decolorization of methylene blue with h2o2. Applied Surface Science, 478:54–61, 2019.
- [155] Tongqian Zhao, Peng Li, Chao Tai, Jiaping She, Yongguang Yin, Guocheng Zhang, et al. Efficient decolorization of typical azo dyes using low-frequency ultrasound in presence of carbonate and hydrogen peroxide. *Journal of hazardous materials*, 346: 42–51, 2018.
- [156] AH Konsowa. Decolorization of wastewater containing direct dye by ozonation in a batch bubble column reactor. *Desalination*, 158(1-3):233–240, 2003.
- [157] A Özlem Yıldırım, Şermin Gül, Orkide Eren, and Erdal Kuşvuran. A comparative study of ozonation, homogeneous catalytic ozonation, and photocatalytic ozonation for ci reactive red 194 azo dye degradation. *CLEAN–Soil, Air, Water*, 39(8):795–805, 2011.
- [158] Xiaolei Fan, João Restivo, José JM Órfão, Manuel Fernando R Pereira, and Alexei A Lapkin. The role of multiwalled carbon nanotubes (mwcnts) in the catalytic ozonation of atrazine. *Chemical Engineering Journal*, 241:66–76, 2014.
- [159] Juliano Carvalho Cardoso, Guilherme Garcia Bessegato, and Maria Valnice Boldrin Zanoni. Efficiency comparison of ozonation, photolysis, photocatalysis and photoelectrocatalysis methods in real textile wastewater decolorization. *Water research*, 98:39–46, 2016.

[160] Xuejun Quan, Dan Luo, Jun Wu, Ruiheng Li, Wen Cheng, et al. Ozonation of acid red 18 wastewater using o3/ca (oh) 2 system in a micro bubble gas-liquid reactor. Journal of Environmental Chemical Engineering, 5(1):283–291, 2017.

- [161] Mahsa Khajeh, Ensiyeh Taheri, Mohammad Mehdi Amin, Ali Fatehizadeh, and Jorge Bedia. Combination of hydrodynamic cavitation with oxidants for efficient treatment of synthetic and real textile wastewater. *Journal of Water Process Engineering*, 49: 103143, 2022.
- [162] Matej Čehovin, Alojz Medic, Jens Scheideler, Jörg Mielcke, Achim Ried, Boris Kompare, and Andreja Žgajnar Gotvajn. Hydrodynamic cavitation in combination with the ozone, hydrogen peroxide and the uv-based advanced oxidation processes for the removal of natural organic matter from drinking water. *Ultrasonics Sonochemistry*, 37:394–404, 2017.
- [163] Dino Musmarra, Marina Prisciandaro, Mauro Capocelli, Despina Karatza, Pasquale Iovino, Silvana Canzano, and Amedeo Lancia. Degradation of ibuprofen by hydrodynamic cavitation: Reaction pathways and effect of operational parameters. *Ultrasonics Sonochemistry*, 29:76–83, 2016.
- [164] Roberto Andreozzi, Vincenzo Caprio, Amedeo Insola, and Raffaele Marotta. Advanced oxidation processes (aop) for water purification and recovery. Catalysis today, 53(1):51–59, 1999.
- [165] Collin G Joseph, Gianluca Li Puma, Awang Bono, and Duduku Krishnaiah. Sonophotocatalysis in advanced oxidation process: a short review. *Ultrasonics Sonochemistry*, 16(5):583–589, 2009.
- [166] L Bilińska, M Gmurek, and S Ledakowicz. Textile wastewater treatment by aops for brine reuse. Process Safety and Environmental Protection, 109:420–428, 2017.
- [167] Dengsheng Ma, Huan Yi, Cui Lai, Xigui Liu, Xiuqin Huo, Ziwen An, Ling Li, Yukui Fu, Bisheng Li, Mingming Zhang, et al. Critical review of advanced oxidation processes in organic wastewater treatment. Chemosphere, 275:130104, 2021.
- [168] Ikechukwu A Ike, Karl G Linden, John D Orbell, and Mikel Duke. Critical review of the science and sustainability of persulphate advanced oxidation processes. *Chemical Engineering Journal*, 338:651–669, 2018.
- [169] David B Miklos, Christian Remy, Martin Jekel, Karl G Linden, Jörg E Drewes, and Uwe Hübner. Evaluation of advanced oxidation processes for water and wastewater treatment—a critical review. Water research, 139:118–131, 2018.
- [170] Pooja Jain, Vinay M Bhandari, Kshama Balapure, Jyotsnarani Jena, Vivek V Ranade, and Deepak J Killedar. Hydrodynamic cavitation using vortex diode: An efficient approach for elimination of pathogenic bacteria from water. *Journal of environmental management*, 242:210–219, 2019.

[171] Mojca Zupanc, Martin Petkovšek, Jure Zevnik, Gregor Kozmus, Alenka Šmid, and Matevž Dular. Anomalies detected during hydrodynamic cavitation when using salicylic acid dosimetry to measure radical production. *Chemical Engineering Journal*, 396:125389, 2020.

- [172] Chih-Shan Li and Yu-Chun Wang. Surface germicidal effects of ozone for microorganisms. *Aiha Journal*, 64(4):533–537, 2003.
- [173] Chunchieh Tseng and Chihshan Li. Inactivation of surface viruses by gaseous ozone. Journal of environmental health, 70(10):56–63, 2008.
- [174] Jingxin Yang, Cheng Luo, Tingting Li, Jie Cao, Wenyi Dong, Ji Li, and Jun Ma. Superfast degradation of refractory organic contaminants by ozone activated with thiosulfate: Efficiency and mechanisms. *Water research*, 176:115751, 2020.
- [175] Mohammad Mehrjouei, Siegfried Müller, and Detlev Möller. A review on photocatalytic ozonation used for the treatment of water and wastewater. *Chemical Engineering Journal*, 263:209–219, 2015.
- [176] Jacek Nawrocki and Barbara Kasprzyk-Hordern. The efficiency and mechanisms of catalytic ozonation. *Applied Catalysis B: Environmental*, 99(1-2):27–42, 2010.
- [177] PL Smedley, HB Nicolli, DMJ Macdonald, AJ Barros, and JO Tullio. Hydrogeochemistry of arsenic and other inorganic constituents in groundwaters from la pampa, argentina. *Applied geochemistry*, 17(3):259–284, 2002.
- [178] Wolfgang Driehaus, Reiner Seith, and Martin Jekel. Oxidation of arsenate (iii) with manganese oxides in water treatment. Water Research, 29(1):297–305, 1995.
- [179] Kevin R Henke. Arsenic in natural environments. Arsenic: Environmental chemistry, health threats and waste treatment, pages 69–235, 2009.
- [180] Manish Kumar, Ritusmita Goswami, Arbind Kumar Patel, Medhavi Srivastava, and Nilotpal Das. Scenario, perspectives and mechanism of arsenic and fluoride co-occurrence in the groundwater: a review. *Chemosphere*, 249:126126, 2020.
- [181] Pooja Sevak and Bhupendra Pushkar. Arsenic pollution cycle, toxicity and sustainable remediation technologies: A comprehensive review and bibliometric analysis. *Journal of Environmental Management*, 349:119504, 2024.
- [182] Norman Neill Greenwood and Alan Earnshaw. *Chemistry of the Elements*. Elsevier, 2012.
- [183] Tsung-Lin Tsai, Chin-Chi Kuo, Ling-I Hsu, Shih-Fen Tsai, Hung-Yi Chiou, Chien-Jen Chen, Kuang-Hung Hsu, and Shu-Li Wang. Association between arsenic exposure, dna damage, and urological cancers incidence: A long-term follow-up study of residents in an arseniasis endemic area of northeastern taiwan. *Chemosphere*, 266: 129094, 2021.

[184] Sachin V Jadhav, Eugenio Bringas, Ganapati D Yadav, Virendra K Rathod, Inmaculada Ortiz, and Kumudini V Marathe. Arsenic and fluoride contaminated groundwaters: a review of current technologies for contaminants removal. *Journal of environmental management*, 162:306–325, 2015.

- [185] Howlader Rahidul Hassan. A review on different arsenic removal techniques used for decontamination of drinking water. Environmental Pollutants and Bioavailability, 35 (1):2165964, 2023.
- [186] MA Sanjrani, B Zhou, H Zhao, SA Bhutto, AS Muneer, and SB Xia. Arsenic contaminated groundwater in china and its treatment options, a review. *Applied Ecology & Environmental Research*, 17(2), 2019.
- [187] Harshith Govindappa, Gholamreza Abdi, UT Uthappa, Ganesan Sriram, Sung Soo Han, and Mahaveer Kurkuri. Efficient separation of arsenic species of oxyanion as (iii) and as (v) by using effective polymer inclusion membranes (pim). *Chemosphere*, 316:137851, 2023.
- [188] Arpan Sarkar and Biswajit Paul. The global menace of arsenic and its conventional remediation-a critical review. *Chemosphere*, 158:37–49, 2016.
- [189] Pengbo Hu, Shujuan Wang, and Yuqun Zhuo. Arsenic adsorption enhancement performances of mn-modified γ -al2o3 with flue gas constituents involved. *Chemosphere*, 288:132653, 2022.
- [190] Erhan Demirbas, Mehmet Kobya, Mehmet Salim Oncel, Emrah Şık, and Aysegul Yagmur Goren. Arsenite removal from groundwater in a batch electrocoagulation process: Optimization through response surface methodology. Sep. Sci. Technol., 54(5):775–785, 2019. URL https://doi.org/10.1080/01496395.2018.1521834.
- [191] Jinyoung Chun, Hongshin Lee, Sang-Hyup Lee, Seok-Won Hong, Jaesang Lee, Changha Lee, and Jinwoo Lee. Magnetite/mesocellular carbon foam as a magnetically recoverable fenton catalyst for removal of phenol and arsenic. Chemosphere, 89(10):1230–1237, 2012.
- [192] Sixto Malato, Manuel I Maldonado, Pilar Fernandez-Ibanez, Isabel Oller, Inmaculada Polo, and Ricardo Sánchez-Moreno. Decontamination and disinfection of water by solar photocatalysis: The pilot plants of the plataforma solar de almeria. *Materials Science in Semiconductor Processing*, 42:15–23, 2016.
- [193] Maria Battistel, Lucien Stolze, Muhammad Muniruzzaman, and Massimo Rolle. Arsenic release and transport during oxidative dissolution of spatially-distributed sulfide minerals. *Journal of Hazardous Materials*, 409:124651, 2021.
- [194] Huihui Zhou, Guijian Liu, Liqun Zhang, and Chuncai Zhou. Mineralogical and morphological factors affecting the separation of copper and arsenic in flash copper

smelting slag flotation beneficiation process. *Journal of Hazardous Materials*, 401: 123293, 2021.

- [195] Zhenyao Han, Nguyen Thi Hong Nhung, Yongxiang Wu, Minyi Huang, Chunlin He, Siminig Lu, Gjergj Dodbiba, Yuezou Wei, Akira Otsuki, and Toyohisa Fujita. Arsenic (iii) oxidation and removal from artificial mine wastewater by blowing o2 nanobubbles. *Journal of Water Process Engineering*, 47:102780, 2022.
- [196] Mohammad T ALSamman, Sebastián Sotelo, Julio Sánchez, and Bernabé L Rivas. Arsenic oxidation and its subsequent removal from water: An overview. Separation and Purification Technology, 309:123055, 2023.
- [197] Michael C Dodd, Ngoc Duy Vu, Adrian Ammann, Van Chieu Le, Reinhard Kissner, Hung Viet Pham, The Ha Cao, Michael Berg, and Urs Von Gunten. Kinetics and mechanistic aspects of as (iii) oxidation by aqueous chlorine, chloramines, and ozone: relevance to drinking water treatment. *Environmental science & technology*, 40(10): 3285–3292, 2006.
- [198] Olivier X Leupin and Stephan J Hug. Oxidation and removal of arsenic (iii) from aerated groundwater by filtration through sand and zero-valent iron. *Water Research*, 39(9):1729–1740, 2005.
- [199] Bruce A Manning, Scott E Fendorf, Benjamin Bostick, and Donald L Suarez. Arsenic (iii) oxidation and arsenic (v) adsorption reactions on synthetic birnessite. Environmental Science & Technology, 36(5):976–981, 2002.
- [200] Sung-Hwan Yoon, Jai H Lee, SangEun Oh, and Jae E Yang. Photochemical oxidation of as (iii) by vacuum-uv lamp irradiation. *Water research*, 42(13):3455–3463, 2008.
- [201] Kevin A Bierlein, Maryam Rezvani, Scott A Socolofsky, Lee D Bryant, Alfred Wüest, and John C Little. Increased sediment oxygen flux in lakes and reservoirs: The impact of hypolimnetic oxygenation. Water Resources Research, 53(6):4876–4890, 2017.
- [202] Carolina P Funkey, Daniel J Conley, Nina S Reuss, Christoph Humborg, Tom Jilbert, and Caroline P Slomp. Hypoxia sustains cyanobacteria blooms in the baltic sea. Environmental Science & Technology, 48(5):2598–2602, 2014.
- [203] Anna Melnikova, Antonio Faggiano, Marco Visconti, Raffaele Cucciniello, Patrizia Iannece, Natalia Kostryukova, Antonio Proto, Antonino Fiorentino, and Luigi Rizzo. Photo driven homogeneous advanced oxidation coupled to adsorption process for an effective arsenic removal from drinking water. *Journal of Environmental Management*, 349:119568, 2024.
- [204] Zhiming Yang, Shaobo Liu, Xiaofei Tan, Hailan Yang, Xinjiang Hu, Yanling Gu, and Chuang Li. Tuned bimetallic mofs with balanced adsorption and non-radical oxidizing activities for efficient removal of arsenite. Separation and Purification Technology, 330:125359, 2024.

[205] Guiyuan Cai, Yu Tian, Lipin Li, Wenxuan Zhang, Rui Huang, Jun Zhang, Qinyu Wang, Hua Xu, and Yifeng Zhang. Sulfite activation of fe-mn bimetallic oxides for rapid oxidative removal of as (iii) in water: Involvement of active mn (iii). Chemical Engineering Journal, 479:147539, 2024.

- [206] Ahmad Shahedi, Ahmad Khodadadi Darban, Ahmad Jamshidi-Zanjani, Mehdi Homaee, and Fariborz Taghipour. Effect of ozonation and uv-led combination on simultaneous removal of toxic elements during electrocoagulation. *Environmental Science and Pollution Research*, 31(4):5847–5865, 2024.
- [207] Min-Tian Gao, Makoto Hirata, Hirokazu Takanashi, and Tadashi Hano. Ozone mass transfer in a new gas-liquid contactor-karman contactor. Separation and purification technology, 42(2):145–149, 2005.
- [208] L Joseph Boilyky. The mass transfer of ozone into water: energy requirements-state of the art. 1981.
- [209] Snigdha Khuntia, Subrata Kumar Majumder, and Pallab Ghosh. Oxidation of as (iii) to as (v) using ozone microbubbles. *Chemosphere*, 97:120–124, 2014.
- [210] Ying Tang, Meiyi Zhang, Jing Zhang, Tao Lyu, Mick Cooper, and Gang Pan. Reducing arsenic toxicity using the interfacial oxygen nanobubble technology for sediment remediation. Water Res., 205:117657, 2021. URL https://doi.org/10. 1016/j.watres.2021.117657.
- [211] Daisuke Kobayashi, Yoshiyuki Hayashida, Kazuki Sano, and Koichi Terasaka. Agglomeration and rapid ascent of microbubbles by ultrasonic irradiation. *Ultrasonics sonochemistry*, 18(5):1193–1196, 2011.
- [212] Shinya Kato, Daigo Matsuoka, and Nobuhiko Miwa. Antioxidant activities of nano-bubble hydrogen-dissolved water assessed by esr and 2, 2-bipyridyl methods. *Materials Science and Engineering: C*, 53:7–10, 2015. doi: https://doi.org/10.1016/ j.msec.2015.03.064.
- [213] Chihiro Minamoto, Nonoka Fujiwara, Yutaka Shigekawa, Kaori Tada, Jun Yano, Takashi Yokoyama, Yoshikazu Minamoto, and Susumu Nakayama. Effect of acidic conditions on decomposition of methylene blue in aqueous solution by air microbubbles. *Chemosphere*, 263:128141, 2021. doi: https://doi.org/10.1016/j. chemosphere.2020.128141.
- [214] Muhammad A Rauf, Mohammed A Meetani, A Khaleel, and Amal Ahmed. Photocatalytic degradation of methylene blue using a mixed catalyst and product analysis by lc/ms. *Chemical Engineering Journal*, 157(2-3):373–378, 2010. doi: https://doi.org/10.1016/j.cej.2009.11.017.
- [215] Haosheng Sun, Jun Qin, Ludong Yi, Yinghao Ruan, Yanan Sun, Jun Wang, and Dawei Fang. Study on negative pressure assisted hydrodynamic cavitation (npa-hc)

degradation of methylene blue in dye wastewater. Chemical Engineering Research and Design, 181:1–13, 2022. doi: https://doi.org/10.1016/j.cherd.2022.03.003.

- [216] Wei Fan, Wen-gang An, Ming-xin Huo, Wu Yang, Sui-yi Zhu, and Shan-shan Lin. Solubilization and stabilization for prolonged reactivity of ozone using micro-nano bubbles and ozone-saturated solvent: A promising enhancement for ozonation. Separation and Purification Technology, 238:116484, 2020.
- [217] Yunxian Liu, Bing Wang, Dan Zhao, Wenhui Jin, Feng Xu, Yujia Gao, Wen Shi, and Hongyang Ren. Investigation of surfactant effect on ozone bubble motion and mass transfer characteristics. *Journal of Environmental Chemical Engineering*, 11 (5):110805, 2023.
- [218] Chikang Wang, Chien-Yu Lin, and Guan-Yun Liao. Degradation of antibiotic tetracycline by ultrafine-bubble ozonation process. *Journal of Water Process Engineering*, 37:101463, 2020.
- [219] Tao Yang, Lei Zhang, Fen Liu, Chunming Cheng, and Guochao Li. Hydrodynamic cavitation–impinging stream for enhancing ozone mass transfer and oxidation for wastewater treatment. *Journal of Water Process Engineering*, 58:104799, 2024.
- [220] L Carvalho, T De Koe, and P Tavares. An improved molybdenum blue method for simultaneous determination of inorganic phosphate and arsenate. *Restoration*, 1(1), 1998.
- [221] Susanna Tsang, Frank Phu, Marc M Baum, and Gregory A Poskrebyshev. Determination of phosphate/arsenate by a modified molybdenum blue method and reduction of arsenate by s2042-. *Talanta*, 71(4):1560–1568, 2007.
- [222] VV Tien, DV Bay, DX Thu, and TV Chung. Analysis of arsenic from water by spectrophotometric method. *Int. J. Dev. Res*, 5:4987–4991, 2015.
- [223] N Otgon, G Zhang, and C Yang. Arsenic removal from waste water by ozone oxidation combined with ferric precipitation. *Mongolian Journal of Chemistry*, 17(43):18–22, 2016.
- [224] Nayeem K Ibnul and Carl P Tripp. A solventless method for detecting trace level phosphate and arsenate in water using a transparent membrane and visible spectroscopy. *Talanta*, 225:122023, 2021.
- [225] PH Sarkodie, D Nyamah, and EH Amonoo-Niezer. Speciation of arsenic in some biological samples from obuasi and its surrounding villages. In *Pp. 146ÿ154 in:* National symposium proceedings ÿ the mining industry and the environment, April 14ÿ15, Kumasi, UST, 1997.
- [226] Clàudia Fontàs, Ruben Vera, Anna Batalla, Spas D Kolev, and Enriqueta Anticó. A novel low-cost detection method for screening of arsenic in groundwater. Environmental Science and Pollution Research, 21(20):11682-11688, 2014.

[227] Kalyani Agarwal, Mohit Trivedi, and Neelkanth Nirmalkar. Does salting-out effect nucleate nanobubbles in water: Spontaneous nucleation? *Ultrasonics sonochemistry*, 82:105860, 2022.

- [228] SD Razumovskii, ML Konstantinova, TV Grinevich, GV Korovina, and V Ya Zaitsev. Mechanism and kinetics of the reaction of ozone with sodium chloride in aqueous solutions. *Kinetics and Catalysis*, 51:492–496, 2010. doi: https://doi.org/10.1134/ S0023158410040051.
- [229] BG Ershov and PA Morozov. The kinetics of ozone decomposition in water, the influence of ph and temperature. Russian Journal of Physical Chemistry A, 83(8): 1295–1299, 2009. doi: https://doi.org/10.1134/S0036024409080093.
- [230] María Eugenia Lovato, Carlos A Martín, and Alberto E Cassano. A reaction kinetic model for ozone decomposition in aqueous media valid for neutral and acidic ph. Chemical Engineering Journal, 146(3):486–497, 2009. doi: https://doi.org/10.1016/ j.cej.2008.11.001.
- [231] JN Israelachvili. Intermolecular and surface forces: with applications to colloidal and biological systems/jacob n. *Israelachvili. London: London: Academic*, 1985.
- [232] L De Rond, SFWM Libregts, LG Rikkert, CM Hau, E Van Der Pol, R Nieuwland, TG Van Leeuwen, and FAW Coumans. Refractive index to evaluate staining specificity of extracellular vesicles by flow cytometry. *Journal of Extracellular Vesicles*, 8(1):1643671, 2019. doi: https://doi.org/10.1080/20013078.2019.1643671.
- [233] Craig F Bohren and Donald R Huffman. Absorption and scattering of light by small particles. John Wiley & Sons, 2008.
- [234] Kenta Kakiuchi, Takehiro Miyasaka, Norikazu Harii, and Shinji Takeoka. Development of quantitative and concise measurement method of oxygen in fine bubble dispersion. *PloS one*, 17(2):e0264083, 2022.
- [235] Marina Sabelfeld and Sven-Uwe Geißen. Effect of helical structure on ozone mass transfer in a hollow fiber membrane contactor. *Journal of Membrane Science*, 574: 222–234, 2019. doi: https://doi.org/10.1016/j.memsci.2018.10.056.
- [236] Bing Wang, Huan Zhang, Qingjie Meng, Hongyang Ren, Mingyang Xiong, and Chunyang Gao. The enhancement of ozone—liquid mass transfer performance in a ptfe hollow fiber membrane contactor using ultrasound as a catalyzer. RSC advances, 11(23):14017—14028, 2021. doi: \url{https://doi.org/10.1039/D1RA00452B}.
- [237] Joost H Weijs, James RT Seddon, and Detlef Lohse. Diffusive shielding stabilizes bulk nanobubble clusters. *ChemPhysChem*, 13(8):2197–2204, 2012. doi: https://doi.org/10.1002/cphc.201100807.

[238] Kosuke Ebina, Kenrin Shi, Makoto Hirao, Jun Hashimoto, Yoshitaka Kawato, Shoichi Kaneshiro, Tokimitsu Morimoto, Kota Koizumi, and Hideki Yoshikawa. Oxygen and air nanobubble water solution promote the growth of plants, fishes, and mice. *PLoS One*, 8(6):e65339, 2013.

- [239] Yoshichika Hirahara, Kazuyoshi Iwata, and Katsuhiko Nakamuro. Effect of citric acid on prolonging the half-life of dissolved ozone in water. *Food Safety*, 7(4):90–94, 2019.
- [240] Jeffrey M Small and Holger Hintelmann. Methylene blue derivatization then lc–ms analysis for measurement of trace levels of sulfide in aquatic samples. *Analytical and bioanalytical chemistry*, 387:2881–2886, 2007. doi: https://doi.org/10.1007/s00216-007-1140-3.
- [241] Sabrina Roguai and Abdelkader Djelloul. Structural, microstructural and photocatalytic degradation of methylene blue of zinc oxide and fe-doped zno nanoparticles prepared by simple coprecipitation method. Solid State Communications, 334:114362, 2021. doi: https://doi.org/10.1016/j.ssc.2021.114362.
- [242] Aniruddha Molla, Meenakshi Sahu, and Sahid Hussain. Under dark and visible light: fast degradation of methylene blue in the presence of ag-in-ni-s nanocomposites. *Journal of Materials Chemistry A*, 3(30):15616–15625, 2015. doi: https://doi.org/10.1039/C5TA02888D.
- [243] He Wang, Han Wang, and Qun Yan. Peroxymonosulfate activation by algal carbocatalyst for organic dye oxidation: Insights into experimental and theoretical. Science of the Total Environment, 816:151611, 2022. doi: https://doi.org/10.1016/j.scitotenv.2021.151611.
- [244] Elvana Cako, Kumaravel Dinesh Gunasekaran, Reza Darvishi Cheshmeh Soltani, and Grzegorz Boczkaj. Ultrafast degradation of brilliant cresyl blue under hydrodynamic cavitation based advanced oxidation processes (aops). Water Resources and Industry, 24:100134, 2020. doi: https://doi.org/10.1016/j.wri.2020.100134.
- [245] Baowei Wang, Tingting Wang, and Huijuan Su. A dye-methylene blue (mb)-degraded by hydrodynamic cavitation (hc) and combined with other oxidants. *Journal of Environmental Chemical Engineering*, 10(3):107877, 2022. doi: https://doi.org/10.1016/j.jece.2022.107877.
- [246] LIU Limei, Shuting ZHANG, LÜ Xuebin, YU Xiaoyan, and ZHI Suli. Ozonation of sulfur dioxide in sulphuric acid solution. *Chinese Journal of Chemical Engineering*, 21(7):808–812, 2013.
- [247] Siyuan Wang, Xinghao Wang, Jing Chen, Ruijuan Qu, and Zunyao Wang. Removal of the uv filter benzophenone-2 in aqueous solution by ozonation: kinetics,

- intermediates, pathways and toxicity. Ozone: Science & Engineering, 40(2):122-132, 2018.
- [248] Ruijuan Qu, Bingzhe Xu, Lingjun Meng, Liansheng Wang, and Zunyao Wang. Ozonation of indigo enhanced by carboxylated carbon nanotubes: performance optimization, degradation products, reaction mechanism and toxicity evaluation. Water research, 68:316–327, 2015.
- [249] H Lawrence Clever, Rubin Battino, Hiroshi Miyamoto, Yuri Yampolski, and Colin L Young. Iupac-nist solubility data series. 103. oxygen and ozone in water, aqueous solutions, and organic liquids (supplement to solubility data series volume 7). *Journal of Physical and Chemical Reference Data*, 43(3), 2014.
- [250] John A Roth and Daniel E Sullivan. Solubility of ozone in water. *Industrial & Engineering Chemistry Fundamentals*, 20(2):137–140, 1981.
- [251] Tadao Mizuno and Hiroshi Tsuno. Evaluation of solubility and the gas-liquid equilibrium coefficient of high concentration gaseous ozone to water. Ozone: science & engineering, 32(1):3–15, 2010.
- [252] Marek Solecki. Mass transfer: advancement in process modelling. BoD–Books on Demand, 2015.
- [253] Zachary R Hopkins and Lee Blaney. A novel approach to modeling the reaction kinetics of tetracycline antibiotics with aqueous ozone. Science of the total environment, 468:337–344, 2014.
- [254] Ankush Majumdar, Utpal Ghosh, and Anjali Pal. 2d-bi4nbo8cl nanosheet for efficient photocatalytic degradation of tetracycline in synthetic and real wastewater under visible-light: Influencing factors, mechanism and degradation pathway. *Journal of Alloys and Compounds*, 900:163400, 2022.
- [255] Werner R Haag and Jürg Hoigné. Ozonation of water containing chlorine or chloramines. reaction products and kinetics. Water Research, 17(10):1397–1402, 1983.
- [256] Marc A Boncz, Harry Bruning, Wim H Rulkens, Han Zuilhof, and Ernst JR Sudhölter. The effect of salts on ozone oxidation processes. *Ozone: Science and Engineering*, 27(4):287–292, 2005.
- [257] Grzegorz Boczkaj, Andre Fernandes, and Patrycja Makos. Study of different advanced oxidation processes for wastewater treatment from petroleum bitumen production at basic ph. *Industrial & Engineering Chemistry Research*, 56(31): 8806–8814, 2017.
- [258] Grzegorz Boczkaj and André Fernandes. Wastewater treatment by means of advanced oxidation processes at basic ph conditions: A review. Chemical engineering journal, 320:608–633, 2017.

[259] Jerry J Wu, M Muruganandham, and SH Chen. Degradation of dmso by ozone-based advanced oxidation processes. *Journal of Hazardous Materials*, 149(1):218–225, 2007.

- [260] Mohammad A Alsheyab and Aurelio H Muñoz. Reducing the formation of trihalomethanes (thms) by ozone combined with hydrogen peroxide (h2o2/o3). *Desalination*, 194(1-3):121–126, 2006.
- [261] Pan Li, Masayoshi Takahashi, and Kaneo Chiba. Enhanced free-radical generation by shrinking microbubbles using a copper catalyst. *Chemosphere*, 77(8):1157–1160, 2009.
- [262] Rama Pulicharla, Satinder Kaur Brar, Tarek Rouissi, Serge Auger, Patrick Drogui, Mausam Verma, and Rao Y Surampalli. Degradation of chlortetracycline in wastewater sludge by ultrasonication, fenton oxidation, and ferro-sonication. *Ultrasonics sonochemistry*, 34:332–342, 2017.
- [263] Nuanqin Zhang, Junyi Chen, Zhanqiang Fang, and Eric Pokeung Tsang. Ceria accelerated nanoscale zerovalent iron assisted heterogenous fenton oxidation of tetracycline. *Chemical Engineering Journal*, 369:588–599, 2019.
- [264] Ying Zhang, Jiabin Zhou, Junhui Chen, Xiaoqiong Feng, and Weiquan Cai. Rapid degradation of tetracycline hydrochloride by heterogeneous photocatalysis coupling persulfate oxidation with mil-53 (fe) under visible light irradiation. *Journal of hazardous materials*, 392:122315, 2020.
- [265] Hyejung Lee, Eunyoung Lee, Chang-Hee Lee, and Kisay Lee. Degradation of chlorotetracycline and bacterial disinfection in livestock wastewater by ozone-based advanced oxidation. *Journal of Industrial and Engineering Chemistry*, 17(3):468–473, 2011.
- [266] Ashutosh Agarwal, Wun Jern Ng, and Yu Liu. Principle and applications of microbubble and nanobubble technology for water treatment. *Chemosphere*, 84(9): 1175–1180, 2011.
- [267] Seung Hee Chae, Min Sik Kim, Jae-Hong Kim, and John D Fortner. Nanobubble reactivity: evaluating hydroxyl radical generation (or lack thereof) under ambient conditions. ACS Es&t Engineering, 3(10):1504–1510, 2023.
- [268] Kyuichi Yasui. On some aspects of nanobubble-containing systems. *Nanomaterials*, 12(13):2175, 2022.
- [269] Erika Reisz, Clemens von Sonntag, Agnes Tekle-Röttering, Sergej Naumov, Winfried Schmidt, and Torsten C Schmidt. Reaction of 2-propanol with ozone in aqueous media. *Water research*, 128:171–182, 2018.
- [270] JJ Wu, JS Yang, M Muruganandham, and CC Wu. The oxidation study of 2-propanol using ozone-based advanced oxidation processes. Separation and Purification Technology, 62(1):39–46, 2008.

[271] Min Fu, Chenxi Yuan, Jinwu Bai, and Youzhou He. Degradation of tetracycline in wastewater by persulfate activated with micro-nano bubbles. *Available at SSRN* 4055015.

- [272] Gui Yang, Yujun Liang, Zhuoran Xiong, Jian Yang, Kun Wang, and Zikang Zeng. Molten salt-assisted synthesis of ce4o7/bi4moo9 heterojunction photocatalysts for photo-fenton degradation of tetracycline: Enhanced mechanism, degradation pathway and products toxicity assessment. Chemical Engineering Journal, 425: 130689, 2021.
- [273] Cui Lai, Ziwen An, Huan Yi, Xiuqin Huo, Lei Qin, Xigui Liu, Bisheng Li, Mingming Zhang, Shiyu Liu, Ling Li, et al. Enhanced visible-light-driven photocatalytic activity of bismuth oxide via the decoration of titanium carbide quantum dots. *Journal of colloid and interface science*, 600:161–173, 2021.
- [274] Min Wang, Siyan Li, Jin Kang, Yiwu Tang, Jiadian Wang, Zhenqi Xu, and Jiayun Liu. Enhanced tetracycline degradation by nc codoped fe2o3 with rich oxygen vacancies in peroxymonosulfate assisting photoelectrochemical oxidation system: performance, mechanism and degradation pathway. Chemical Engineering Journal, 451:138611, 2023.
- [275] Yishuang Bi, Lihui Huang, Xiaoyang Song, Ting Sun, and Shimin Xu. Fe-based prb system with ultrasound synergistically enhances the degradation of tetracycline. Chemical Engineering and Processing-Process Intensification, 197:109687, 2024.
- [276] Narjess Zaghbani, Amor Hafiane, and Mahmoud Dhahbi. Separation of methylene blue from aqueous solution by micellar enhanced ultrafiltration. Separation and Purification Technology, 55(1):117–124, 2007.
- [277] Thi Thuy Bui and Mooyoung Han. Decolorization of dark green rit dye using positively charged nanobubbles technologies. Separation and Purification Technology, 233:116034, 2020.
- [278] Ping Ma, Chao Han, Qiongqiong He, Zhenyong Miao, Mingqiang Gao, Keji Wan, and Enle Xu. Oxidation of congo red by fenton coupled with micro and nanobubbles. Environmental Technology, 44(17):2539–2548, 2023.
- [279] Abhispa Sahu and Jordan C Poler. Removal and degradation of dyes from textile industry wastewater: Benchmarking recent advancements, toxicity assessment and cost analysis of treatment processes. *Journal of Environmental Chemical Engineering*, page 113754, 2024.
- [280] MA Adelin, G Gunawan, M Nur, A Haris, DS Widodo, and L Suyati. Ozonation of methylene blue and its fate study using lc-ms/ms. In *Journal of physics: conference series*, volume 1524, page 012079. IOP Publishing, 2020.

[281] Snigdha Khuntia, Subrata Kumar Majumder, and Pallab Ghosh. Removal of ammonia from water by ozone microbubbles. *Industrial & Engineering Chemistry Research*, 52(1):318–326, 2013.

- [282] Sabrina Sorlini and Francesca Gialdini. Conventional oxidation treatments for the removal of arsenic with chlorine dioxide, hypochlorite, potassium permanganate and monochloramine. Water Research, 44(19):5653–5659, 2010.
- [283] Stephan J Hug and Olivier Leupin. Iron-catalyzed oxidation of arsenic (iii) by oxygen and by hydrogen peroxide: ph-dependent formation of oxidants in the fenton reaction. Environmental science & technology, 37(12):2734–2742, 2003.
- [284] Ganesh Ghurye and Dennis Clifford. As (iii) oxidation using chemical and solid-phase oxidants. *Journal-American Water Works Association*, 96(1):84–96, 2004.
- [285] Ganesh Ghurye and Dennis A Clifford. Laboratory study on the oxidation of arsenic III to arsenic V. National Risk Management Research Laboratory, Office of Research and ..., 2001.
- [286] Dennis Charles Johnson, DT Napp, and Stanley Bruckenstein. Electrochemical reduction of ozone in acidic media. *Analytical Chemistry*, 40(3):482–488, 1968.
- [287] Dariush Shahidi, René Roy, and Abdelkrim Azzouz. Advances in catalytic oxidation of organic pollutants—prospects for thorough mineralization by natural clay catalysts. *Applied Catalysis B: Environmental*, 174:277–292, 2015.
- [288] Pierre Boule, Detlef W Bahnemann, PKJ Robertson, et al. Environmental photochemistry part II. Springer, 2005.
- [289] Johnnie N Moore, Jeffrey R Walker, and Thomas H Hayes. Reaction scheme for the oxidation of as (iii) to as (v) by birnessite. *Clays and Clay Minerals*, 38:549–555, 1990.
- [290] Eberhard Rischbieter, Hendrik Stein, and Adrian Schumpe. Ozone solubilities in water and aqueous salt solutions. *Journal of Chemical & Engineering Data*, 45(2): 338–340, 2000.
- [291] JL Sotelo, FJ Beltran, FJ Benitez, and J Beltran-Heredia. Henry's law constant for the ozone-water system. *Water research*, 23(10):1239–1246, 1989.
- [292] Fernando J Beltran. Ozone reaction kinetics for water and wastewater systems. crc Press, 2003.
- [293] Ulrik K Klaening, Benon HJ Bielski, and K Sehested. Arsenic (iv). a pulse-radiolysis study. *Inorganic Chemistry*, 28(14):2717–2724, 1989.

Chapter A

Appendix A

Chapter B

Appendix A

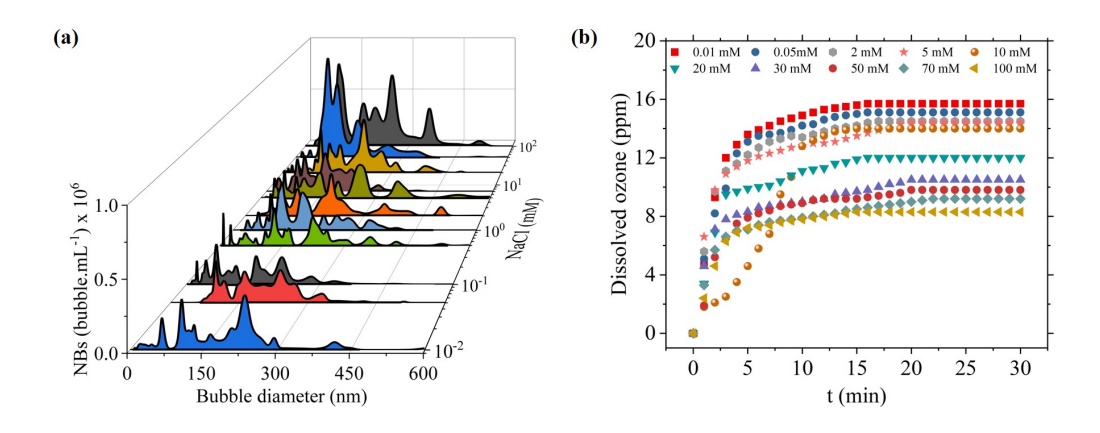


Figure B.1: Ozone nanobubble preparation in the presence of monovalent salt (NaCl) (a) 3D representation of bubble number density of NBs at different concentrations of salts (0.1-100 mM) (b) Dissolved ozone concentration at every one-minute time interval for a period of 30 minutes.

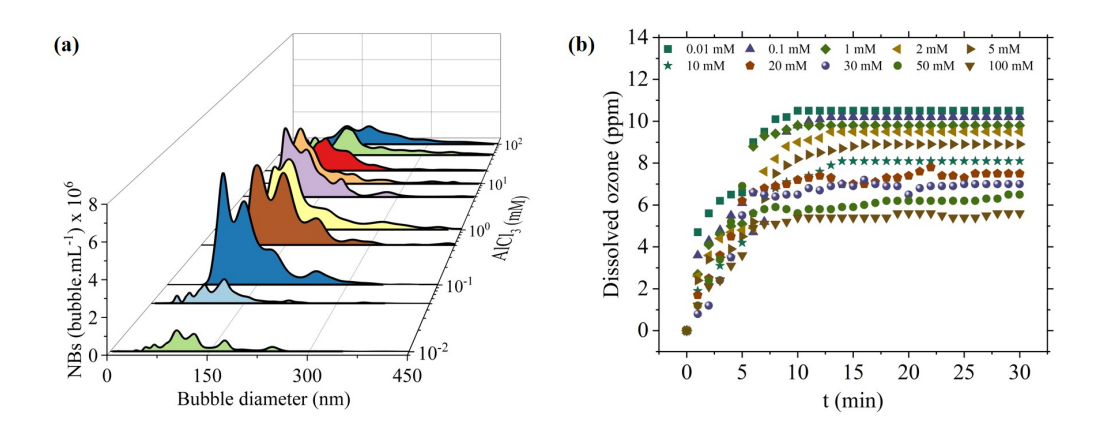


Figure B.2: Ozone nanobubble preparation in the presence of trivalent salt ($AlCl_3$) (a) 3D representation of bubble number density of NBs at different concentrations of salts (0.1-100 mM) (b) Dissolved ozone concentration at every one-minute time interval for a period of 30 minutes.

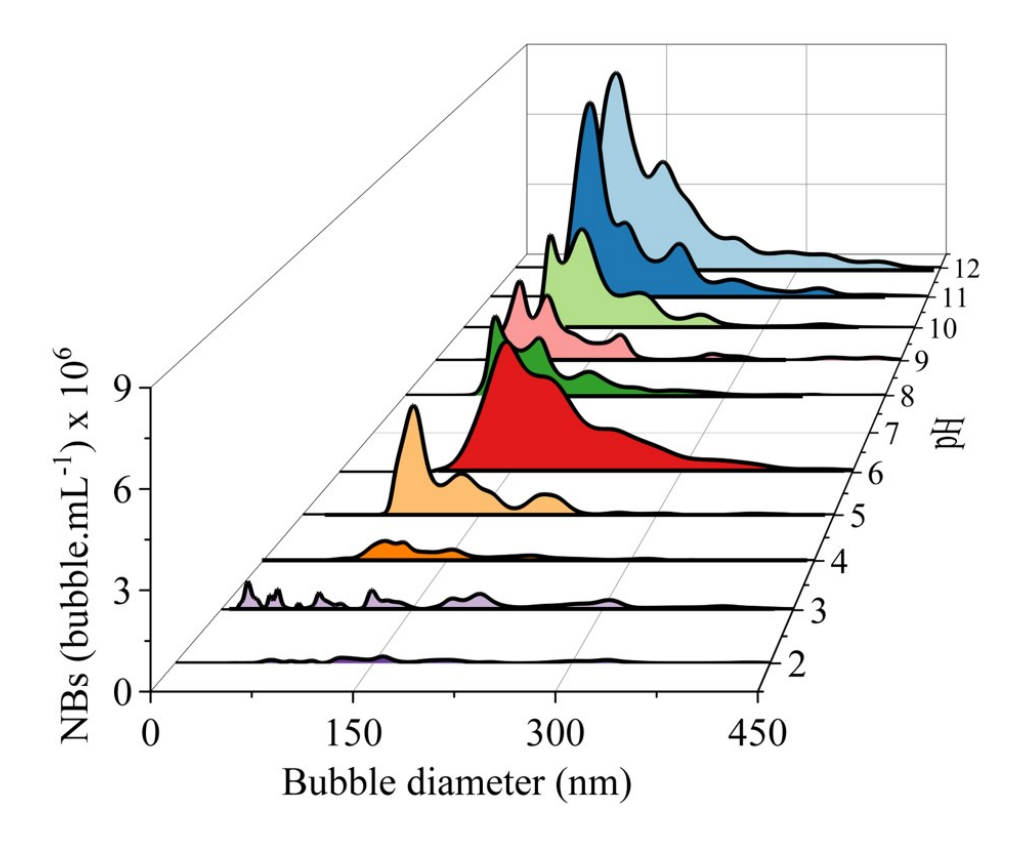


Figure B.3: 3D representation of Ozone nanobubble preparation at different pH (2-12).

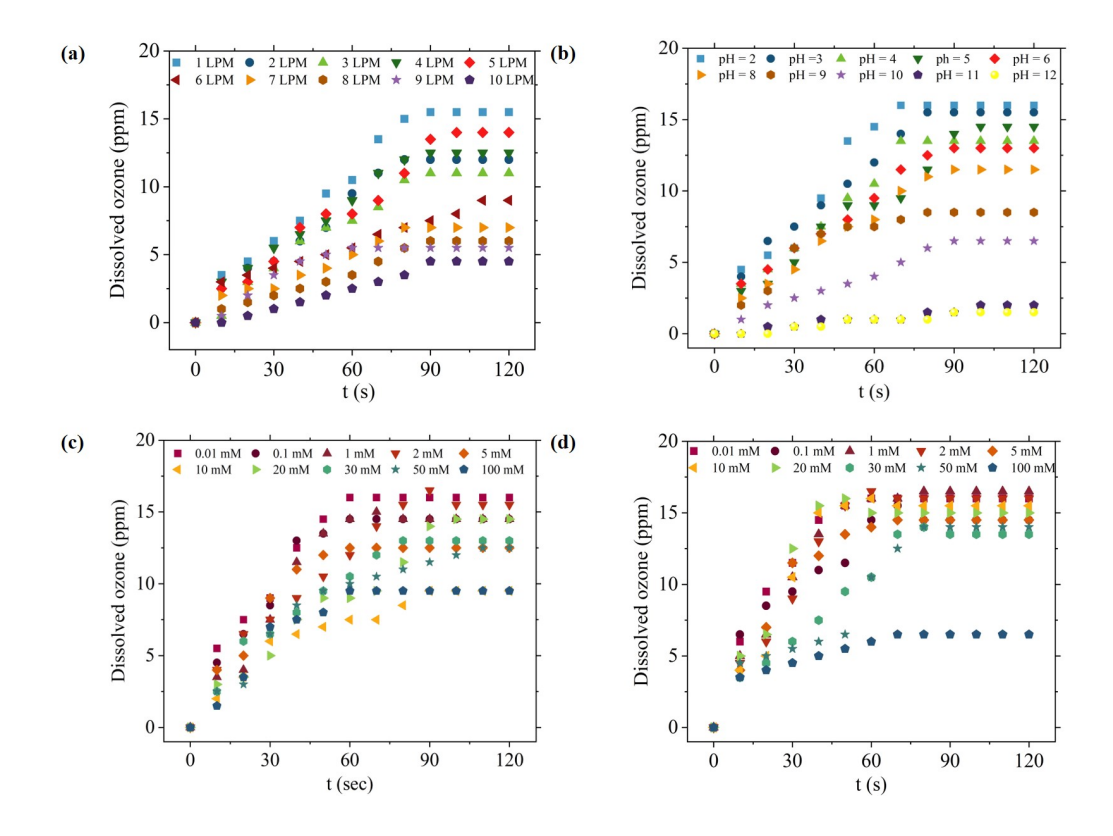


Figure B.4: Dissolved ozone concentration during ozone dissolution (1:5) at various conditions (a) varying ozone flow rates (1-10 LPM) (b) varying pH (2-12) (c) monovalent salt (NaCl) (d) trivalent salt (AlCl_3)

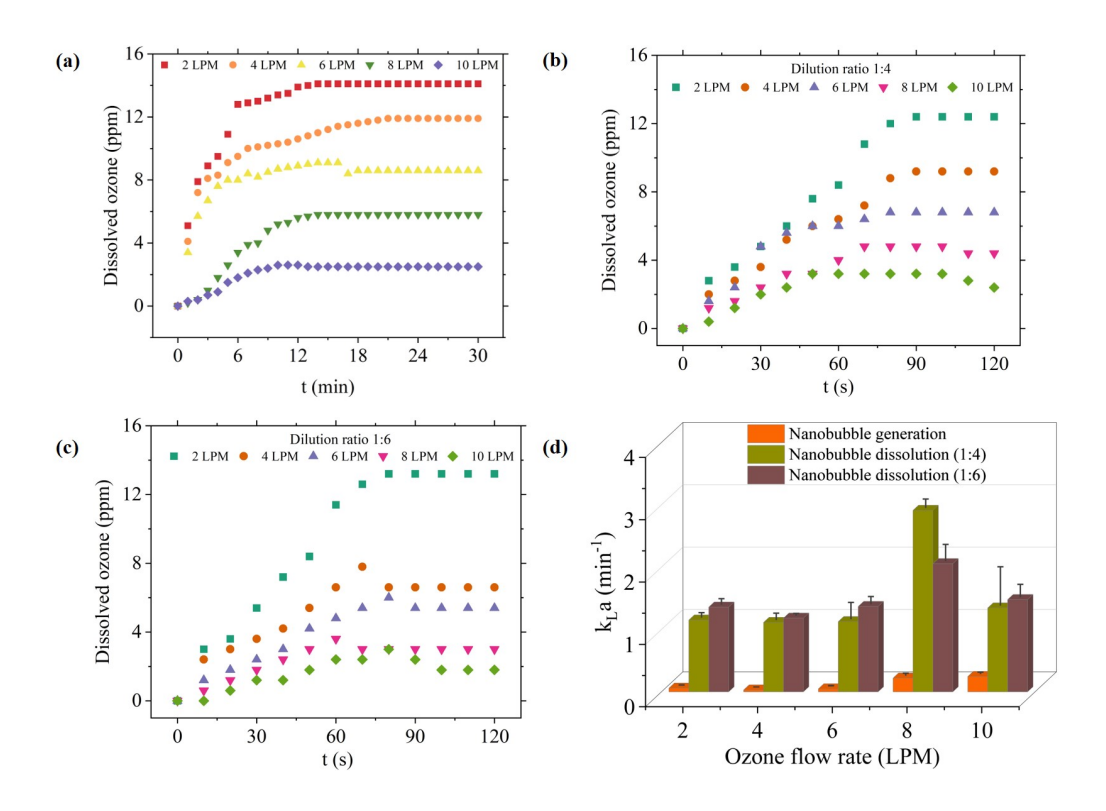


Figure B.5: (a) Dissolved ozone at different ozone flow rates (b) increase in dissolved ozone at 1:4 dilution ratio (c) increase in dissolved ozone at 1:6 dilution ratio (d) mass transfer coefficient at different conditions.

Chapter C

Appendix B

C.1 Determination of volumetric mass transfer coefficient (Model development)

The calculation of the volumetric mass transfer coefficient is presented here. Firstly, the ozone decomposition constant k_d were calculated using Eq 7. It was found by determining the slope of the curve fit of ozone concentration vs time. Further this value of k_d was substitutes in Eq 6. On further integrating Eq 6, k_L a values were determined by curve fitting as shown in Fig (ii). Sample calculations for one particular case have been mentioned below in Figure C.1:

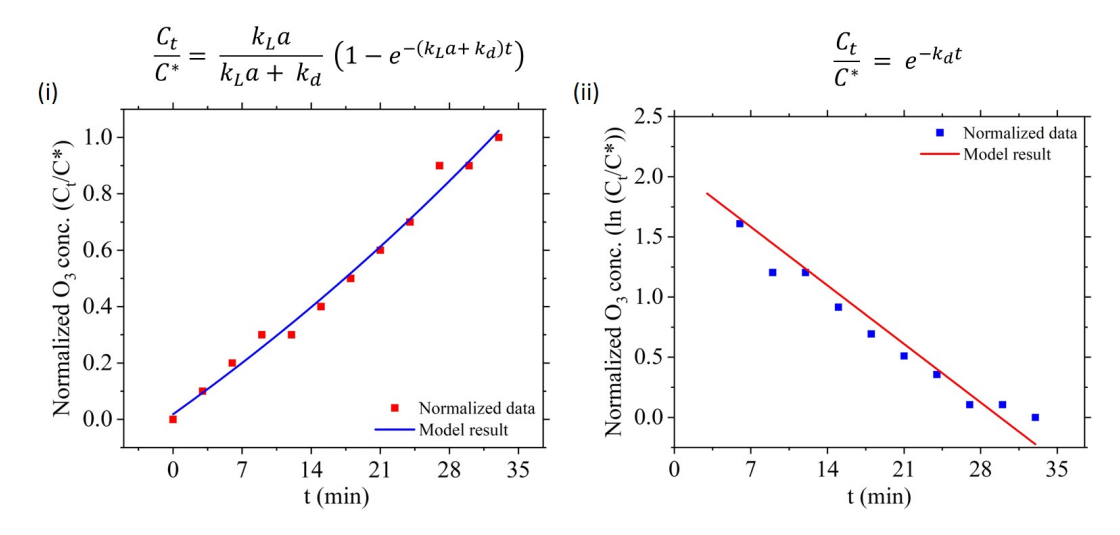


Figure C.1: Sample calculations for (i) k_La (ii) k_d.

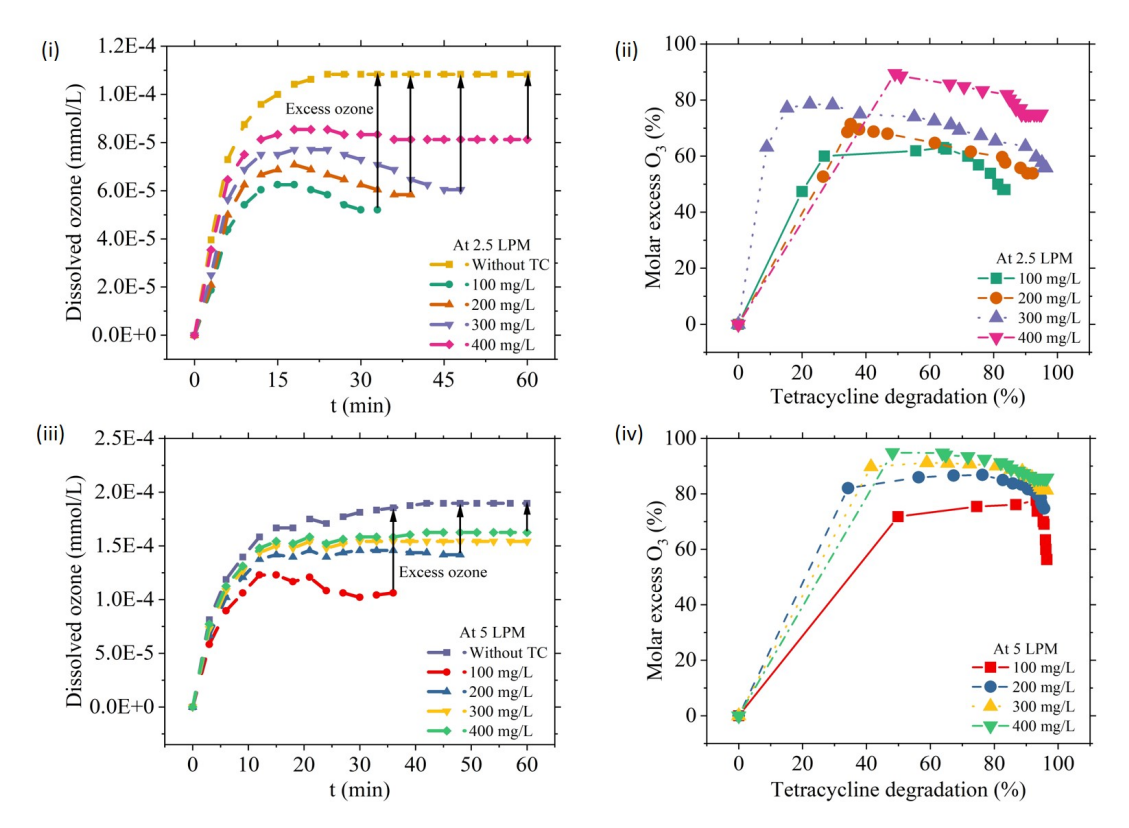


Figure C.2: (i) Dissolved ozone measurements in pure water and during TC degradation (2.5 LPM) (ii) Comparison of molar excess of O3 to degradation efficiency (%) of TC at 2.5 LPM (iii) Dissolved ozone measurements in pure water and during TC degradation (5 LPM) (iv) Comparison of molar excess of O3 to degradation efficiency (%) of TC at 5 LPM.

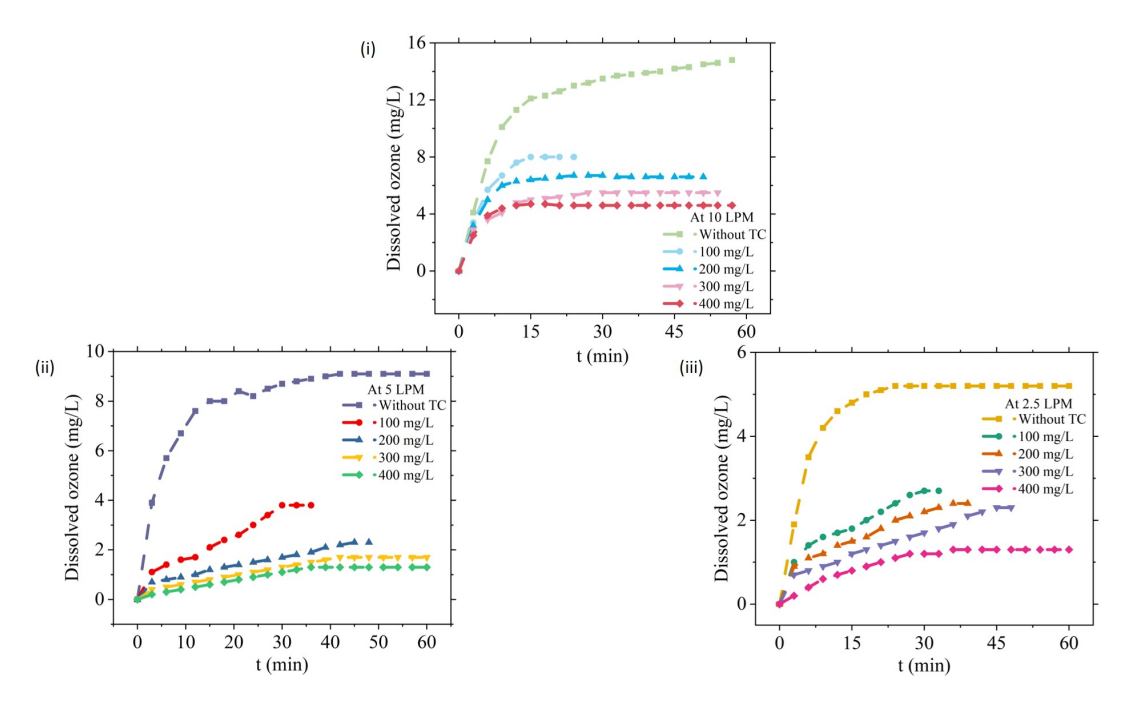


Figure C.3: Comparison of dissolved ozone in pure water and during degradation of TC (100-400 mg/L) (i) 10 LPM (ii) 5 LPM (iii) 2.5 LPM.

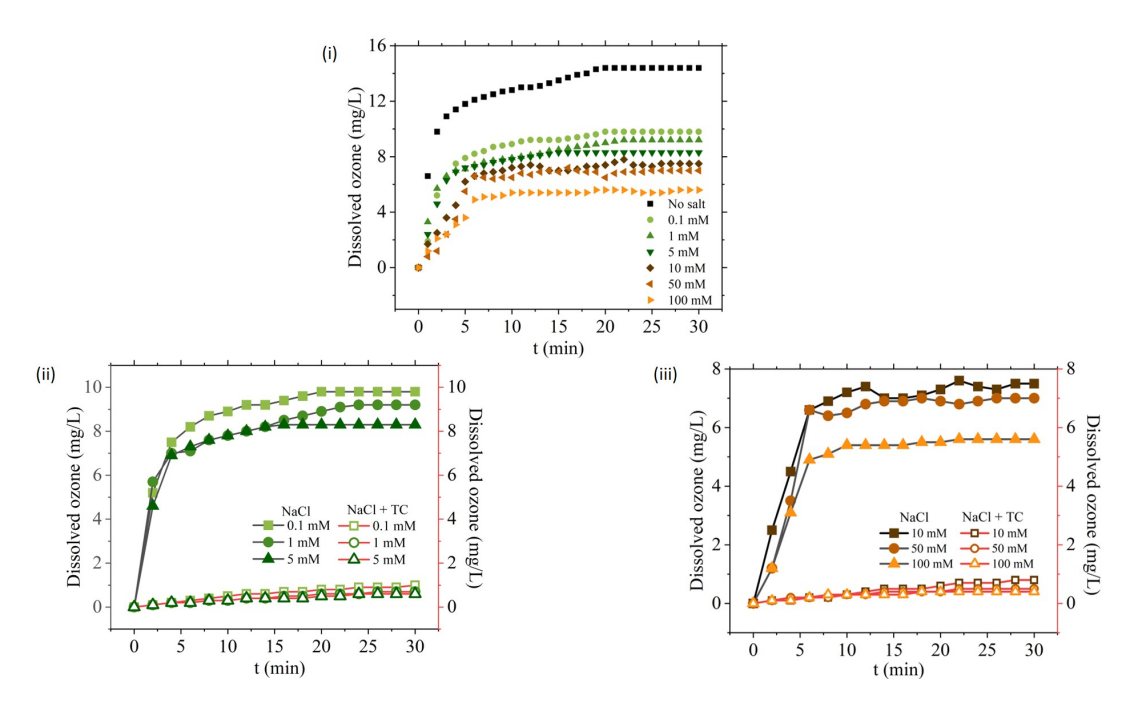


Figure C.4: (i) Comparison of dissolved ozone in presence of pure water to different salt concentrations (ii) Comparison of dissolved ozone in presence of only NaCl to NaCl + TC (0.1, 1, 5mM) (iii) Comparison of dissolved ozone in presence of only NaCl to NaCl + TC (10, 50, 100 mM).

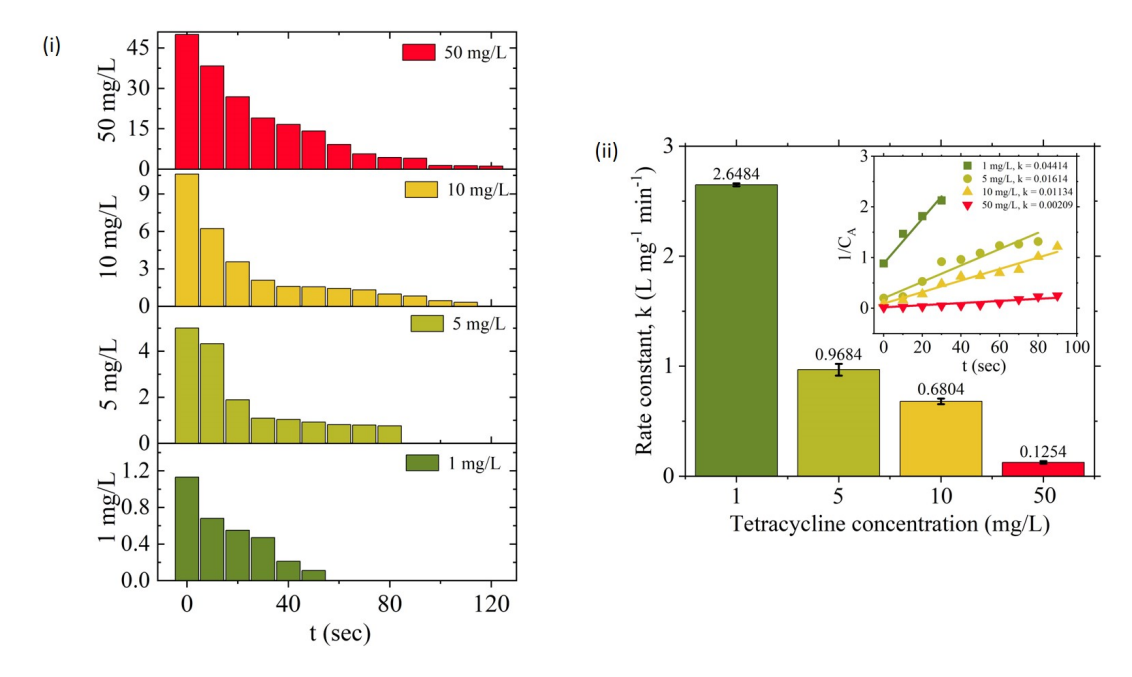


Figure C.5: (i) Tetracycline degradation at low concentrations (1-50 mg/L) (ii) Kinetics with rate constant k at 10 LPM ozone flow rates.

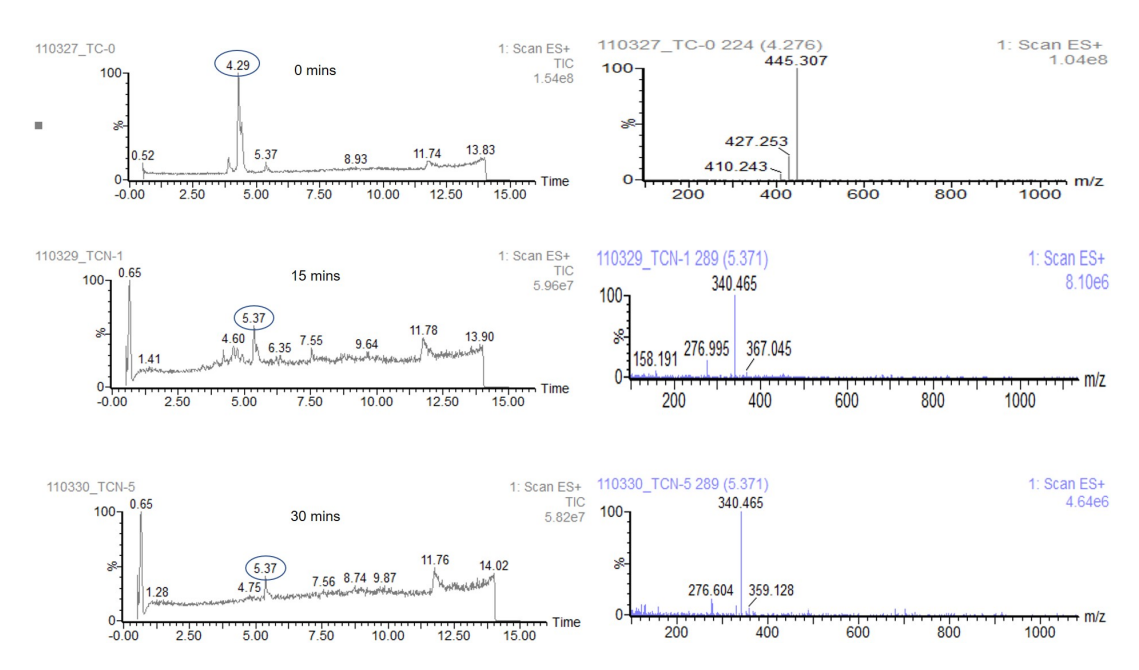


Figure C.6: LC-MS peaks with MS spectra during TC degradation at an interval of 5 minutes.

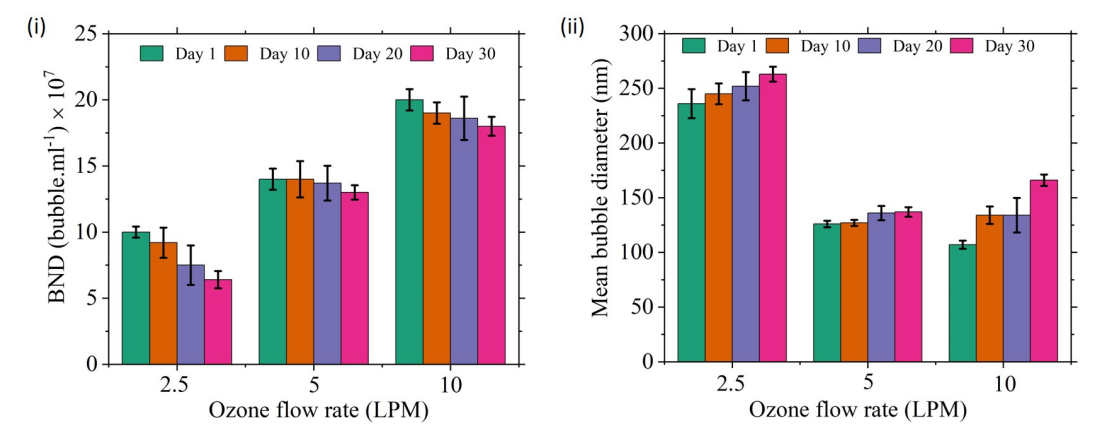


Figure C.7: Stability of ozone nanobubbles at different ozone flow rates (2.5, 5 and 10 $\rm L/min$) over a period of 30 days (i) Bubble number density (bubble.mL⁻¹) (ii) Mean bubble diameter (nm

Figure C.8: Scheme 1

m/z: 362.05 (100.0%), 363.05 (14.7%), 364.05

Figure C.9: Scheme 2

m/z: 362.05 (100.0%), 363.05 (14.7%), 364.05 (2.5%), 364.06 (1.0%)

Figure C.10: Scheme 3

m/z: 226.05 (100.0%), 227.05 (11.2%), 228.05 (1.8%)

m/z: 339.06 (100.0%), 340.06 (15.9%), 341.06 (1.9%), 341.07 (1.1%)

Figure C.11: Scheme 4

Chapter D

Appendix C

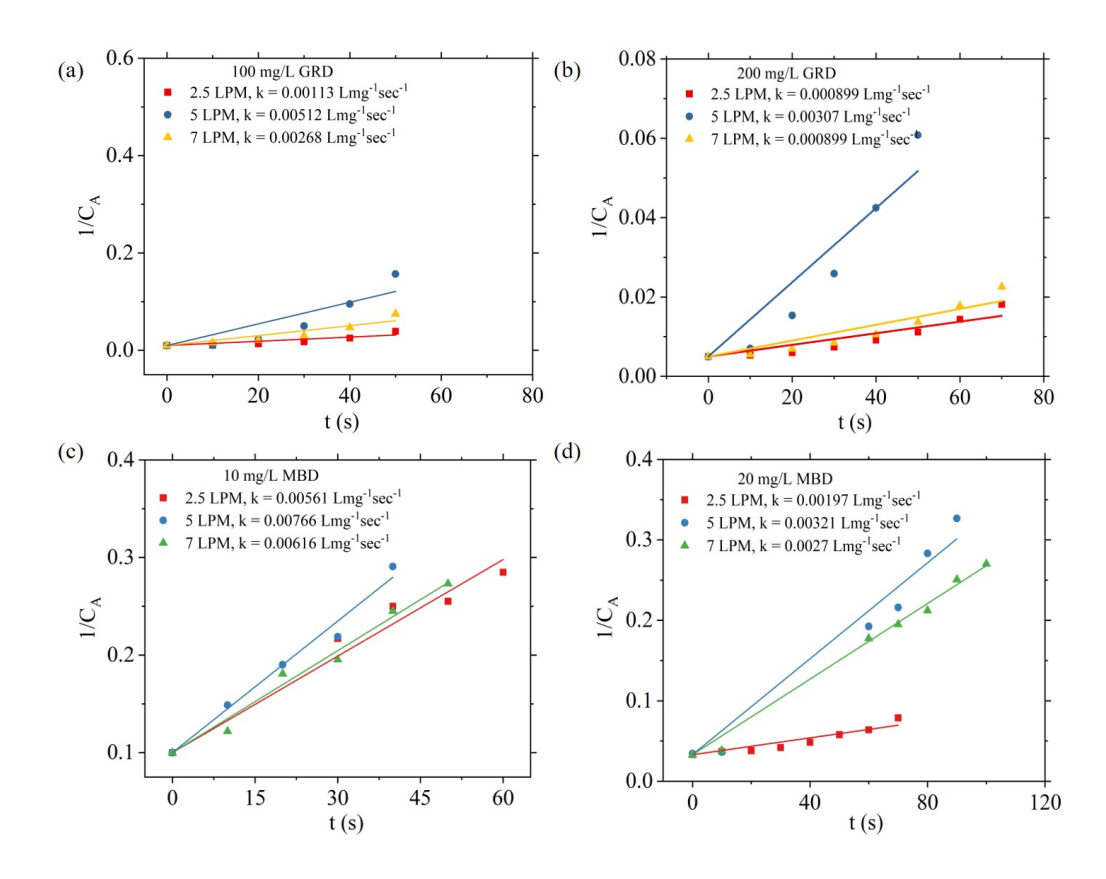


Figure D.1: Kinetic study for effect of ozone flow rates (a) 100 mg/L green rit dye (b) 200 mg/L green rit dye (c) 10 mg/L methylene blue dye (d) 20 mg/L methylene blue dye

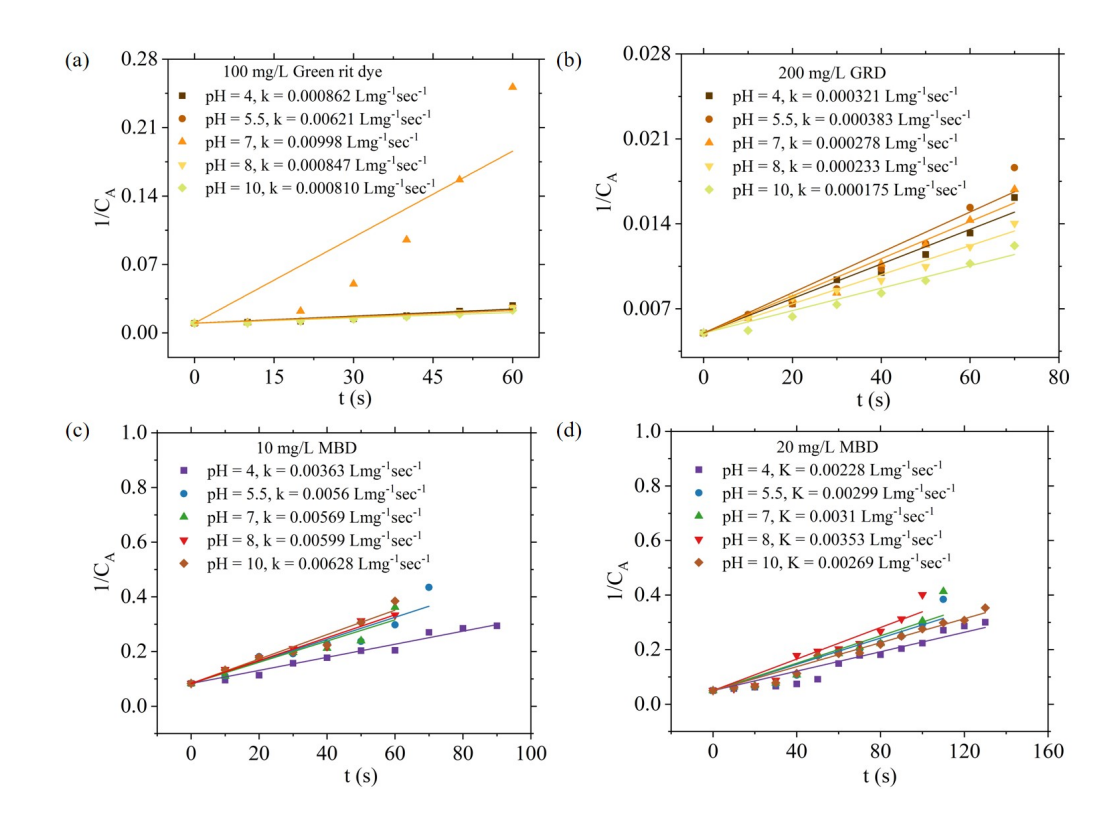


Figure D.2: Kinetic study for effect of pH on (a) 100 mg/L green rit dye (b) 200 mg/L green rit dye (c) 10 mg/L methylene blue dye (d) 20 mg/L methylene blue dye

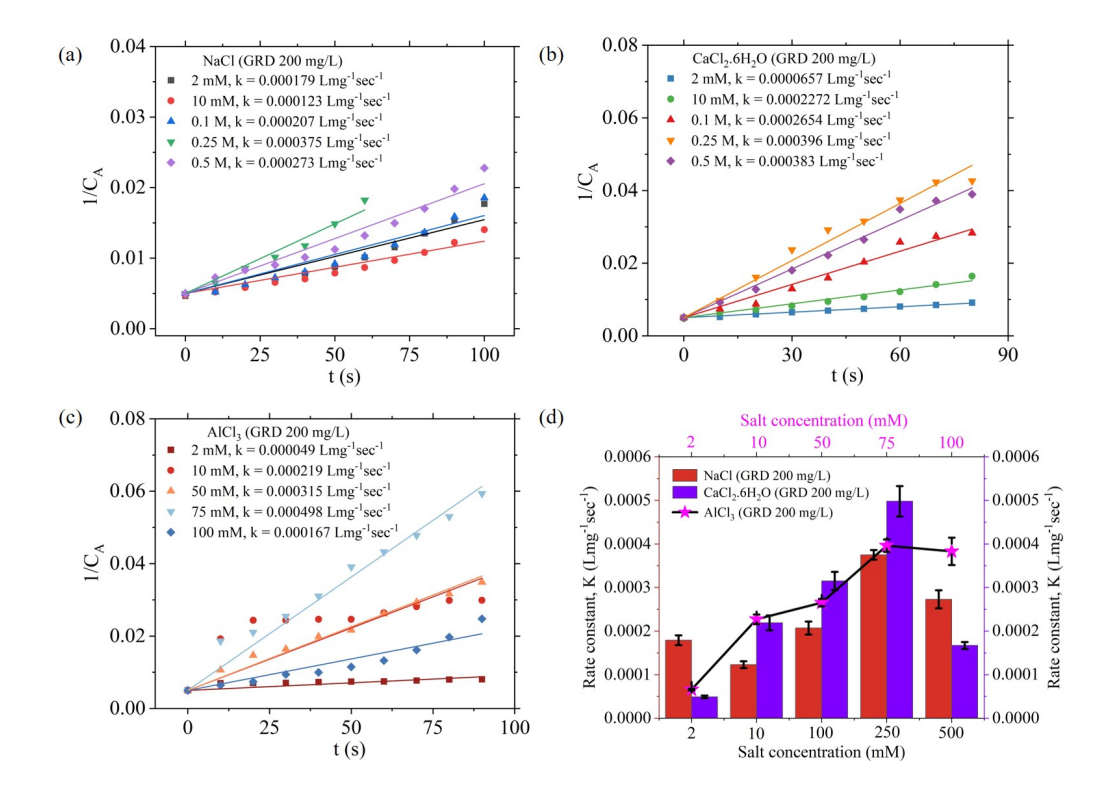


Figure D.3: Kinetic study on effect of salts on green rit dye (200 mg/L) (a) Monovalent salt (b) Divalent salt (c) Trivalent salt (d) Rate constant k for all three salts

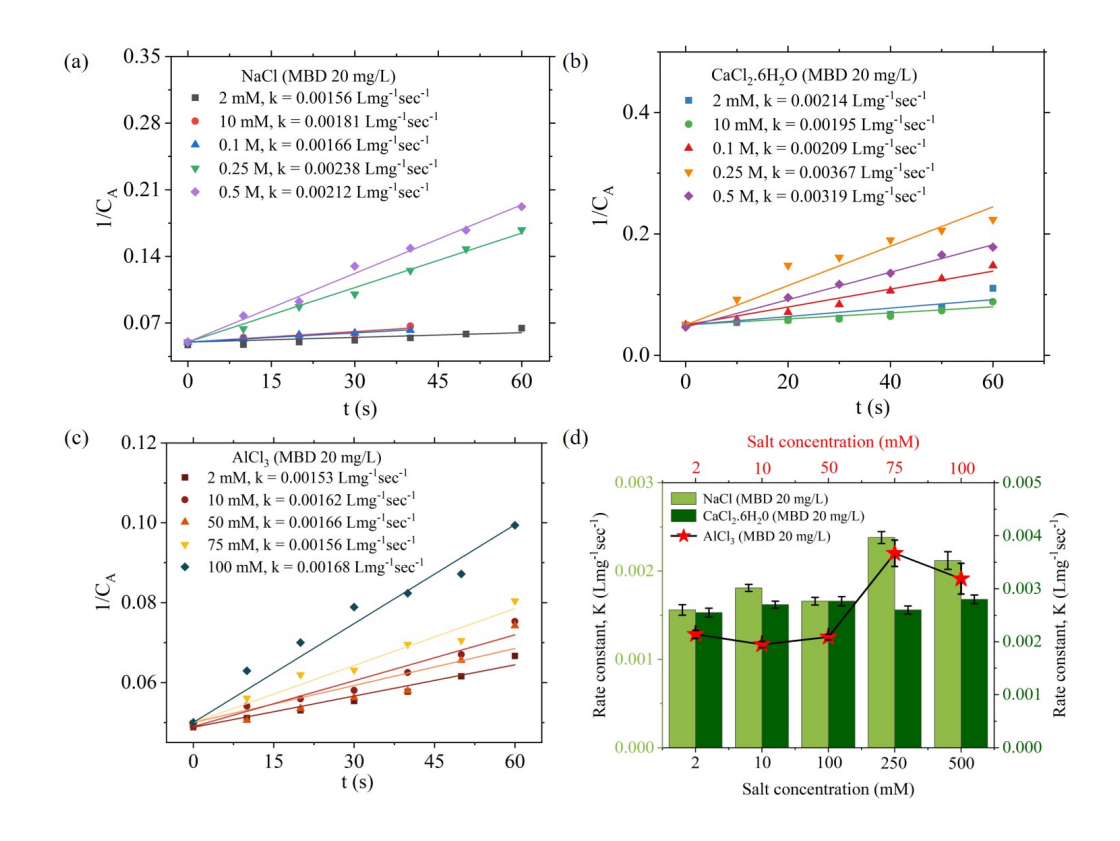


Figure D.4: Kinetic study on effect of salts on methylene blue dye (20 mg/L) (a) Monovalent salt (b) Divalent salt (c) Trivalent salt (d) Rate constant k for all three salts

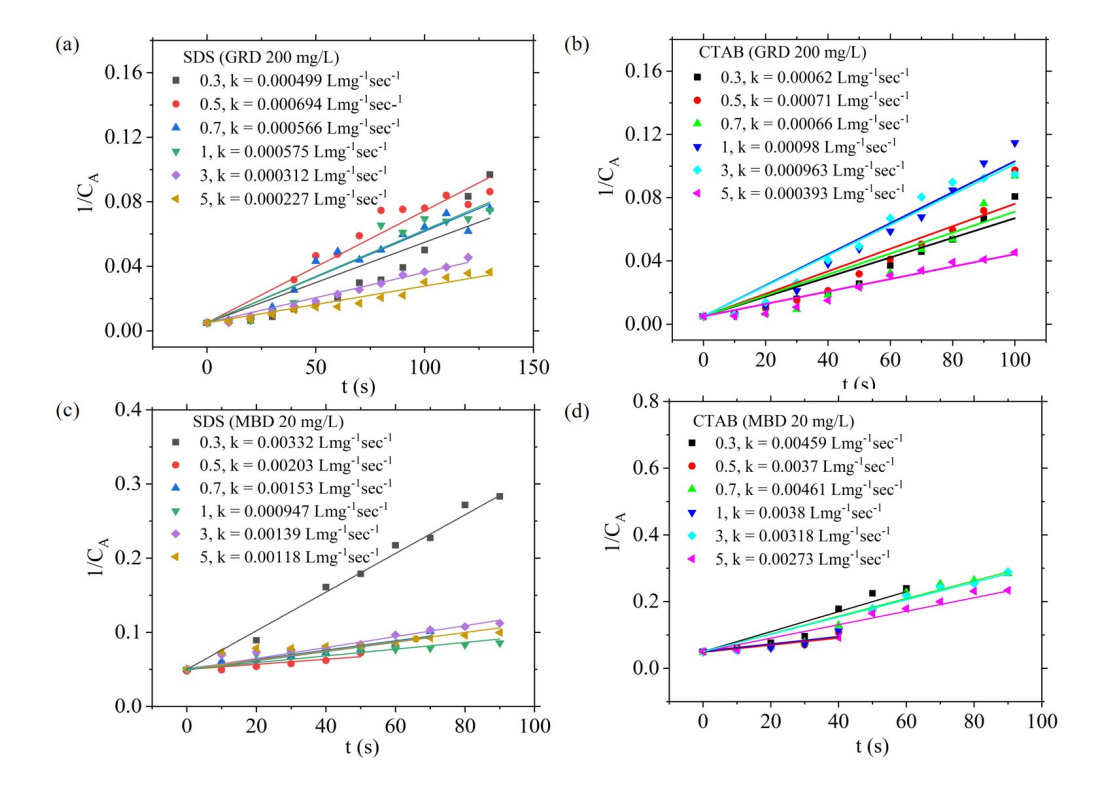


Figure D.5: Kinetic study on the effect of surfactants (a) SDS on green rit dye (200 mg/L) (b) CTAB on green rit dye (200 mg/L) (c) SDS on methylene blue dye (20 mg/L) (d) CTAB on methylene blue dye (20 mg/L)

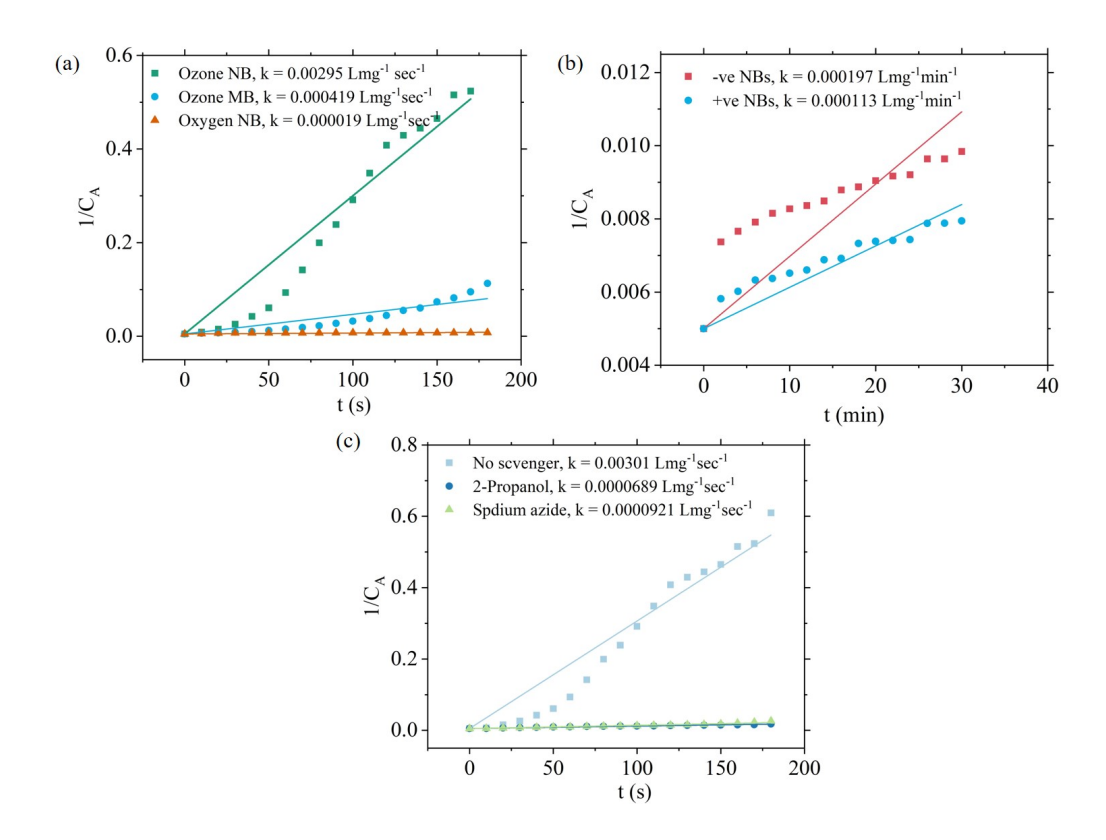


Figure D.6: Kinetic study on (a) Comparison of ozone and oxygen MB's and NB's (b) Negative and positive oxygen NB's (c) Radical scavenging experiments

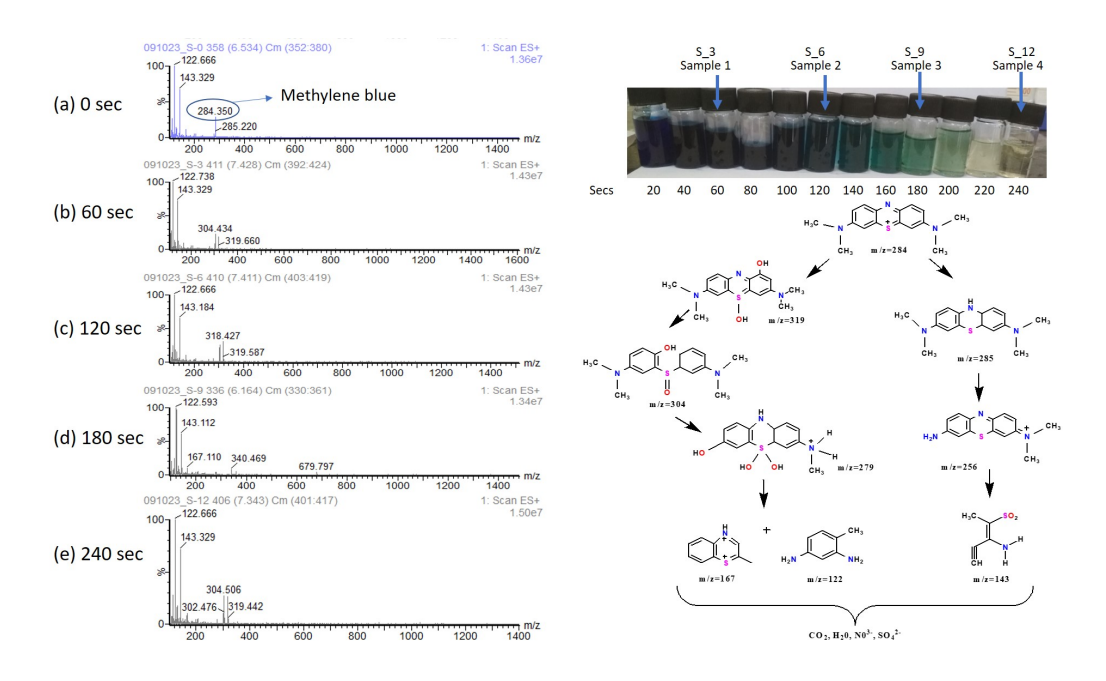


Figure D.7: Analysis of intermediates formed during ozonation of 100 mg/L methylene blue by LC-MS analysis showing MS spectra and the possible degradation mechanism.

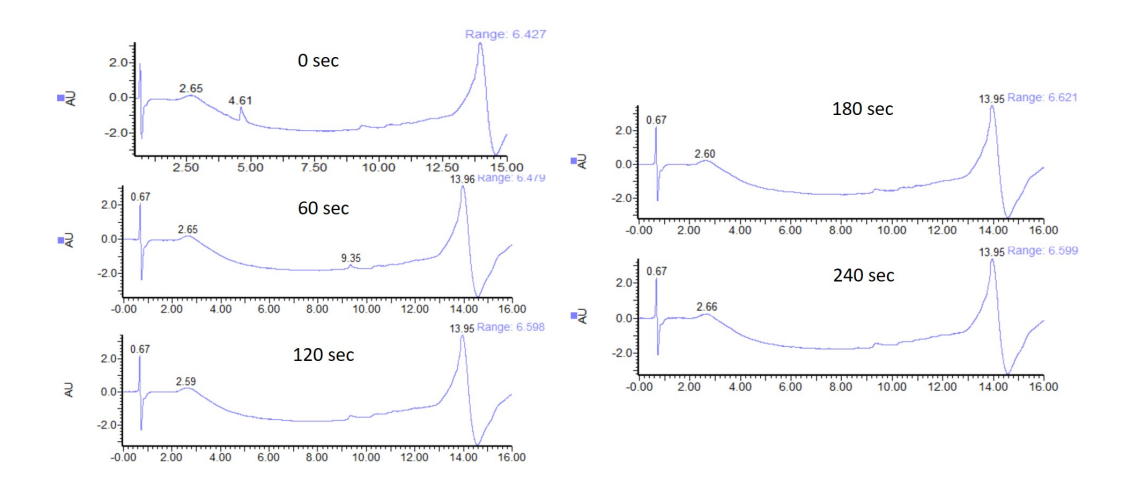


Figure D.8: LC chromatograms for the LC-MS analysis of the methylene blue dye.